



Burianova, Valeriia (2025) *The synthesis and development of radionuclide based tracers for the imaging of diseases*. PhD thesis.

<https://theses.gla.ac.uk/85384/>

Copyright and moral rights for this work are retained by the author

A copy can be downloaded for personal non-commercial research or study, without prior permission or charge

This work cannot be reproduced or quoted extensively from without first obtaining permission from the author

The content must not be changed in any way or sold commercially in any format or medium without the formal permission of the author

When referring to this work, full bibliographic details including the author, title, awarding institution and date of the thesis must be given

Enlighten: Theses

<https://theses.gla.ac.uk/>
research-enlighten@glasgow.ac.uk

The Synthesis and Development of Radionuclide Based Tracers for the Imaging of Diseases

Valeriia Burianova, MSc

Thesis is submitted in fulfilment of the requirements for the Degree of
Doctor of Philosophy



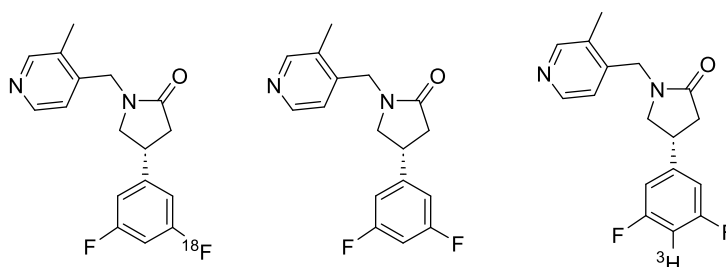
**University
of Glasgow** | School of
Chemistry

School of Chemistry
College of Science and Engineering
University of Glasgow

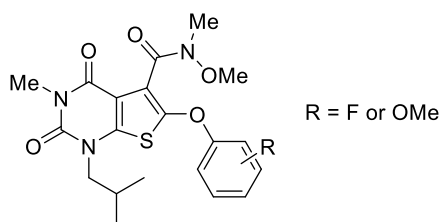
June 2025

Abstract

This PhD focused on the development of synthetic methods for the preparation of known and novel PET imaging agents targeting the central nervous system. The first project created a second-generation enantioselective synthesis of [^{18}F]SynVesT-1, a PET imaging agent for the synaptic vesicle protein 2A (SV2A), along with its non-radiofluorinated standard. Additionally, a modification of this route allowed the synthesis of the novel radioligand, [^3H]SynVesT-1, for SV2A autoradiography.



The next project focused on the synthesis of novel PET imaging agents for the monocarboxylate transporters-1 and -2. A small library of fluorinated and methoxylated 6-substituted thieno[2,3-*d*]pyrimidinedione-5-carboxamide analogues was synthesised via an eight-step route. The physicochemical properties of the developed compounds were evaluated using HPLC methodology, with all showing favourable characteristics.



The final project was dedicated to the development of novel fluorescent α -amino acids via derivatisation of tryptophan at C2-position through alkenylation (Horner-Wadsworth-Emmons and Wittig) and arylation (Suzuki-Miyaura) reactions. The resulting amino acids showed excellent photophysical properties, solvatochromism and pH sensitivity.

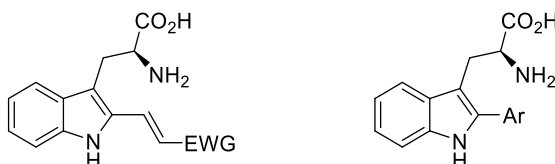


Table of Contents

Abstract.....	1
Table of Contents.....	2
Acknowledgment.....	4
Authors Declaration	6
List of Abbreviations.....	7
1. Introduction	11
1.1 Positron Emission Tomography	11
1.1.1 Physics and instrumentation of PET.....	12
1.1.2 PET radiotracers	13
1.2 Synaptic Vesicle Protein 2	18
1.2.1 Imaging of synaptic density	19
1.2.2 Known synthetic approaches to [¹⁸ F]SynVesT-1	24
1.2.3 Enantioselective synthesis of nonacetamide PET imaging agents....	28
1.2.4 Previous work in the Sutherland group.....	29
1.3 Monocarboxylate Transporters	32
1.3.1 MCT1–4 inhibitors	33
1.3.2 PET imaging agent targeting MCT	39
1.3.3 Previous work in the Sutherland group.....	41
2. Results and Discussion.....	47
2.1 Development of SV2A Imaging Agents.....	47
2.1.1 Project aims	47
2.1.2 Development of a second-generation route for SynVest-1 and precursor for [¹⁸ F]SynVesT-1.....	52
2.1.3 Application of the second-generation route for the synthesis of [¹⁸ F]SynVesT-1 precursor.....	58
2.1.4 Radiosynthesis of [¹⁸ F]SynVesT-1	60

2.1.5	Synthesis of precursor for [³ H]SynVesT-1	64
2.1.6	Conclusions and future work	74
2.2	Development of New PET Imaging Agents Targeting MCT1/MCT2	76
2.2.1	Project aims.....	76
2.2.2	Synthesis of the phenoxy thieno[2,3- <i>d</i>]pyrimidinedione derivatives ..	78
2.2.3	Synthesis of the methoxylated MCT1/2 inhibitors.....	84
2.2.4	Synthesis of phenylamino thieno[2,3- <i>d</i>]pyrimidinedione derivatives.....	87
2.2.5	Evaluation of physicochemical properties	90
2.2.6	Conclusions and future work	94
2.3	Development of New Fluorescent Tryptophan-Based α -Amino Acids	96
2.3.1	Fluorescence imaging	96
2.3.2	Fluorescent amino acids	99
2.3.3	Project aims	102
2.3.4	Synthesis of tryptophan analogues via olefination reactions	103
2.3.5	Synthesis of tryptophan analogues via the Suzuki-Miyaura reaction	117
2.3.6	Conclusions and future work	128
3.	Experimental Section	130
3.1	General Experimental	130
3.2	SV2A PET Imaging Agent Experimental.....	131
3.3	New PET Imaging Agents Binding MCT1 and MCT2 Experimental.....	147
3.4	Fluorescent Tryptophan Derivatives Experimental	169
4.	References.....	191
5.	Appendices	204
	Appendix A. Figures and Schemes.....	204
	Appendix B. Chiral HPLC Traces.....	206
	Appendix C. Determination of Physicochemical Properties	216

Acknowledgment

Firstly, I would like to thank my PhD supervisor, Professor Andrew Sutherland, for giving me an opportunity to do this PhD in his group and for his constant support, guidance and prompt feedback at all times. It was a great honour for me to learn chemistry from you, and I hope I did remember something from the group problem sessions. I would also like to thank my second PhD supervisor, Dr. Drew Thomson for all his help and support during this PhD. Thank you to Professor Justin Hargreaves for being such a great Head of School, always ready to help every team member. I would also like to thank the EPSRC for funding this PhD as well as the University of Glasgow for providing the international student fee waiver.

Thank you to all the technical staff who supported the services at the University: Finlay and Karen (stores), Alec (NMR), Giovanni and Eirinn Rose (MS), Stuart, Arlene and Iain (IT). Many thanks to the School of Chemistry and the COSE Graduate school teams for their support. I would also like to thank everyone in the West of Scotland PET RPU, especially Dr Dmitry Solovyev, Dr Sally Pimlott, Dr Sue Champion, and Dr Gavin Brown for my 1-month internship there and amazing introduction to radiochemistry I received during that time. Additionally, thanks to Dr Will Peveler for the fluorimeter training and all the help with fluorescence.

To earlier members of the Sutherland group: Beckie, Leanne, Liyao, Amy, Rochelle, Lachlan, Nina – thank you for welcoming me to the team. And huge thanks to the current group members: Holly (thanks for the Christmas tree!), Olivia, Juwon, Eoghan, Layal, Pankaj – thank you for your help, support and making my PhD such an enjoyable time. Thank you to Arthur for being such a great student. Also, thanks to all the Hartley group members, especially Stuart for his help and to Pat and Claudia for making the lab a fun place to work in. Special thanks to the best technician a Loudon lab could ever have, Gillian, for all the work you've done and for all the support you've given me, you're amazing. Also, thanks to Marina from the Bell's group for being a Meladze girl. My huge thanks go to Hollie from the Prunet group for being such an amazing friend, I'm so glad I had a chance to meet you. Another special thanks to Olya from the Hedley group, who I couldn't imagine this PhD without and I'm glad we've shared all the up and downs of the past 4 years together.

Special thanks to all the members of my previous research groups: Krasavin and Kukushkin research groups from SPbU. I'm grateful for an opportunity to work with you and learn from you.

I can't even imagine completing this PhD without my husband, Pete, one of the best synthetic chemists I know, who taught me so much and supported me through both the highs and the lows. I don't even know how to express my gratitude to my whole family, who have supported me throughout this journey and loved me in their own special way. Huge thanks to my Mum, a true hero, who fought her cancer diagnosis last year; thank you for finally accepting that I want to be a chemist. Special thanks to my Dad, Natasha, and Sasha who have always been there for me, helped in any way they could and supported my wild ideas. Enormous thanks to my Grandma, Grandpa, Masha, and Ulyana for loving and supporting me despite 2000 km between us. To my school and Uni besties who were also doing their PhDs at the same time in one way or another, Natasha, Gelya, Leshia, Ilya (and your mum!), Firuza, Dasha&Dasha, Polina, Sasha, I don't know what I would do without you. Thank you for all our chats, and all the love and support you've given me for the past 20+ years. Special shout-out my Glasgow squad – Maria, Karthi&Joyce, Olya&Andrei. I was lucky to meet you in my early PhD years and I'm grateful we're still friends after all this time.

"I gave my blood, sweat, and tears for this"

Taylor Swift, *You're on Your Own, Kid*

Authors Declaration

I declare that, except where explicit reference is made to the contribution of others, this thesis represents the original work of Valeriia Burianova and has not been submitted for any other degree at the University of Glasgow or any other institution. The research was carried out at the University of Glasgow in the Loudon Laboratory under the supervision of Professor Andrew Sutherland between October 2021 to March 2025. Aspects of the work described herein have been published elsewhere as listed below.

H. McErlain, E. B. McLean, T. E. F. Morgan, **V. K. Burianova**, A. A. S. Tavares and A. Sutherland, Organocatalytic Asymmetric Synthesis of SynVesT-1, a Synaptic Density Positron Emission Tomography Imaging Agent, *J. Org. Chem.*, 2022, **87**, 14443–14451.

V. Burianova, H. McErlain, A. Sutherland, Transition-Metal-Mediated Radiohalogenation using Aryl Boron Reagents, *Synthesis*, 2024, **56**, 1402–1414.

V. Burianova, L. Zeng, A. Thom, N. Radcliffe-Kennedy, S. Magennis, A. Sutherland, Environment-Sensitive Fluorescent Tryptophan Analogues via Indole C-2 Alkenylation Reactions, *Chem. Commun.*, 2025, **61**, 11621–11624.

C. Wimberley, C. J. Alcaide-Corral, T. E. F. Morgan, M. G. Macaskill, B. Andrews, H. McErlain, **V. K. Burianova**, A. Sutherland, A. A. S. Tavares. Characterization of in vivo binding kinetics and non-displaceable binding of [¹⁸F]SynvesT-1 in the rat brain. *EJNMMI Research*, **15**(1), 72.

Signature

Printed Name

Valeriia Burianova

List of Abbreviations

Ac	acetyl
α -CHC	alpha cyano-4-hydroxycinnamic acid
AcOH	acetic acid
Ar	aromatic
ATP	adenosine triphosphate
a.u.	arbitrary unit
<i>rac</i> -BINAP	(\pm)-2,2'-bis(diphenylphosphino)-1,1'-binaphthalene
BMIM	1-butyl-3-methylimidazolium
Boc	<i>tert</i> -butyloxycarbonyl
BODIPY	boron-dipyrromethene
BPO	benzoyl peroxide
Bq	becquerel
Cbz	carboxybenzyl
CD147	cluster of differentiation 147
clogP	calculated partition coefficient
COSY	homonuclear correlation spectroscopy
cm	centimetre
CNS	central nervous system
cryo-EM	cryo-electron microscopy
CT	computed tomography
d	doublet
dba	dibenzylideneacetone
DBU	1,8-diazabicyclo[5.4.0]undec-7-ene
deg	degree
DEPT	distortionless enhancement by polarisation transfer
DIDS	4,4'-diisothiocyanatostilbene-2,2'-disulfonate
DIPEA	<i>N,N'</i> -diisopropylethylamine
DIBAL-H	diisobutylaluminium hydride
DMA	dimethyl acetamide
DMF	<i>N,N'</i> -dimethylformamide
DMSO	dimethylsulfoxide
dppf	1,1'-bis(diphenylphosphino)ferrocene
ee	enantiomeric excess

eq.	equivalent
<i>er</i>	enantiomeric ratio
ESI	electrospray ionisation
Et	ethyl
EtOAc	ethyl acetate
EtOH	ethanol
EWG	electron-withdrawing group
FDA	Food and Drug Administration
[¹⁸ F]FDG	2-deoxy-2-[¹⁸ F]fluoro-D-glucose
[¹⁸ F]Flac	¹⁸ F-labelled lactic acid
[¹⁸ F]FP	[¹⁸ F]fluoropyruvate
FRET	fluorescence resonance energy transfer
g	gram
GFP	green fluorescent protein
GM	Goeppert-Mayer
h	hour
HADA	3-(7-hydroxycoumarin)-carboxamide-D-alanine
HBTU	O-(benzotriazol-1-yl)- <i>N,N,N',N'</i> -tetramethyluronium hexafluoro-phosphate
Het	heterocycle
HMBC	heteronuclear multiple bond correlation
HPLC	high performance liquid chromatography
HAS	human serum albumin
HSQC	heteronuclear single quantum correlation spectroscopy
HWE	Horner-Wadsworth-Emmons
Hz	Hertz
IAM	immobilised artificial membrane
IC ₅₀	half-maximal inhibitory concentration
ICG	indocyanine green
<i>J</i>	coupling constant
keV	kiloelectron volt
<i>K_m</i>	membrane partition coefficient
LDA	lithium diisopropylamide
log <i>P</i>	partition coefficient
LOR	line of response

M	molar
m	multiplet
MCT	monocarboxylate transporter
Me	methyl
MeCN	acetonitrile
MeOH	methanol
MHz	megahertz
min	minute
mL	millilitre
mmol	millimole
mol	mole
Mp	melting point
MRI	magnetic resonance imaging
MW	molecular weight
<i>m/z</i>	mass to charge ratio
N/A	not available
NBS	<i>N</i> -bromosuccinimide
NCS	<i>N</i> -chlorosuccinimide
NETs	neuroendocrine tumours
NIR	near-infrared
NIS	<i>N</i> -iodosuccinimide
nm	nanometer
NMR	nuclear magnetic resonance
NMP	<i>N</i> -methylpyrrolidone
PBS	phosphate-buffer saline
<i>p</i> -CMBS	<i>para</i> -chloromercuribenzenesulfonate
PET	positron emission tomography
PG	protecting group
Ph	phenyl
pin	pinacol
P_m	membrane permeability
PPA	polyphosphoric acid
%PPB	the percentage of plasma protein binding
ppm	parts per million
py	pyridine

q	quartet
RCC	radiochemical conversion
RCP	radiochemical purity
RCY	radiochemical yield
RPU	Radiopharmaceutical Production Unit
rt	room temperature
s	singlet
sec	second
S _N Ar	nucleophilic aromatic substitution
SV2	synaptic vesicle protein 2
t	triplet
TBAI	tetrabutylammonium iodide
TBAOTf	tetrabutylammonium trifluoromethanesulfonate
^t Bu	<i>tert</i> -butyl
TEAB	tetraethylammonium bromide
temp.	temperature
TEMPO	(2,2,6,6-tetramethylpiperidin-1-yl)oxyl
Tf	trifluoromethanesulfonyl
TFA	trifluoroacetic acid
THF	tetrahydrofuran
TMHD	2,2,6,6-tetramethyl-3,5-heptanedione
TMS	trimethylsilyl
UV	ultraviolet
vis	visible
v/v	volume/volume
XPhos	2-dicyclohexylphosphino-2',4',6'-triisopropylbiphenyl
3D	three dimensional
°C	degrees centigrade
ε	molar extinction coefficient
Φ _F	fluorescence quantum yield
λ _{abs}	absorbance maximum
λ _{em}	emission maximum

1. Introduction

1.1 Positron Emission Tomography

Medical imaging is widely used for disease monitoring, diagnosis and evaluation of treatment effectiveness. In research settings, imaging plays a crucial role in metabolic and anatomic studies, providing insights into the interior of the human or animal body and its internal process. The choice of imaging technique depends on the aim of the examination. One of the first imaging techniques enabling visualisation of internal structures in living organisms was X-ray. X-Rays were discovered in the late nineteenth century by Wilhelm Röntgen.¹ Since then, many visualising techniques, such as magnetic resonance imaging (MRI), computed tomography (CT), and sonography have been presented. Positron emission tomography (PET) was one of most recent advancements in this field. Today, PET imaging is widely utilised in both medical diagnostics and research practice. Clinical and research PET imaging is widely used for cancer diagnosis and management, as well as in cardiology, neurology, and psychiatry.²

In cancer treatment, the data obtained using PET imaging is important in disease staging as well as in developing a treatment plan and assessment of the response to therapy. PET is an essential diagnostic tool for evaluation of tumour recurrence, and surgery preparation. In some cases, using PET imaging helps to avoid biopsy and surgical intervention.^{3,4} In cardiology, PET imaging is used for the detection and management of coronary artery disease and assessment of ventricular function and myocardial viability.⁵ PET can help with identifying myocardial regions with reduced blood flow but preserved metabolism, indicating areas that may benefit from revascularisation.⁶ In neuropsychiatry, using PET is helpful in the pathophysiological studies of epilepsy and seizures.⁷ Furthermore, PET has shown to be effective in the early detection and differential diagnosis of various neurological conditions, including Alzheimer and Parkinson's diseases.²

All of this is made possible due to PET's high spatial resolution and high sensitivity, short acquisition type, and excellent quantitative capabilities. Despite its advantages, it remains an expensive method, that typically requires access to a cyclotron or radionuclide generator and involves exposure to radiation for both patients and staff.

However, new developments are being made every day to make this method faster, more affordable and safer.

1.1.1 Physics and instrumentation of PET

The PET imaging technique employs beta-decay of short-lived isotopes. These radionuclides are usually produced either using a cyclotron or a generator.² Following the production, the radionuclides undergo a radiolabelling process with the precursor of choice after which the resulting radiopharmaceutical is isolated, purified and subjected to quality control. Typically, the radiopharmaceuticals (or tracers as they are administered at very low dose) are synthesised, purified, analysed and formulated on site, although those containing isotopes with a longer half-life can be produced externally. Usually, a timescale of three isotope half-lives is considered acceptable for the total synthesis time to ensure a sufficient activity is available for the administration. A PET tracer is then administered intravenously (more rarely through inhalation), and the patient imaged in the PET scanner. When radioisotopes undergo beta decay, emission of a positron (${}^0_1\beta^+$), the antiparticle of the electron occurs.

${}^A_ZX \rightarrow {}^A_{Z-1}Y + {}^0_1\beta^+ + \nu + Q(+e^-)$, where A_ZX is a parent isotope, ${}^A_{Z-1}Y$ is a daughter isotope, Q is energy and ν is the neutrino.

After the positron loses kinetic energy by interactions with the surrounding matter, it eventually collides with an electron.² This results in annihilation and production of two gamma photons of 511 keV, which are emitted at 180° to each other (**Figure 1**). This makes it possible to localise their source, the tissue of interest and where the PET tracer accumulated, using the straight line of coincidence (also called the line of response, LOR). The emitted radiation is detected using scintillation detectors, which are usually arranged in a circular ring. The scintillation detectors are the most commonly used in PET imaging due to its high stopping efficiency and energy resolution. These detectors consist of a scintillator coupled to a photodetector to detect visible light. Various models of PET scanners exist, however, PET scanners combined either with computed tomography (for both research and clinical imaging) or with magnetic resonance imaging (mostly for research purposes) have become increasingly popular in recent decades. Data from the CT or MRI scanners is

merged with PET data, reconstructed and used to generate three dimensional (3D) images of the patient's body. These integrated systems provide both metabolic and anatomic information.

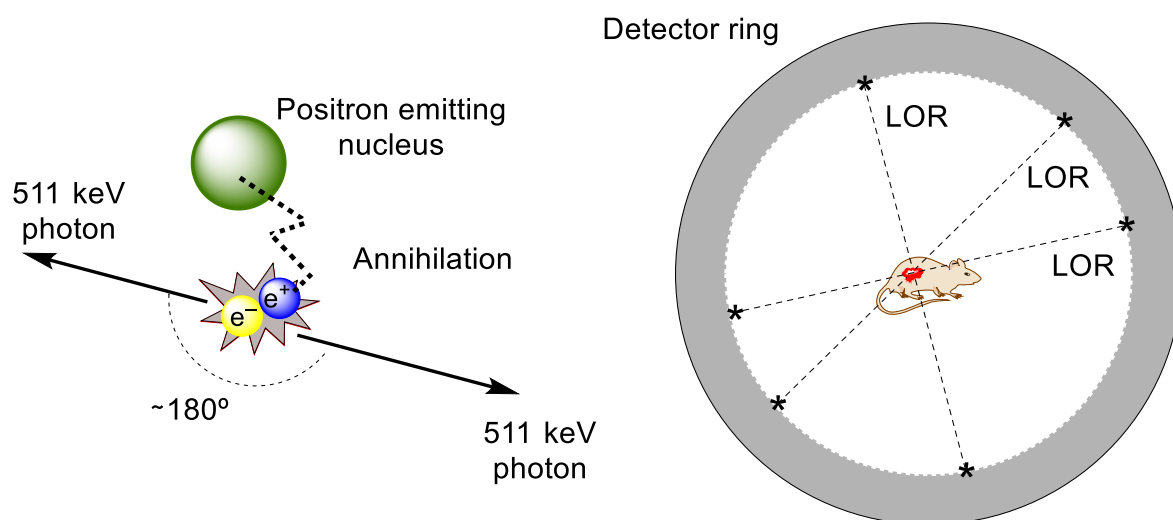


Figure 1. Positron and electron annihilation scheme. Process of detection of annihilation cases in PET scanner.⁸

1.1.2 PET radiotracers

One of the most essential parts of the PET-tracer is the short-lived isotope. The selection of isotopes depends on experiment conditions and the study's objectives (**Table 1**). Due to limitations related to the half-life of certain radionuclides, the most commonly used isotopes in PET radiopharmaceuticals include ^{11}C , ^{18}F , ^{64}Cu , ^{68}Ga and ^{89}Zr .⁹ Radioisotopes are typically produced using a cyclotron, which generates them by bombarding stable isotopes with protons or deuterons. Another method for producing certain radionuclides involves the use of generators (^{68}Ga or ^{82}Rb , **Table 1**), in which the long-lived parent radioisotope decays into a daughter radioisotope, which is then extracted for further use.

The most obvious isotope for use in PET is ^{11}C , as most developed PET tracers are organic molecules, allowing radiolabelling without altering their chemical structure. However, the short half-life of the ^{11}C radionuclide (20.4 min) limits its applications as such a short half-life period restricts radiolabelling only to last-stage procedures. Typically, radiolabelling is performed using either $[^{11}\text{C}]\text{CO}_2$ or its secondary precursors, such as $[^{11}\text{C}]\text{methyl iodide}$ and $[^{11}\text{C}]\text{CO}$.¹⁰

Table 1. Most commonly used isotopes in PET imaging.^{2,11}

Radionuclide	Half-life	Production route
^{11}C	20.34 min	$^{14}\text{N}(\text{p},\alpha)^{11}\text{C}$
^{13}N	9.97 min	$^{16}\text{O}(\text{p},\alpha)^{13}\text{N}$
^{15}O	122.27 sec	$^{14}\text{N}(\text{d},\text{n})^{15}\text{O}$
^{18}F	109.8 min	$^{18}\text{O}(\text{p},\text{n})^{18}\text{F}$
^{44}Sc	3.9 h	$^{44}\text{Ti} / ^{44}\text{Sc}$ generator $^{44}\text{Ca} (\text{p},\text{n})^{44}\text{Sc}$
^{64}Cu	12.7 h	$^{64}\text{Ni}(\text{p},\text{n})^{64}\text{Cu}$
^{68}Ga	67.7 min	$^{68}\text{Ge} / ^{68}\text{Ga}$ generator $^{68}\text{Zn}(\text{p},\text{n})^{68}\text{Ga}$
^{82}Rb	1.25 min	$^{82}\text{Sr} / ^{82}\text{Rb}$ -Generator
^{89}Zr	78 h	$^{89}\text{Y}(\text{p},\text{n})^{89}\text{Zr}$
^{124}I	4.2 d	$^{124}\text{Te}(\text{d},2\text{n})^{124}\text{I}$

Despite these limitations, one ^{11}C -labelled PET tracer, $[^{11}\text{C}]\text{choline}$ (**Figure 2**), has been approved by the United States Food and Drug Administration (FDA) for “prostate cancer recurrence evaluation for subsequent histological confirmation”.¹² Additionally, this radiotracer is used for PET imaging of brain tumours, as well as in the detection of prostate cancer.^{13,14} Beyond $[^{11}\text{C}]\text{choline}$, numerous ^{11}C -based PET radiopharmaceuticals are widely utilised in both clinical and research settings. Other major ^{11}C -labelled PET tracers include $[^{11}\text{C}]\text{methionine}$ and $[^{11}\text{C}]\text{acetate}$, which are both widely used for cancer imaging, and the latter one is also used for cardiac imaging.^{15,16}

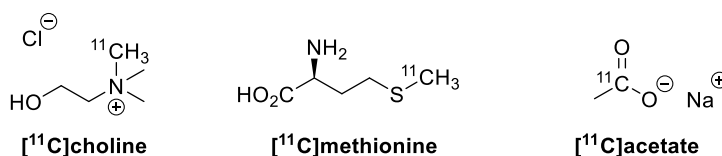


Figure 2. Major ^{11}C -labelled PET tracers.

Although various PET-tracers have been developed using different radionuclides, ^{18}F remains the most commonly used in clinical practice due to its relatively long half-life time (109.8 min). Additionally, the small size of fluorine makes it a preferred substitute for hydrogen in drug discovery, as the C–H to C–F substitution is the most structurally conservative on steric grounds.¹⁷ However, due to fluorine's high electronegativity, this substitution can significantly change the electronic properties of the final molecule potentially affecting its binding to the target.

Up to 2023, nineteen radiopharmaceuticals have been approved by the FDA and eleven of which contain fluorine-18.¹² This includes the most widely used PET-tracer, 2-deoxy-2- ^{18}F fluoro-D-glucose (^{18}F FDG) (**Figure 3**). Similar to ordinary glucose, ^{18}F FDG is taken up by cells, but cannot be metabolised in the same way as glucose due to the C2 fluorine-18 substitution. As a result, ^{18}F FDG accumulates well in cells particularly in cancer cells, which have higher glucose consumption.¹⁸

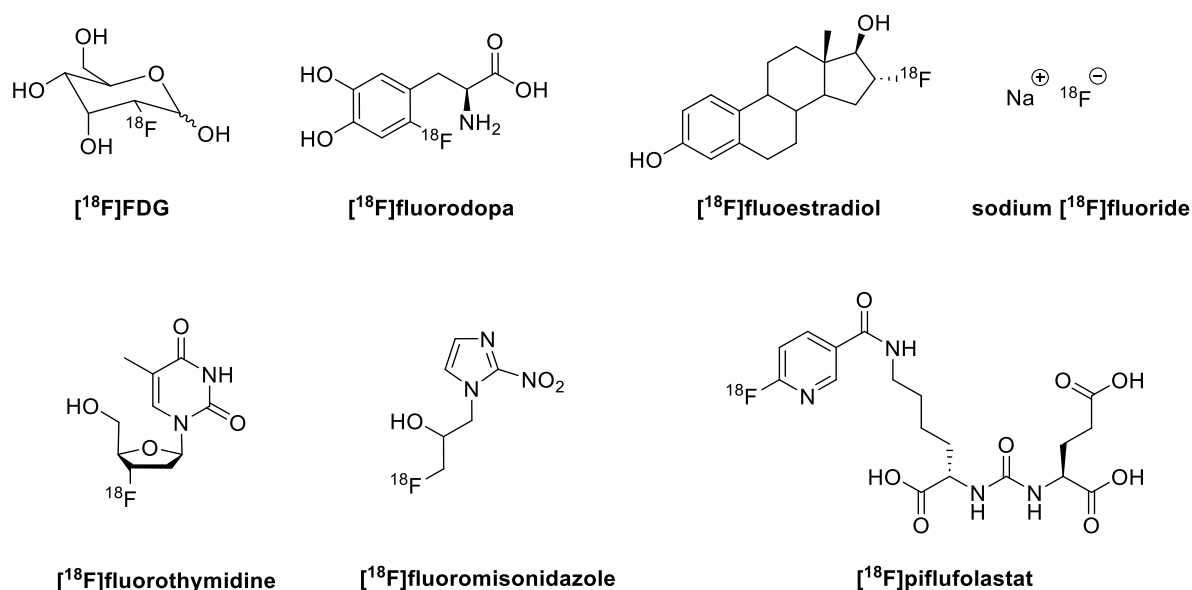


Figure 3. Major ^{18}F -labelled PET tracers.

The use of ^{18}F FDG PET is being widely explored for various clinical and research applications, such as oncology,¹⁹ cardiology,²⁰ the diagnosis of neurological conditions including dementias and epilepsy,²¹ and the detection of infectious and inflammatory diseases, including COVID-19.^{22,23}

While ^{18}F FDG remains the most commonly used PET tracer, its limitations, such as low sensitivity for certain health conditions, lack of selectivity in some cases, have

driven the development of novel radioactive compounds.²⁴ Some other major ^{18}F -labelled PET tracers include:

- [^{18}F]fluorodopa, widely used for diagnosis of Parkinson disease;¹²
- [^{18}F]fluoroestradiol, for imaging of oestrogen-receptor positive breast cancer;²⁵
- sodium [^{18}F]fluoride, for imaging of atherosclerosis and bone metastases detection;^{12,26}
- [^{18}F]fluorothymidine, for imaging of cytostatic therapy response;²⁷
- [^{18}F]fluoromisonidazole, for hypoxia imaging in solid tumours;²⁸
- [^{18}F]piflufolastat (Pylarify®), for metastatic prostate cancer imaging.²⁹

Several ^{18}F -labelling strategies have been developed over time. These include classic nucleophilic radiofluorination using [^{18}F]F⁻, electrophilic radiofluorination using [^{18}F]F₂ gas or secondary electrophilic radiofluorinating agents, as well as transition metal-mediated radiofluorination, and the use of ^{18}F -prelabelled prosthetic groups.³⁰ Among these, the most common approach is nucleophilic radiofluorination, which is also used in the synthesis of [^{18}F]FDG for clinical PET imaging.

Other radionuclides such as ^{64}Cu , ^{68}Ga , ^{89}Zr are mostly used for the imaging with larger PET tracers including peptides, peptidomimetics and antibodies. These radioisotopes usually form complexes with chelating agents attached to the selected peptide or antibody. Compared to small-molecule radiopharmaceuticals, these PET tracers offer improved imaging as they bind with high affinity to specific proteins. The peptide-based radiotracers are significantly cheaper than antibody-based PET tracers and are comparatively easier to synthesise while offering high affinity and specificity for selected targets. Peptide-based PET tracers can be labelled with a wide range of radionuclides, including ^{11}C and ^{18}F , but they are commonly utilised with radiometals.³¹ Notable peptide radiopharmaceuticals for PET imaging include:

- [^{68}Ga]Ga-PSMA-11, for prostate cancer PET imaging;¹²
- [^{68}Ga]Ga-DOTATOC, [^{68}Ga]Ga-DOTATATE and [^{64}Cu]DOTATATE, for imaging somatostatin receptor (SSTR)-positive neuroendocrine tumours (NETs);¹²
- [^{64}Cu]Cu-ATSM, for hypoxia imaging.³²

PET imaging using monoclonal antibodies or their fragments, also called immunoPET, provides high target specificity, although it has certain limitations, including high production costs, slow kinetics, and high background activity in some organs.³³ As a result, these radiotracers are less commonly used and are primarily employed for imaging of various cancers. One example is ⁸⁹Zr-trastuzumab, a monoclonal antibody for imaging of HER2-positive breast cancer.³⁴

1.2 Synaptic Vesicle Protein 2

Synaptic vesicle protein 2 (SV2) is an integral 12-transmembrane domain glycoprotein expressed in the secretory vesicles in neurons and endocrine cells.^{35,36} There are three isoforms of SV2, A, B, and C, which are similar in structure but differ in expression pattern.^{35,37} The SV2A is the predominant isoform, ubiquitously expressed in the brain's grey matter, with peak levels in the basal ganglia and thalamus, and present in all synaptic terminals of all neurons (**Figure 4**). The SV2B is mostly expressed in such brain structures as the cortex and hippocampus. Although neurons typically express only one isoform, the expression patterns of SV2A and SV2B overlap in certain regions. The SV2C isoform structurally resembles other two isoforms but has a highly restricted distribution.

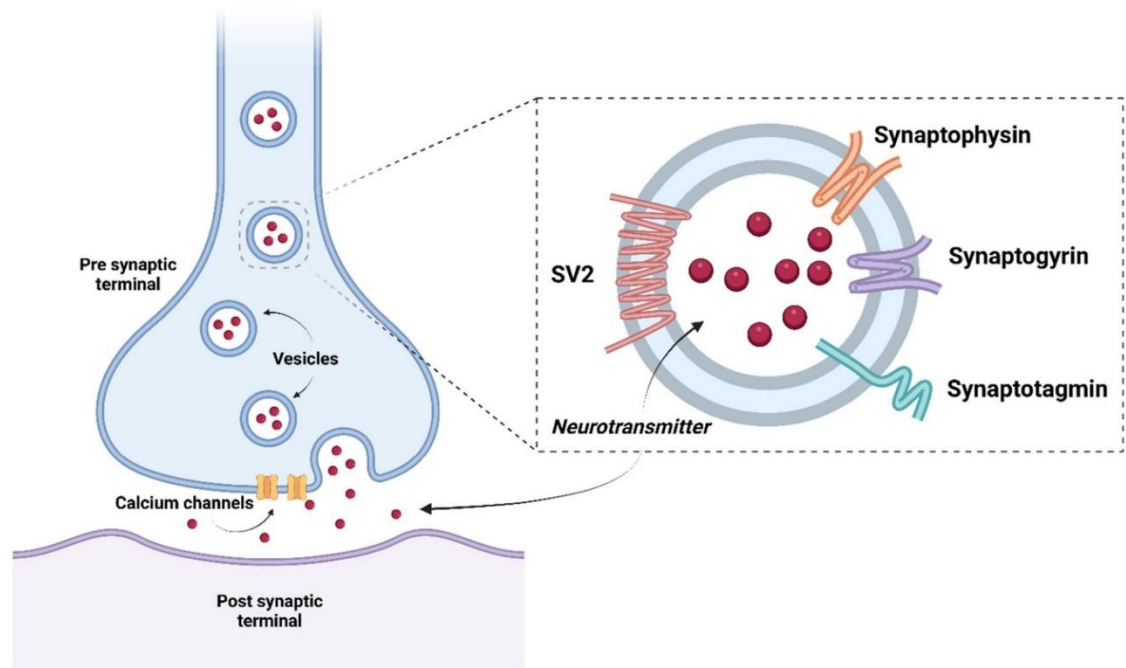


Figure 4. The location of SV2 in the vesicle in the presynaptic terminal, with the SV2A isoform being ubiquitously expressed, while the SV2B and SV2C are more limited in distribution.³⁸ (Reprinted with permission from Figure 1 of S. L. Martin et al., *J. Neurosci. Res.*, 2023, **102** (3), e25253. Copyright 2023 John Wiley and Sons)

The SV2 proteins are believed to play an important role in key vesicular processes.³⁵ The SV2 proteins are thought to regulate a maturational step of vesicles during calcium-induced exocytosis. The SV2A protein was also shown to have interactions

with synaptotagmin 1, a Ca^{2+} sensor in membrane, and to regulate presynaptic Ca^{2+} levels. The SV2A was also shown to participate in mediating galactose transport. The SV2 proteins are also believed to have various other functions, including control of the entry of neurotoxins, in particular the botulinum toxins, and interacting with extracellular proteins and adenosine triphosphate (ATP).

Traditionally, the SV2A has been associated with epilepsy, as after levetiracetam was discovered as an antiepileptic drug, it was later found that the SV2A protein is its target.³⁹ Another antiepileptic drug, brivaracetam, has also been shown to bind to SV2A (**Figure 5**).

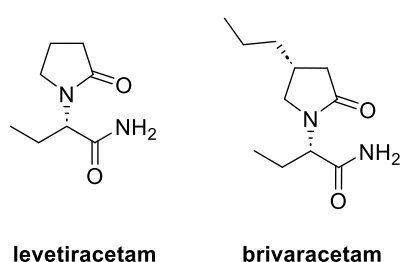


Figure 5. Structure of antiepileptic drugs levetiracetam and brivaracetam.

Racetams are the class of drug that have a pyrrolidone core.

In addition, the SV2A has been recognised as a promising biomarker of synaptic density.³⁹ As a result, the quantification of SV2A proteins is used to measure the synaptic density *ex vivo* and *in vivo*. Furthermore, it is utilised to identify the synaptic dysfunction, which is associated with neurological conditions such as Parkinson's and Alzheimer's diseases, and psychiatric conditions such as schizophrenia.

1.2.1 Imaging of synaptic density

Over the past decade, growing evidence suggests that many neurodegenerative disorders are associated with reduced synaptic density or synapse dysfunction.³⁹ However, for comparison, it is also essential to understand what synaptic density looks like in a healthy brain. Synaptic density imaging can be conducted using various biomarkers. This can be performed both *in vivo* and *ex vivo*, with electron microscopy being one of the methods used for the latter. This method enables detailed visualisation of synapses; however, it is expensive, time-consuming and does not provide a full picture of brain. Other methods, such as histology and

immunohistochemistry, are more cost-effective, however, like electron microscopy they are limited to the analysis of postmortem tissue. When it comes to measuring synaptic density *in vivo* and following brain changes due to aging and development, an MRI-based method that measure glutamate level are available. However, this approach has rather low specificity and sensitivity. PET imaging of SV2A protein has been validated in both animals and humans. Even though this method requires administration of radiopharmaceuticals, it allows proper *in vivo* evaluation of synaptic density.

As an initial attempt to develop a SV2A PET tracer, levetiracetam was introduced as a ^{11}C -labelled PET imaging agent (**Figure 6**).⁴⁰ However, due to the modest binding affinity for SV2A ($K_i = 1.74 \mu\text{M}$) it was not further used for *in vivo* PET imaging.³⁶ Later, new nonacetamide ligands binding to the SV2A protein were developed and evaluated as PET agents in nonhuman primates, [^{11}C]UCB-A, [^{18}F]UCB-H, [^{11}C]UCB-J (**Figure 6**).³⁶ [^{11}C]UCB-A was tested in mini-pigs, rats and rhesus monkeys, however, it exhibited slow kinetics, characterised by prolonged retention in brain tissue, making it unsuitable for PET imaging. [^{18}F]UCB-H displayed good kinetics in rats and non-human primates and progressed to human PET imaging, where it showed acceptable dosimetry. However, its radiosynthesis proved challenging and its specific binding was low. Among these, [^{11}C]UCB-J demonstrated the best preliminary results for preclinical PET imaging studies due to its rapid and high brain uptake, reversible binding kinetics, and relatively low nonspecific binding in white matter. In clinical studies, [^{11}C]UCB-J also confirmed the data obtained in preclinical studies and proved to be an excellent candidate for PET imaging of SV2A. This imaging agent was widely used for various preclinical and clinical studies for example in studying epilepsy, Parkinson's disease, Alzheimer's disease, depression in humans.

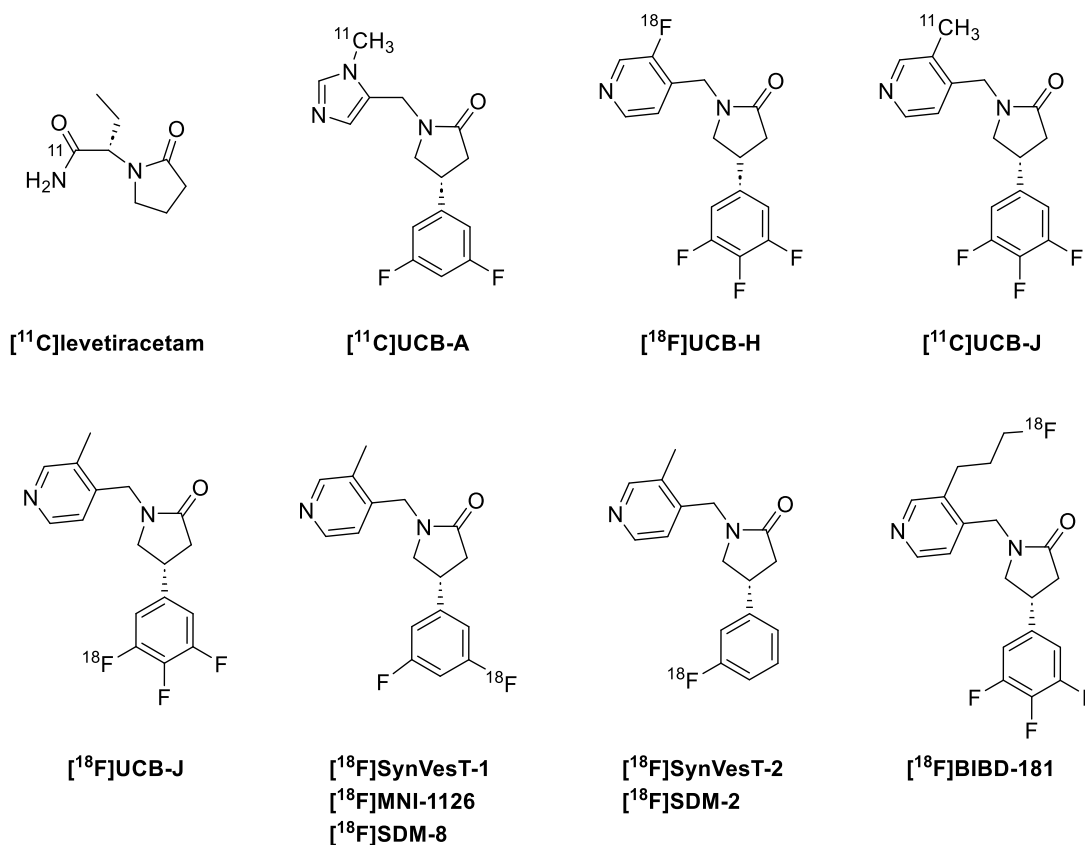


Figure 6. SV2A PET imaging agents reported in the literature.³⁹

One of the major achievements for this tracer was the creation of an *in vivo* high-resolution 3D human brain atlas of synaptic density using the *in vivo* [¹¹C]UCB-J PET data in combination with *in vitro* [³H]UCB-J autoradiography (**Figure 7**).⁴¹ The atlas, available in both *fsaverage* and *MNI152* templates, revealed distinctive cortical and subcortical gradients of synaptic density. This reflected functional topography of the brain, demonstrating the synapse organisation from core sensory to high-order integrative cortical areas. In particular, the study found high *in vivo* SV2A density in the neocortex, with highest densities in the posterior cingulate, precuneus, and gyri of the temporal cortex. For the subcortical regions, the highest density was observed in the putamen and caudate. Although regional PET estimates of *in vivo* SV2A binding generally correlated well with postmortem autoradiography data, some notable differences, particularly in the hippocampus were observed.

Despite the success of [¹¹C]UCB-J, due to the short half-life of the ¹¹C-isotope (20.4 min), the development of other PET tracers with longer half-life isotopes was initiated. The labelling of UCB-J with fluorine-18 led to the discovery of [¹⁸F]UCB-J

(**Figure 6**). Although the imaging results with [^{18}F]UCB-J proved to be as good as for the ^{11}C -labelled analogue, the radiolabelling process was found to be complex for this molecule.⁴²

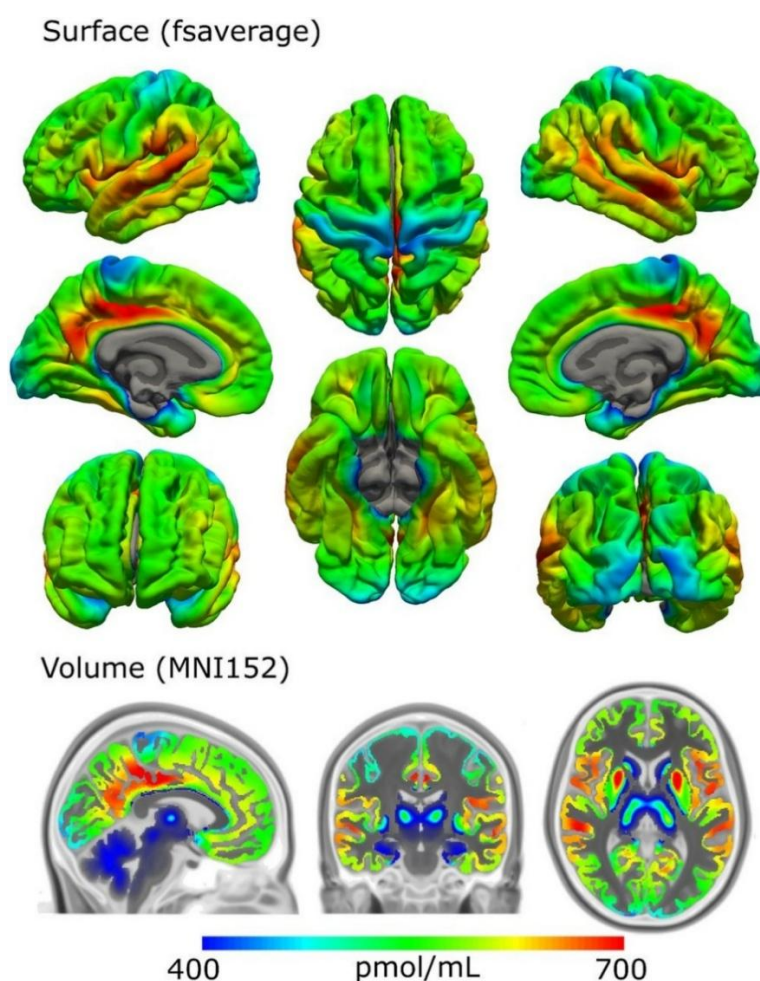


Figure 7. Average *in vivo* SV2A density maps on the FreeSurfer *fsaverage* surface (top) and in the *MNI152* volume space (bottom).⁴¹ (Reprinted from Figure 2 of A. Johansen *et al.*, *J. Neurosci.*, 2024, **44** (33), e1750232024, under the terms of the Creative Commons Attribution 4.0 International License)

This led to the development of ^{18}F -labelled analogues of UCB-J such as [^{18}F]SynVesT-1 and [^{18}F]SynVesT-2 (**Figure 6**).³⁶ Li and co-workers presented the synthesis and structure-activity study of four radiofluorinated analogues of [^{11}C]UCB-J, and as a result, the *in vivo* evaluation of their best candidate, [^{18}F]SynVesT-1, for PET imaging of SV2A. This molecule demonstrated outstanding imaging characteristics in humans, possessing very high brain uptake, fast and reversible kinetics, excellent test-retest reproducibility and binding specificity to

SV2A.⁴² It is worth noting that both the racemate and the (*R*)-enantiomer demonstrated similar brain distribution; however, the uptake value of the (*R*)-enantiomer was approximately twice as high as that of the racemate (**Figure 8**). Meanwhile, the (*S*)-enantiomer displayed low binding affinity to SV2A, leading to non-specific homogeneous brain uptake.⁴³ The (*R*)-enantiomer under the name [¹⁸F]MNI-1126 entered phase I clinical trials for evaluation as an imaging marker for synaptic density loss in brain of patients with probable Parkinson's or Alzheimer diseases.

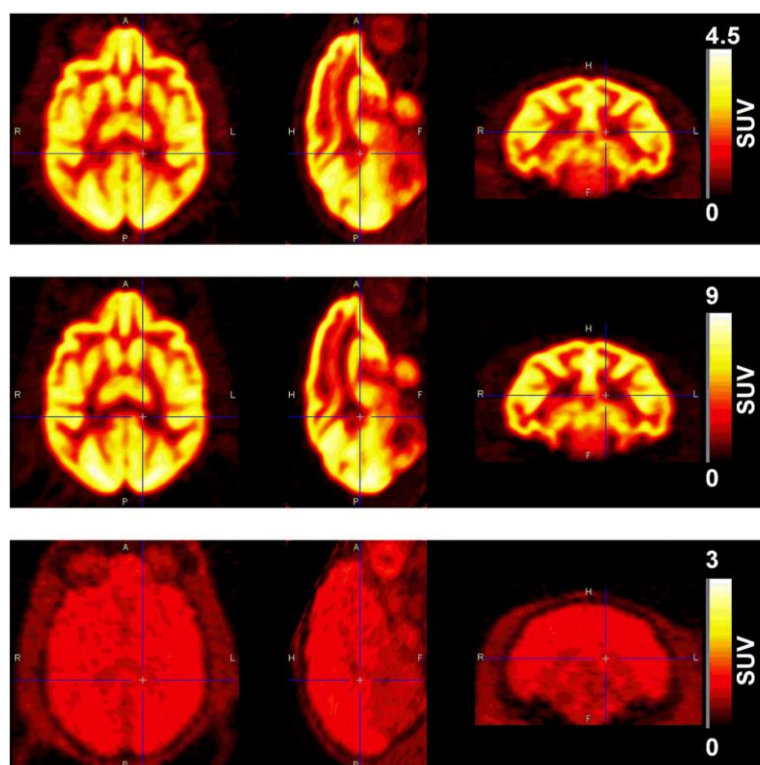


Figure 8. The comparison of the racemate (top), (*R*)-enantiomer (middle) and (*S*)-enantiomer (bottom) of [¹⁸F]SynVesT-1 in the same rhesus monkey (standardised uptake value (SUV) 30–120 min post-injection).⁴³ (Reprinted with permission from Figure 4 of C. C. Constantinescu *et al.*, *Mol. Imaging Biol.*, 2019, **21**, 509–518.

Copyright 2019 John Wiley and Sons)

To investigate synaptic density changes during brain aging, studies in healthy mice were conducted using PET imaging with [¹⁸F]SynVesT-1 to track the synapse alterations.⁴⁴ Three groups of mice of different ages underwent PET imaging using [¹⁸F]SynVesT-1. This study showed that only slight reduction of synaptic density in the oldest group of mice was observed, suggesting that synaptic density stays quite stable during the life of mice. Similar results were achieved for the human PET study

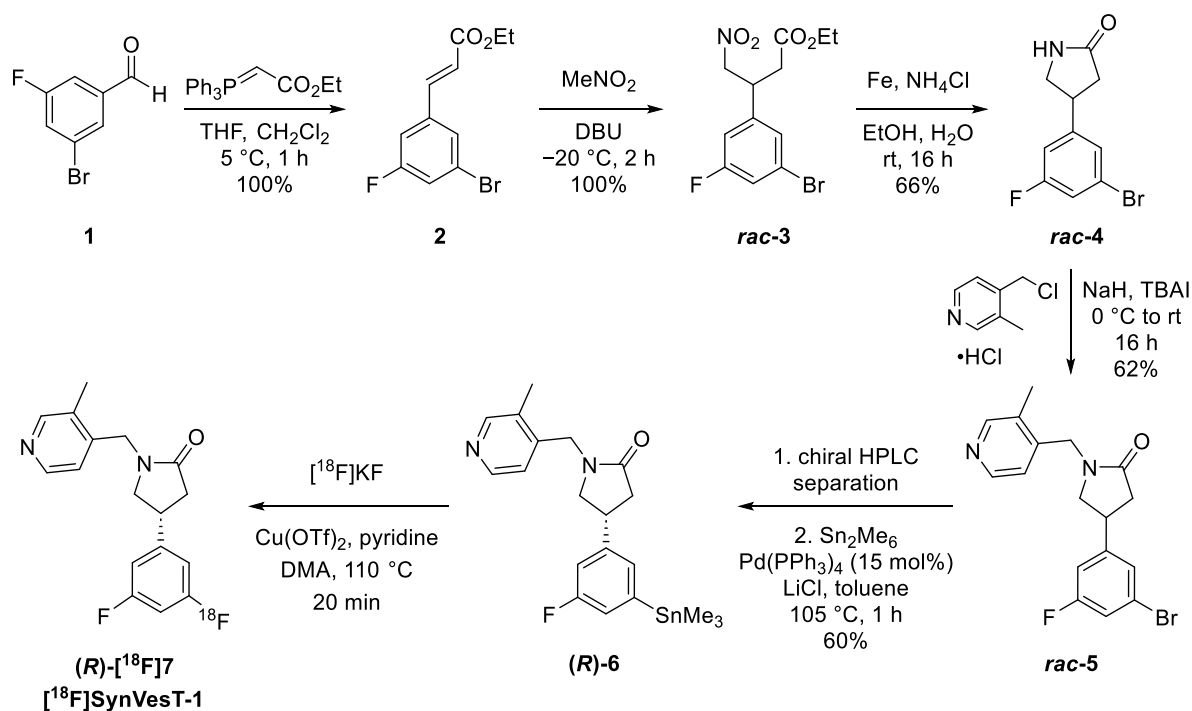
using [^{11}C]UCB-J or combined [^{11}C]UCB-J/[^{18}F]FDG imaging. In these studies, individuals of different age (78 people, 19–85 years old) or two cohorts of young (24.8 years old, 11 people) and old people (72.7 years old, 15 people) were compared. These studies reported that synaptic density in humans was stable during aging.^{45,46} However, longitudinal aging studies in which the same subject undergoes PET imaging with [^{18}F]SynVesT-1 or other SV2A binding tracers at different ages would possibly be more sensitive for detecting age-related changes in brain.⁴⁴

As for the other analogues, [^{18}F]SynVesT-2 also demonstrated imaging characteristics suitable for large scale clinical trial investigations, showing higher specific binding signals compared to [^{11}C]UCB-J and exhibiting faster kinetics.⁴⁷ Recently, [^{18}F]BIBD-181 has been presented as a novel PET imaging agent for targeting SV2A and demonstrated excellent qualities in small animal PET imaging studies (**Figure 6**).⁴⁸

1.2.2 Known synthetic approaches to [^{18}F]SynVesT-1

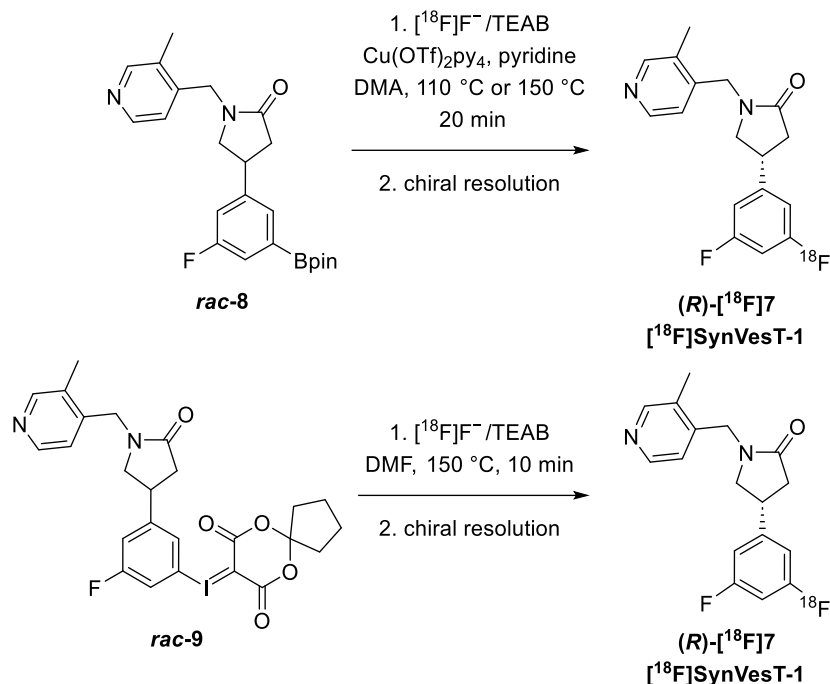
The synthesis of [^{18}F]SynVesT-1 was first proposed by two research groups around the same time. Huang and co-workers described a racemic synthetic approach for (*R*)-[^{18}F]**7** (reported under name [^{18}F]SDM-8, **Scheme 1**).^{49,50} They attempted the synthesis and radiofluorination of three different precursors, with organotin precursor (*R*)-**6** giving the best results. This approach began with the Wittig reaction of 3-bromo-5-fluorobenzaldehyde (**1**) with (carbethoxymethylene)-triphenylphosphorane. The resulting unsaturated ester **2** was subjected to a conjugate addition reaction with nitromethane to form **3**. The nitro group was then reduced, enabling an intramolecular lactamisation reaction to proceed. This was then followed by alkylation of lactam **4** with 4-(chloromethyl)-3-methylpyridine hydrochloride. After that, a chiral semipreparative high performance liquid chromatography (HPLC) separation (performed by a specialist separation company) was conducted to afford the (*R*)-enantiomer of the brominated intermediate **5** (>99% ee). The resulting chiral material was submitted to a Pd-catalysed stannylation reaction with hexamethylditin. The radiofluorination of the organotin precursor (*R*)-**6** was performed by the protocol developed by Scott and Sanford using copper triflate in presence of pyridine as a catalyst, providing the desired radiolabelled

tracer in 24% radiochemical yield (RCY, mean, HPLC incorporation yield, decay-uncorrected) and high molar activity 241.7 MBq/nmol (mean, by the end of synthesis, $n = 4$).⁵⁰



Scheme 1. Synthetic route for (*R*)-enantiomer of [¹⁸F]SynVesT-1 by Huang and coworkers.⁴⁹

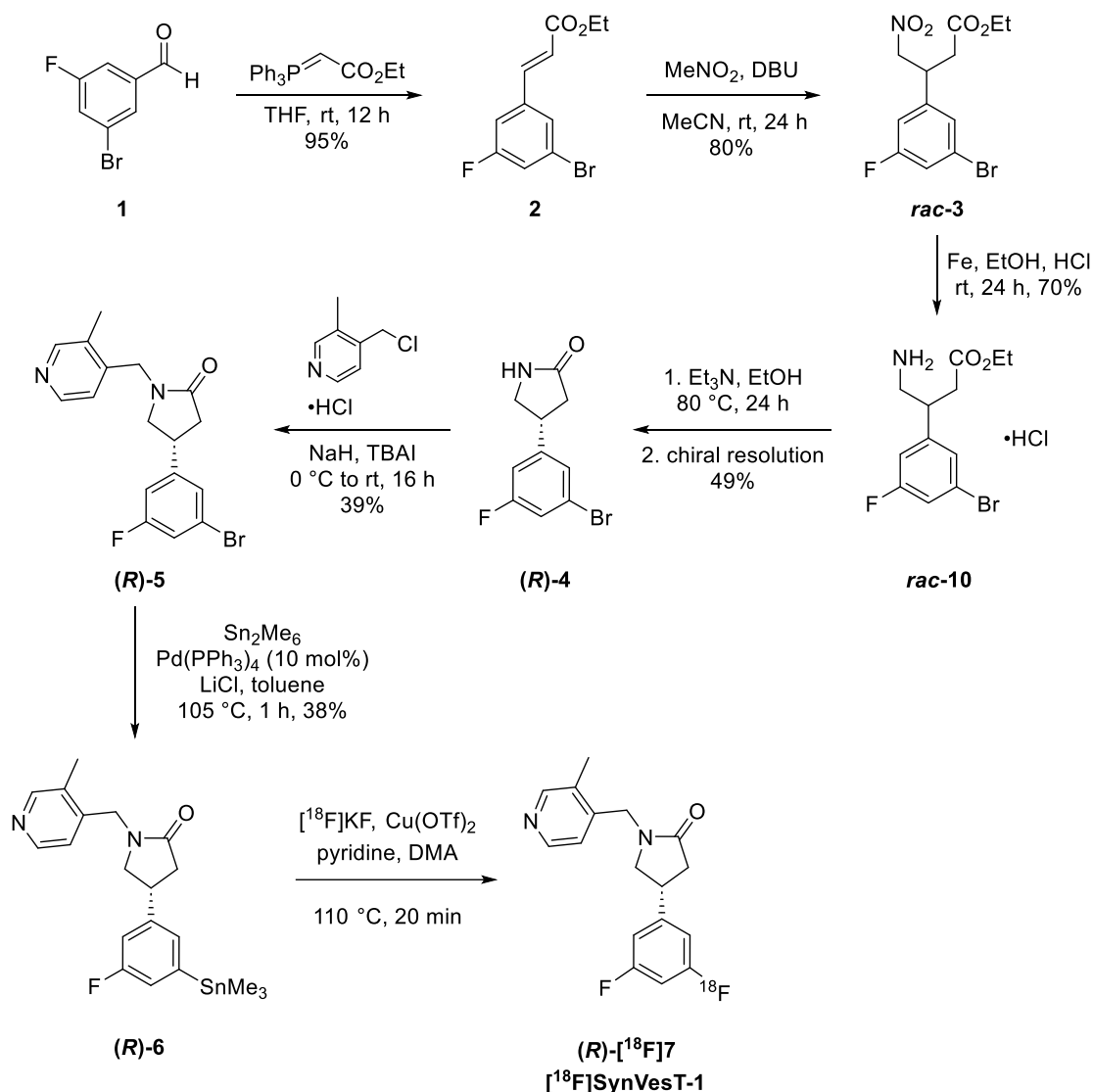
The radiofluorination of the boronic ester **8** and iodonium **9** precursors required higher reaction temperatures, which led to the racemisation of the product.⁴⁹ As a result, radiofluorination was performed on the racemic precursors followed by the chiral resolution of the radiolabelled material (**Scheme 2**). Thus, [¹⁸F]SynVesT-1 was obtained from iodonium precursor **9** in <1% RCY (decay-uncorrected) and moderate molar activity of 25.6 MBq/nmol ($n = 2$). Radiofluorination of boronic ester precursor **8** was attempted using the protocol developed by Gouverneur and co-workers.⁵¹ This approach led to better results, providing the desired [¹⁸F]SynVesT-1 in 11% (reaction at 150 °C) and 6% RCY (reaction at 110 °C, both are HPLC incorporation yields, decay-uncorrected).



Scheme 2. Radiofluorination of boronate and iodonium precursors of $[^{18}\text{F}]\text{SynVesT-1}$.⁴⁹

A slightly different approach for the synthesis of (*R*)- $[^{18}\text{F}]\text{7}$ (under name $[^{18}\text{F}]\text{MNI-1126}$) was reported by Invicro, LLC.⁴³ Similar chemistry was employed to form nitro ester **3**; however, the nitro group reduction and cyclisation were conducted in two separate steps and the chiral resolution using semipreparative chiral HPLC was performed one step earlier, allowing subsequent steps with only (*R*)-enantiomer from that stage onward (**Scheme 3**). The radiofluorination was undertaken using tin precursor (*R*)-**6** by the method developed by Scott and Sanford resulting in the product with high specific activity (99.6 MBq/nmol) and in 9.7% RCY (*n* = 3).⁵⁰

Based on these developed syntheses, a good manufacturing practice (GMP) compliant automated radiosynthesis of $[^{18}\text{F}]\text{SynVesT-1}$ utilising the radiofluorination of the organotin precursor was developed in 2024.⁵² This protocol allows consistent production of a high-quality pharmaceutical-grade solution of $[^{18}\text{F}]\text{SynVesT-1}$ suitable for clinical imaging studies.



Scheme 3. Another approach for the synthesis of [¹⁸F]SynVesT-1 reported by Invicro, LLC.⁴³

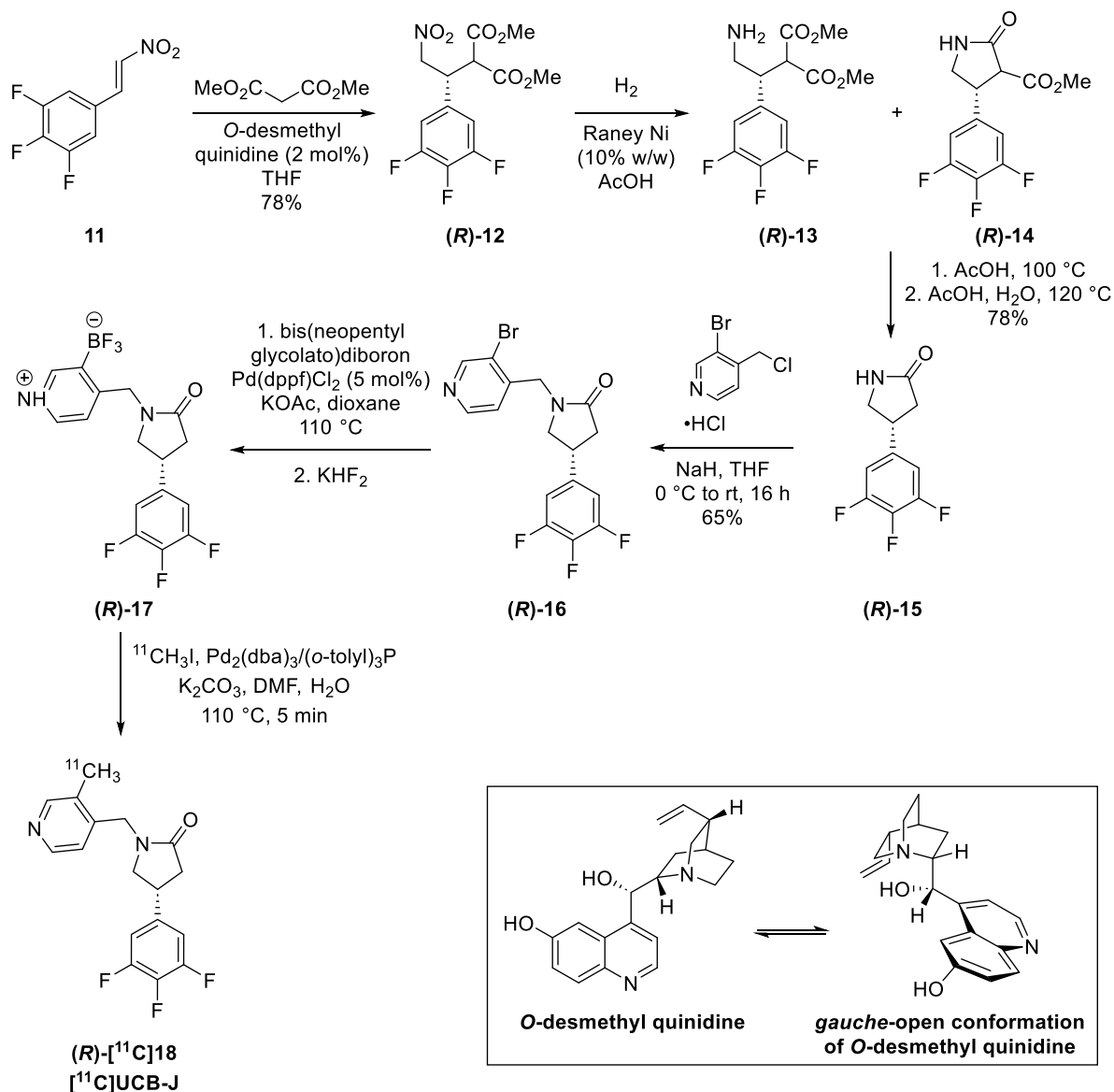
As for the other analogues, the same racemic approach is typically used for the synthesis of [¹⁸F]SynVesT-2, as proposed by the same group.⁴⁷ Instead of starting with 3-bromo-5-fluorobenzaldehyde, the synthesis began with 3-bromobenzaldehyde, which was submitted to the same synthetic route, and the corresponding organotin precursor was radiofluorinated under same conditions.

The main issue of the synthesis of the (*R*)-enantiomers of all of the mentioned nonacetamides is that the synthetic pathways typically involve the synthesis of a racemate, followed by chiral preparative HPLC separation in the later stages, and in some cases even chiral resolution of the radiolabelled material.^{47–49} Clearly, it is not only time-consuming but also requires the use of an expensive preparative chiral

HPLC system (and the expertise of a specialist chromatography company to separate multigram quantities) and results in the loss of the activity of the desired radiolabelled material. Utilising the racemic approach also means the loss of 50% of synthesised advanced intermediate, if the chiral resolution is performed at the earlier stages.

1.2.3 Enantioselective synthesis of nonacetamide PET imaging agents

The first enantioselective synthesis of nonacetamides was attempted in 2016 by Huang and co-workers.⁵³ They reported the synthesis of [¹¹C]UCB-J using *O*-desmethyl quinidine as a chiral organocatalyst in the first step, which was a conjugate addition of dimethyl malonate to nitrostyrene **11** (**Scheme 4**). *O*-Desmethyl quinidine catalyst, a cinchona amine-based organocatalyst, was reported to work through the adoption of a *gauche*-open conformation, forming hydrogen bonding between the phenolic hydroxy moiety of the catalyst and both the conjugate donor and acceptor and between the quinuclidine moiety of the catalyst and the conjugate donor.⁵⁴ These interactions direct the addition of the nucleophile and control enantioselectivity of the reaction. The conjugate addition step was then followed by nitro group reduction using Raney Ni catalyst, resulting in a mixture of amine (**R**)-**13** and lactam (**R**)-**14** (75:25). The mixture was subjected to a cyclisation and hydrolysis/decarboxylation step to yield lactam (**R**)-**15**. The resulting lactam (**R**)-**15** was alkylated using 4-(chloromethyl)-3-bromopyridine hydrochloride. This synthesis was conducted on a multigram scale and provided the desired intermediate in 94% *ee*. The bromide (**R**)-**16** was then converted into a BF₃ leaving group in a two-step process. The final step, the radiolabelling of the obtained precursor (**R**)-**17** using [¹¹C]CH₃I, provided access to the desired [¹¹C]UCB-J (**R**)-**18**.

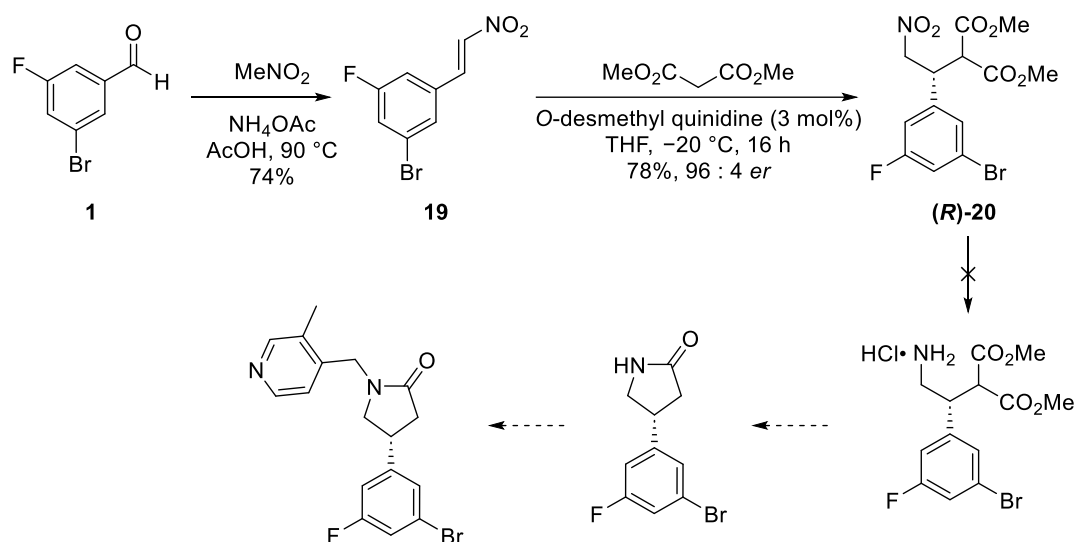


Scheme 4. Synthesis of [^{11}C]UCB-J reported by Huang and co-workers.⁵³

1.2.4 Previous work in the Sutherland group

Based on the previous enantioselective approach for the synthesis of [^{11}C]UCB-J, an attempt was made in the Sutherland group by Holly McErlain to adapt this for the preparation of [^{18}F]SynVesT-1.⁵⁵ 2-Bromo-4-fluorobromobenzaldehyde (**1**) which was reacted with nitromethane via a Henry reaction to give the corresponding nitrostyrene **19** in 74% yield (**Scheme 5**). Nitrostyrene **19** was submitted to an enantioselective Michael addition reaction with dimethyl malonate in the presence of *O*-desmethyl quinidine (3 mol%) at $-20\text{ }^\circ\text{C}$ and this provided access to the desired intermediate **(R)-20** in 78% yield and 96:4 *er*. Further the reduction of nitro-group was investigated, however, after screening various reaction conditions, the

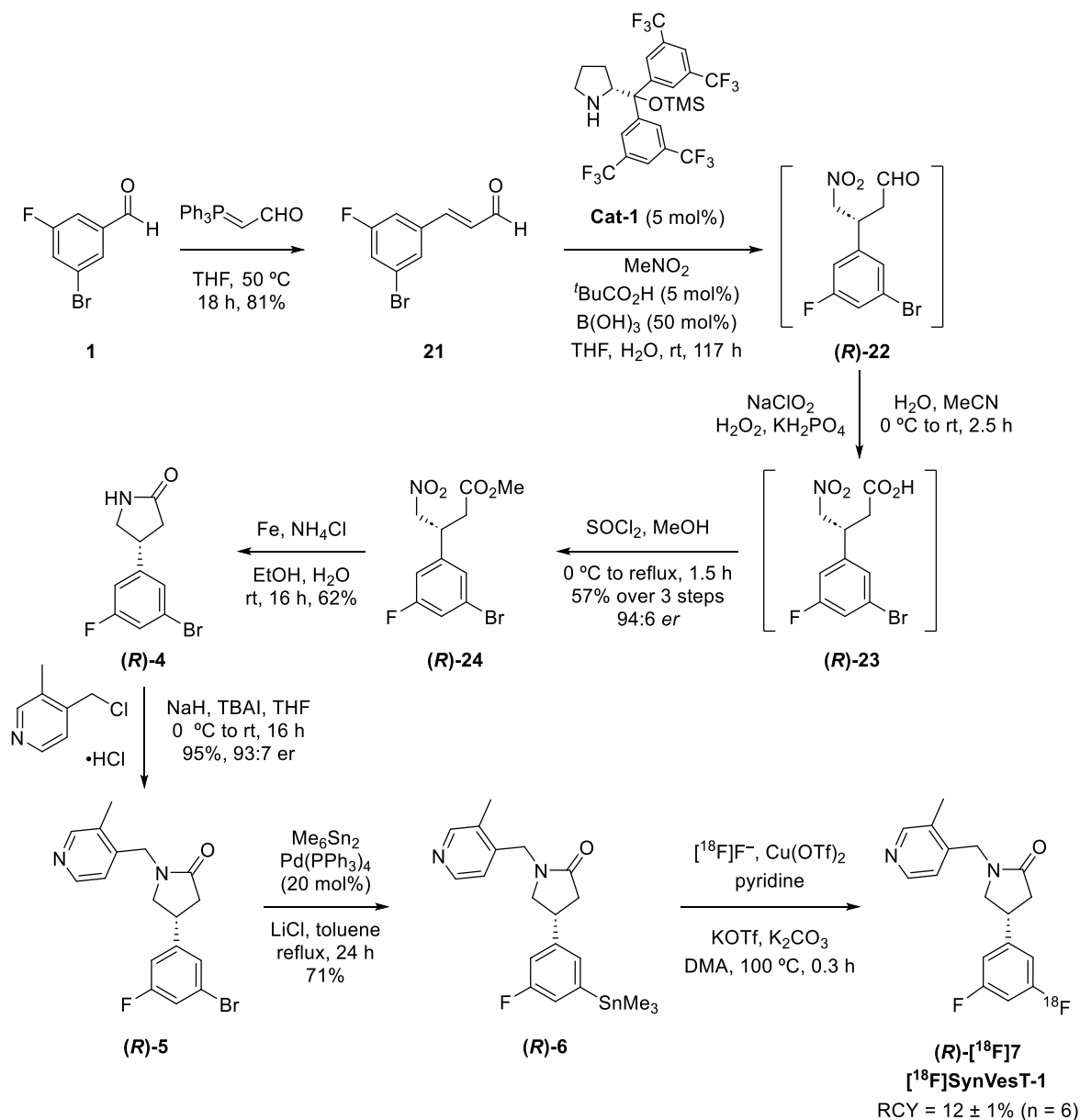
desired product was not achieved as the reaction did not proceed and only starting materials were isolated. As this step was problematic, this approach was abandoned, and other options were explored.



Scheme 5. Enantioselective synthesis of [^{18}F]SynVesT-1 precursor attempted in the Sutherland group.⁵⁵

Due to these limitations, another alternative enantioselective synthetic route for the preparation of [^{18}F]SynVesT-1 was developed by the Sutherland group (**Scheme 6**).⁵⁶ In the first step, 3-bromo-5-fluorobenzaldehyde **1** underwent a Wittig reaction to install the alkene moiety. An asymmetric conjugate addition of nitromethane was conducted next in the presence of Jørgensen-Hayashi organocatalyst **Cat-1** (5 mol%) and a mixture of pivalic and boric acids as cocatalysts. Despite a reaction time of five days, this gave access to the desired enantioenriched nitroaldehyde (**R**)-**22** which was used without any purification in the next step. This was then followed by Pinnick-type oxidation of the aldehyde to the carboxylic acid and esterification to form the enantioenriched 4-nitrobutanoate (**R**)-**24** in 57% yield over three steps and 94:6 *er*. The subsequent nitro-reduction and *in-situ* cyclisation provided access to lactam in 62% yield. *N*-Alkylation of the lactam using 4-(chloromethyl)-3-methylpyridine hydrochloride under basic conditions and in the presence of tetrabutylammonium iodide (TBAI) as a catalyst gave the bromide intermediate (**R**)-**5** in 95% yield. Stannylation of intermediate (**R**)-**5** using a palladium-catalysed reaction with hexamethylditin gave the desired organotin precursor (**R**)-**6** in 71% yield. The radiolabelling of the resulted organotin precursor (**R**)-**6** was then performed using copper-mediated radiofluorination, which provided the desired (**R**)-

[¹⁸F]7 in 12% RCY (n = 6), >99% radiochemical purity (RCP) and 50.9 GBq/μmol molar activity. This synthetic route was found to generate material of suitable enantiomeric quality that could be used for *in vivo* PET imaging of SV2A. The same approach was used to synthesise a non-radioactive standard SynVesT-1.



Scheme 6. Asymmetric synthesis of [¹⁸F]SynVesT-1 developed in the Sutherland group.⁵⁶

1.3 Monocarboxylate Transporters

Monocarboxylate transporters (MCTs) are a family of solute carrier 16A transporters (SLC16A), which play an essential role in the transport of short chain monocarboxylates, hormones, nutrients and amino acids.⁵⁷ Among the fourteen isoforms of this family, the proton-dependent MCTs 1–4 have been the most investigated due to their critical role in the transport of products of the glycolysis cycle such as lactate, pyruvate and ketonic compounds such as acetoacetate and β -hydroxybutyrate across the plasma membrane.⁵⁸ The MCT1 is ubiquitously distributed in the human body, while others are expressed in various tissues. The other members of the MCT family, isoforms 5–14 have not been extensively characterised, however, recent studies have provided insight into their function. Specifically, it is reported that MCT6 is involved in drug transport, MCT7 facilitates ketone body transport, MCT8 and MCT10 participate in thyroid hormone transport, with MCT10 additionally mediating aromatic amino acids transport. MCT9 functions as a carnitine efflux transporter, while MCT12 serves as a creatine transporter.⁵⁷

The isoforms 1 and 4 of the MCTs are overexpressed in various types of cancers (e.g., colon, brain, breast, bone, and kidney) and are associated with poorer prognosis in certain cancers.⁵⁸ The overexpression of these proteins is connected with the energy metabolism in cancer cells, glycolytic pathway, known as the Warburg effect (**Figure 9**).⁵⁹ Malignant tumours are able to adjust their metabolism to sustain proliferation, invasion and metastasis as well as other energy-intensive processes essential for their progression.⁶⁰ Cancer cells preferentially metabolise glucose to lactate via accelerated glycolysis, even if enough oxygen is present, rather than following oxidative phosphorylation, as observed in healthy cells. Cancer cells consume much more glucose to compensate for the significantly lower ATP production in glycolysis, which is eighteen times lower than in oxidative phosphorylation. This increased glucose consumption, accelerated metabolism, and lactic acid accumulation is called the Warburg effect. As MCTs 1–4 are responsible for lactate transfer, high expression of these proteins helps cancer cells to maintain an appropriate pH for tumour growth, therefore contributing to proliferation. Currently, it is widely accepted that MCT4 is predominantly expressed in hypoxic/glycolytic cancer cells, whereas MCT1 is overexpressed in oxidative cancer cells, which are adapted to utilise lactate as an energy source.⁶¹ The role of

MCTs in the proliferation of cancer made them promising drug targets for cancer treatment, as well as for diagnostic markers.⁶²

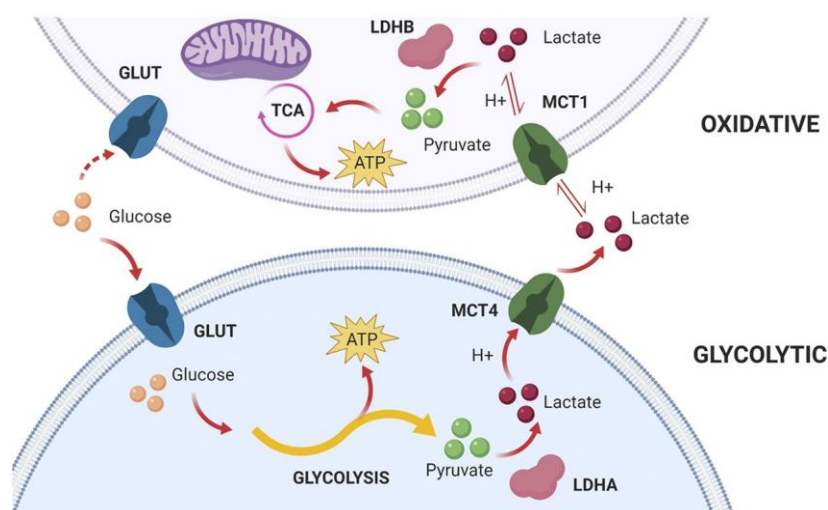


Figure 9. A representation of the Warburg Effect. GLUT – glucose transporter; H^+ – proton; LDHA/B – lactate dehydrogenase A/B; TCA – tricarboxylic acid cycle.⁵⁸ (Reprinted with permission from Figure 5 of M. A. Felmlee *et al.*, *Pharmacol. Rev.*, 2020, **72** (2), 466–485. Copyright 2020 Elsevier)

Apart from using MCTs as cancer biomarkers, the cellular distribution of the MCT1 and MCT2 were found to be perturbed in the hippocampus of patients with temporal lobe epilepsy.⁶³ These changes may represent an adaptive response to maintain high lactate levels in epileptic tissue, potentially suppressing epileptic activity by lowering cyclic adenosine monophosphate (cAMP) levels via the lactate receptor GPR81 in the hippocampus. It was suggested that this deviation in MCT function may further contribute to the pathophysiology of temporal lobe epilepsy by affecting brain energy homeostasis, mitochondrial function, glutamatergic and GABAergic neurotransmission, and lactate circulation in the brain.⁶³

1.3.1 MCT1–4 inhibitors

The inhibition of MCTs has mostly been investigated for cancer treatment purposes. Various compounds have been reported to inhibit MCTs, and many of them simultaneously inhibit multiple MCTs isoforms. Several potent dual MCT1/4 inhibitors have been developed; however, the primary challenge associated with

these is the widespread expression of MCT4 in skeletal muscles and heart. Thus, inhibition of this isoform can lead to major undesirable side effects.⁶⁴

Another important aspect is that some of the inhibitors seem to bind with the chaperone proteins of MCTs rather than binding directly to MCT.⁵⁹ One of these proteins, basigin (or CD147, cluster of differentiation 147), especially basigin 2, is associated with MCT1, 3, 4, 11 and 12 and has been demonstrated to interact with MCTs through noncovalent interactions (**Figure 10**).⁶⁵ Another chaperon protein known as embigin or gp70 is associated with MCT2 and can act as a chaperone protein for the MCT1 in the absence of basigin. These highly glycosylated chaperone proteins are essential for MCTs and for plasma membrane expression and activity.⁶⁶

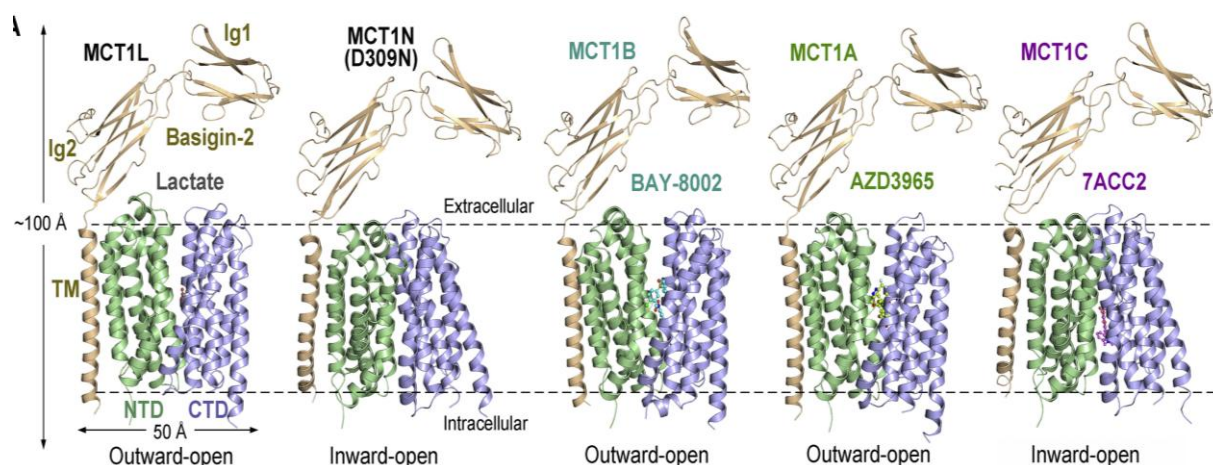


Figure 10. Structures of the wild type MCT1/Basigin-2 complex bound to lactate D309N, AZD3965, BAY-8002, and 7-AAC2. NTD is an amino terminal domain; CTD is a carboxy terminal domain; Ig is an immunoglobulin; TM is a transmembrane segment.⁶⁷ (Reprinted with permission from Figure 1 of Wang, N., *et al. Cell*, 2021, **184**(2), 370–383. Copyright 2021 Elsevier)

Inhibition of the chaperon proteins rather than the MCTs could be an effective strategy for disrupting lactate homeostasis.⁵⁹ However, this approach would also simultaneously affect several isoforms at the same time. Considering that these proteins have biological functions beyond acting as chaperones for MCTs and these roles are also crucial for non-malignant cells, inhibiting basigin and embigin could

also lead to undesirable side effects, which is why the common approach is to target MCTs directly.

One of the first developed MCT inhibitors, 4,40-diisothiocyanatostilbene-2,20-disulfonate (DIDS, **Figure 11**) contains two highly reactive isothiocyanate groups. This compound was reported to be reactive toward lysine side chains not only on MCT1 but also on embigine, cross-linking MCT to its chaperon-protein.⁶⁶ High reactivity of this inhibitor to lysine could mean that various other protein targets may also be covalently modified.⁵⁹ Similarly, inhibition of basigin was demonstrated for *para*-chloromercuribenzenesulfonate (*p*-CMBS, **Figure 11**). This compound is highly electrophilic due to the presence of the mercury atom, which binds to sulfhydryl groups of cysteine side chains in proteins. It was shown that *p*-CMBS binds cysteines of basigin, not on MCTs, and that affects isoform selectivity of the inhibitor.⁵⁹

Another series of compounds, derivatives of α -cyano-4-hydroxycinnamic acid (α -CHC, **Figure 11**) were also reported to inhibit MCTs. However, as strong Michael acceptors, they can also covalently bind all the accessible cysteine residues, including those in CD147.⁵⁹ In some cases, the binding with CD147 was shown to be preferable. Those compounds may also target some other cysteine reactive members of the proteome, which means there may be some limitations in therapeutic use due to target selectivity. Furthermore, the lead compound of α -CHC series demonstrated poor oral bioavailability and toxicity at high concentrations.⁶⁸

Recently, another small molecule NGY-091, developed by Nirogy Therapeutics (structure is not revealed) has been reported to act as a dual MCT1/4 inhibitor, blocking both lactate import and lactate export *in vitro*.⁶⁹ This compound demonstrated a potent *in vitro* cytotoxicity against cancers in multiple cancer cell lines.

Greater success has been achieved in developing selective MCT1 inhibitors compared to MCT4 inhibitors as among the four predominant isoforms MCT4 exhibits lower affinity for various substrates, even for lactate.⁶⁴ For instance, another series of MCTs inhibitors which showed better isoform selectivity is coumarin derivatives, such as 7AAC2 (**Figure 11**). These highly electrophilic compounds are

reported to be potent MCT1 inhibitors.⁶⁸ Although they demonstrate quite high inhibition activity to MCT, they only affect lactate export capabilities of MCTs, whereas lactate export capabilities are retained despite the fact that MCTs are bidirectional transporters.

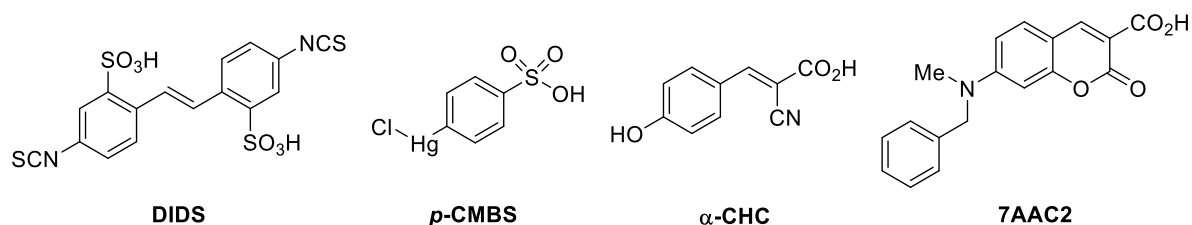


Figure 11. Proposed MCT inhibitors.⁵⁹

Another small molecule CYT-0851 has been initially developed, patented and underwent phase I clinical trial as a RAD51 inhibitor (**Figure 12**).⁷⁰ However, recent studies have revealed that CYT-0851 is more likely to act as a MCT1 inhibitor.⁷¹ Therefore, further investigation are now being conducted to determine the mechanism of inhibition of MCT1 by CYT-0851.⁷² It was confirmed that this compound is a dose-dependent MCT1 inhibitor with an IC₅₀ value of 134 nM and effectively disrupts lactate transport.⁷³ This compound also entered phase I clinical trials as a MCT inhibitor in combination with two chemotherapy drugs for the treatment of advanced solid tumours.⁷¹

A new class of potent MCT1 inhibitors, indole derivatives, has recently been introduced. The lead compound **25** of the new class has been reported to exhibit low-nanomolar inhibitory activity against MCT1, while showing no activity against MCT4 (**Figure 12**).⁷⁴ It also demonstrated great antiproliferative effect against two MCT1-expressing cancer cell lines. Molecular docking studies, using the cryo-electron microscopic (cryo-EM) structure of MCT1, have demonstrated a strong binding affinity to the MCT1 protein, specifically binding to the MCT rather than the chaperon protein.

In 2018, Bayer AG reported the compound BAY8002 (**Figure 12**), which demonstrated IC₅₀ values of 1, 5 and >500 nM against MCT1, 2 and 4 respectively, making it a selective dual inhibitor for MCT1/2.⁷⁵ Due to the high sequence similarity of MCT1 and MCT2, selective inhibition of each isoform remains quite challenging

to achieve. Although this is not a major concern, given that MCT2 plays a smaller role in human cancers compared to MCT1.⁵⁹ No significant off-target activity was reported for this small molecule and it exhibited significant suppression of the bidirectional transport of lactate. Using cryo-EM data, it was reported that MCT1 in complexation with BAY8002 exhibited an outward-open conformation (**Figure 10**).⁶⁷

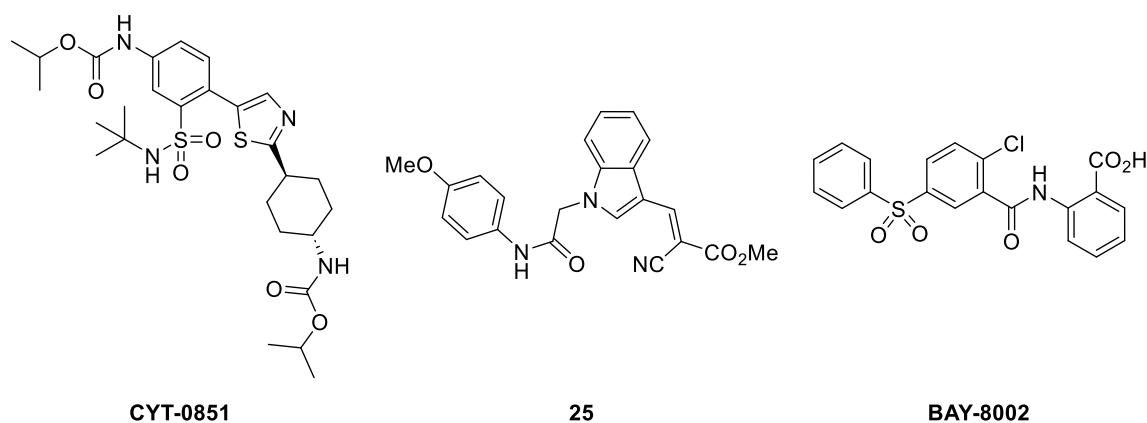


Figure 12. Proposed MCT inhibitors.⁵⁹

Potent MCT inhibitors were reported by AstraZeneca (**Figure 13**) and those included the pyrrolopyridazinones **26**, fused uracil pyrroles **27**, and fused uracil thiophenes **28**.⁵⁹ These compounds inhibit MCT1 as well as MCT2, avoiding inhibition of MCT4. Although compounds **26–28** from the series demonstrated tumour regression in *in vivo* experiments with Raji Burkitt lymphoma and oestrogen receptor-positive MCF7 breast cancer cells, they turned out to have poor pharmacokinetic properties. That is why further optimisation of the fused uracil thiophene series was performed, leading to substitution of the highly metabolically labile thioether and naphthyl moieties. This resulted in the clinical compound AR-C155858, which had much improved pharmacokinetic properties. Further modification of this compound led to AZD3965, a pyrrole pyrimidine derivative which is a specific MCT1 inhibitor (**Figure 13**).⁶⁰ This compound partially inhibits MCT2 with 6-fold lower activity and does not show any inhibitory activity for MCT3 and MCT4. In 2013, AZD3965 underwent clinical studies for the treatment of advanced solid tumours and lymphomas that express MCT1.^{76,77} The first dose of AZD3965 in a patient with metastatic melanoma led to a temporary suspension of recruitment due to a potential drug-related effect. However, it was later discovered that the patient had “hyper-Warbugism”, which is a rare condition where a high tumour burden is linked to excessive glucose uptake and lactate efflux from cancer cells.

After the clinical trial resumed, the screening for the plasma lactate level was added to the safety protocol and patients with excessive glucose level were excluded from the trial.⁷⁸ The results of the clinical trials demonstrated that AZD3965 is generally well-tolerated and can be given to patients at doses that engage the drug target with a maximum tolerated dose of 20 mg a day.⁷⁷

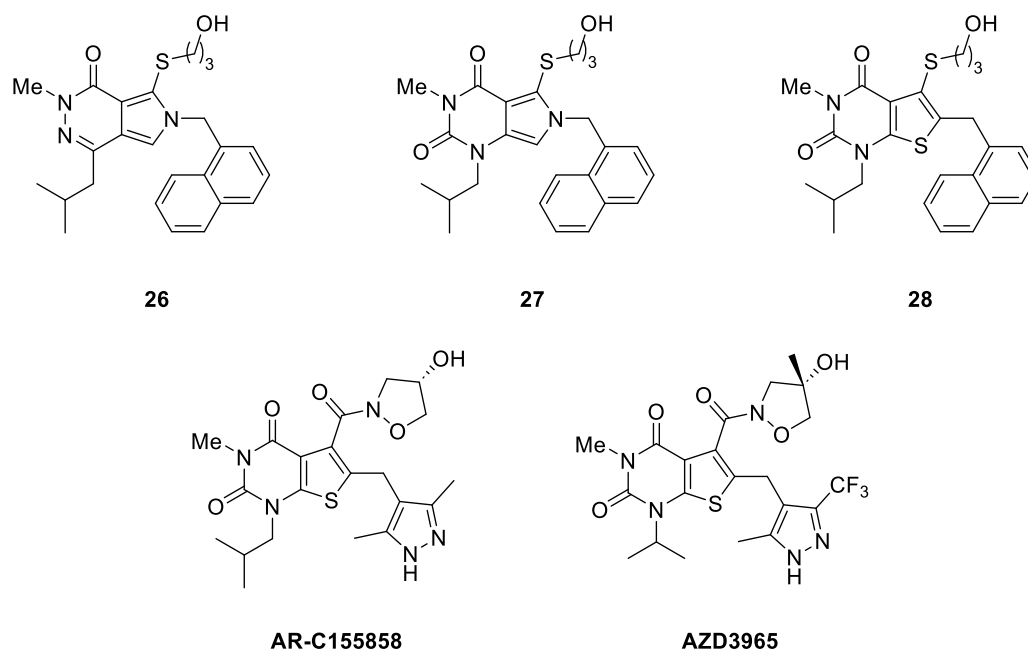


Figure 13. Potent MCT1/MCT2 inhibitors from AstraZeneca and CRUK.^{59,60}

The phase I expansion study of this inhibitor in patients with large B-cell and Burkitt lymphomas showed a noticeable reduction in tumour [¹⁸F]FDG uptake in one patient as detected by [¹⁸F]FDG-PET. However, the other four patients who underwent research PET imaging showed no changes.⁷⁶

Nevertheless, the recent studies have reported that certain cancer cells develop resistance to MCT1 inhibitors following prolonged exposure.⁷⁵ This resistance has been reported to arise from metabolic adaptations, including upregulation of other isoforms such as MCT2 and MCT4, as well as a shift to oxidative phosphorylation. This could limit the use of MCT inhibitors as a monotherapy; however, when used in combination with other anti-tumour treatments, they may offer promising results.^{79,80}

1.3.2 PET imaging agent targeting MCT

PET imaging of MCTs is not widely used, although, several tracers were developed for this application. All of these tracers were designed with the intention of using MCTs as a tumour biomarker. One of the first radiolabelled molecules for this application, [^{18}F]fluoropyruvate ([^{18}F]FP, **Figure 14**) was developed as an analogue of 3-bromopyruvate, a potent agent for cancer therapy, which was hypothesised to enter tumour cells via MCT4.⁸¹ [^{18}F]Fluoropyruvate was used as a PET imaging agent for visualising the metabolic adaptation of cancer cells. However, this radiolabelled compound showed low uptake in the selected cancer cell line (0.08% of the applied dose) with no time dependent uptake, which was not observed for other radiolabelled compounds used in the same study. Also no significant changes were observed in the uptake of the tracer in the blocking experiment using excess of pyruvate. It was proposed that this happened due to the low affinity of [^{18}F]fluoropyruvate with the target protein, which prevent its transport into the cells. A lack of recognition of this compound by the MCTs has also been proposed. The *in vivo* evaluation of this tracer showed no uptake of [^{18}F]FP in any organs except for bones probably due to metabolism of the tracer in the blood and liver.

^{18}F -Labelled lactic acid ([^{18}F]Flac, **Figure 14**) was the next attempt to develop a selective PET tracer targeting MCT to evaluate MCT1-dependent lactate uptake in tumour cells.⁸² While the radiolabelling of the 3-position of lactate was found to be challenging, [^{18}F]Flac was successfully synthesised in good RCY and with a good regioselectivity in favour of desired (\pm)-[^{18}F]-3-fluoro-2-hydroxypropionate vs. (\pm)-[^{18}F]-2-fluoro-3-hydroxypropionate. The *in vitro* assessment of this PET tracer in two cancer cell lines showed that uptake of [^{18}F]Flac is 1–2 times of that of [^{18}F]fluoropyruvate but blocking experiments with MCT1 inhibitors led to a significant decrease in [^{18}F]Flac uptake. *In vivo* imaging in mice with [^{18}F]Flac showed labelling of tumours, gut and liver. However, the tracer could not distinguish between MCT1-silenced and control tumours, likely due to compensatory MCT4 upregulation.

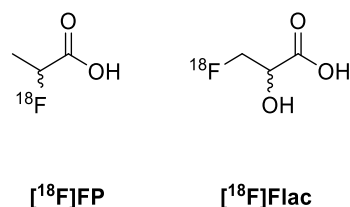
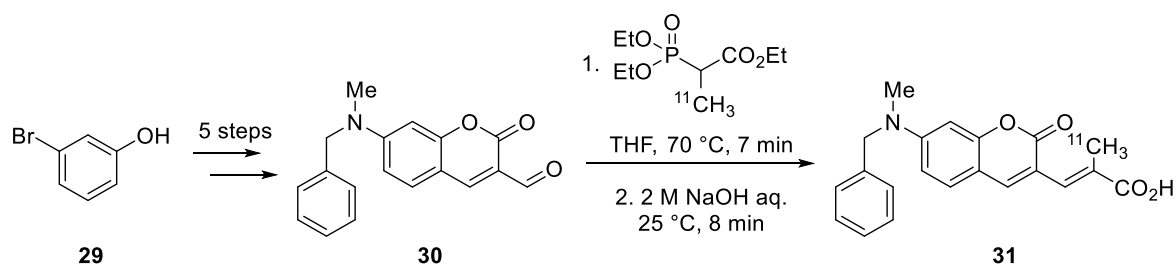


Figure 14. Previously developed PET tracers targeting MCTs.

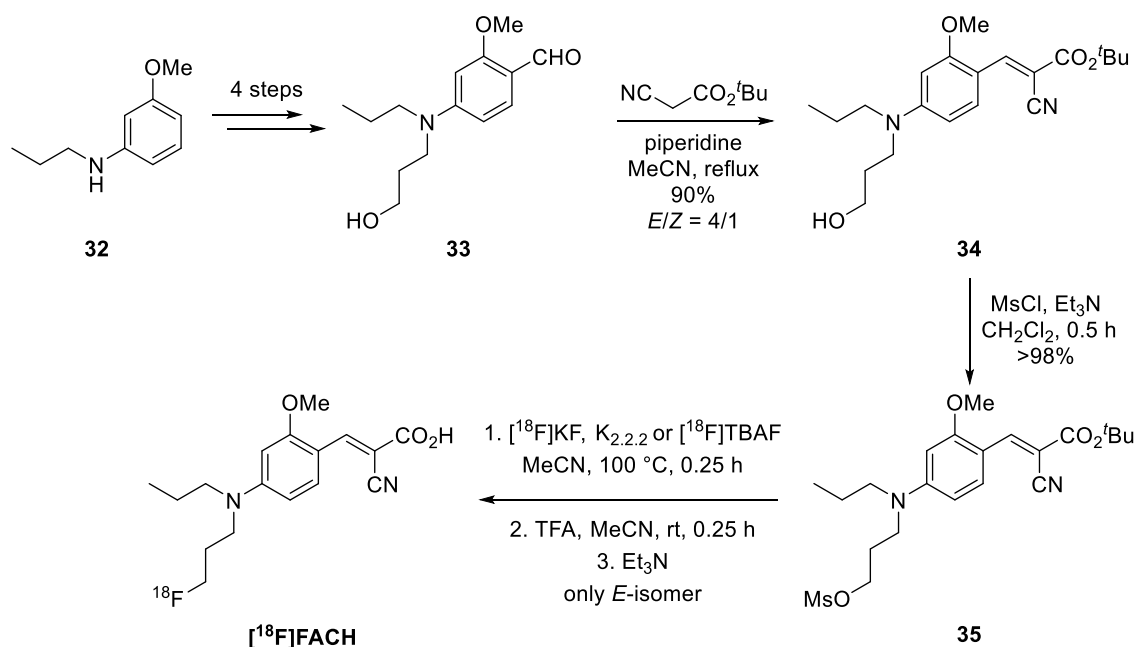
Another attempt to develop a PET tracer for MCT imaging involved the ^{11}C -labelling of one of the coumarin derivatives **31** (**Scheme 7**). This radioligand was evaluated in a tumour mouse model by a dynamic PET study.⁸³ The radiosynthesis of this compound was relatively straightforward and the desired radiotracer was obtained via the Horner-Wadsworth-Emmons reaction of the corresponding coumarin aldehyde **30** with ^{11}C -labelled phosphonate ester in 5.9% RCY with an *E/Z* ratio of 9:1 (**Scheme 7**). However, *in vivo* imaging using this PET tracer showed low tumour uptake with a peak value of only 1.9% injected dose/g and with the highest uptake in liver.⁸³



Scheme 7. Synthesis of ^{11}C -labelled coumarin PET tracer.

Another developed PET tracer was a ^{18}F -fluorinated α -CHC derivative, $[^{18}\text{F}]\text{FACH}$ (**Scheme 8**).⁸⁴ The non-radiative standard FACH demonstrated high MCT1 and MCT4 inhibition, with IC_{50} values of 11 nM and 6.5 nM, respectively. Precursor synthesis was achieved in six steps through standard *N*-alkylation of 3-methoxy-*N*-propylaniline **32**, followed by the protection of hydroxy group (**Scheme 8**). Vilsmeier-Haack formylation then gave benzaldehyde intermediate **33**. After deprotection, Knoevenagel condensation of compound **34** with *tert*-butyl cyanoacetate was conducted. Mesylation provided the desired precursor **35** for radiolabelling as a mixture of *E*- and *Z*-isomers (4:1, respectively). Radifluorination and deprotection gave the desired $[^{18}\text{F}]\text{FACH}$ in 39.6% RCY and > 98% RCP. After the deprotection step, only the more stable *E*-isomer was observed.⁸⁴ Preclinical evaluation of this PET tracer was later conducted in healthy mice and piglets.⁸⁵ Despite the ubiquitous

distribution of MTCs, the results of this study in mice showed specific uptake of [^{18}F]FACH only in kidneys, probably due to the fact that this compound can also act as a substrate for MTCs and can be accumulated intracellularly. The other organs that have high expression of MTCs, such as intestine, liver, heart and blood cells did not demonstrate any specific uptake of this tracer possibly due to restricted transporter availability on the cell membrane in these organs. Another possible explanation could be the the [^{18}F]FACH uptake into these cells is hindered under physiological conditions. This may be due to a transport gradient of MCTs, which is directed from the intracellular to the extracellular side. The results from piglet imaging were similar although accompanied by rapid metabolism of [^{18}F]FACH. It was concluded that further studies are necessary to establish the exact mechanism of tracer uptake.⁸⁵



Scheme 8. Synthesis of [^{18}F]FACH.

1.3.3 Previous work in the Sutherland group

The Sutherland group has also been interested in the development of PET imaging agents targeting MCT1 and MCT2. Since the AR-class of compounds developed by AstraZeneca has shown both high affinity and high selectivity for MCT1/MCT2, a library of new fused uracil thiophene derivatives was introduced by our research group and were tested for inhibition of lactate uptake of MCT1, MCT2 and MCT4. In particular, Kerry O'Rourke and Erin Johnstone developed a reliable and scalable

route for the synthesis of a thieno[2,3-*d*]pyrimidinedione-5-carboxamide derivatives **36**, **37** and **38** (Figure 15).^{86,87}

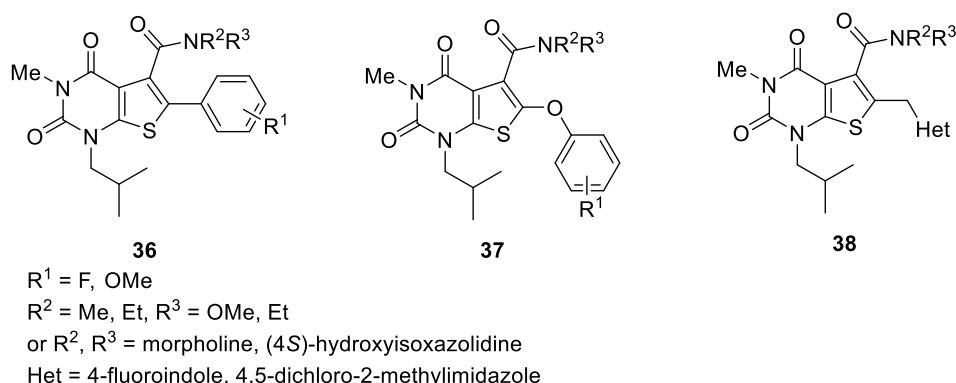
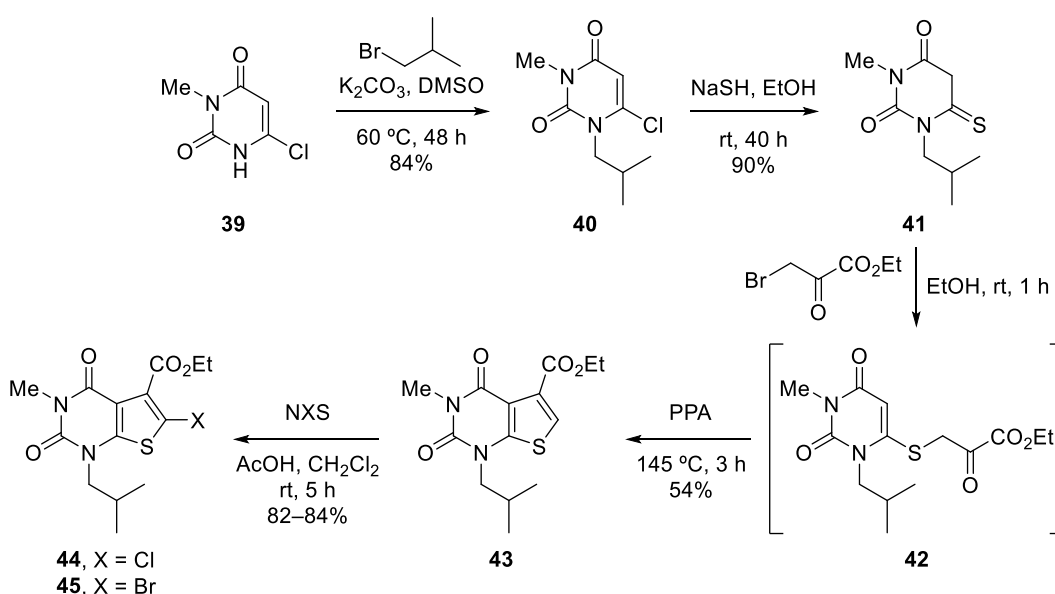


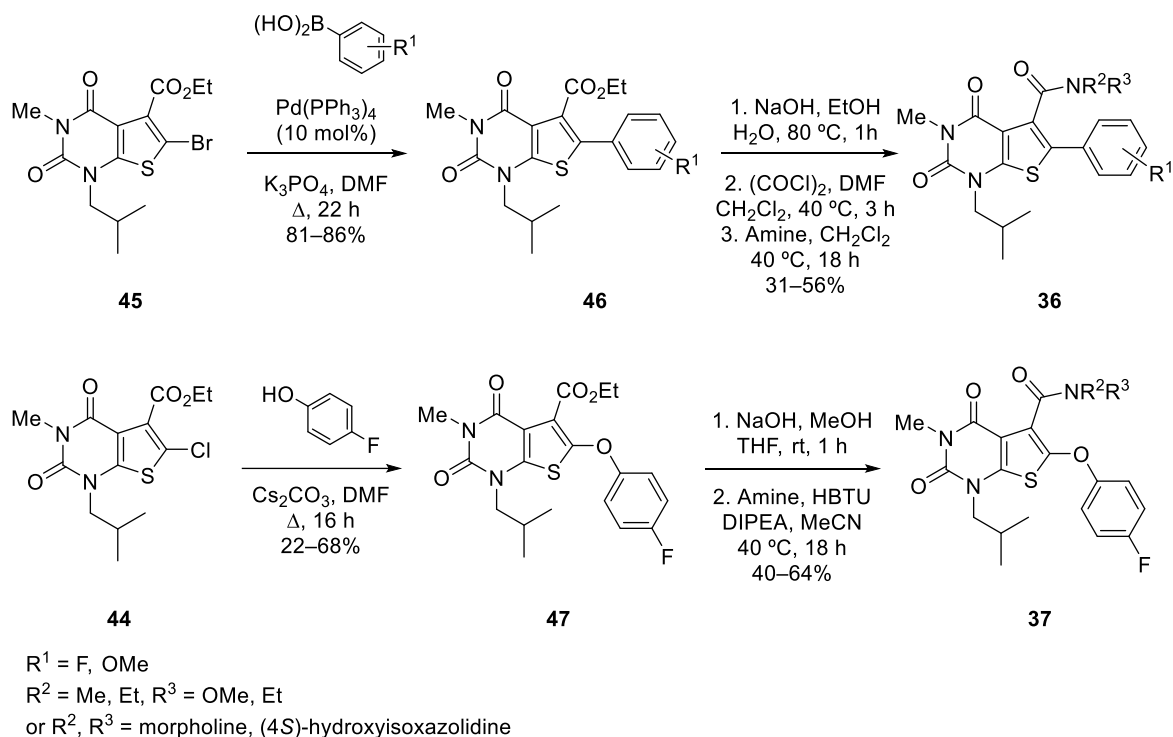
Figure 15. MCT1/MCT2 inhibitors developed in the Sutherland group.^{86,87}

These compounds were prepared in two stages. The first stage involved the synthesis of halogenated intermediates **44** and **45** in five steps from 6-chloro-3-methyluracil **39**.^{86,87} *N*-Alkylation of 6-chloro-3-methyluracil **39** using isobutyl bromide was followed by a substitution reaction with NaSH, which led to the formation of mercaptouracil **41**. *S*-Alkylation of the obtained mercaptouracil **41** with ethyl 3-bromopyruvate, followed by cyclisation in presence of polyphosphoric acid (PPA) gave thienopyrimidinedione **43** (Scheme 9). This key intermediate was used for late-stage halogenation of the thiophene ring using *N*-chlorosuccinimide (NCS) or *N*-bromosuccinimide (NBS).



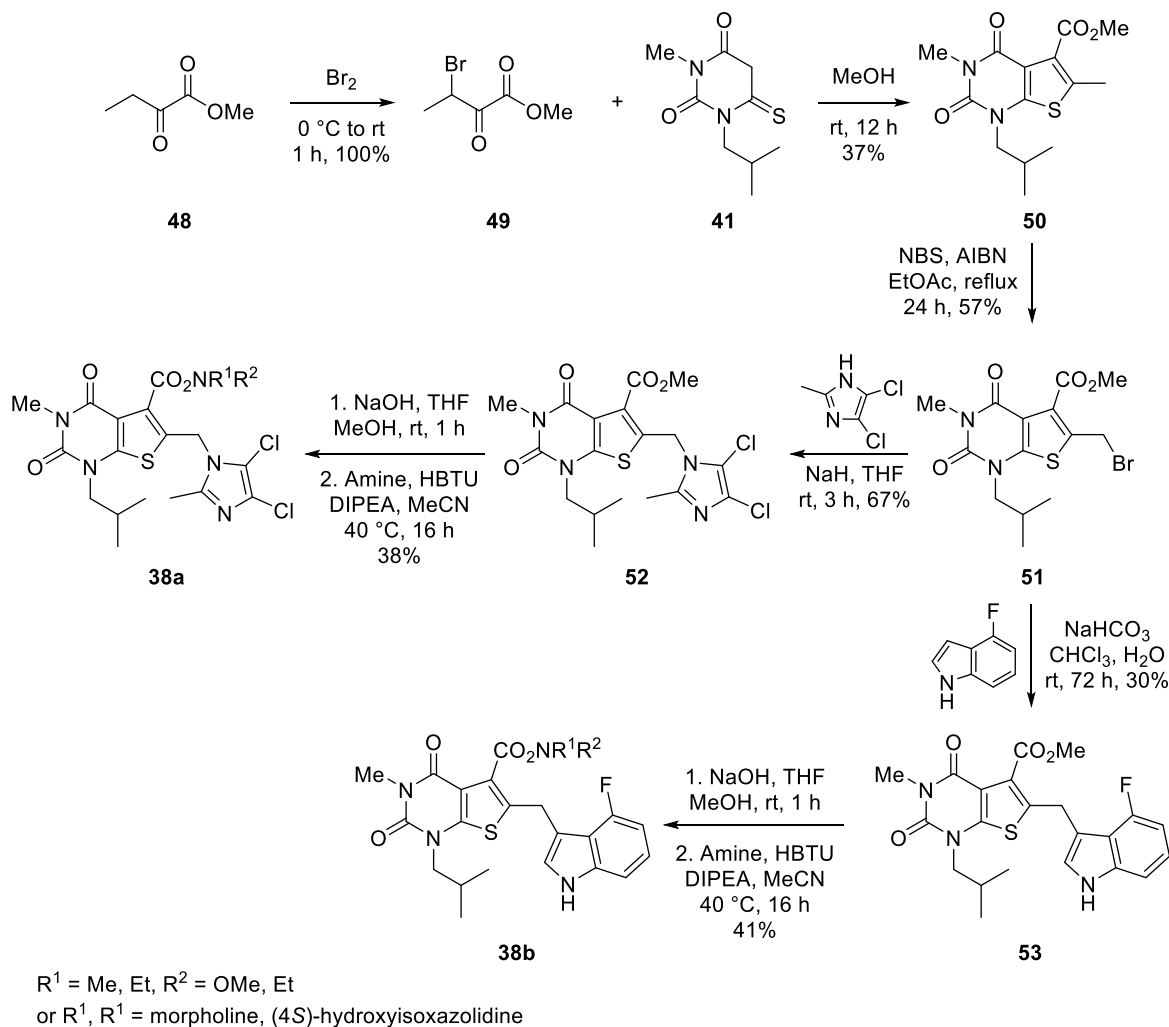
Scheme 9. Synthetic route to halogenated thieno[2,3-*d*]pyrimidinediones.^{86,87}

The second stage involved Suzuki or nucleophilic aromatic substitution (S_NAr) reactions, which allowed introduction of arenes bearing either fluorine or methoxy groups (**Scheme 10**).^{86,87} Ester hydrolysis, acid chloride formation and aminolysis gave two series of novel carboxamide targets: 5-carboxamide-6-aryl **36** and 5-carboxamide-6-phenoxy **37** derivatives.



Scheme 10. Synthesis of 5-carboxamide-6-aryl **36** and 5-carboxamide-6-phenoxy **37** derivatives from halogenated thienopyrimidinediones **44** and **45**.^{86,87}

Another library of thienopyrimidinedione derivatives was also made, bearing heterocycles at the 6-position, connected to the main thienopyrimidinedione core with a methylene linker (**Scheme 11**). These compounds were synthesised starting from the 6-methyl thienopyrimidinedione precursor **50**, which was obtained via *S*-alkylation of mercaptouracil **41** with methyl 3-bromo-2-oxobutanoate **49**, followed by a cyclisation reaction. The resulting 6-methyl thienopyrimidinedione **50** was then brominated using NBS in presence of azobisisobutyronitrile (AIBN) to facilitate the introduction of the heterocyclic moiety under basic conditions. Subsequent ester hydrolysis and amide coupling reactions provided access to two analogues **38a** and **38b**, which were evaluated for MCT inhibition with thienopyrimidinedione derivatives **36** and **37**.⁸⁷



Scheme 11. Synthesis of the second library of potential MCT inhibitors.

The partition coefficient ($\log P$), permeability (P_m), the membrane partition coefficient (K_m) and the percentage of plasma protein binding (%PPB) of the target thieno[2,3-*d*]pyrimidinedione-5-carboxamides **36**, **37** and **38** were evaluated using HPLC methods. The physicochemical values of most of the compounds were found to be within the acceptable limits for the potential PET tracers,¹²⁰ so they were tested as inhibitors of lactate uptake of MCT1, MCT2 or MCT4 in *Xenopus oocytes*, which are a common model system for studying MCT.^{88,89} One of the phenoxy derivatives (**37a**) showed a significant decrease in lactate uptake against MCT1 (**Figure 16**). It was proposed that a spacer atom between the thiophene and aromatic ring systems was important for high affinity with MCT1.⁸⁶

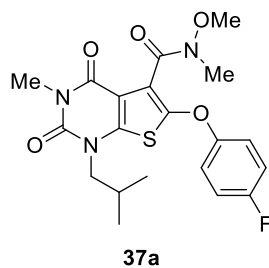


Figure 16. The compound that showed significant decrease in lactate uptake in the previous studies in the Sutherland group.

1.4 Conclusions

In summary, imaging plays a crucial role in both clinical practice and research as it enables non-invasive visualisation of the body's internal structures and physiological processes. With significant advancements in this field, PET has emerged as one of the important imaging techniques, which is widely used due to its high spatial resolution, short acquisition time and high sensitivity. This imaging technique employs radiopharmaceuticals that contain short-lived isotopes. The most commonly used isotopes for this method are ^{11}C and ^{18}F , which are widely used for labelling of small molecules, peptides and antibodies. The most widely employed PET imaging agent remains [^{18}F]FDG, although numerous other tracers have been developed or are under development, offering higher selectivity for specific application.

In recent decades, imaging of synaptic density in the brain has gained significant attention as researchers seek to understand brain function and the changes that occur during aging and the development of various neurological conditions. This can be accomplished using various techniques, but PET imaging has been primarily used for these purposes, suggesting the imaging of the SV2A protein, which is ubiquitously expressed in the neurons that play an important role in neurotransmission. This protein has been used as a non-invasive biomarker of synaptic density, and several imaging agents has been developed for this application, with the nonacetamide radioligands demonstrating the best imaging results. However, these imaging agents could benefit from the optimisation of their synthesis as it would enable faster and more-cost-effective production.

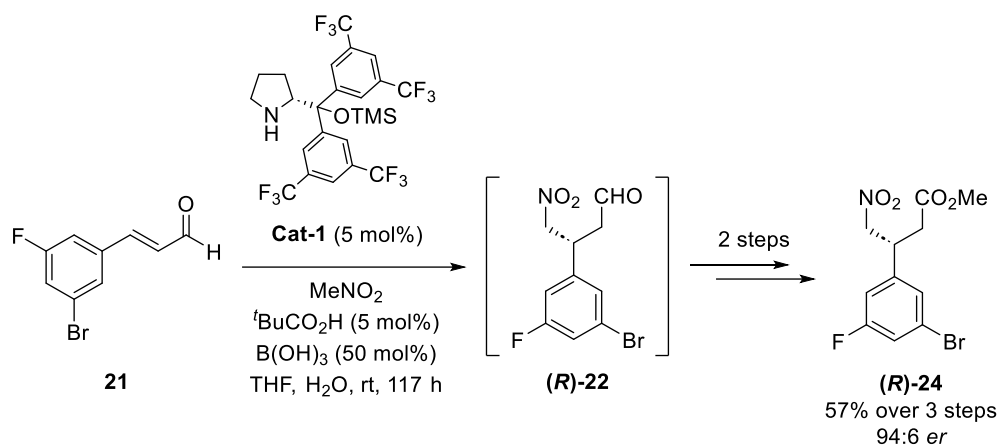
Other proteins, which have gained considerable attention is the family of MCT proteins, which play an important role in monocarboxylate transport. The expression of these transporter proteins is known to be perturbed in the brain of temporal lobe epilepsy patients, however, MCTs has gained more popularity due to their role in regulating metabolism of cancer cells. Due to its function and overexpression in cancer cells, various inhibitors of these proteins have been developed to be used in anticancer therapy. Several PET imaging agents targeting MCTs has also been developed, although a tracer that shows acceptable imaging properties is yet to be discovered.

2. Results and Discussion

2.1 Development of SV2A Imaging Agents

2.1.1 Project aims

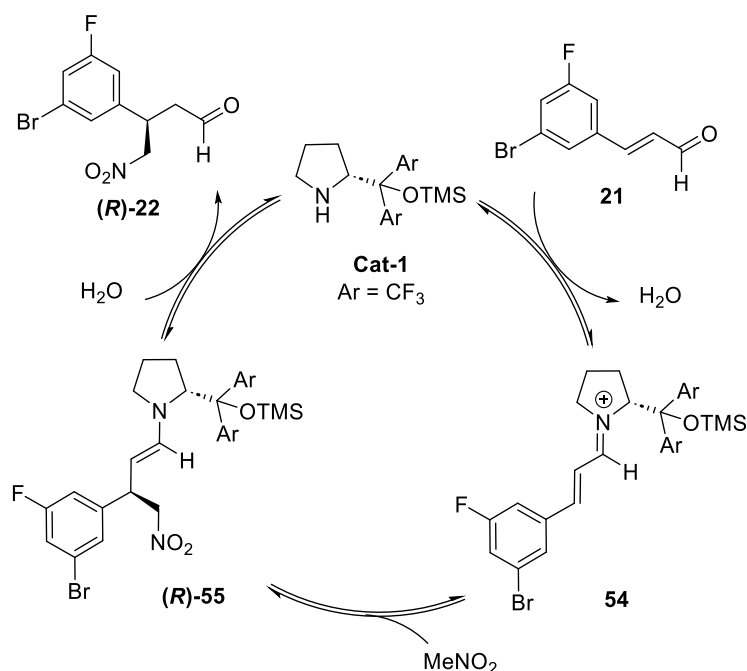
As previously discussed in the Chapter 1.1, [^{18}F]SynVesT-1 is recognised as a prominent PET tracer with high affinity for the SV2A protein.^{43,90,91} SV2A is a validated biomarker of synaptic density and is commonly used to assess the synaptic changes in healthy brain associated with normal aging as well as in various neurological conditions, including dementia and epilepsy.^{35,37,39} [^{18}F]SynVesT-1 is the (*R*)-enantiomer of nonacetamide [^{18}F]7, as this stereoisomer demonstrated the most favourable imaging characteristics. To date, this radioligand has been synthesised as a racemate, with chiral resolution performed using an advanced intermediates or the radiolabelled compound.^{43,49} Due to the importance of the development of an enantioselective approach for the synthesis of [^{18}F]SynVesT-1 and other related tracers, the Sutherland group reported the first asymmetric synthesis for the preparation of the desired (*R*)-enantiomer of this molecule.⁵⁶ This approach developed by Holly McErlain, will be further referred to as the first-generation synthetic route to [^{18}F]SynVesT-1. The key step of this first-generation synthetic route was an organocatalytic conjugate addition of a cinnamaldehyde with nitromethane (**Scheme 12**). Using the chiral 3,5-di(trifluoromethyl)phenyl Hayashi-Jørgensen organocatalyst **Cat-1** enabled the formation of intermediate nitroaldehyde (**R**)-22 as early as the second step in the eight-step synthetic route. The ester intermediate (**R**)-24 was isolated in 57% yield over three steps and 94:6 *er*.⁵⁶



Scheme 12. Key step of the first-generation synthetic route developed in the Sutherland group.⁵⁶

Asymmetric organocatalysis played a key role in enabling the first-generation route for the production of [^{18}F]SynVesT-1. Emerging in the latter half of the 20th century, organocatalysis has become an important field in synthetic organic chemistry. As an acknowledgement of the importance of this field, in 2021, David McMillan and Benjamin List were awarded with the Nobel prize in Chemistry “for the development of asymmetric organocatalysis”. The main idea of the organocatalytic approach is that organic molecules can act as catalysts to promote chemical reactions, affording products with high enantioselectivity. Compared to conventional transition metal catalysis, the advantages of the organocatalytic approach include the avoidance of air and moisture sensitive transition metal complexes.⁹² In addition, these reactions generally do not require harsh conditions and are relatively straightforward to perform on a large scale. Organocatalysts are typically non-toxic and do not contaminate the final products or reaction equipment with transition metals.

While a wide range of organocatalytic reactions has been developed over the past fifty years, the first reports of organocatalytic reactions can be found as early as in 1860, when Justus von Liebig reported the conversion of cyanogen into oxamide in the presence of acetaldehyde.⁹³ Then, an asymmetric intramolecular aldol reaction of triketone promoted by L-proline was reported in 1970s by two separate groups from Hoffmann-La Roche and Schering AG.^{94,95} However, rapid development of this field did not start until the beginning of 21st century when the term organocatalysis was introduced.⁹⁶ One of the first reactions catalysed by L-proline (**Figure 17**), an asymmetric aldol condensation reaction between acetone and aromatic and aliphatic aldehydes, which gave the aldol products in up to 96% *ee*, was reported

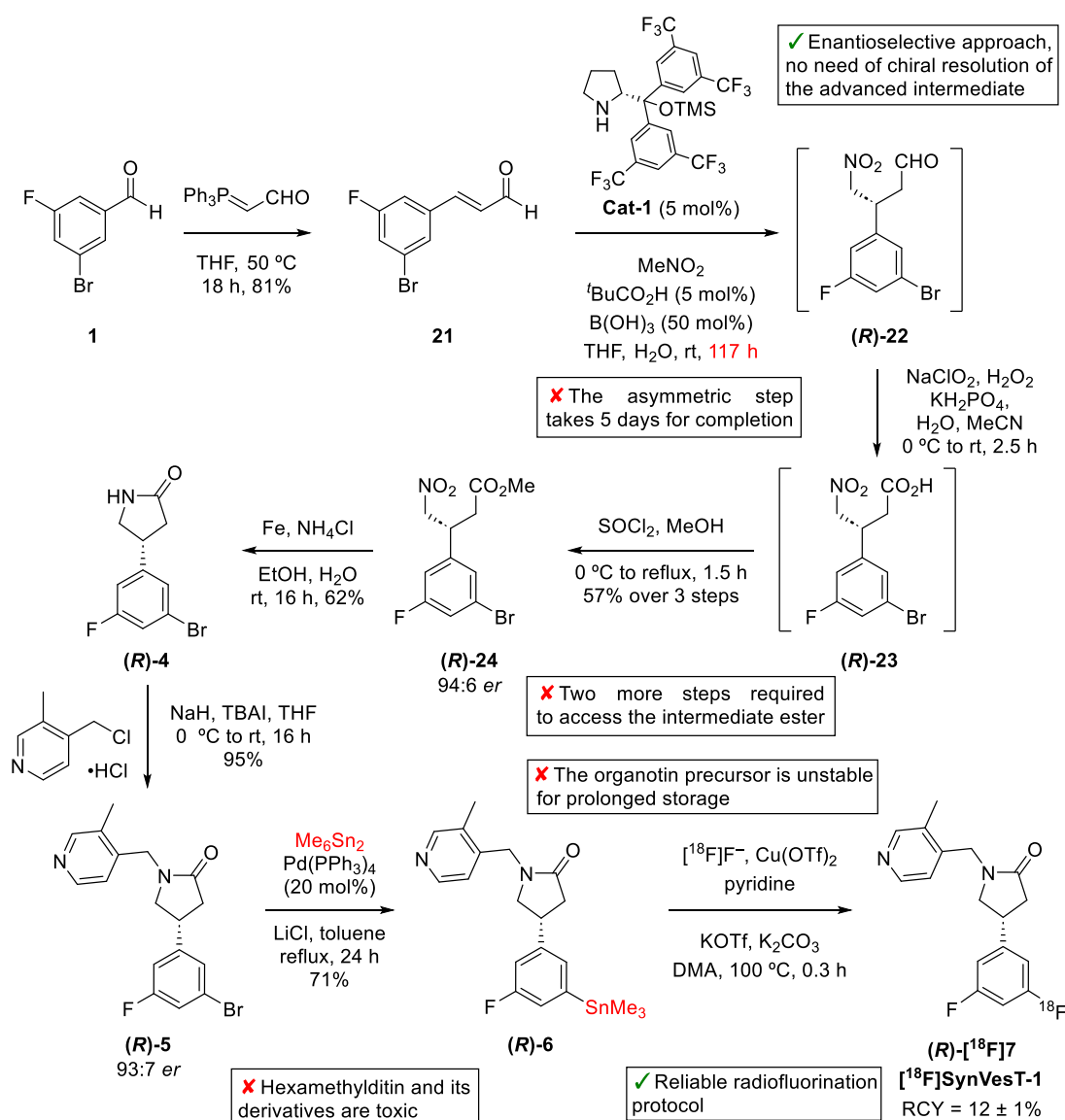


Scheme 13. Catalytic cycle of the asymmetric conjugate addition catalysed by proline-derived catalysts.¹⁰⁰

This transformation enables the efficient asymmetric synthesis of the [¹⁸F]SynVesT-1. The presented approach avoids the need for preparative chiral HPLC resolution step which would otherwise result in the loss of 50% of the synthesised intermediate (**Scheme 14**). The first-generation route also incorporates a reliable radiofluorination step, affording the desired PET tracer in 12% RCY, high molar activity and radiochemical purity. The [¹⁸F]SynVesT-1 synthesised using this protocol has been routinely used by the Tavares group at the University of Edinburgh for SV2A PET imaging applications. However, there were several aspects of the designed synthetic approach that could be further optimised. Firstly, despite the use of the Hayashi-Jørgensen catalyst, the asymmetric conjugate addition reaction required five days for completion, and it required two more steps to access the ester intermediate **(R)-24**. Furthermore, despite the organostannyl precursor **(R)-6** generating better radiofluorination results in the earlier studies, the use of this precursor remains challenging. The synthesis of this precursor involves handling hexamethylditin, a highly toxic reagent, that poses significant risks. It can be fatal if it comes into contact with skin or is swallowed or inhaled, requiring careful attention and quenching procedures. In addition, tin byproducts are generated during radiofluorination, requiring additional precautions to prevent tin contamination of the final radiopharmaceutical. Additionally, it was observed that

this precursor is not stable during prolonged storage, even at low temperatures (<6 °C).

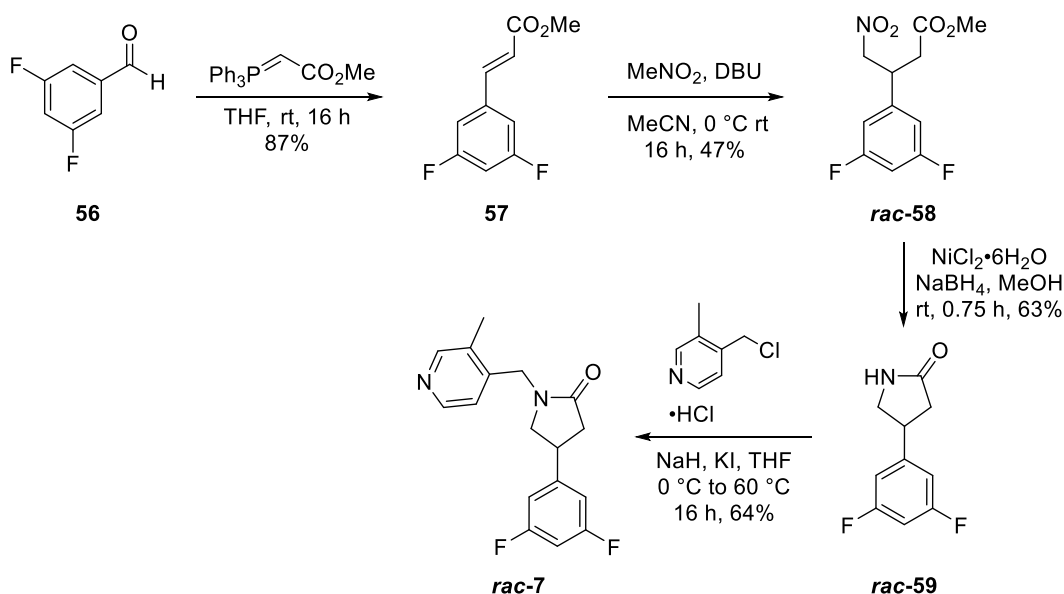
[¹⁸F]SynVesT-1 is an important PET imaging agent, routinely used by several research groups including our collaborators at the University of Edinburgh and has a potential for clinical application. Therefore, it was necessary to revise the current approach to improve the efficiency and address the challenges of the first-generation route. Thus, the aim of this project was to develop second generation route for the synthesis of [¹⁸F]SynVesT-1 and its non-radioactive standard, optimising asymmetric conjugate addition and oxidation/esterification steps. Furthermore, a different type of radiofluorination precursor was deemed necessary to avoid working with toxic and unstable tin compounds.



Scheme 14. First-generation route for the synthesis of [¹⁸F]SynVesT-1.⁵⁶

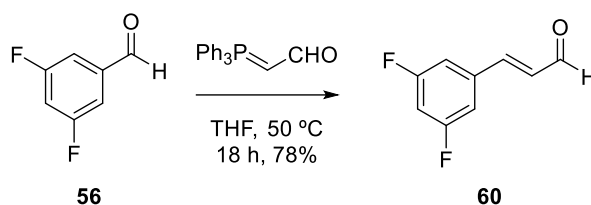
2.1.2 Development of a second-generation route for SynVest-1 and precursor for [¹⁸F]SynVesT-1

To confirm the enantioselectivity of the route which would be developed, the racemate of SynVesT-1 was prepared as previously synthesised in our group using the standard procedure (**Scheme 15**).⁴³ Starting from commercially available 3,5-difluorobenzaldehyde (**56**), this was reacted with methyl (triphenylphosphoranylidene)acetate via a Wittig reaction, which gave the *E*- α,β -unsaturated ester **57** in 87% yield. Conjugate addition of nitromethane with **57** then provided access to the γ -nitroester intermediate **rac-58** under basic conditions overnight and in 47% yield. Nitro group reduction using nickel(II) chloride and sodium borohydride and subsequent *in situ* lactamisation of the resulting amine provided lactam **rac-59** in 63% yield. This was then followed by the alkylation reaction using 4-(chloromethyl)-3-methylpyridine hydrochloride under basic conditions and in the presence of catalytic potassium iodide. At 60 °C and a reaction time of 18 h, this gave the desired **rac-7** in 64% yield. Compounds **rac-58**, lactam **rac-59** and **rac-7** were used as standards for chiral HPLC analysis. The same approach was employed for the synthesis of racemates of brominated lactam **rac-4** and bromide precursor **rac-5**, which were also used for the chiral HPLC evaluation of the corresponding enantioenriched material.



Scheme 15. Synthesis of racemate **rac-7**.

The optimisation study was started with the synthesis of non-radioactive standard SynVesT-1. To start the optimisation study of the conjugate addition step, appropriate cinnamaldehyde was synthesised starting from 3,5-difluorobenzaldehyde **56** in a Wittig reaction with (triphenylphosphoranylidene)acetaldehyde at 50°C and with a reaction time of 16 h. This reaction successfully yielded the desired product **60** in 78% on a multigram scale (**Scheme 16**). The intermediate cinnamaldehyde was exclusively formed as a *E*-isomer due to the resonance stabilisation of the phosphonium ylide by the carbonyl moiety. The reaction selectivity was confirmed by ^1H nuclear magnetic resonance (NMR) spectroscopy, demonstrating vicinal C–H signals sharing $^3J_{\text{HH}}$ coupling of 16 Hz.



Scheme 16. The Wittig reaction step.

Thus, once sufficient amount of the cinnamaldehyde intermediate had been generated, the optimisation of the stereoselective conjugate addition step was undertaken. Initially, increasing the amount of **Cat-1** was found to accelerate the reaction, although a reaction time of 60 hours was still required (**Table 2**, entry 1). Exploring other catalysts along with co-catalytic acids was proposed to reduce the reaction time as well as enhance the *er* value. There are two main Hayashi-Jorgensen organocatalysts employed in organic synthesis (**Figure 18**). 3,5-Di(trifluoromethyl)phenyl catalyst **Cat-1** has improved stability in comparison to bis-phenyl analogue **Cat-2** due to the presence of the strong electron-withdrawing trifluoromethyl groups. Moreover, these substituents also introduce additional steric bulk which is thought to enhance the steric control over the reaction.⁹⁸ This catalyst was employed in the first-generation route and although it provided reasonable stereoselectivity, the reaction rate remained slow. Therefore, as bis-phenyl catalyst **Cat-2** is supposed to be more active, it was evaluated in the conjugate addition step to determine its impact on reaction rate.

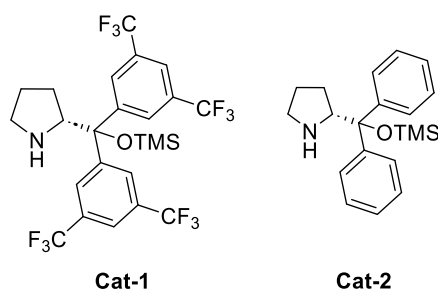
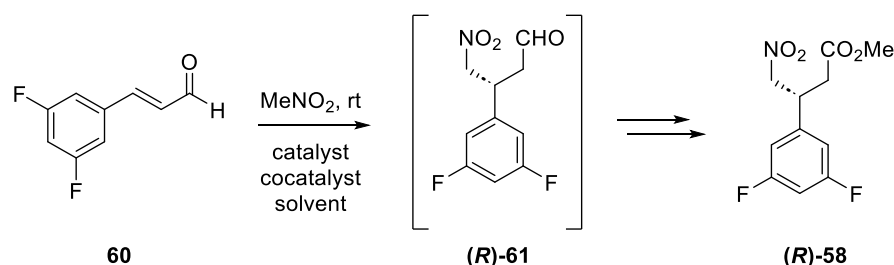


Figure 18. Structures of **Cat-1** and **Cat-2**.

Hence, bis-phenyl Hayashi-Jørgensen organocatalyst **Cat-2** (**Figure 18**) was tested in the conjugate addition reaction of nitromethane under standard conditions (**Table 2**, entry 2) followed by the oxidation/esterification of aldehyde **60**. The application of the new catalyst did speed up the reaction rate and the reaction reached full conversion after 18 h, although the overall yield after oxidation/esterification step remained low. Next, the co-catalytic acid and solvent were also changed as benzoic acid in methanol was more commonly used with the bis-phenyl organocatalyst. Thus, using **Cat-2** in the presence of benzoic acid and methanol resulted in the same reaction time but a slightly higher yield of the final product (entry 3).

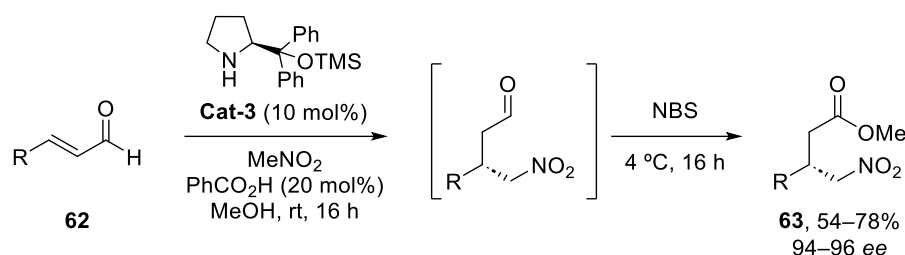
Table 2. Optimisation of the asymmetric conjugate addition step.*



Entry	Catalyst	Cocatalysts/solvents	Reaction time	Overall yield of (R)-58	<i>er</i>
1	Cat-1 (10 mol%)	<i>t</i> BuCO ₂ H (10 mol%), B(OH) ₃ (100 mol%), THF, H ₂ O	60 h	14%	94:6
2	Cat-2 (10 mol%)	<i>t</i> BuCO ₂ H (10 mol%), B(OH) ₃ (100 mol%), THF, H ₂ O	18 h	14%	99:1
3	Cat-2 (10 mol%)	PhCO ₂ H (20 mol%), MeOH	18 h	23%	99:1

*Oxidation and esterification steps were performed as shown in **Scheme 14**.

Given the improvement of the reaction time for the conjugate addition step, methods to enhance the overall yield of the ester (**R**)-**58** were investigated. It was proposed that alternative reactions for the oxidation and esterification steps might result in improved yields. Jørgensen and co-workers previously reported a two-step one-pot procedure for converting cinnamaldehydes **62** into methyl (*S*)-3-phenyl-4-nitrobutanoates **63** in good yields and high ee using bis-phenyl catalyst **Cat-3**, benzoic acid, NBS and methanol (**Scheme 17**).¹⁰¹

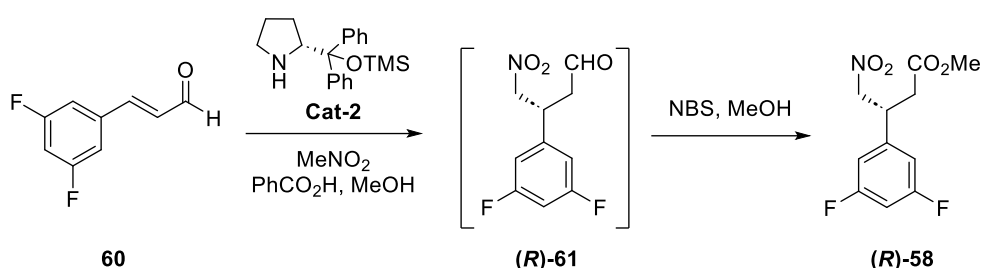


Scheme 17. Two-step, one-pot asymmetric synthesis of γ -nitroesters.¹⁰¹

An optimisation study of this one-pot, two-step method was then conducted using cinnamaldehyde **60** as a substrate (**Table 3**). The conjugate addition step was carried out at 0 °C over 18 hours using standard catalyst loading of 10 mol%. The oxidative esterification step was performed one-pot with 1.3 equivalents of NBS at 0 °C overnight. Both steps were initially carried out under an argon atmosphere (entry 1); however, it was later found that the conjugate addition step does not require inert atmosphere (entry 2). To increase the rate of the second step, the reaction was performed at a higher temperature (entry 3). Although this reduced the reaction time, it resulted in a lower yield probably due to the decomposition of the starting material. Increasing the quantity of NBS did not affect the yield or the reaction time (entry 4). It was previously suggested in the literature that the oxidation step proceeded via radical formation,¹⁰² however, Jørgensen and co-authors in their paper proposed an electrophilic mechanism for this reaction (**Scheme 18**). To establish the mechanism of the oxidative esterification step and use this information to find optimal reaction conditions, a radical trap, [(2,2,6,6-tetramethylpiperidin-1-yl)oxyl (TEMPO)], was used. Although the addition of TEMPO stopped the reaction, which would confirm the radical mechanism of this reaction (**Table 3**, entry 5), performing the reaction in the air did not affect the yield (entry 6). Consequently, both steps were subsequently performed under ambient atmosphere. The yield obtained in the reaction with 5 mol% of catalyst **Cat-2** was comparable to that with

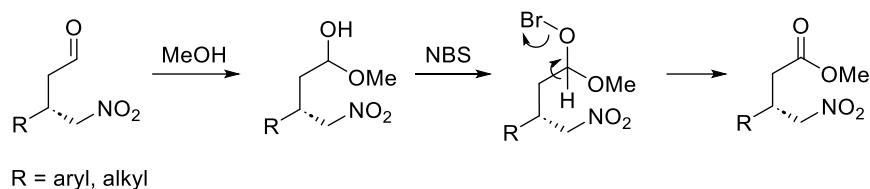
10 mol% (entries 6 and 7). However, for greater efficiency, the higher catalyst loading was preferred. Therefore, after the optimisation study, the reaction conditions were used as presented in the Jørgensen's procedure (Entry 7).¹⁰¹ Thus, the synthesis of ester **(R)**-**58** from cinnamaldehyde **60** was achieved in 36 h using a new two-step, one-pot approach compared to 124 h and three steps required by the first-generation route, with equal organocatalyst loading (10 mol%).

Table 3. Optimisation study of the asymmetric conjugate addition/oxidative esterification steps.



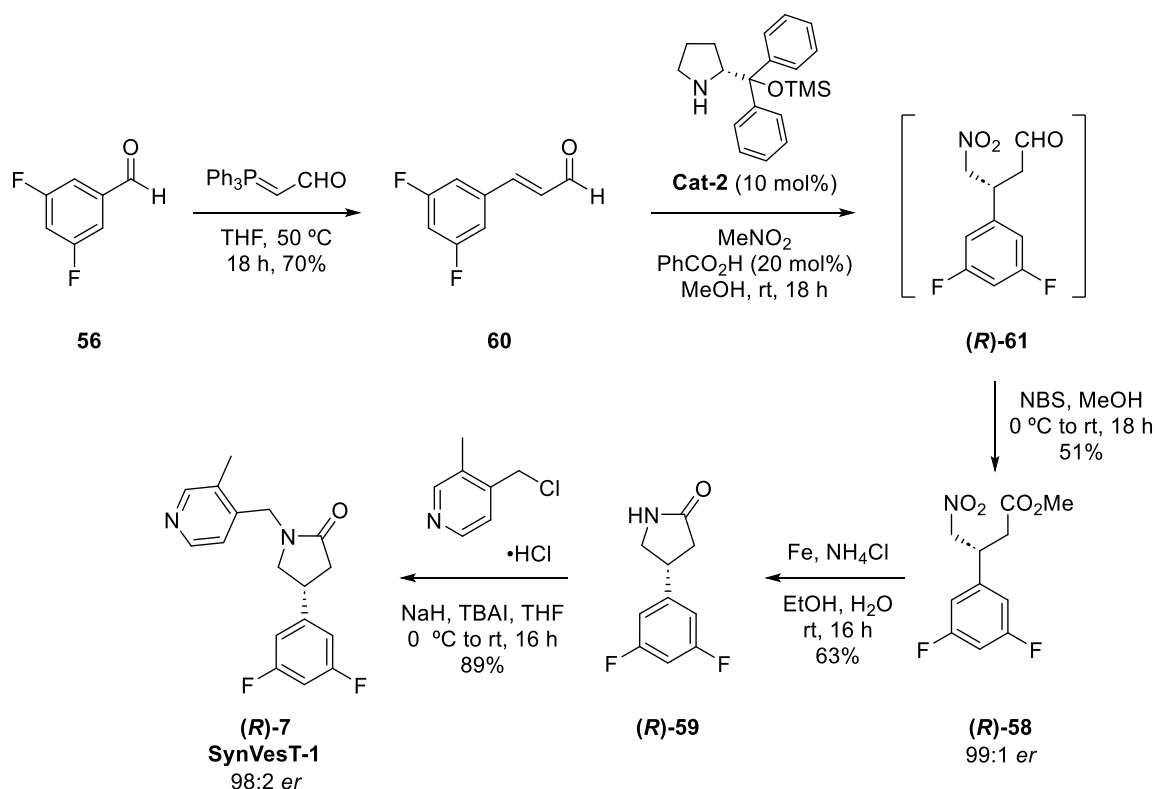
Entry	Catalyst loading	NBS eq.	Temp. of 2 nd step (°C)	Reaction time (1 st /2 nd step)	Inert atmosphere		Overall yield after 2 steps
					1 st step	2 nd step	
1	10 mol%	1.3	0 ^a	18/18 h	+	+	43%
2	10 mol%	1.3	0 ^a	18/18 h	-	+	49%
3	10 mol%	1.3	0 to 64	18/4 h	-	+	37%
4	10 mol%	1.5	0 ^a	18/18 h	-	+	51%
5 ^b	10 mol%	1.3	0 ^a	18/18 h	-	+	0% ^c
6	10 mol%	1.3	0 ^a	18/18 h	-	-	48%
7	5 mol%	1.3	0 ^a	48/18 h	-	-	50%

^a Kept in the ice bath overnight. After 18 h the temperature of the bath would usually reach 15 °C. ^b TEMPO was used as a radical inhibitor. ^c Undefined products.



Scheme 18. Mechanism of the oxidative esterification proposed by Jørgensen and co-authors.¹⁰¹

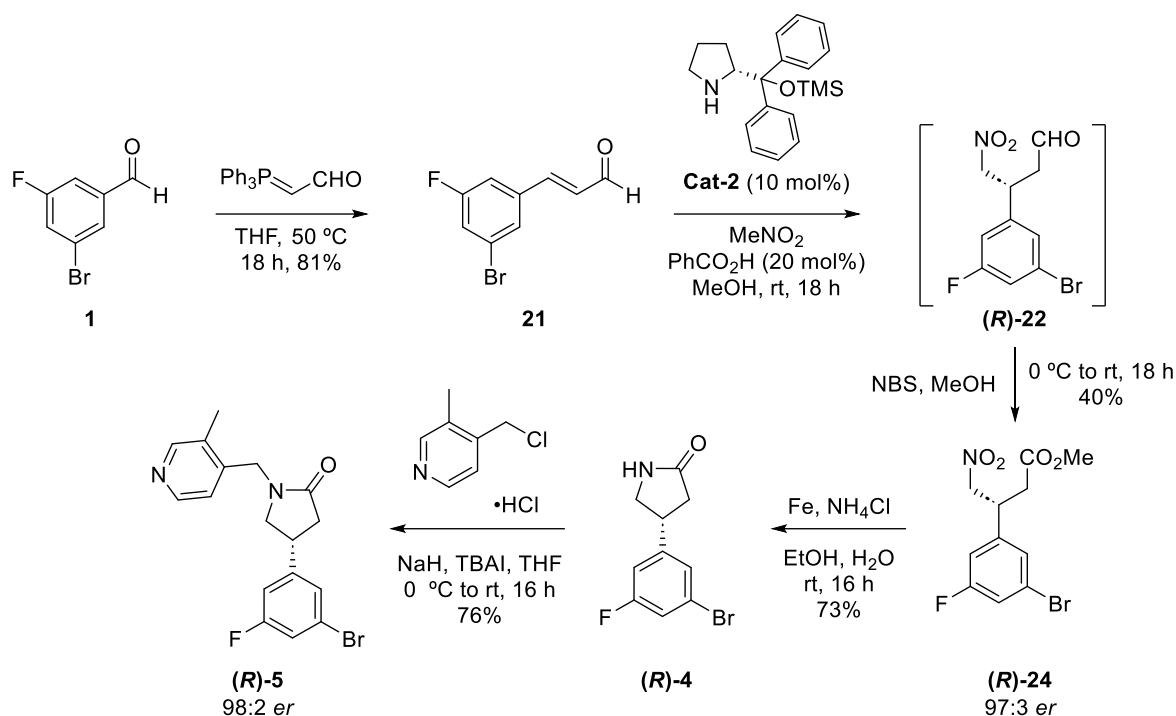
Following optimisation of the one-pot, two step method, subsequent steps were repeated as described for the first-generation route (**Scheme 19**). The nitro group reduction was conducted in the presence of iron powder and ammonium chloride, which allowed the formation of the corresponding amine. The resulting amine underwent lactamisation upon basic quenching and provided the desired lactam (**R**)-**59** in 63% yield. Lactam intermediate (**R**)-**59** then was introduced to the Finkelstein-type reaction. Alkylation of lactam (**R**)-**59** was then performed using 4-(chloromethyl)-3-methylpyridine hydrochloride and TBAI as a catalyst under basic conditions. Under these conditions, the alkylating agent was converted to the iodide to introduce a better leaving group for the nucleophilic substitution reaction and then was attacked by the lactam. This reaction yielded the desired (**R**)-**7** SynVesT-1 in 89% overnight at room temperature. Analytical chiral HPLC was then performed to determine the *er* of the target compound using racemate of this compound. The HPLC analysis revealed that the target compound (**R**)-**7** was synthesised in 98:2 *er*. This represents a substantial improvement on the first-generation synthesis, which produced (**R**)-**7** in 93:7 *er*. The resulting material was used as a non-radioactive HPLC standard during the development of the radiofluorination procedure.



Scheme 19. Optimised second generation synthesis of **(R)-7**.

2.1.3 Application of the second-generation route for the synthesis of [¹⁸F]SynVesT-1 precursor

Upon completion of the second-generation route to non-radioactive SynVesT-1, the same approach was used to synthesise the bromide precursor for [¹⁸F]SynVesT-1 (**Scheme 20**). Firstly, 3-bromo-5-fluorobenzaldehyde **1** was subjected to the Wittig reaction under standard conditions to obtain exclusively *E*-cinnamaldehyde **21** (confirmed by ¹H NMR spectroscopy) in 81% yield. The one-pot, two-step process was then performed in the presence of organocatalyst **Cat-2**, benzoic acid in methanol solution, followed by addition of NBS to convert cinnamaldehyde **21** to the ester **(R)-24**. The intermediate ester **(R)-24** was isolated in 40% yield with an *er* value of 96:4, which was confirmed by analytical chiral HPLC. This is slightly higher than the *er* value obtained from the first-generation route (94:6 *er*, **Scheme 14**). The ester **(R)-24** was then subjected to nitro group reduction, lactamisation and alkylation reactions under standard conditions (**Scheme 20**). It should be noted that the *er* value was retained during these two steps.

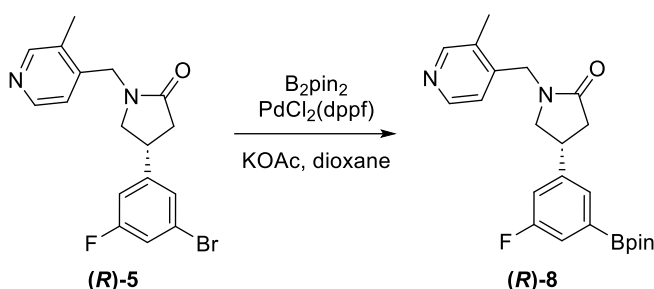


Scheme 20. Optimised second generation route for the synthesis of the bromide precursor **(R)-5**.

After successful optimisation of the key step for the synthesis of **(R)-5**, an alternative precursor to an organotin compound for radiofluorination was investigated. The boronic ester precursor was identified as a suitable alternative for the toxic and unstable organotin precursor. A method for the synthesis of a boronic ester precursor of [^{18}F]SynVesT-1 had been previously reported, however, the product was isolated in a low 36% yield.⁴⁹ The optimisation of the conditions of the Miyaura reaction was started by a MSci student Louise Black (**Table 4**). First, the reaction at 80 °C was attempted, however, only 88% conversion, resulting in a 51% yield was observed after 24 h (entry 1). After raising the reaction temperature to 100 °C, the reaction reached full conversion after 1 h and the desired boronic ester **(R)-8** was isolated in 65% yield (entry 2). Reducing the catalyst loading (entry 3) and the amount of bis(pinacolato)diboron (B_2pin_2) (entry 4) did not affect the efficiency of the borylation reaction as the full conversion was achieved in each case. The lower yield observed in entry 3 is likely due to the product loss during purification. Thus, using 5% of the Pd catalyst and 1.1 equivalents of B_2pin_2 , the desired organoboron precursor **(R)-8** was isolated in 63% yield. Boronic ester **(R)-8** was found to be unstable on silica or neutral alumina, which excluded the purification of this compound using chromatography methods. Instead, recrystallisation from hot hexane was determined as the most suitable purification method for **(R)-8**, however,

the loss of some material could be observed while using this purification technique. The prior filtration through a silica pad was still necessary for successful recrystallisation as it helped to hydrolyse and remove some of the borylated side products.

Table 4. Optimisation study of the synthesis of boronic ester precursor (**R**)-8.



Entry	B ₂ Pin ₂ (eq.)	PdCl ₂ (dppf) (mol%)	Time (h)	Temperature (°C)	Isolated yield (%)
1 ^a	1.5	8.7	24	80	51
2	1.5	8.7	1	100	65
3	1.5	5	1	100	51
4	1.1	5	1	100	63

^a Performed by Louise Black.

2.1.4 Radiosynthesis of [¹⁸F]SynVesT-1

After the successful synthesis of the boronic ester precursor, the optimisation of the radiofluorination procedure was performed at both PET Radiopharmaceutical Production Unit (RPU), West of Scotland PET centre and by the Tavares group at the University of Edinburgh.

The optimisation at the PET RPU was initiated using the standard procedure for the organotin precursor as it was important to keep the reaction temperature below 120 °C to avoid racemisation.⁵⁶ The automated radiofluorination was performed using customised RNPlus Synthra module (**Figure 19**).

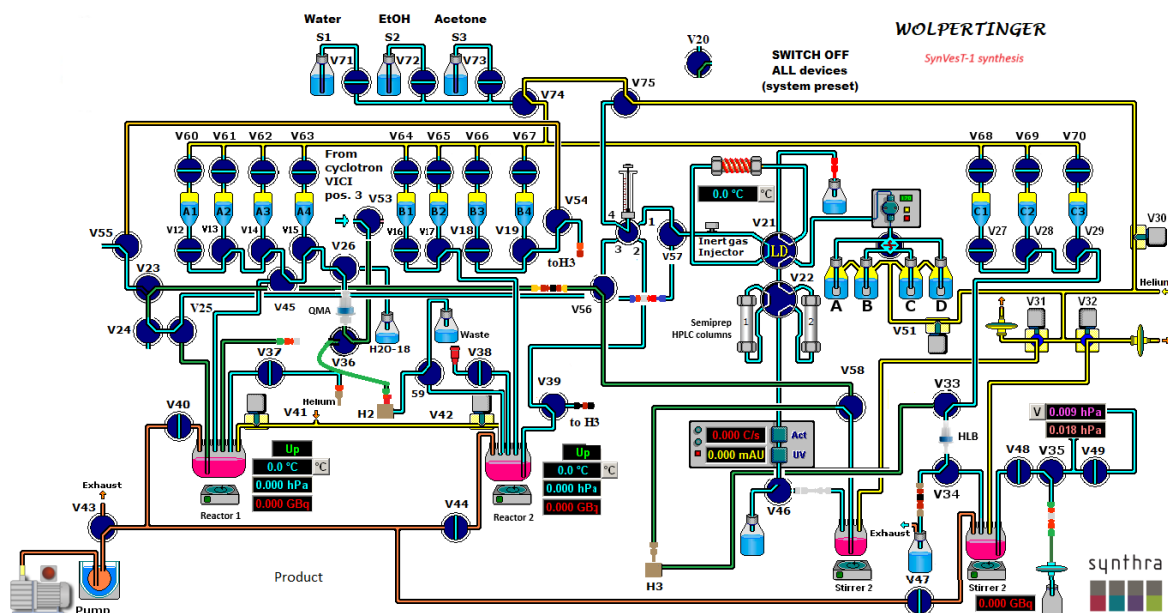
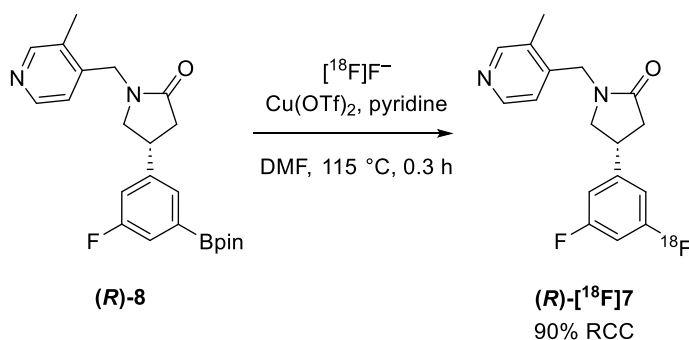


Figure 19. Automated synthesiser scheme used for [^{18}F]SynVesT-1 synthesis at the PET RPU, West of Scotland PET centre.

First, no-carrier added aqueous [^{18}F]fluoride was produced *via* the $^{18}\text{O}(\text{p},\text{n})^{18}\text{F}$ nuclear reaction by irradiation of ^{18}O -enriched water by a cyclotron. Cyclotron target water containing [^{18}F]fluoride was transferred to and trapped on a QMA SepPakPlus Light cartridge (V53 to QMA, **Figure 19**). The trapped [^{18}F]fluoride was eluted into a glassy carbon reaction vessel using a solution of tetrabutylammonium trifluoromethanesulfonate (TBAOTf) in water/acetonitrile (Reactor 2). Using TBAOTf instead of standard potassium triflate helped to increase the amount of activity washed to the reactor from the cartridge and improve the reaction conversion. Azeotropic drying of the [^{18}F]fluoride *in vacuo* was then performed, and the solution of boronic ester precursor (**R**)-**8**, copper triflate catalyst and pyridine in anhydrous *N,N*-dimethylformamide was added to the reactor. It was important to dissolve the precursor (**R**)-**8** immediately prior the start of the synthesis as previous reports indicated that this type of precursor decomposed if left with the catalyst for extended period. The reaction mixture was then heated to 115 °C for 20 minutes while being stirred (**Scheme 21**). After that an aliquot was removed for analysis by analytical radioHPLC to allow radiochemical conversion (RCC) calculation and product identity (**Figure 20**). During this optimisation study the RCC up to 90% was achieved and it was confirmed that the desired [^{18}F]SynVesT-1 was obtained using analytical radioHPLC. However, when purification was attempted using a semi-preparative HPLC system, the product became trapped in the system. A similar issue was

observed with radio thin-layer chromatography (radio-TLC), as all activity remained at the baseline. This was initially thought to be caused by the formation of a complex of the radiolabelled product, which is used in larger excess as radiofluorination reactions are typically performed under pseudo-first-order reaction conditions with respect to fluoride. Another possibility was that the boronic ester or its derivative could bind to the column, causing the product to adhere to the sorbent especially given that only a small amount of the product is formed compared to the amount of starting material used. To address this issue, a cartridge filtration prior semi-preparative HPLC purification was proposed. Several cartridges were evaluated with the Oasis® HLB cartridge providing the best results allowing the reaction mixture to pass through while retaining the product, which could be eluted using ethanol. Although, installing the cartridge before the semipreparative HPLC column during the radiolabelling process did not lead to the expected result, a small amount of the [^{18}F]SynVesT-1 was recovered during the purification though it was not sufficient to calculate the radiochemical yield and molar activity.



Scheme 21. Radiofluorination procedure developed in the PET RPU.

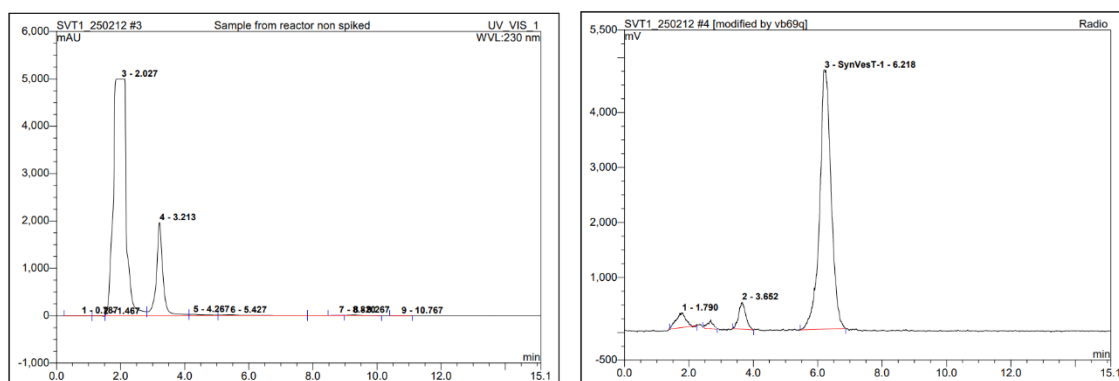
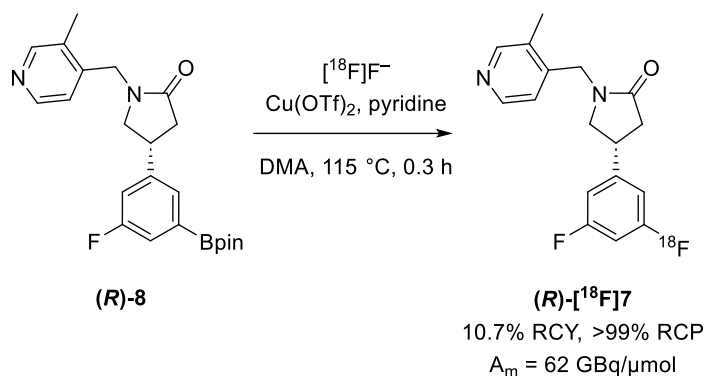


Figure 20. UV-vis (left) and radio (right) HPLC traces of the reactor aliquot. [^{18}F]SynVesT-1 signal was only observed in the radio-channel due to the low concentration.

Our collaborators from the Tavares group at the University of Edinburgh also tested the radiofluorination of the boronic ester precursor **(R)-8** procedure using a different module type, TRACERlab FX_{FN}. It was independently confirmed that using *N,N'*-dimethylformamide (DMF) as a radiofluorination reaction solvent resulted in only a trace amount of [¹⁸F]SynVesT-1 as detected on the semi-preparative HPLC column. Several reported radiofluorination procedures of boronic esters have been performed in DMF.⁵¹ However, this substrate is sensitive to the reaction solvent, so the further radiolabelling reactions were conducted using anhydrous dimethyl acetamide (DMA) as a solvent. Using the same conditions as for the organotin precursor also resulted in traces of the product recovered from the semi-preparative HPLC column. To improve the reaction, the order of reagent addition was changed as this had proven effective for some other borylate precursors.¹⁰³ The modified radiofluorination procedure, in which fluoride was first dissolved in half of the reaction solvent, heated at 100 °C for 5 minutes, and the remaining reagents were then added in the second half of the solvent proved to be successful. The reaction temperature was kept at 115 °C and the reaction time was also 20 min (**Scheme 22**). Fewer impurities were observed on the semi-preparative chromatogram, and the results were comparable to those obtained with the organotin precursor. The desired [¹⁸F]SynVesT-1 was synthesised using this approach in 10.7% RCY, > 99% RCP and with the molar activity by the end of the synthesis of 62 GBq/μmol (n = 2). No racemisation of the product was observed using these reaction conditions despite the previous reports.⁴⁹

In summary, this precursor delivered radiofluorination results comparable with the organotin compound, while also allowing work with a much less toxic precursor and reagents for its synthesis (**Scheme 22**). Also, it was confirmed that this precursor is stable enough for prolonged storage as no changes were observed by ¹H NMR spectroscopy of the material after a year in the fridge. Moreover, the developed second-generation synthetic route offered a more efficient synthesis of the boronic ester precursor **(R)-8** and provided the bromide intermediate **(R)-5** with the improved enantiomeric ratio of 98:2.



Scheme 22. Radiofluorination of boronic ester precursor **(R)-8**.

2.1.5 Synthesis of precursor for [^3H]SynVesT-1

2.1.5.1 Synthesis [^3H]SynVesT-1 using first-generation route

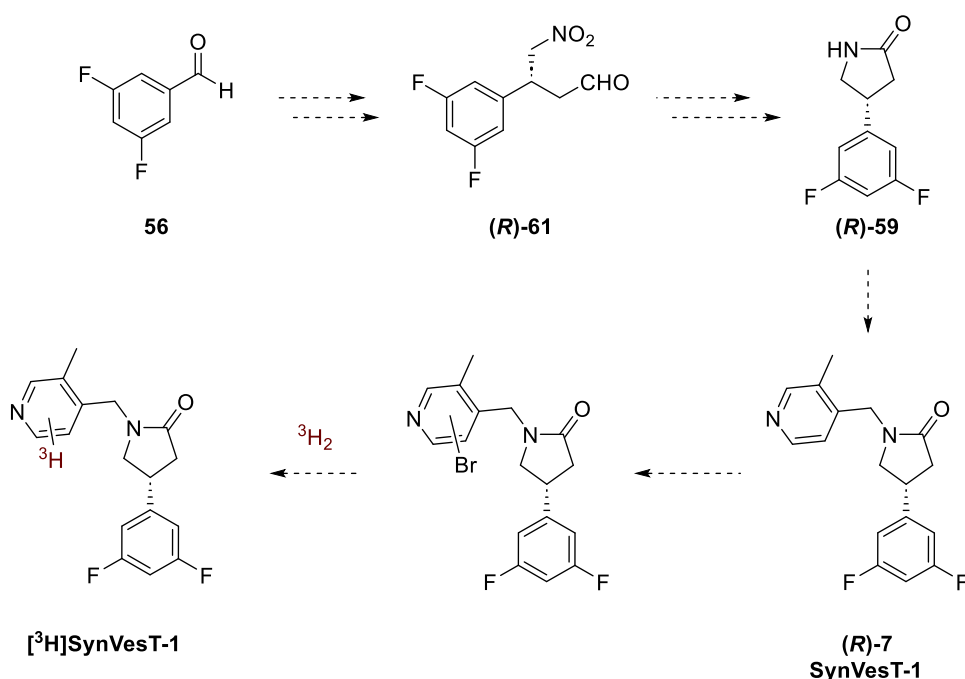
Another part of this project required the synthesis of [^3H]SynVesT-1, which would be used by our collaborators at the University of Edinburgh to develop synaptomics as a new technology for studying human synaptopathy in clinical applications. For this study, it was necessary to conduct an autoradiography studies targeting the SV2A protein.

Autoradiography is an *in vitro* imaging technique which allows visualisation of the radioligand distribution in the tissue.¹⁰⁴ Frozen tissues are typically incubated with the solution of a radiolabelled compound, which has specific binding with the chosen biological target. Using a photosensitive film or phosphor imaging plate, the accumulation of the imaging agent is then localised. This method has high spatial resolution and enables quantification and localisation of the imaging agent in the tissue. Using this method, dissociation constant K_d and inhibition constant K_i can be calculated, as well as the density of the binding sites B_{max} . A radiolabelled imaging agent with high binding specificity is typically required, as non-specific binding of this ligand can lead to the incorrect results. As for the radioisotope, tritium is a commonly used for autoradiography due to its longer half-life (12.33 years).

As nonacetamide ligands (**Figure 6**) showed high specific binding to SV2A, their tritium labelled analogues are commonly used in the autoradiography studies. For instance, [^3H]UCB-J is the most commonly used imaging agent used in the autoradiography of SV2A.^{105,106} Autoradiography studies have also been conducted

using [^{18}F]SynVesT-1, however, a tritium-labelled analogue of this molecule has not yet been employed.¹⁰⁷ To characterise binding properties of SynVesT-1 using a radioligand with a longer half-life and obtain higher spatial resolution, so that changes in demyelination and subsequent remyelination processes could be observed, access to [^3H]SynVesT-1 was required.

For the synthesis of a tritium labelled SynVesT-1 derivative, it was decided to repeat the original route to non-radiofluorinated standard SynVesT-1 (**(R)**-**7**) using the first-generation route. This is because the development of this imaging agent had started prior to the optimisation of the second-generation route.⁵⁶ After synthesising SynVesT-1, the late-stage modification to incorporate the tritium label would be conducted. The initial plan was to introduce a halogen into the pyridine ring of SynVesT-1 for subsequent hydrogenation using tritium gas (**Scheme 23**).

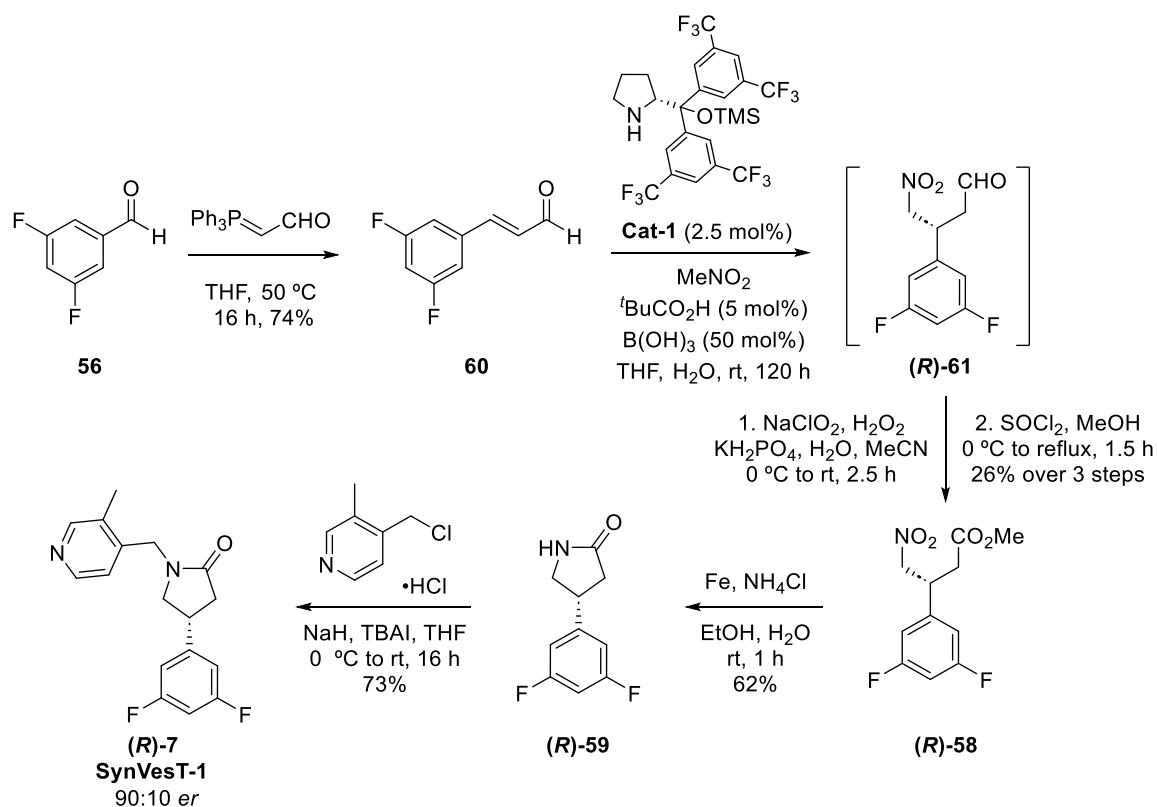


Scheme 23. Proposed route to [^3H]SynVesT-1.

The route started from the Wittig reaction of commercially available 3,5-difluorobenzaldehyde **56** with (triphenylphosphoranylidene)acetaldehyde under standard conditions (**Scheme 24**). This reaction resulted into the formation of *E*-cinnamaldehyde **60** in 70% yield after 18 h at 50 °C. Next, the asymmetric conjugate addition of nitromethane with *E*-cinnamaldehyde **60** was performed in the presence of Hayashi-Jørgensen's organocatalyst **Cat-1**, using pivalic and boric acids as

cocatalysts. This resulted in the formation of the (**R**)-**61** as the major product. The addition product (**R**)-**61** was found to be unstable on silica and was used without any purification in the next step. A Pinnick-type oxidation involving mixture of sodium chlorite and hydrogen peroxide as oxidants in a potassium dihydrophosphate buffer gave the corresponding carboxylic acid. Carboxylic acid was then esterified using thionyl chloride and methanol. Ester (**R**)-**58** was obtained in 26% yield over the three steps.

The obtained yield for ester (**R**)-**58** was lower than expected for this reaction (usually 50%). On checking catalyst **Cat-1**, it was found that it had degraded by 50% (**Figure 21**). According to the ^1H NMR spectrum of the catalyst sample, degradation had occurred by loss of the trimethylsilyl-group (TMS) (**Cat-4**), which has been described in the literature.¹⁰⁸ Although the prolinol degradation by-product **Cat-4** can catalyse conjugate addition, this process is less effective, resulting in longer reaction time, other addition products and lower yields (**Scheme S1, Appendix A**).¹⁰⁹



Scheme 24. Asymmetric synthesis of (**R**)-**7**.

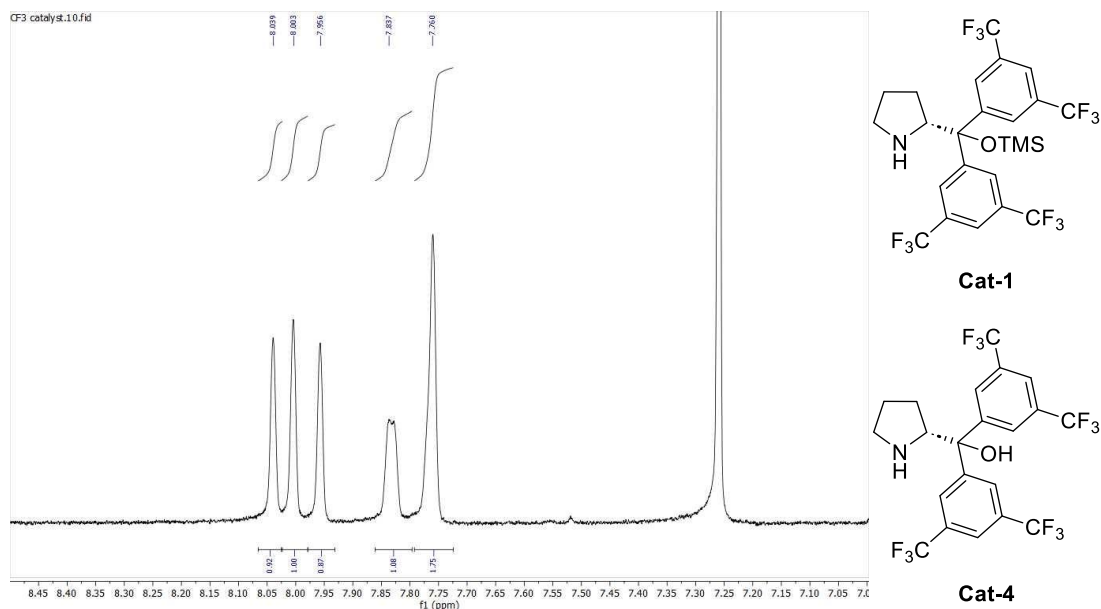
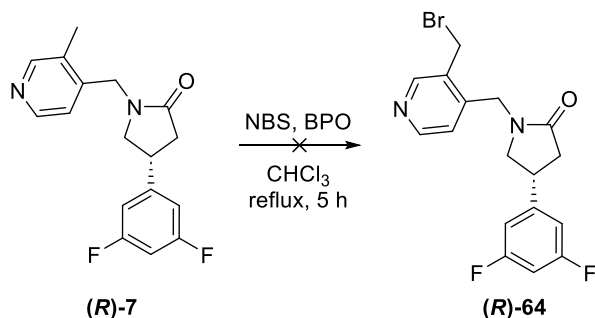


Figure 21. Part of the ^1H NMR spectrum of the degraded catalyst **Cat-1**: peaks at δ 7.76, 7.84, and 8.00 ppm are from the TMSO-catalyst (**Cat-1**), whereas δ 7.76, 7.96, and 8.04 ppm are assigned to the HO-catalyst (**Cat-4**).

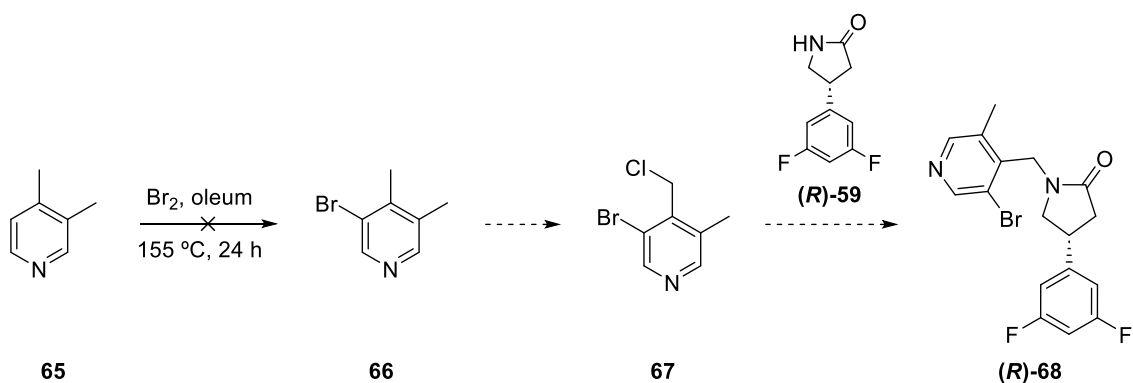
It was decided to proceed with the synthesised material to evaluate whether the proposed approach was viable. The esterification step was then followed by the nitro group reduction reaction, which was conducted in the presence of iron powder as the reducing reagent (**Scheme 24**). This reaction was complete after 1 h at room temperature and followed by a base quench, which gave lactam **21** in 62% yield. Coupling of lactam (**R**)-**59** with alkyl halide in the presence of NaH as a base and a catalytic amount of TBAI provided SynVesT-1 in 73% yield. The *er* value for the final compound was determined as 90:10. As expected, the *er* value of the synthesised material was lower as the unprotected prolinol **Cat-4** is a less effective asymmetric organocatalyst than the original Hayashi-Jørgensen organocatalyst **Cat-1**.¹⁰⁹

After completion of this synthetic route, bromination of SynVesT-1 to afford the precursor for tritium-labelling was attempted. Following literature precedent, treatment of the compound with NBS in the presence of benzoyl peroxide (BPO) under reflux did not lead to the formation of the desired product (**R**)-**7** (**Scheme 25**).¹¹⁰ Inspection of the reaction mixture by ^1H NMR spectroscopy showed only decomposition of the starting material.



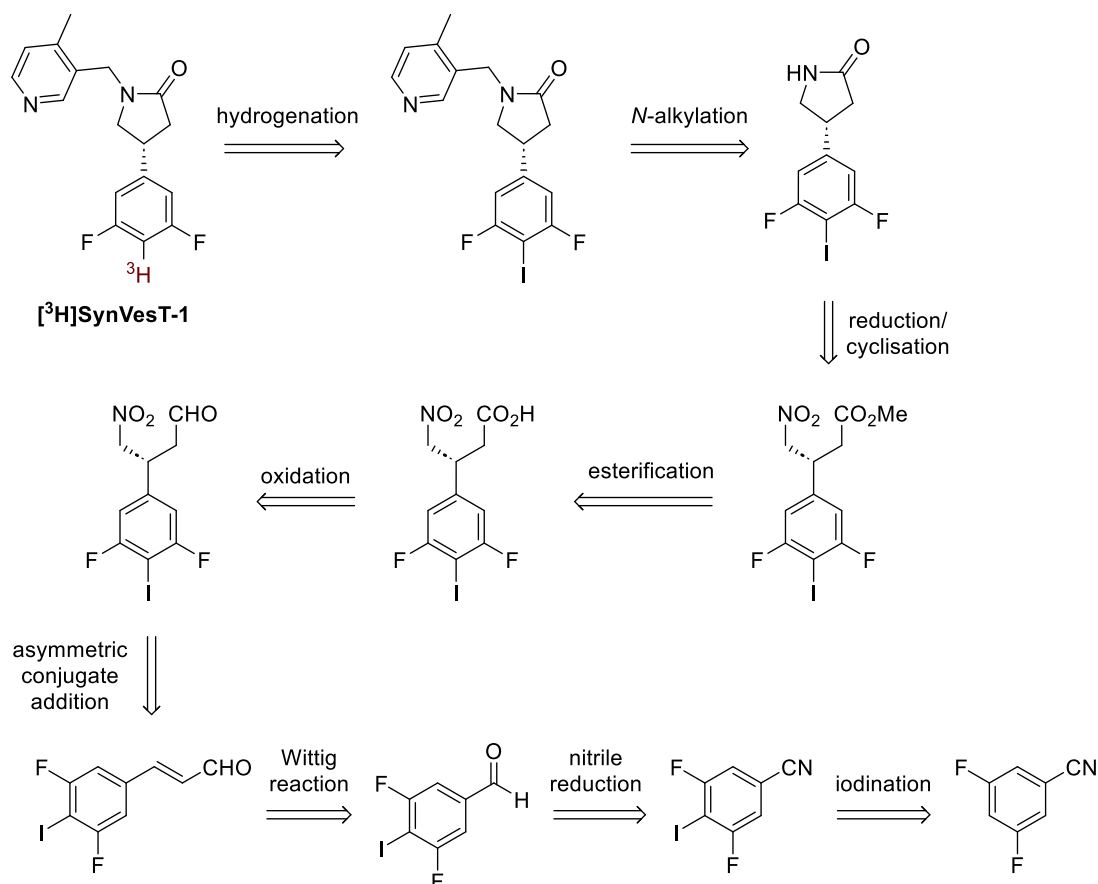
Scheme 25. Attempted bromination of **SynVesT-1**.

After unsuccessful late-stage bromination of **(R)-7**, it was decided to introduce the bromine moiety an earlier stage and during the synthesis of the alkylation agent, which would be later coupled with lactam **(R)-59** (**Scheme 26**). The modified synthesis of alkyl halide **67** began from commercially available 3,4-lutidine **65**. Regioselective bromination using bromine and oleum at 155 °C was attempted using a published procedure.¹¹¹ However, the starting material **65** was found to be resistant to the harsh conditions, and after 24 hours, only 3,4-lutidine was recovered.



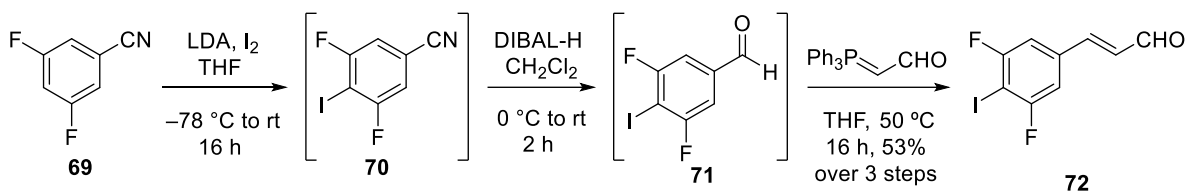
Scheme 26. Attempted bromination of 3,4-lutidine.

After these unsuccessful attempts to introduce a halogen functional group during the later stages of **(R)-7** synthesis, it was decided to introduce the halogen moiety at the beginning of the route. Li and co-workers reported the synthesis of a racemic iodinated precursor for [¹⁸F]UCB-J.¹¹² Therefore, a new proposed synthetic route was developed involving the synthesis of an iodinated precursor for tritium labelling using similar early steps. This would involve the preparation of an iodinated cinnamaldehyde, followed by our previous developed approach (**Scheme 27**).



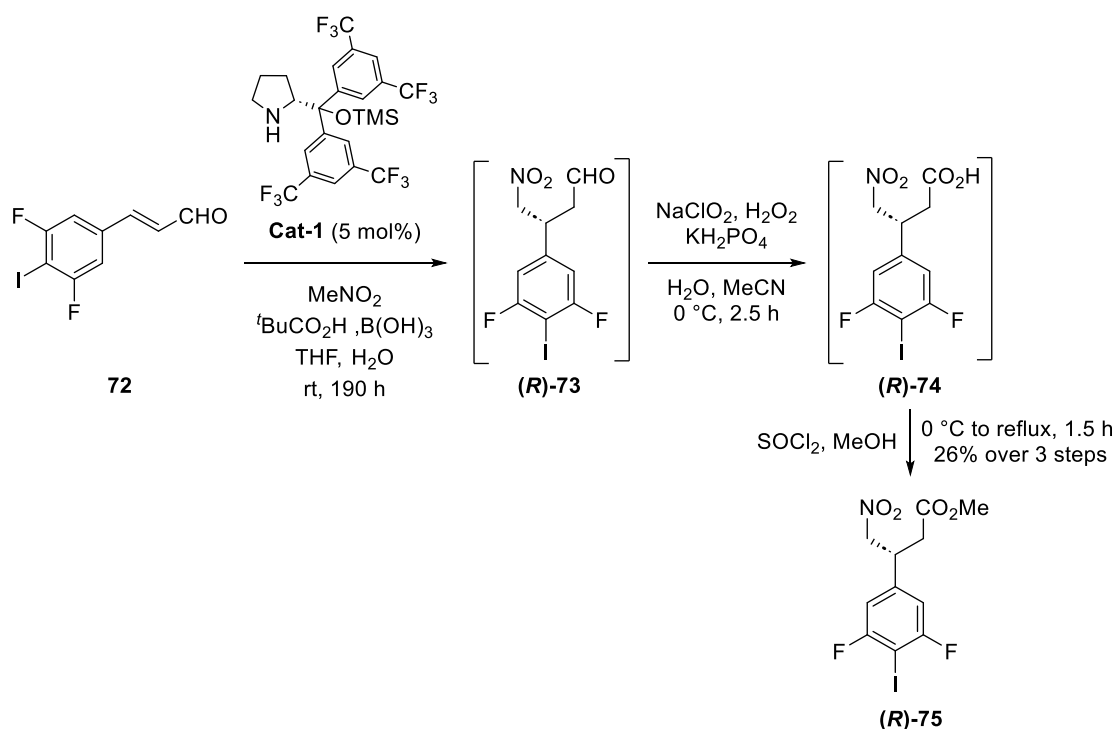
Scheme 27. Retrosynthesis of [³H]SynVesT-1.

The route began with the iodination of commercially available 3,5-difluorobenzonitrile **69**, conducted using lithium diisopropylamide as a base (**Scheme 28**). Although the published procedure reported a 1 h reaction, the best yield was achieved when left overnight.¹¹² The obtained material **70** was used without any purification as separating the product from other minor impurities turned out to be challenging. To retain the iodide, nitrile reduction was performed using mild conditions using DIBAL-H as a reducing agent. After 2 h, the reaction achieved completion and due to instability of the product to silica gel, the compound **71** was used immediately for the subsequent Wittig reaction. After the standard Wittig reaction with (triphenylphosphoranylidene)-acetaldehyde under normal conditions and with a reaction time of 16 h, cinnamaldehyde **72** was isolated in 53% yield over the three steps. Only the *E*-isomer was formed as confirmed by ¹H NMR spectroscopy, however, there were other *E*-alkenes formed in this reaction.



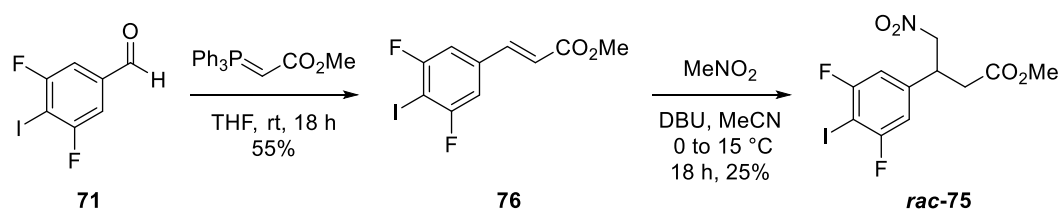
Scheme 28. Synthesis of cinnamaldehyde **74**.

α,β -Unsaturated aldehyde **72** was then used for an asymmetric conjugate addition with nitromethane under standard conditions and using Hayashi-Jørgensen's organocatalyst **Cat-1** (**Scheme 29**). As previously mentioned, the catalyst used was a mixture with the deprotected prolinol derivative **Cat-4**, although, this had not been identified at the time. During the first attempt using this mixture of catalysts (5 mol%) led to the product conversion of 50% over five days. Adding more reagents (everything except for catalyst) only improved the conversion to 70% over 24 h. For this reason, the catalyst loading was increased to 10 mol% (which gave only 5 mol% of effective catalyst loading) and due to presence of weak electron-withdrawing iodide substituent, the reaction took 190 h to reach 95% conversion. After this step, the resulting material (**R**)-**73** without purification was subjected to a Pinnick-type oxidation and subsequent esterification using thionyl chloride and methanol. Ester (**R**)-**75** was obtained in 26% yield over the three steps. However, the yield would have been higher if pure catalyst **Cat-1** was used.



Scheme 29. Conjugate addition and esterification/lactamisation steps.

Concurrently, a corresponding racemic nitro ester (**R**)-**75** was synthesised to evaluate the enantioselectivity of the conjugate addition step using a similar approach as for the previous targets from this project (**Scheme 30**). Aldehyde **71** was submitted to a Wittig reaction with methyl (triphenylphosphoranylidene)acetate. This provided the desired methyl cinnamate **76**, which was isolated in 50% yield after overnight reaction at room temperature. Formation of only the *E*-isomer was confirmed by ¹H NMR spectroscopy, and as in the previous case other *E*-alkenes were present in the crude reaction mixture. The resulting ester derivative **76** the underwent conjugate addition with nitromethane under basic conditions to provide the desired racemic γ-nitroester **rac-75** in 25% yield. Though the yield was low, it gave enough material to perform analytical chiral HPLC.



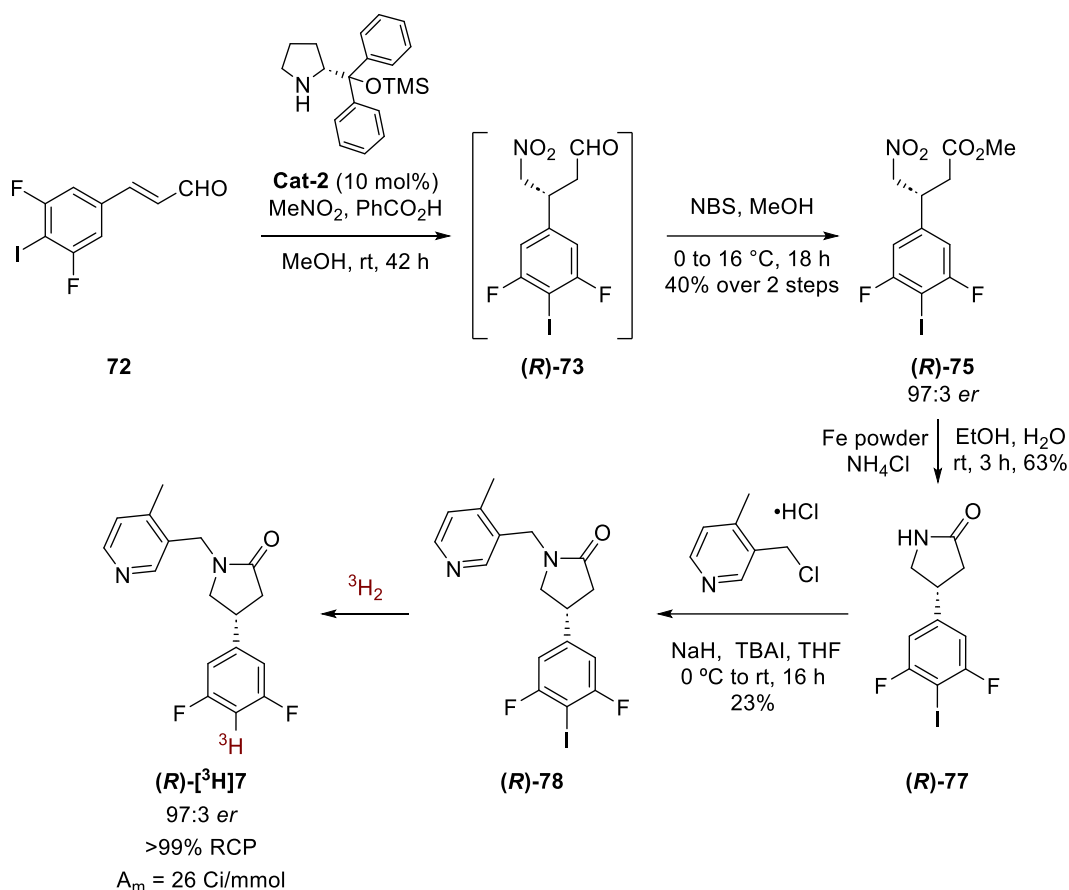
Scheme 30. Synthesis of racemic ester **rac-75**.

Having both racemate **rac-75** and enantioenriched ester (**R**)-**75** in hand, the chiral HPLC was conducted under standard conditions. The *er* value of racemate **rac-75** was confirmed by analytical chiral HPLC. Using this as a standard, the *er* value of the enantioenriched material (**R**)-**75** was determined to be 81:19, which was unexpectedly low. Apparently, the use of decomposed catalyst not only affected the yield of the conjugate addition reaction but also the enantioselectivity of the conjugation addition reaction with this substrate. Due to both factors, the decision to switch the approach was taken as by that point as the second-generation route using bis-phenyl organocatalyst **Cat-2** for a conjugate addition step as well as oxidative esterification step using NBS as an oxidant, had proved to be more efficient and faster.

2.1.5.2 Synthesis of [³H]SynVesT-1 using second-generation route

Given the known lower reactivity of the iodinated substrate **72** compared to difluorocinnamaldehyde, the conjugate addition step was tested using 10 mol% of bis-phenyl catalyst **Cat-2** (**Scheme 31**). The conjugate addition of nitromethane took

42 h for completion in the presence of catalyst **Cat-2** and benzoic acid in methanol. A significant improvement was still observed compared to the reaction in the presence of catalyst **Cat-1**, which required 190 h to reach 95% conversion although this result was achieved with 5 mol% catalyst loading. Regardless, it confirmed the assumption that introduction of the iodide-substituent changes the electronic system of the whole molecule resulting in longer reaction times for some the steps of the described route. The next step, oxidation of the resulting aldehyde **(R)-73** to ester **(R)-75**, was performed as a one-pot process with the conjugate addition step using NBS. This one-pot two-step procedure provided the desired methyl ester in 40% yield over two steps and with an *er* value 97:3. The second-generation approach provided the desired intermediate much faster and with higher enantioselectivity. The following nitro-group reduction and *in situ* cyclisation step in the presence of iron powder after basic quench gave lactam **(R)-77** in 63% yield after 3 h. The alkylation of lactam **(R)-77** using alkyl halide in the presence of sodium hydride and TBAI however reached only 65% conversion within the standard 18 h reaction time, which resulted into the isolation of desired precursor **(R)-78** in 23% yield. Once again, the presence of the iodine substituent significantly affected the outcome of this reaction. However, as a sufficient amount of precursor **(R)-78** was prepared for tritium labelling, no further optimisation was conducted. This material was then sent to Novandi Chemistry AB, where the labelling procedure was developed using tritium gas and the imaging agent [³H]SynVesT-1 **(R)-[³H]7** was obtained in >99% radiochemical purity and a molar activity of 26 Ci/mmol. The *er* value of the tritium labelled compound was also analysed and shown to be 97:3. Thus, the enantiopurity of the target compound had been retained during the synthetic route and the final step tritium labelling.



Scheme 31. Synthesis of [³H]SynVesT-1.

The radiolabelled material was used by Kelly Panichnantakul for autoradiography studies at the University of Edinburgh as part of her PhD project, which currently is being prepared for publication. One of the first studies performed using this imaging agent focused on investigating the *in vitro* binding properties of [³H]SynVesT-1 to SV2A in both healthy and cuprizone model mice. Cuprizone models are widely used to study demyelination and remyelination processes. These animal models are commonly employed in the study of Multiple Sclerosis; however, this pathology is common for many neurodegenerative disorders. In this case, mice are administered the copper-chelating agent cuprizone, a neurotoxin that induces reversible remyelination (**Figure 22**).¹¹³

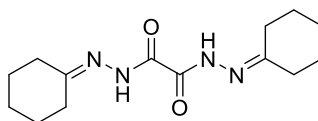


Figure 22. Structure of cuprizone.

As a result of this study, the K_d value for SynVesT-1 was confirmed as 10 nM, which matched the previous data obtained using [^{18}F]SynVesT-1. Very low non-specific binding of [^3H]SynVesT-1 along with high binding potential and ligand affinity was observed, which was consistent with previously reported values in healthy control mice using [^{18}F]SynVesT-1 autoradiography (**Figure 23**).¹⁰⁷ In addition, a decrease in SV2A receptor density was observed during demyelination with a subsequent recovery during remyelination, which reflected the changes in synaptic density and activity previously reported in the cuprizone model.^{114,115} These findings further support that SynVesT-1 is highly specific and sensitive ligand for SV2A, emphasising its potential as an effective *in vivo* biomarker of synaptic pathology.

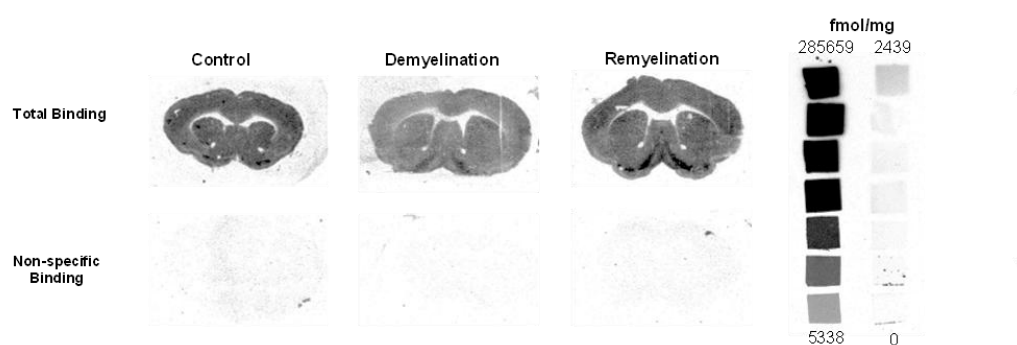


Figure 23. Autoradiograms of mouse brain sections incubated with [^3H]SynVesT-1 (top) and adjacent sections co-incubated with non-radioactive SynVesT-1 (bottom). Performed by Kelly Panichnantakul as a part of her PhD project, unpublished data.

2.1.6 Conclusions and future work

In summary, a second-generation route was developed for the synthesis of the [^{18}F]SynVesT-1, a PET imaging agent targeting SV2A, along with its non-radiofluorinated standard SynVesT-1. This new synthetic approach was based on the first-generation route previously developed by the Sutherland group but enabled a significantly shorter and more efficient synthesis of both enantioenriched γ -nitro ester intermediates (**(R)-24** and (**R)-58** through a one-pot, two-step process completed in 42 hours compared to the previous 121 hours and three-step synthesis. This process involved a conjugate addition of nitromethane catalysed by the more selective bis-phenyl Hayashi-Jørgensen organocatalyst **Cat-2** and the more effective benzoic acid cocatalyst. A single step oxidative esterification of the

resulting enantioenriched aldehyde using NBS completed the shortened synthesis of **(R)-24** and **(R)-58**. The developed approach not only accelerated the overall process but also provided access to both intermediates in improved enantiomeric ratios, 96:4 for **(R)-24** and 98:2 for **(R)-58**, compared to 94:6 and 93:7 respectively in the previous approach. For the synthesis of [^{18}F]SynVesT-1, the second-generation route also included the development of a non-toxic and more stable organoboron radiofluorination precursor **(R)-8**, which was successfully radiofluorinated to produce the target tracer [^{18}F]SynVesT-1 in high radiochemical conversion, along with high radiochemical purity and molar activity, comparable to that of the organotin precursor **(R)-6**.

In addition, a novel [^3H]SynVesT-1 radioligand synthesis was established using a second-generation route, enabling access to the desired tritium-labelled compound **(R)-[^3H]7** with high radiochemical purity, molar activity and enantioselectivity. Access to [^3H]SynVesT-1 allowed our collaborators at the University of Edinburgh to perform autoradiography studies and explore binding properties of this compound in detail.

Future work on this project will focus on further optimising the automated radiofluorination of **(R)-8** to achieve superior radiochemical yield and molar activity, thereby enabling a more efficient synthesis of [^{18}F]SynVesT-1.

2.2 Development of New PET Imaging Agents Targeting MCT1/MCT2

2.2.1 Project aims

As previously discussed in Chapter 2, MCTs are a group of transporter proteins that are ubiquitously expressed in human tissues, with isoforms 1 and 4 overexpressed in various type of cancers.^{57,58,80} The compound AZD3965 is among the most successful, selective and potent MCT1/2 inhibitors and underwent clinical trials for the treatment of solid tumours.⁷⁷ In addition to serving as cancer biomarkers, the distribution of MCT1 and MCT2 has been reported to differ in the hippocampus of patients with temporal lobe epilepsy compared to that of the healthy brain.⁶³ However, despite the prominence of this biological target, no successful PET imaging agents have been developed to date. The Sutherland group has focused on developing PET tracers targeting MCT1/2 for application in epilepsy studies. Based on the clinical candidate from AstraZeneca, several libraries of potential selective MCT1/2 inhibitors were developed in the Sutherland group by former group members.^{86,87} One lead compound, 6-phenoxy thienopyrimidinedione **37a**, demonstrated a significant decrease in lactate uptake against MCT1 in an activation assay in *Xenopus* oocytes (**Figure 24**). Continuing with the development of an effective PET tracer targeting MCT1/2, the aim of this project was to expand the previous libraries by synthesising more 6-substituted thieno[2,3-*d*]pyrimidinedione-5-carboxamides including phenoxy derivatives bearing fluoro or methoxy substituents (**37**, **Figure 24**), in order to evaluate their inhibitory activity against MCT1/2. Additionally, the synthesis of aniline derivatives **79** was explored as any bridge atom between the thiophene core and the aryl moiety could potentially improve the performance of the compounds during biological testing as evidenced by previous studies.⁸⁶ Upon completion of the libraries, the evaluation of physicochemical properties was to be conducted in order to identify the compounds that meet the specified standards for neurological PET tracers using protocols previously described.¹¹⁶ Once suitable compounds are determined, they would be subjected to the biological testing as lactate uptake inhibitors.

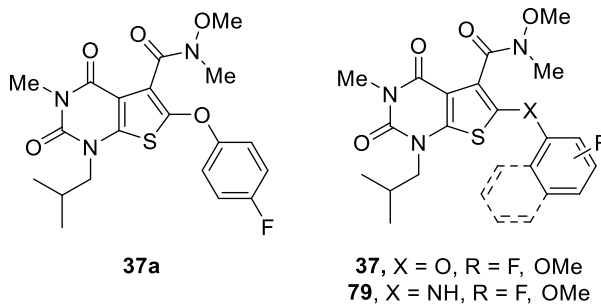
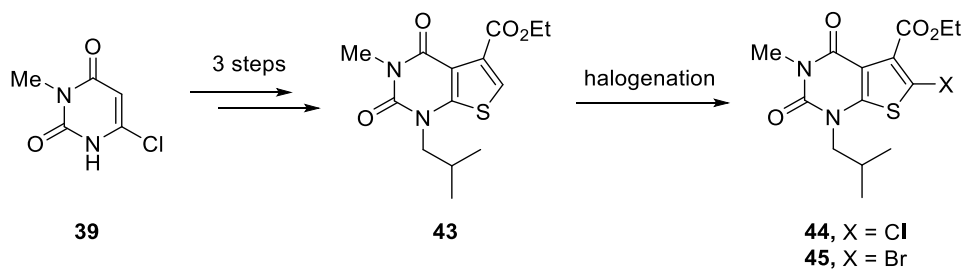


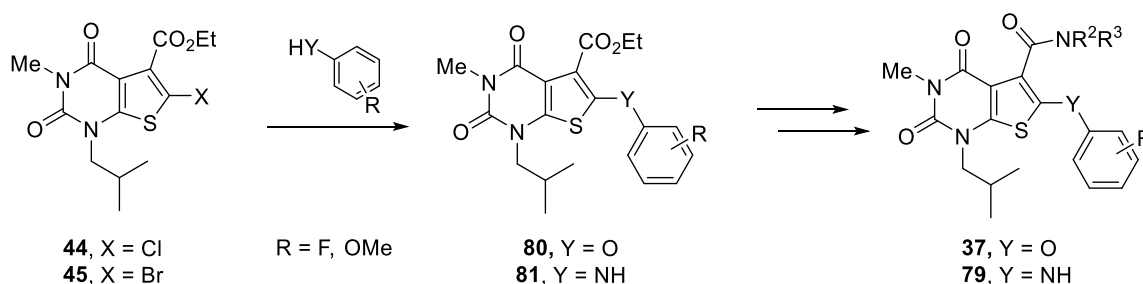
Figure 24. Previously developed and proposed thymidine-thiophene analogues.

In this project, thieno[2,3-*d*]pyrimidinediones **43** would serve as a universal intermediate and would be obtained using the synthetic route previously developed by Kerry O'Rourke and Erin Johnstone in the group (**Scheme 32**). This would be done starting from 6-chloro-3-methyluracil (**39**) which in the three steps could be converted to key thieno[2,3-*d*]pyrimidinedione intermediate **43**. Halogenation of the thiophene ring would then give advanced intermediates **44** and **45**.



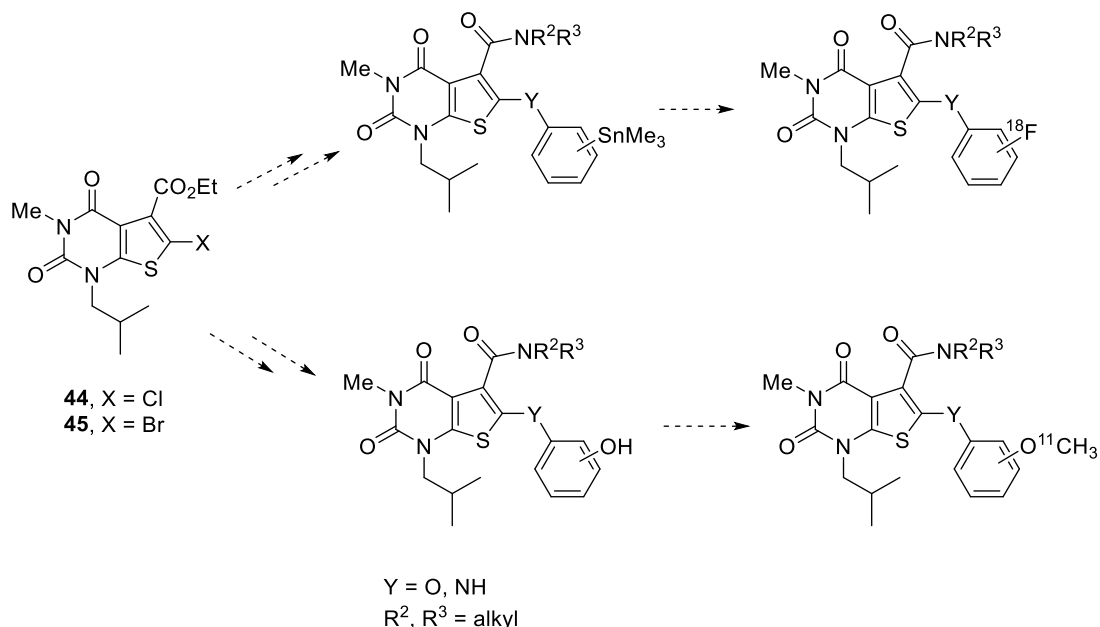
Scheme 32. Synthetic route to halogenated thieno[2,3-*d*]pyrimidinediones.

The resulting halogenated thieno[2,3-*d*]pyrimidinediones **44** and **45** would be reacted with substituted phenols and anilines (**Scheme 33**). The obtained intermediate esters **80** and **81** would be hydrolysed giving access to carboxylic acids, which would then undergo an amide coupling reaction giving access to the desired 6-substituted thieno[2,3-*d*]pyrimidinedione-5-carboxamides.



Scheme 33. Synthesis of the final thieno[2,3-*d*]pyrimidinedione targets.

The lead compound would be later synthesised as a carbon-11 or fluorine-18 labelled analogue. The key intermediate **44** and **45** also would allow the synthesis of the radiolabelling precursors by installation of the corresponding aryl group in the final stages (**Scheme 34**).

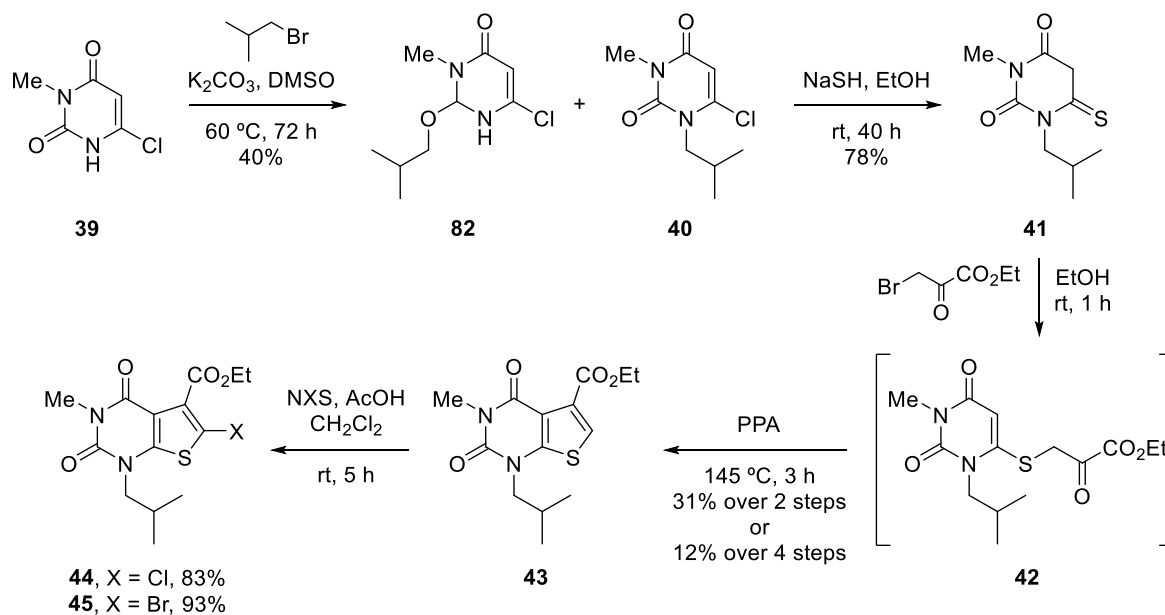


Scheme 34. Synthesis of ^{18}F - and ^{11}C -labelled analogues of the developed thienopyrimidinedione derivatives.

2.2.2 Synthesis of the phenoxy thieno[2,3-*d*]pyrimidinedione derivatives

Synthesis of the thieno[2,3-*d*]pyrimidinedione intermediate began with alkylation of 6-chloro-3-methyluracil (**39**) using potassium carbonate and isobutyl bromide at 60 °C (**Scheme 35**). Under these conditions, both the *N*- and *O*-alkylation occurred, however, the formation of the *N*-alkylated product **40** was favoured with a typical ratio of 9:1 (**40:82**) was achieved. It was reported that an increase in reaction temperature resulted in greater formation of the *O*-alkylated product **82**, yielding a 5:1 mixture.⁸⁶ Therefore, a longer reaction time was preferred. The best isolated yield of 40% of 6-chloro-1-isobutyl-3-methyl-2,4-(1*H*,3*H*)-pyrimidinedione **40** was achieved a reaction time of 72 h. However, in routine procedure the mixture was typically used after aqueous work-up without further separation of the regioisomers as formation of the *O*-alkylated product **82** was not considered problematic as it did not react in the subsequent step. Subsequently, the resulting alkylated intermediate **40** was then submitted to a reaction with sodium hydrosulfide to form thioamide **41**

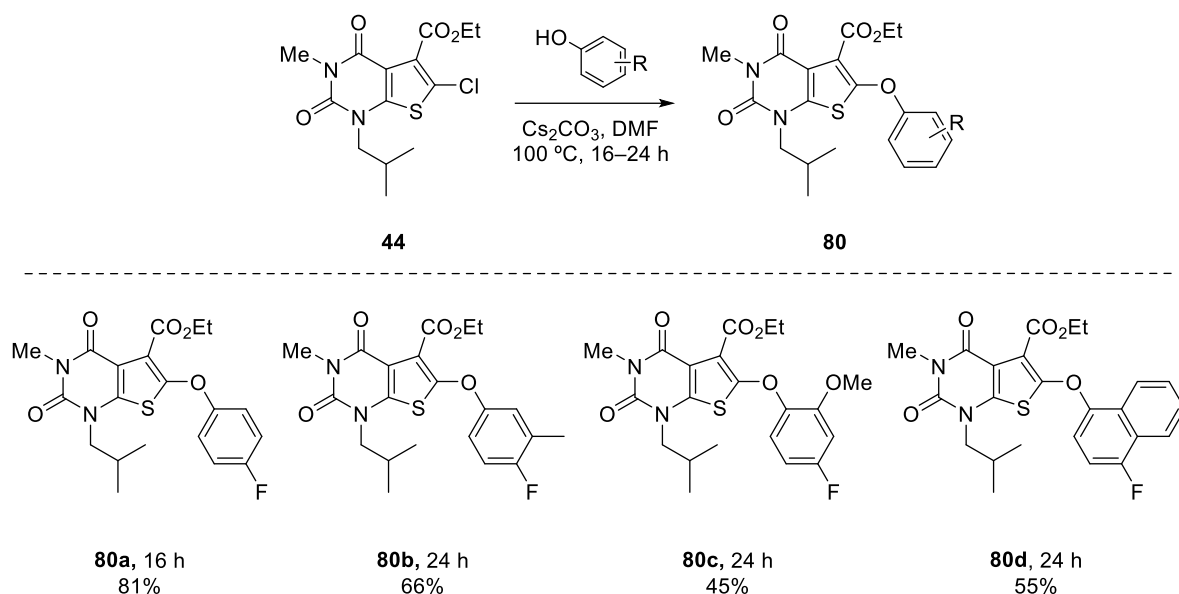
in 78% yield after 24 h. This reaction proceeded with minimal byproduct formation, typically allowing the material to be used directly in the next step without any purification. Thioamides are known to undergo thione-thiol tautomerisation; however, the NMR spectra in CDCl₃ showed the presence of only one tautomer, thione **41**. S-Alkylation of **41** using 3-bromopyruvate at room temperature was followed by subsequent cyclisation of **42** in the presence of PPA at 145 °C which provided the thieno[2,3-*d*]pyrimidinedione **43** after 3 hours in 31% yield over 2 steps. When performed on a multigram scale without intermediate purification between steps, this synthetic route gave the desired thieno[2,3-*d*]pyrimidinedione **43** in 12% yield over four steps, with up to 1 g of the intermediate **43** being produced using this approach. This product served as an intermediate for further diversification at the 6-position of the thienopyrimidinedione core. Thus, 6-chlorinated thieno[2,3-*d*]pyrimidinedione was obtained from the reaction of **44** with NCS and acetic acid in 83% yield. Similarly, a clean reaction of **43** with NBS under the identical conditions resulted in 6-bromothieno[2,3-*d*]pyrimidinedione **45** in 93% yield.



Scheme 35. Synthetic route to the 6-halogenated thieno[2,3-*d*]pyrimidinedione intermediates.

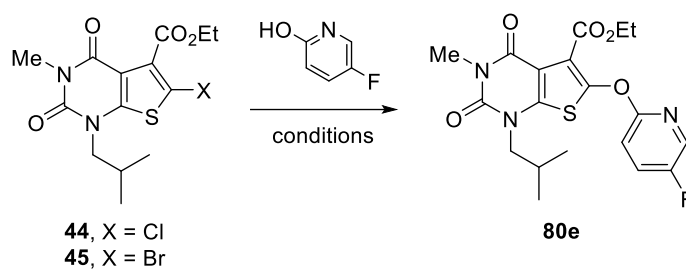
As described in previous work, 6-chlorothieno[2,3-*d*]pyrimidinedione **44** reacted with phenols to afford phenoxy derivatives in higher yields compared to the bromo-derivative **45** as it is typically observed in aromatic nucleophilic substitution reactions.⁸⁶ Therefore, chloro-derivative **44** was used in further reactions with

phenols (**Scheme 36**). The first reaction was carried out with 4-fluorophenol to obtain the standard, which could be later used to compare the inhibitory activity of the other compounds in the library. The chlorinated substrate **44** reacted with 4-fluorophenol under basic condition reaching full conversion after 16 hours at 100 °C and resulting in the formation of desired 6-phenoxy derivative **80a** in 81% yield. However, the reaction of 6-chlorothieno[2,3-*d*]pyrimidinedione **44** with 4-fluoro-3-methylphenol under the same conditions only reached 80% conversion overnight. Increasing the amount of phenol had no effect, but increasing the reaction time to 24 hours led to reaction completion, and the desired phenoxy product **80b** was isolated in 66% yield. With the aim of evaluating the effect of different substituents attached to the aryl moiety on inhibitory activity, 4-fluoro-2-methoxyphenol was also employed in a reaction with the same substrate **44**. Although this phenol was expected to be more nucleophilic due to the presence of a strong electron-donating group at the *ortho* position, steric hindrance from this substituent may have reduced its reactivity as only 50% of the starting material **44** was consumed under standard conditions after 16 hours. After 24 hours, 65% conversion was achieved, however, even despite quite a modest yield of 45%, sufficient amount of material **80c** was generated and so no further optimisation was conducted. In a study conducted by AstraZeneca, it was reported that bicyclic thienopyrimidinedione derivatives (quinoline, azaindole, benzimidazole) displayed nanomolar binding affinity for the MCT1 target and possessed good metabolic stability.¹¹⁷ To obtain structurally similar compounds but bearing a fluorine label, intermediate **44** was coupled with 4-fluoro-1-naphthol under standard conditions (**Scheme 36**). After 24 h, the reaction achieved 90% conversion which led to the isolation of the desired product **80d** in 55% yield.



Scheme 36. S_NAr reaction with fluorinated phenols.

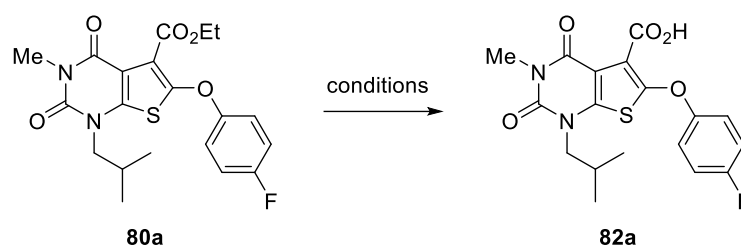
To introduce a heteroatom into the aryl moiety of the potential MCT1/2 inhibitor, 5-fluoro-2-hydroxypyridine was investigated as a nucleophile for installation at the 6-position of thieno[2,3-*d*]pyrimidin-2(1*H*)-one. Using the 6-chlorothienopyrimidin-2(1*H*)-one intermediate **44**, the coupling with the corresponding phenol was attempted under standard basic conditions at 100 °C (**Table 5**, entry 1). However, no reaction was observed and this led to the isolation of starting material **44**. Even with an increase in temperature, the desired product was not formed and only decomposition of the starting material **44** was observed (entry 2), which was likely due to the low nucleophilicity of the 2-hydroxypyridine. So instead, the same nucleophile was tested using an Ullmann-type coupling in the presence of a copper catalyst (entry 3).¹¹⁸ However, due to challenging purification of the reaction mixture when using *N*-methylpyrrolidone (NMP) as the solvent, an alternative attempt was made using DMF as the solvent (entry 4). Unfortunately, only the product of debromination **43** was isolated which would prove that the oxidative addition of substrate to catalyst took place, however, the subsequent ligand exchange with the pyridine and reductive elimination did not happen. Alternatively, coordination of the 2-hydroxypyridine with the copper catalyst may have been too effective, also inhibiting the cross-coupling reaction. At this stage, attempts to synthesise derivative **80e** were discontinued and the focus was redirected towards other targets.

Table 5. Attempted reactions of **44** and **45** with 6-chlorothienopyrimidinedione.

Entry	Starting material	Reagents/solvent	Temperature (°C)	Time (h)	Result
1	44	Cs ₂ CO ₃ /DMF	100	18	No reaction
2	44	Cs ₂ CO ₃ /DMF	130	24	44 + decomposition products
3	45	CuI, TMHD, Cs ₂ CO ₃ /NMP	120	18	43
4	45	CuI, TMHD, Cs ₂ CO ₃ /DMF	120	18	43

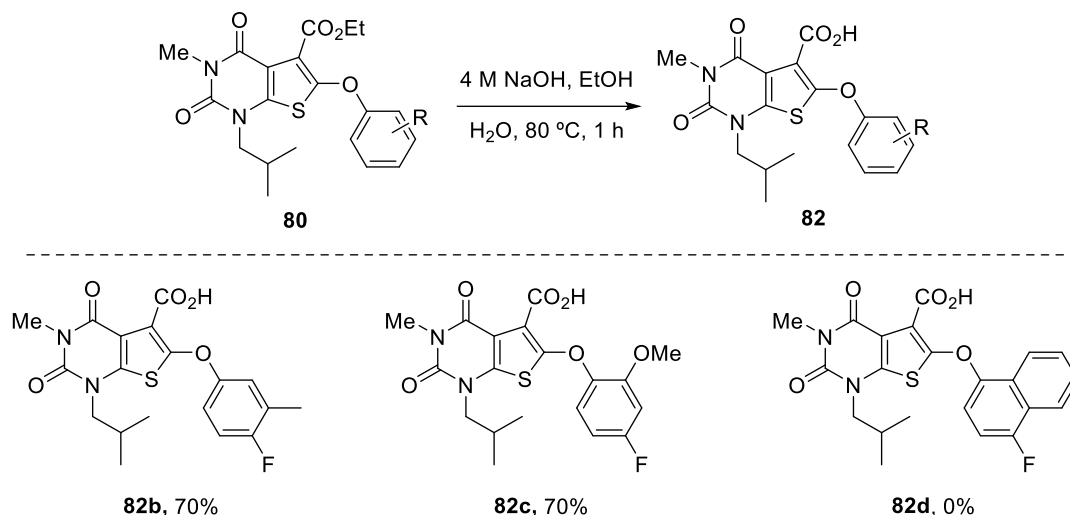
TMHD – 2,2,6,6-tetramethyl-3,5-heptanedione

Hydrolysis of esters **80a–d** was subsequently investigated. Initially, the standard conditions previously applied for the earlier libraries – 10% sodium hydroxide solution in a mixture of tetrahydrofuran (THF) and methanol was investigated (MeOH was used as a co-solvent to ensure reaction mixture homogeneity) (**Table 6**, entry 1).⁸⁶ Surprisingly, the desired carboxylic acid was achieved in only 28% yield from the ester hydrolysis of thieno[2,3-*d*]pyrimidinedione **80a**. Thus, optimisation of the reaction was initiated. Hydrolysis using a 10% sodium hydroxide solution at an elevated temperature of 40 °C was then attempted, but in this case the carboxylic acid **82a** was isolated in a lower yield of 14% (entry 2). The low yield was attributed to possible decomposition of the starting material **80a**. Therefore, a milder base, caesium carbonate, was subsequently investigated. The reaction at room temperature did not lead to the formation of any product, and similarly no conversion was observed at 40 °C, with only starting material **80a** being recovered (entry 3). Increasing the reaction temperature to 65 °C (entry 4) and extending the reaction time to 24 hours led to the isolation of **82a** in 72% yield (entry 5).

Table 6. Optimisation of ester hydrolysis of **80a**.

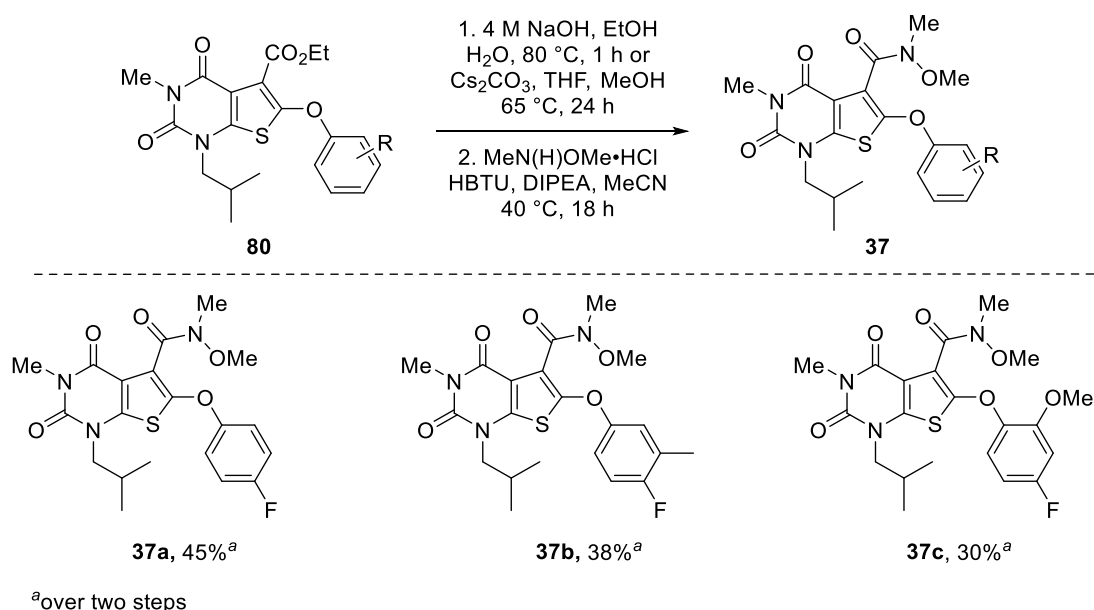
Entry	Base	Temperature (°C)	Time (h)	Solvents	Yield (%)
1	10% NaOH solution	rt	1	THF/MeOH	28
2	10% NaOH solution	40	1	THF/MeOH	18
3	Cs ₂ CO ₃	rt to 40	24	THF/MeOH	–
4	Cs ₂ CO ₃	65	16	THF/MeOH	68
5	Cs ₂ CO ₃	65	24	THF/MeOH	72

Ester hydrolysis of **80b** and **80c** was then attempted under these conditions, however, it gave only traces of the desired carboxylic acids. Instead, more forcing conditions, involving 4 M sodium hydroxide, but for a shorter reaction time of 1 hour were used and gave both carboxylic acids **82b** and **82c** in 70% yield (**Scheme 37**). The resulting carboxylic acids were found to be relatively unstable, therefore, were used immediately without further purification in the subsequent amide coupling reaction. Ester hydrolysis of **80d** did not proceed within the standard 1-hour reaction time and an increase in time (16 hours) only resulted in the decomposition of the starting material. Due to the high cost of the 4-fluoronaphthol, no further attempts were made to perform ester hydrolysis of the compounds **80d**, and it was subsequently removed from the library.



Scheme 37. Ester hydrolysis of **80**.

The final step of the described synthetic route was the amide coupling of the carboxylic acids with *N,O*-dimethylhydroxylamine to form the target Weinreb amides **37** (**Scheme 38**). Under the previous standard conditions, used in the previous reports using a combination of HBTU as a coupling agent and Hünig's base gave the corresponding 5-carboxamides in 38–45% yield over two steps.⁸⁶

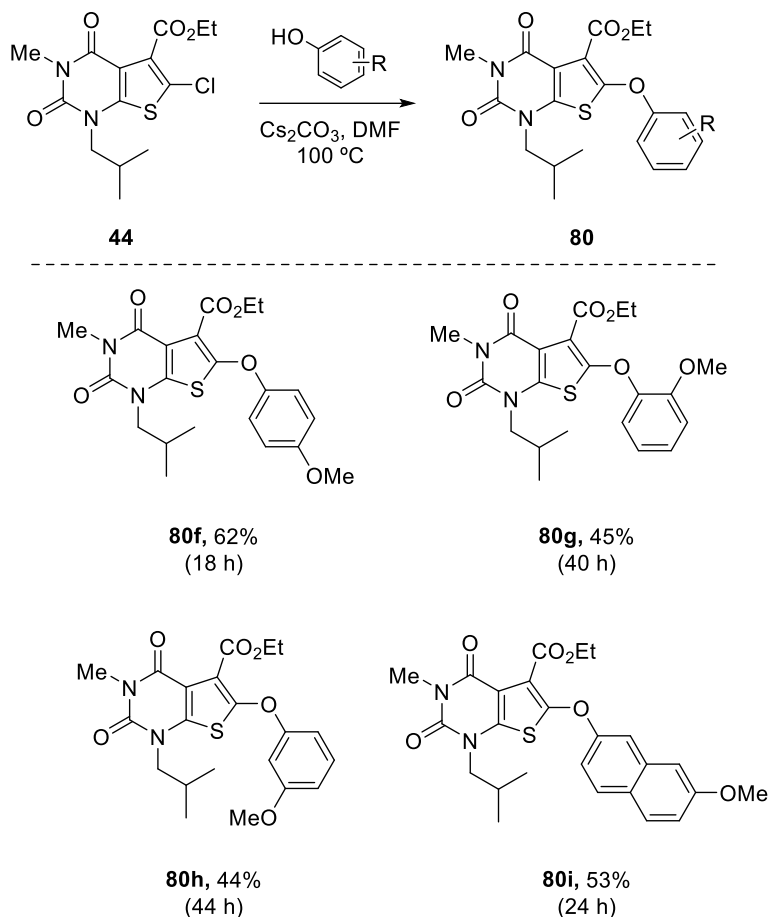


Scheme 38. Formation of the Weinreb amides with *N,O*-dimethylhydroxylamine.

2.2.3 Synthesis of the methoxylated MCT1/2 inhibitors

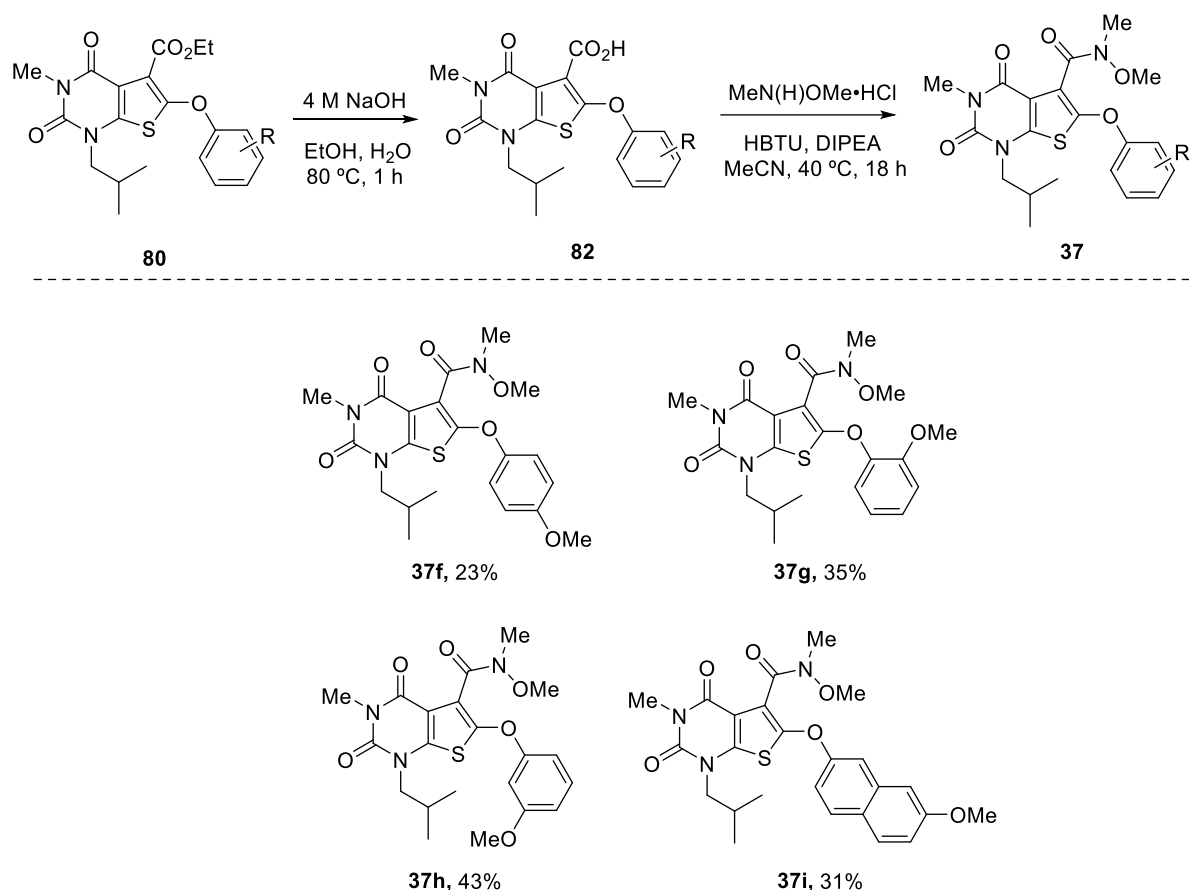
Upon completion of the synthesis of the fluorinated targets, a small library of methoxylated compounds was generated. The inclusion of methoxy-group to the

final inhibitors would enable synthesis of ^{11}C -labelled compounds for PET imaging. To achieve this, three phenols as well as a naphthol were reacted with 2-chlorothiophene **44** under standard conditions (**Scheme 39**). It is worth noting that reactions with methoxylated phenols required a higher loading of nucleophile compared to the 4-fluorophenol (2 equivalents vs standard 1.5 equivalents). Under optimised conditions, the reaction with 4-methoxyphenol was completed after 18 hours, resulting in the isolation of the desired phenoxy derivative **80f** in 62% yield. The reaction with 2-methoxyphenol under the same conditions reached 90% conversion after 40 hours, and the desired product **80g** was isolated from the reaction mixture in 45% yield. The reduced reactivity of this phenol can again be explained by the steric hindrance caused by the methoxy substituent. Similar results were observed for 3-methoxyphenol as the full conversion was only achieved after 44 hours at 100 °C, with the desired phenoxy derivative **80h** isolated in 44% yield. In this case, the methoxy group did not have any electron-donating effect due to absence of resonance effect, instead acting as an inductive electron-withdrawing group. As previously mentioned, the compounds with the bicyclic aryl moiety exhibited promising results in the AstraZeneca *in vitro* assay.¹¹⁷ Since the previous attempt to synthesise a fluorophenoxy derivative **82d** was unsuccessful due to challenges with ester hydrolysis step and the high cost of the 4-fluoronaphthol, the synthesis of methoxy analogue **80i** was attempted. Accordingly, the reaction of the 6-chlorothieno[2,3-*d*]pyrimidinedione **44** with 6-methoxynaphthol after 24 hours afforded the corresponding naphthol derivative **80i** in 53% yield.



Scheme 39. Synthesis of the methoxyphenoxy-thienopyrimidinedione derivatives.

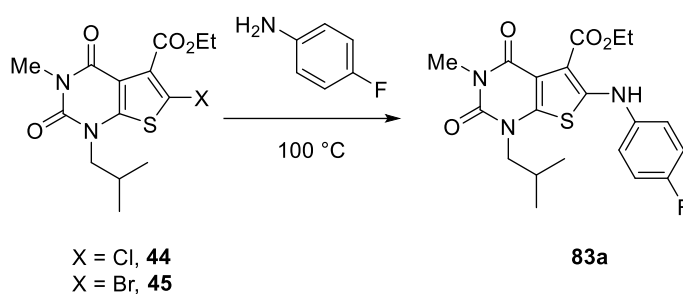
Once the intermediate phenoxy ester derivatives **80f–i** had been successfully synthesised, the subsequent ester hydrolysis and amide coupling steps were performed using established procedures. Sodium hydroxide was used as a base for ester hydrolysis and *N,O*-dimethylhydroxylamine in combination with HBTU and Hünig's base were used for preparation of the Weinreb amides (**Scheme 40**). The intermediate carboxylic acids **82f–i** were found to be more stable compared to fluorophenyl analogues **82a–c**; however, they were still used without purification in the subsequent amide coupling step. The target Weinreb amides **37f–i** were obtained in 23–43% yield over the two steps, in similar results to that observed for the fluorinated analogues **37a–c**.



Scheme 40. Ester hydrolysis and amide coupling reactions of substrates **37f–i**.

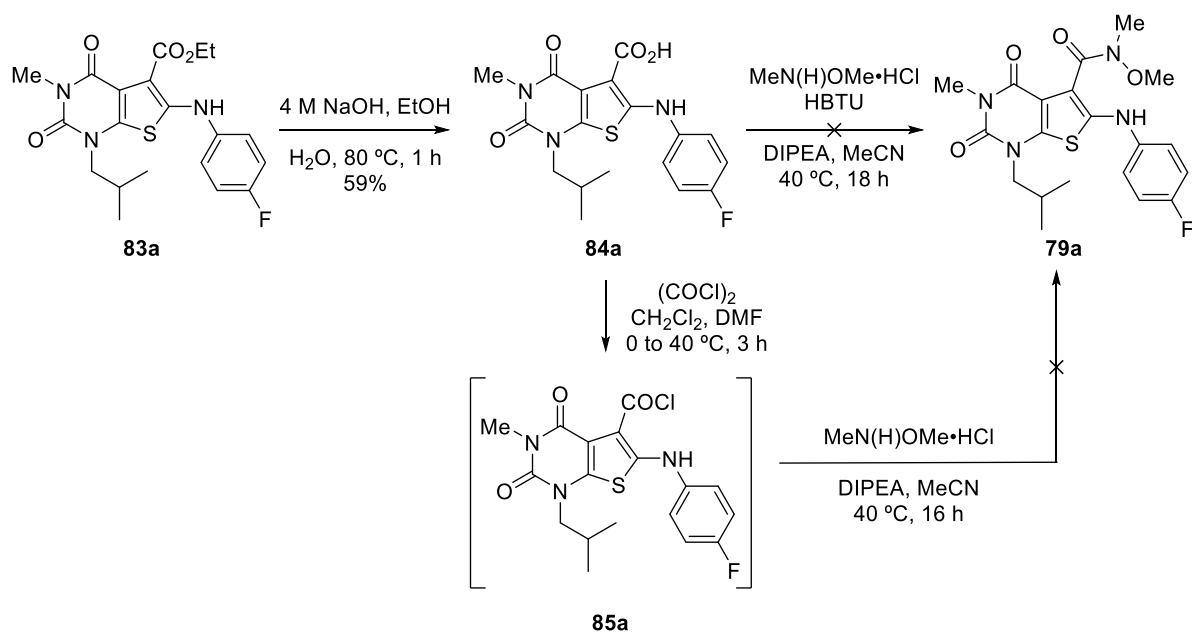
2.2.4 Synthesis of phenylamino thieno[2,3-*d*]pyrimidinedione derivatives

Given the interest in diversifying the libraries by varying bridging heteroatoms between the thiophene core and aryl side chain, a new series of potential MCT1/2 inhibitors featuring a fluorinated aniline moiety at the C6-position was also investigated. First, the incorporation of 4-fluoroaniline was attempted (**Table 7**). The $\text{S}_{\text{N}}\text{Ar}$ reactions of both 6-chloro and 6-bromo substrates **44** and **45** with this nucleophile were initially explored; however, in both cases only the starting materials were recovered (entries 1 and 2). Instead, a Buchwald-Hartwig type reaction was attempted for the coupling of **45** with 4-fluoroaniline using the conditions previously reported for related compounds.¹¹⁹ Initially, the use of palladium(II) acetate gave no product (entry 3). However, switching to $\text{Pd}(\text{dba})_2$ as the catalyst gave coupled product **83a** in 23% yield after 16 h (entry 4). Using a longer reaction time finally yielded **83a** in 68% yield (entry 5), however this reaction turned out to be not reproducible.

Table 7. Coupling of **44** and **45** with 4-fluoroaniline.

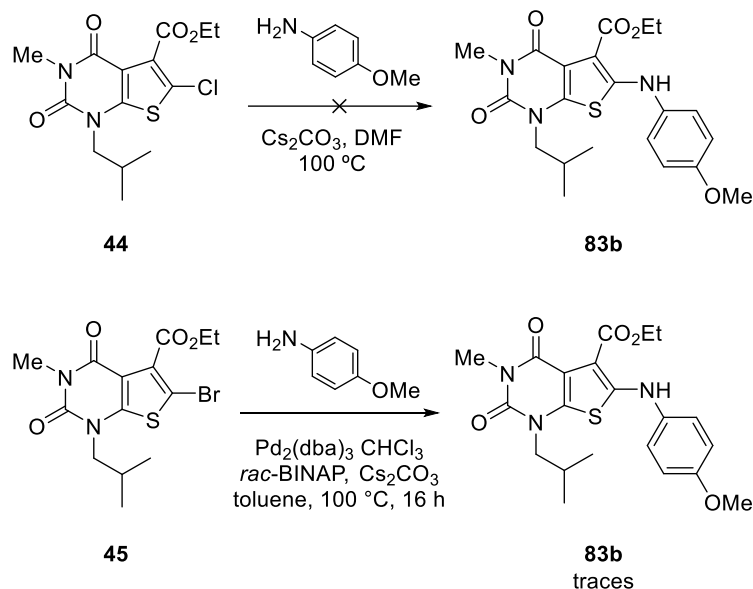
Entry	X	Reagents	Solvent	Time (h)	Yield (%)
1	Cl	Cs ₂ CO ₃	DMF	16	–
2	Br	Cs ₂ CO ₃	DMF	16	–
3	Br	Pd(OAc) ₂ (3 mol%), <i>rac</i> -BINAP, Cs ₂ CO ₃	toluene	16	–
4	Br	Pd(dba) ₂ (10 mol%), <i>rac</i> -BINAP, Cs ₂ CO ₃	toluene	16	23
5	Br	Pd(dba) ₂ (10 mol%), <i>rac</i> -BINAP, Cs ₂ CO ₃	toluene	24	68

While the optimisation study of the Buchwald-Hartwig reaction was ongoing, the material prepared for initial reaction was used to explore the ester hydrolysis and amide coupling steps. Ester hydrolysis of **83a** using 4 M sodium hydroxide gave carboxylic acid **84a** in 59% yield (**Scheme 41**). Attempted coupling of carboxylic acid **84a** with *N,O*-dimethylhydroxylamine in the presence of HBTU and Hünig's base did not yield the expected Weinreb amide **79a** and only starting material was recovered. Instead, a different synthetic approach was attempted via an acid chloride formation as an alternative activated form of the carboxylic acid. However, the subsequent amide coupling reaction did not yield the desired Weinreb amide **79a**, however, this could be caused by the fact that acyl chloride **85a** did not form either. Given the challenges encountered with the Buchwald-Hartwig reaction and amide coupling steps, the synthesis of analogue **79a** was abandoned, in favour of switching to a stronger nucleophile which was expected to provide more reliable and consistent results.



Scheme 41. Attempted amide synthesis with **79a**.

As previously noted, since the synthesis of thienopyrimidinedione derivative **79a** bearing a 4-fluoroaniline substituent was unsuccessful, efforts focused on the synthesis of the corresponding 4-methoxyaniline derivative **83b** (**Scheme 42**). Due to the higher nucleophilicity of this species, aromatic nucleophilic substitution of the 6-chlorinated substrate **44** was investigated. However, this reaction did not lead to the formation of the desired product, and only starting materials were isolated. Instead, a Buchwald-Hartwig type reaction using $\text{Pd}_2(\text{dba})_3$ as a catalyst was attempted under the previously used for 4-fluoroaniline reaction conditions, despite poor reproducibility.¹¹⁹ Unfortunately, this reaction only yielded traces of the desired product. Due to these challenges, the aniline library was entirely discontinued, and subsequent efforts were primarily directed towards the phenol derivatives in the further study.



Scheme 42. Attempted coupling of 6-halogenated thieno[2,3-*d*]pyrimidinediones with 4-methoxyaniline.

2.2.5 Evaluation of physicochemical properties

As a result, two small libraries of novel fluorinated and methoxylated phenoxy-thieno[2,3-*d*]pyrimidinedione derivatives were synthesised through the established seven step route. The next stage involved evaluation of the physicochemical properties, such as membrane permeability (P_m), membrane partition coefficient (K_m) and determination of the calculated partition coefficient (clogP).

As these compounds were developed as potential PET imaging agents targeting MCT1/2 proteins located in the central nervous system (CNS), they were required to meet specific criteria in terms of physicochemical properties, derived for CNS-targeted PET tracers, which are outlined in **Table 8**.¹²⁰ These values are based on an investigation performed by our collaborators that examined ten imaging agents used in clinical studies as PET and single photon emission computed tomography (SPECT) tracers. The four presented parameters play a crucial role in understanding compounds' behaviour and their interactions within the biological environment. In the study, upper limits for these four physicochemical parameters were established using HPLC methodologies, enabling early identification and exclusion of unsuitable compounds, thereby avoiding unnecessary use of time and resources in subsequent imaging agent development. The first important criterion was identified was $\log P$, which is derived from partition coefficient (P) and reflects the distribution of a

compound between the lipophilic and hydrophilic environments. $\log P$ is a measure of lipophilicity of a compound and indicates its ability to cross the blood-brain barrier. This value is determined as:

$$\log P = \log_{10} \left(\frac{[\text{compound}]_{\text{octanol}}}{[\text{compound}]_{\text{water}}} \right)$$

The next parameter, the membrane partition coefficient K_m , represents the distribution of a compound between the membrane and the aqueous phase, providing insight into its interaction with biological membranes.¹¹⁶ The membrane permeability P_m indicates the rate at which a compound crosses the membrane via passive diffusion, and for the compounds that utilises this mechanism P_m is directly proportional to K_m :

$$P_m = \frac{MW}{K_m}$$

The final parameter highlighted in the study, plasma protein binding (%PPB), indicated the proportion of a compound that is reversibly bound to the plasma proteins, thereby influencing the amount of the compound available for biological activity or metabolism.

Table 8. The requirements for the novel CNS PET tracers.

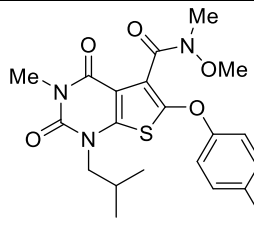
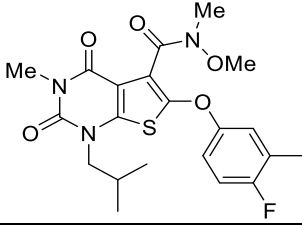
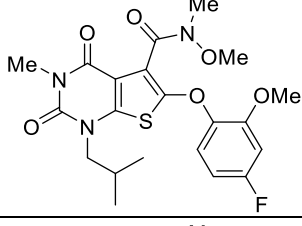
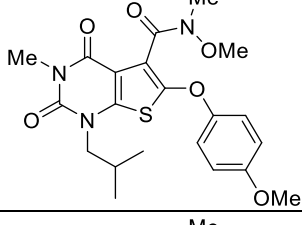
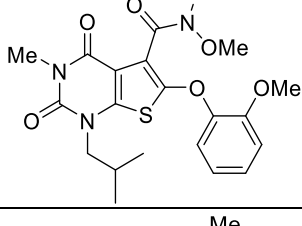
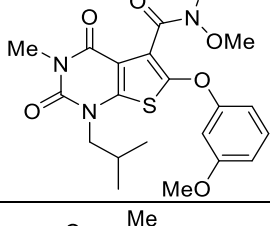
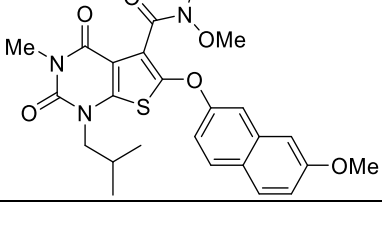
Physicochemical property	Desired value
$\log P$	<4
K_m	<250
P_m	<0.5
%PPB	<95%

Typically, $\log P$ value is determined using the flask method.¹¹⁶ The compound is dissolved and mixed in an equal volume of octanol and water, and the amount of the compound in each phase is subsequently determined. In addition, $\log P$ can also

be determined by HPLC analysis of the compound using a reverse phase HPLC column, where the retention times are used to calculate the chromatographic hydrophobicity index (CHI), which is then employed to determine $\log P$ value. In many cases, $\log P$ is calculated using computational tools that employ various algorithms. One of the most common is the fragment-based approach, in which molecules are broken down into fragments with known $\log P$ values. The resulting calculated value is referred to as $\text{clog}P$.¹²¹ In this work, two different online calculators were used to obtain $\text{clog}P$ and $\text{miLog}P$ values.^{122,123} The K_m value can be evaluated through a liposome partitioning assay, but it is typically calculated using data obtained from HPLC chromatography with an immobilised artificial membrane (IAM) column as was done in this work.¹²⁴ The %PPB value can be determined by equilibrium dialysis, ultrafiltration or ultracentrifugation but the HPLC analysis using a human serum albumin (HSA) column is more commonly employed.¹²⁵ However, this value was not determined in current study due to technical difficulties with the HSA column.

In total in this work, $\text{clog}P$, K_m and P_m values were obtained for seven compounds from two libraries of fluorinated and methoxylated thieno[2,3-*d*]pyrimidinedione derivatives **37** (**Table 9**). Turning to the results of the physicochemical property study, all calculated $\log P$ values were found to be below the established threshold, with the exception of the methoxynaphthol derivative **37i**. However, as the value did not deviate significantly from the desired limit and was a calculated rather than an experimentally measured value, the compound **37i** was retained in the library. The K_m values of all compounds also met the specified criteria, remaining well below the threshold of 250. The P_m value for all the compounds were also found to be well below the threshold, with only methoxynaphthol derivative **37i** approaching the limit yet still remaining within acceptable limits. Thus, all compounds from both libraries **37a-c** and **37f-i** met the requirements for potential PET tracers in terms of physicochemical properties and were selected for subsequent biological evaluation.

Tables 9. Physicochemical properties evaluation of novel thieno[2,3-d]pyrimidinediones **37**.

Compound	Structure	$cLogP^{123}$ $miLogP^{122}$	P_m	K_m	Selected for further testing
37a		2.9825* 3.01**	0.1641	71.53	✓
37b		3.2909* 3.39**	0.2568	115.43	✓
37c		2.9911* 2.80**	0.1469	68.37	✓
37f		2.852* 2.90**	0.1510	67.56	✓
37g		2.852* 2.66**	0.1242	55.60	✓
37h		2.852* 2.88**	0.1682	75.27	✓
37i		4.0052* 4.07**	0.4871	242.36	✓

2.2.6 Conclusions and future work

In conclusion, two libraries of 6-substituted pyrimidinedione derivatives **37a–c** and **37f–i** were synthesised using established an eight-step synthetic route (**Figure 25**). These compounds featured a thienopyrimidindione core, were based on the successful AstraZeneca MCT1 inhibitor clinical candidate AZD3965 and were developed as potential PET imaging agents for neurological applications.⁶⁰ The synthesised compounds had oxygen bridge atom between the thiophene and aryl moieties, as the compounds with this structural element had demonstrated improved results in the previous biological assays.⁸⁶ Attempts were made to synthesise compounds containing *N*-bridge atom; however, the synthesis proved challenging and these compounds were not obtained in this study. The physicochemical properties (*clogP*, *P_m* and *K_m*) of all synthesised compounds were evaluated and all showed values within the acceptable limits, allowing these to proceed to the next step.

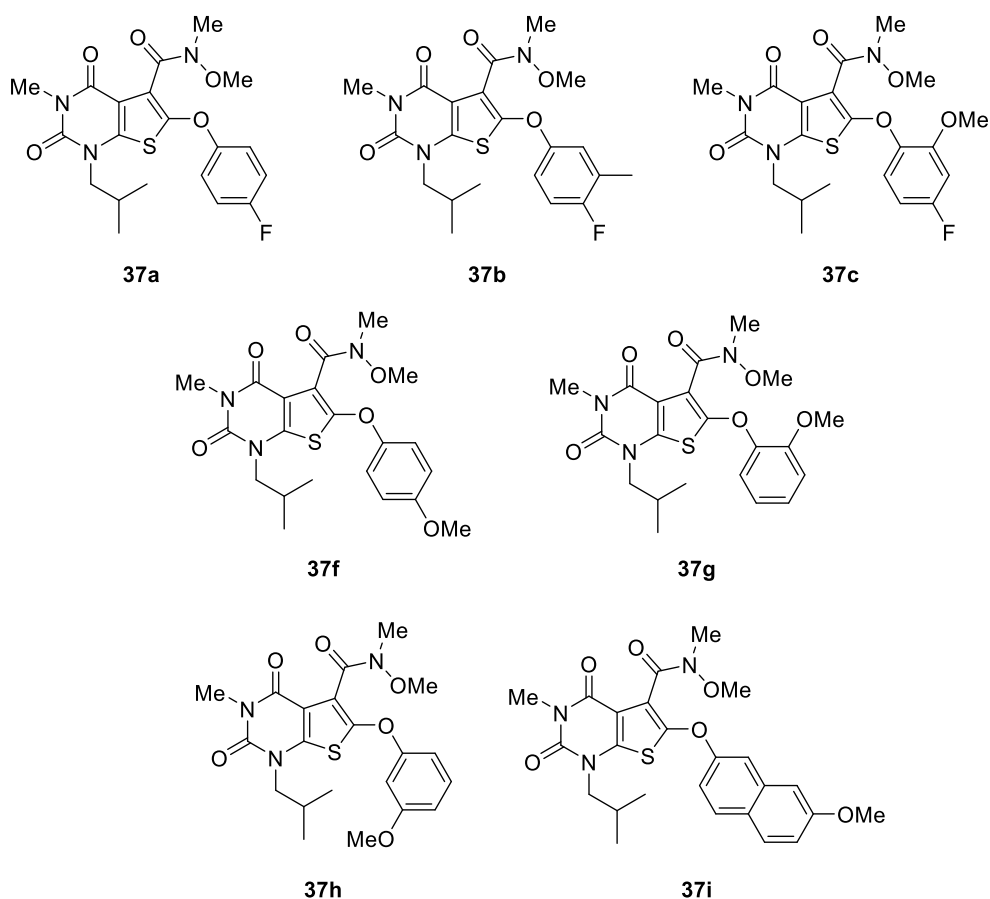


Figure 25. Thieno[2,3-*d*]pyrimidinedione derivatives synthesised in this project.

Future work for this project will involve conducting biological testing of the synthesised phenoxy derivatives **37**, specifically assessing lactate uptake inhibition. For the most potent compound, a carboxamide analogue with (4*S*)-hydroxyisoxazolidine as the amino component will also be synthesised to evaluate any potential differences in activity and stability as these analogues previously demonstrated superior lactate uptake inhibition results (**Figure 26**).^{86,117}. Once the final lead compound is determined, development of the appropriate radiolabelling precursor will be conducted, followed by optimisation of the radiolabelling procedure.

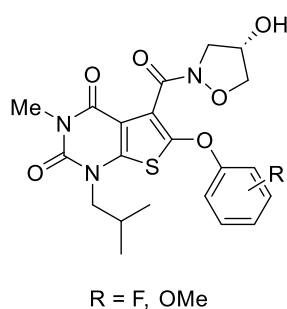


Figure 26. Thieno[2,3-*d*]pyridinedione carboxamide with (4*S*)-hydroxyisoxazolidine amine component.

2.3 Development of New Fluorescent Tryptophan-Based α -Amino Acids

2.3.1 Fluorescence imaging

Another important imaging modality is fluorescence imaging, which utilises fluorescent probes to enable non-invasive visualisation of molecular and cellular processes.^{126,127} Fluorescent probes contain fluorophore that are excited by light at a specific wavelength corresponding to the fluorophore, resulting in emission of light at a different wavelength. This process is illustrated by the Jablonski diagram in **Figure 27**: the photon energy transfers the molecule (A) to a higher excited electronic state S_2 , where it remains for a very brief period (on the order of a few nanoseconds) before undergoing internal conversion of energy (B). The internal conversion typically occurs through vibrational relaxation and heat loss. In the case of fluorescence, when electrons return (C) to the ground state S_0 via the fast singlet state S_1 , the emitted light has a longer wavelength compared to the absorbed light. This difference in wavelength is known as the Stokes shift.

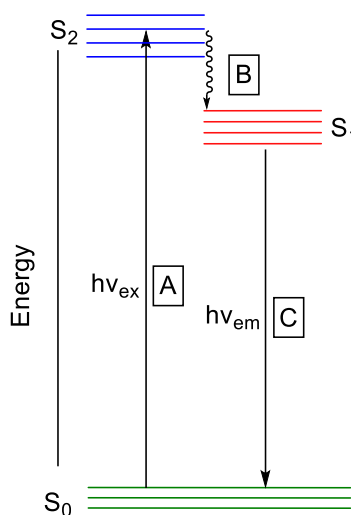


Figure 27. Jablonski diagram for fluorescence process.

Fluorescence imaging has become widely used due to the fact that the use of fluorescent probes is less expensive and less complex, particularly in comparison to radioactive ones, while it is also safer for both patients, clinical staff, and researchers.¹²⁸ The use of fluorescent probes enables visualisation of various processes with high sensitivity and spatial resolution, and it also allows

simultaneous imaging with multiple labels at the same time. In comparison to radiopharmaceuticals, fluorescent probes generally exhibit significantly greater stability. Fluorescence imaging also enables real-time visualisation during a surgery process. However, nuclear and optical imaging should be regarded not as competing methods but rather as complimentary techniques.

Regarding the limitations of optical imaging, it is restricted by light penetration depth.¹²⁹ In addition, fluorescent probes are prone to photobleaching, when the degradation of a fluorophore happens due to the exposure to light. Also, incorporation of a fluorophore into a known molecule often results in significant structural changes as only specific structures with extended conjugation typically exhibit fluorescent properties.

Despite its limitations, fluorescence imaging is widely used in both clinical and research settings. One of the most significant clinical applications of fluorescence is fluorescence-guided surgery, which enables real-time visualisation using fluorescent probes during surgical procedures.¹³⁰ This method is widely employed in oncological surgeries, particularly for performing lymphography. In such cases, the combination of fluorescence imaging with nuclear imaging gives excellent results. In addition to applications in tumour resection, fluorescent probes are extensively used for visualisation during surgeries on urinary and biliary tracts. Another widely used technique is fluorescence microscopy, which allows determination of protein location and interactions and is also employed for visualising ion transport and metabolism, assessing cell viability, neuron tracing, and various other applications.^{131,132} Fluorescence microscopy includes techniques such as two-photon microscopy, wide-field microscopy, total internal reflection fluorescence microscopy, structured light microscopy, laser scanning confocal fluorescence microscopy. Each technique differs in terms of resolution, imaging depth and cost, therefore the choice of a specific method depends on the aim and conditions of the study. These techniques could also be used in combination with other microscopy techniques, such as electron microscopy. Another important approach in fluorescence imaging is near-infrared (NIR) fluorescence imaging, which utilises fluorophores with emission in the near infrared range (above 700 nm).¹²⁹ In clinical practice, this method can be used for visualisation of various type of cancer tumours, such as gastric, breast and gynaecological as well as in imaging

of cardiovascular and infectious diseases.^{133–136} Several other methods exist, including those that combine NIR fluorescence with PET imaging, which is used in the diagnostics of glioblastomas and renal cell carcinomas.^{129,137} Another important fluorescence imaging approach is photoacoustic molecular imaging, where instead of detecting light emission, ultrasound acoustic waves generated as a result of tissue expansion are detected and analysed.^{128,138} This approach is broadly used for the visualisation of cardiovascular system.

Chromophores used in fluorescence imaging can be endogenous, including naturally occurring molecules in the body such as haemoglobin or melanin, which are widely analysed in photoacoustic imaging.¹³⁹ However, exogenous imaging agents are more commonly used; these include a variety of compounds such as proteins, antibodies, peptides, and various small molecules. Among the first group of fluorescent probes, green fluorescent protein (GFP) and its derivatives are among the most well-known fluorescent proteins.¹⁴⁰ GFP was first isolated from jellyfish *Aequoria victoria*. Subsequently, the gene encoding this protein was introduced into the cells of various living organisms, making GFP and its derivatives invaluable tools for cell biology and live-cell imaging.¹⁴¹ As a recognition of the importance of this discovery, the Nobel prize in Chemistry was awarded to Osamu Shimomura, Martin Chalfie and Roger Y. Tsien in 2008. Since the discovery of GFP, numerous other fluorescent proteins have been developed and are now employed in a wide range of applications in cell biology and beyond.^{142,143} Apart from large proteins, numerous fluorescent dyes are also employed for fluorescence imaging both on their own and in conjugation with other molecules. One of the prominent examples among these are cyanine dyes, which include indocyanine green (ICG), one of the most widely used NIR fluorescent imaging agents (**Figure 28**).¹⁴⁴ It has been approved by the FDA for hepatic function studies, ophthalmic angiography, vascular system imaging and in certain cases for lymphatic mapping.¹⁴⁵ It is also used for various other clinical applications.^{146–148} Other cyanine dyes are also commonly used for different applications as well as methylene blue which is another NIR fluorescent probe and has been reported to aid in the detection of small intestinal NETs.¹⁴⁹ Other important groups of fluorescent dyes are fluorescein-based and rhodamine-based dyes.¹⁵⁰ These dyes along with cyanine dyes are also widely used in conjugation with antibodies, nucleotides and peptides for various biomedical imaging purposes.^{150,151} Antibody-dye conjugates are particularly used for cancer visualisation, with several

currently undergoing clinical trials. These include benvazucimab-800CW for breast cancer imaging, FITC-adalimumab for imaging of Crohn's disease,¹⁵² and panitumumab-IRDye800CW for pancreatic adenocarcinoma imaging.¹⁵³ Other notable applications of these dyes involve their use in combination with nanoparticles and liposomes.^{154,155}

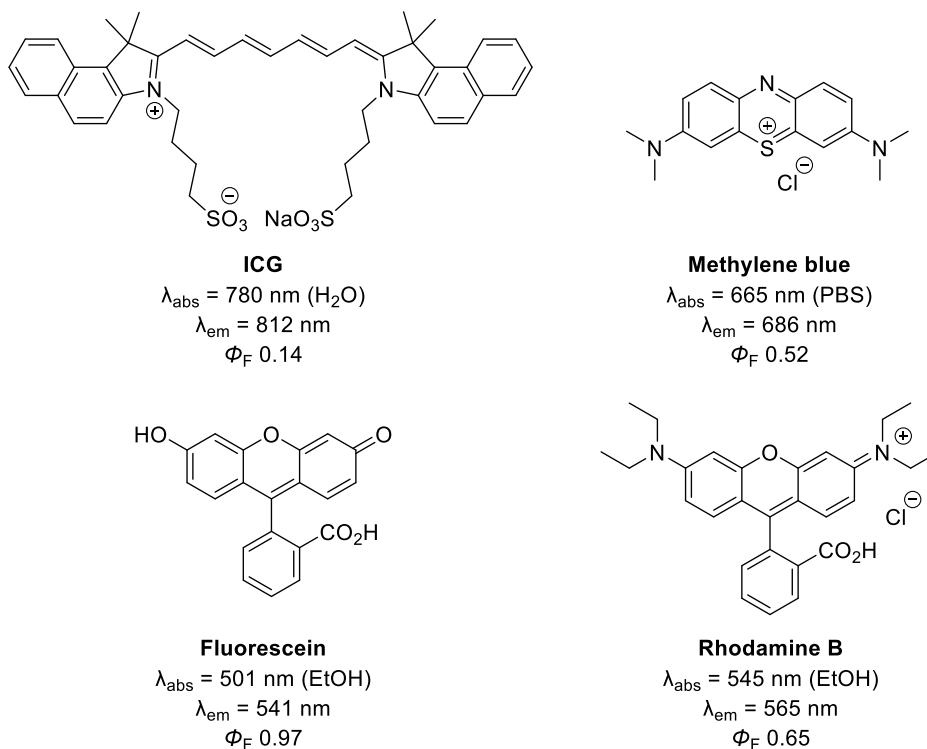


Figure 28. Structure of some fluorescent dyes used for medical applications.^{156–159}

λ_{abs} – absorbance maxima, λ_{em} – emission maxima, Φ_F – quantum yield.

2.3.2 Fluorescent amino acids

Another approach for constructing fluorescent peptides and proteins involves incorporation of fluorescent amino acids.¹⁶⁰ Because of their chemical structure, amino acids cause minimal disruption to the structure and function of peptides or proteins compared to conjugation with fluorescent dyes, which are relatively large.¹⁶¹ Additionally, fluorescent amino acids can be more readily incorporated into peptides and proteins compared to fluorescent dyes, without the need for spacers or linkers. For these reasons, there is considerable interest in the development of the small fluorescent amino acids.

Among naturally occurring α -amino acids, L-tyrosine, L-tryptophan, and L-phenylalanine exhibit fluorescence due to the presence of the aromatic side chains (**Figure 29**).¹⁶² Apart from their abundance in biological tissues, which limits their application as fluorescent probes, these amino acids also have relatively poor optical properties. To minimise tissue autofluorescence caused by naturally fluorescent amino acids, their presence in biological tissues must be taken into account on developing new probes. In particular, compounds should be developed with photophysical properties that differ significantly of those of the natural fluorescent amino acids.

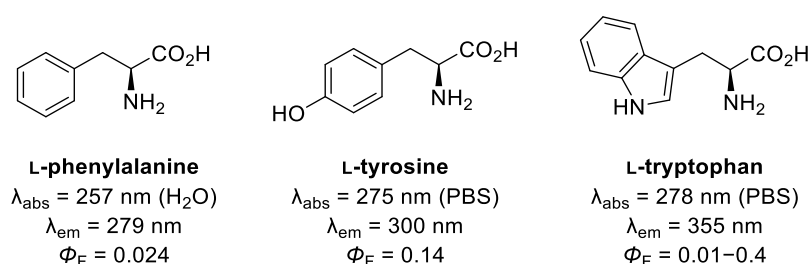


Figure 29. Structure and photophysical properties of natural fluorescent amino acids.^{159,162}

Over the decades, a vast number of unnatural fluorescent amino acids have been reported. For simplicity, they can be categorised into three groups: modified natural amino acids, the amino acids labelled with known fluorophores or *de novo* constructed fluorescent amino acids.¹⁶⁰ 4-Cyanotryptophan represents the first group; the introduction of a cyano-group to the indole ring at C4-position significantly enhances its optical properties and photostability, resulting in an increased quantum yield up to 0.80 and a substantial bathochromic shift of the emission maximum (**Figure 30**).¹⁶¹ This amino acid has been used to replace natural tryptophan in proteins enabling the investigation of protein structure and dynamics, enzyme-catalysed reactions and acting both as a donor and acceptor in fluorescence quenching studies via fluorescence resonance energy transfer (FRET). Labelling of D-alanine with a known fluorophore such as coumarin gave a new fluorescent probe, 3-(7-hydroxycoumarin)-carboxamide-D-alanine (HADA), with enhanced photophysical properties.¹⁶³ This fluorescent probe is widely used for visualisation of internal processes in live bacteria. The introduction of a boron-dipyrromethene (BODIPY) label to tryptophan led to the development of Trp(redBODIPY), which has been employed for live-cell imaging of KRT1-positive cancer cells.¹⁶⁴ *De novo*

constructed unnatural fluorescent amino acids include examples such as acridonylalanine (with a quantum yield of 0.95 in water), which is used in various protein studies as a FRET-sensor.¹⁶⁵

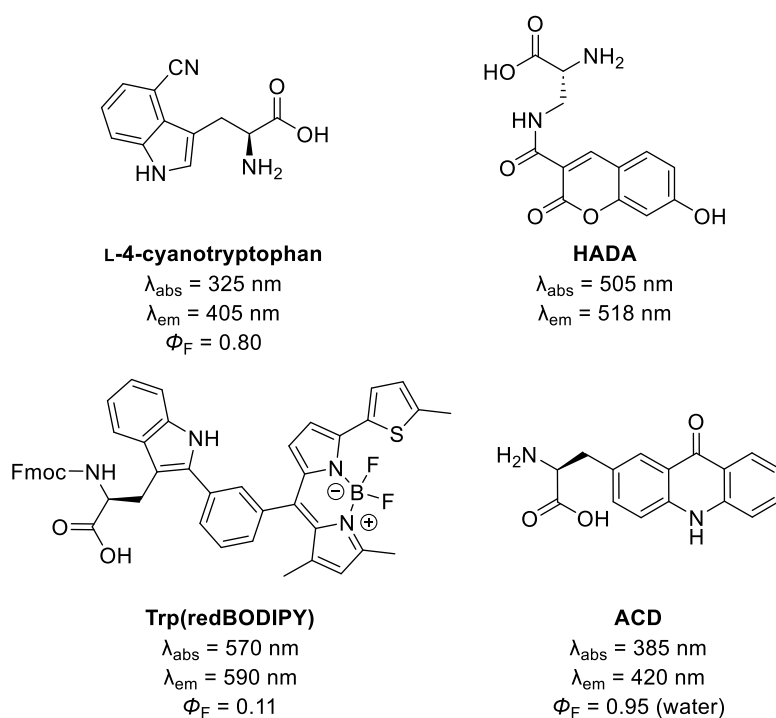


Figure 30. Some of the reported unnatural fluorescent amino acids.

Over the years, the Sutherland group has focused on the development of novel unnatural fluorescent amino acids for various biological applications.^{166–171} As a result, several novel fluorescent amino acids with excellent optical properties have been developed using various synthetic approaches (**Figure 31, 86–89**). These compounds not only exhibited promising, red-shifted emission maxima but also demonstrated high quantum yield and brightness values, making them particularly interesting fluorescent probes. Thus, amino acids **86** and **87** were evaluated as FRET donors within a peptide and were used for monitoring the enzymatic hydrolysis of the serine protease, trypsin.^{167,168} Compound **88** was tested as a reporter of molecular binding events by being installed into a peptide ligand and used to measure the binding of the ligand to a WW domain protein.¹⁶⁹ The last fluorescent amino acid **89** exhibited great potential for biological imaging as it was found to undergo two-photon absorption upon NIR excitation, thereby avoiding the use of UV light and minimising tissue photodamage.¹⁷⁰ Although all of these developed amino acids showed acceptable fluorescent properties, their relatively large size may still lead to potential disruptions within the peptide structure.

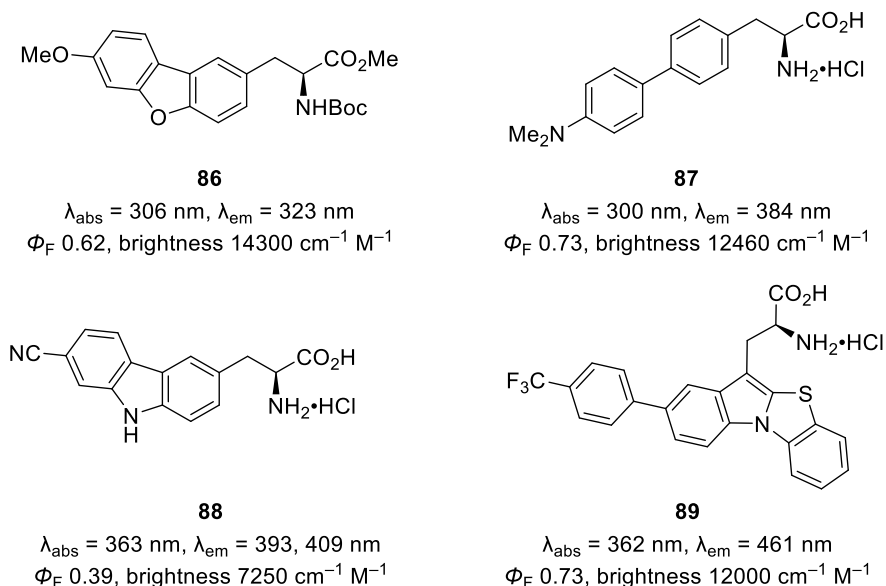


Figure 31. Fluorescent unnatural amino acids developed in the Sutherland group.^{167–170}

2.3.3 Project aims

Despite the extensive pool of developed unnatural fluorescent amino acids, they all have certain limitations such as either large size, which leads to potential perturbations in peptide or protein structures, difficulties with membrane permeability or challenges with incorporating them into peptides and proteins.¹⁷² In addition, some of them still require excitation and/or have emission bands in the UV range which leads to tissue autofluorescence and limits their applicability for cell and deep tissue imaging.¹⁶¹ Some of the reported fluorescent amino acid probes require lengthy and complicated synthesis as well as exhibit limited photostability and are prone to photobleaching.^{162,173} Moreover, certain fluorescent amino acids are toxic in high concentrations.¹⁷⁴ The search for new fluorescent amino acids continues, particularly for specific biological applications; small bright fluorescent amino acids, that are easy to synthesise are of particular interest. Therefore, the aim of this project was to develop novel fluorescent tryptophan analogues. The potential fluorescent amino acids were designed to have excitation wavelength significantly distant from natural amino acids, along with a large Stoke shift. The goal was to achieve rapid synthesis through a relatively short synthetic route of a series of structural analogues, enabling comprehensive photophysical analysis. To achieve this, the strategy involved creating new charge-transfer fluorophores by extending conjugation at the C2-position of the tryptophan indole ring. Incorporation

of new substituents was planned to be achieved through olefination reactions such as Horner-Wadsworth-Emmons (HWE) or Wittig reactions or cross-coupling reactions, such as a Suzuki-Miyaura reaction. In the first case, this would allow the generation of charge transfer-based fluorophores (e.g. **90**) by connection of strong electron-withdrawing groups to the π -excessive indole ring via a double bond (**Figure 32**). In the second case, the aryl moiety would be conjugated with indole ring (**91**), providing compounds with red-shifted absorption and emission, as well as enhanced brightness compared to tryptophan (**Figure 32**).

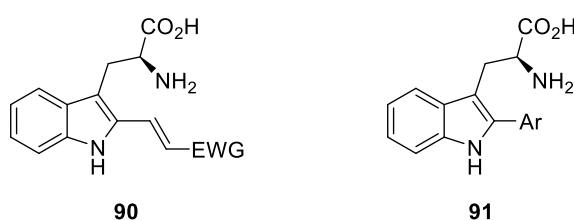
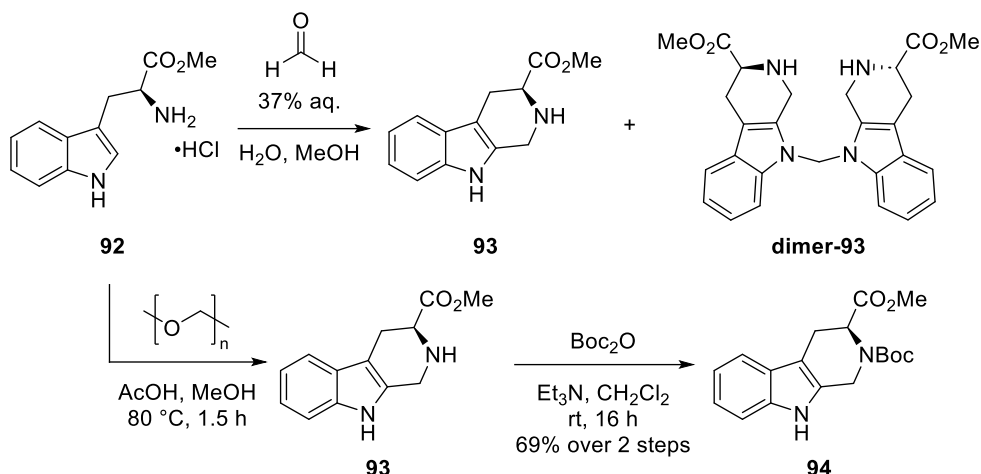


Figure 32. General structures of proposed fluorescent amino acids.

2.3.4 Synthesis of tryptophan analogues via olefination reactions

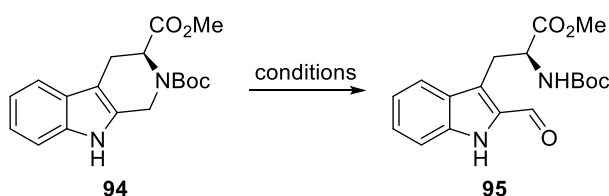
To carry out an alkenylation reaction with tryptophan, it was first necessary to synthesise a universal intermediate bearing a carbonyl group, which could subsequently react with various phosphonium ylides. The synthesis of the intermediate commenced with formation of tetrahydro- β -carboline **94** through a Pictet-Spengler type reaction. Reaction of tryptophan methyl ester with a 37% aqueous formaldehyde solution was attempted at room temperature in a water-methanol solvent mixture, followed by the protection of the secondary amine group (**Scheme 43**).¹⁷⁵ However, despite relatively high mass recovery after the first step (70%), approximately half of the material isolated was a side product, a dimer (**dimer-93**), which could not be separated from the desired product. This type of side product is known to form in the Pictet-Spengler reactions and so alternative reaction conditions were explored to avoid its formation.¹⁷⁶ Instead, the use of more forcing conditions for the reaction of tryptophan methyl ester with paraformaldehyde in the presence of acetic acid at 80 °C resulted in clean access to the product **93** (**Scheme 43**).¹⁷⁷ The resulting material was then subjected to an *N*-protection reaction with Boc₂O under standard basic conditions affording the desired product in 69% yield over two steps.



Scheme 43. Synthesis of tetrahydro- β -carboline **94** via a Pictet-Spengler type reaction.

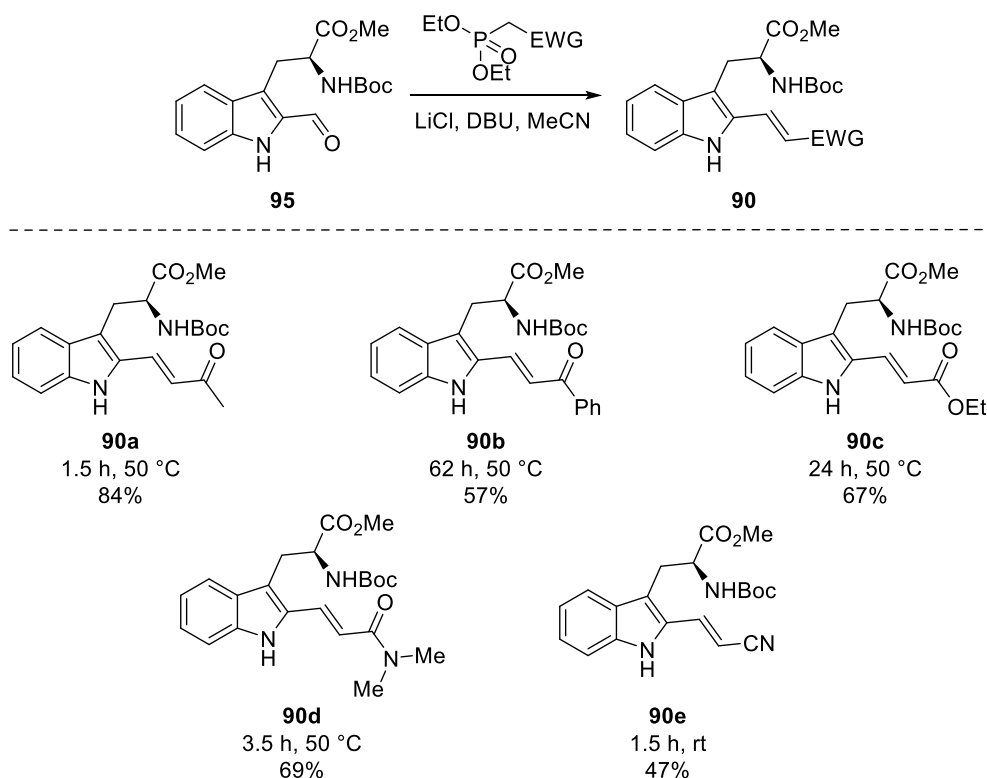
The next step involved oxidation of tetrahydro- β -carboline **94** to afford key aldehyde intermediate **95** (Table 10). First, potassium persulfate was investigated as an oxidant in the presence of a catalytic amount of tetramethylammonium chloride, resulting in the isolation of the formyl derivative **95** in 53% yield after an 8-hour reaction at 40 °C (entry 1).¹⁷⁸ As this was only moderate yielding other reactions were explored. In a previously described reaction for aryl substituted β -carbolines, using hydrogen peroxide and iodine as a catalyst gave no reaction with only the starting material **94** recovered (entry 2).¹⁷⁹ However, when performing SeO₂ oxidative cleavage to form the desired 2-formyl intermediate **95**, the reaction proceeded cleanly, giving the product in 68% yield (entry 3).¹⁸⁰ This procedure was subsequently adopted as the standard reaction protocol.

Table 10. Investigated approaches for the oxidative cleavage of **95**.



Entry	Reaction conditions	Yield
1	K ₂ S ₂ O ₈ , Me ₄ NCl (10 mol%), H ₂ O, DMSO, 40 °C, 8 h	53%
2	30% H ₂ O ₂ in H ₂ O, I ₂ (3 mol%), EtOH, 40 °C, 18 h	94 recovered
3	SeO ₂ , dioxane, 101 °C, 1.5 h	68%

Next, olefination reactions with 2-formyl tryptophan **95** were investigated. While such reactions are well known for various 3-substituted 2-formyl indoles, they had never been previously reported for 2-formyl tryptophan and its derivatives.¹⁸¹ Since alkenylation reactions were regarded as an effective way for derivatising tryptophan while creating a conjugated system, two main reactions of substrate **95** with phosphorus-based reagents were investigated: the HWE reaction and the Wittig reaction. The investigation began with the HWE reaction, which was deemed more advantageous than the Wittig reaction due to its typically higher stereoselectivity, and more efficient product separation. To prevent racemisation of the amino acid, the HWE reaction was conducted under mild Masamune-Roush conditions with phosphonate esters bearing different electron-withdrawing groups (EWGs; ketone, nitrile, ester, amide).¹⁸² The standard reaction conditions employed 1.2 equivalents of the corresponding phosphonate ester, lithium chloride and DBU as the base, varying the temperature and reaction time (**Scheme 44**). The reaction with diethyl (2-oxopropyl)phosphonate gave the desired tryptophan derivative **90a** under standard reaction conditions in 84% yield over 1.5 hour at 50 °C. However, the reaction with a benzoyl phosphonate ester required a longer reaction time of 62 hours and additional portions of DBU and phosphonate ester (1.7 equivalents in total) added after 19 hours. The synthesis of the ester derivative **90c** was achieved via the reaction with triethyl carboxymethylphosphonate over 24 hours at 50 °C; however, an additional portion of the reagent and base was added two hours after the reaction started. Using a higher initial loading of the reagents did not improve the reaction conversion, and additional portions were still required. The amide derivative **90d** was synthesised under standard reaction conditions during a 3.5-hour reaction at 50 °C. The HWE reactions with all these phosphonate esters demonstrated high *E*-selectivity. This was confirmed by ¹H NMR spectroscopy of the crude reaction mixtures, where only the corresponding doublet signals with coupling constants of 15–16 Hz were observed. In contrast, cyanomethylphosphonate ester was found to be much more reactive in the HWE reaction with 2-formyltryptophan **95**, and the addition of this reagent was conducted at 0 °C with subsequent warming of the reaction mixture to room temperature. After 2 hours, both *E*- and *Z*-isomers were observed to be formed in the ¹H NMR spectra with an *E/Z* the ratio of 60/40. The crude reaction mixture was purified by flash column chromatography, and the desired *E*-isomer was isolated in a moderate 47% yield.



Scheme 44. HWE reaction of 2-formyl tryptophan **95** with various phosphonate esters.

After completing synthesis of compounds **90**, their photophysical properties were evaluated. The absorbance maxima (λ_{abs}) for all the compounds of this library were found to be in the range 340–400 nm, with the emission maxima (λ_{em}) fell within the range 437–470 nm (**Table 11, Figure 33**). The modified tryptophan analogues displayed promising bathochromic shift in emission compared to parent L-tryptophan, with the nitrile, ester and amide-substituted derivatives demonstrating the highest emission intensities. For these compounds, molar extinction coefficient (ϵ), quantum yield (Φ_F), and brightness values were determined. Although some of the compounds exhibited very high molar extinction coefficients ($>25000 \text{ cm}^{-1} \text{ M}^{-1}$), their low quantum yield (less than 2%), resulted in weak brightness values. However, it was later found that the fluorescence of these compounds was partly quenched in methanol solutions so other solvents miscible with water were investigated. Tetrahydrofuran was ultimately identified as the most suitable solvent and compounds **90d** and **90e** were reevaluated in this solvent. Although, the emission maxima shifted slightly towards the blue region by 27–30 nm, it remained beyond 400 nm. However, changing the solvent significantly improved the quantum yield values and consequently the brightness values, up by four-fold. Despite this, the

values remained lower than expected. Nevertheless, the results looked promising as the introduction of the new fragment with an EWG at the C2-position of the indole ring did enhance some photophysical properties compared to the parent amino acid.

Table 11. Photophysical data for novel tryptophan analogues **90**.

Compound	Solvent	λ_{abs} (nm)	λ_{em} (nm)	Stokes Shift (nm)	ϵ (cm ⁻¹ M ⁻¹)	Φ_F	Brightness (cm ⁻¹ M ⁻¹)
90a	MeOH	364	470	106	--	--	--
90b	MeOH	400	455	55	--	--	--
90c	MeOH	346	446	100	26600	0.006	170
90d	MeOH	346	437	91	25600	0.017	440
90d	THF	346	410	64	29100	0.036	1060
90e	MeOH	340	437	97	29800	0.018	520
90e	THF	340	425	85	33200	0.063	2100

-- below the limit of detection

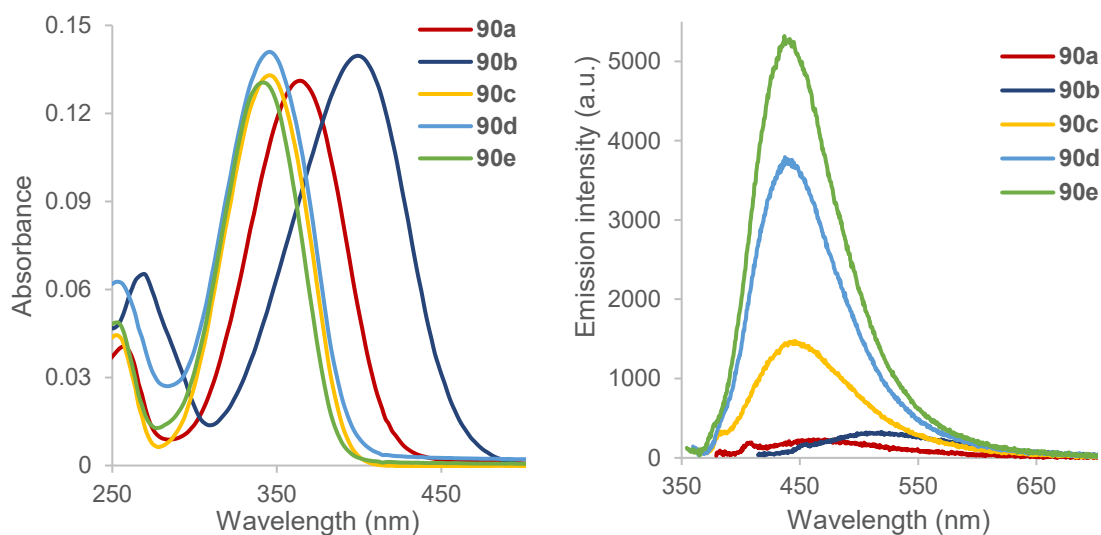
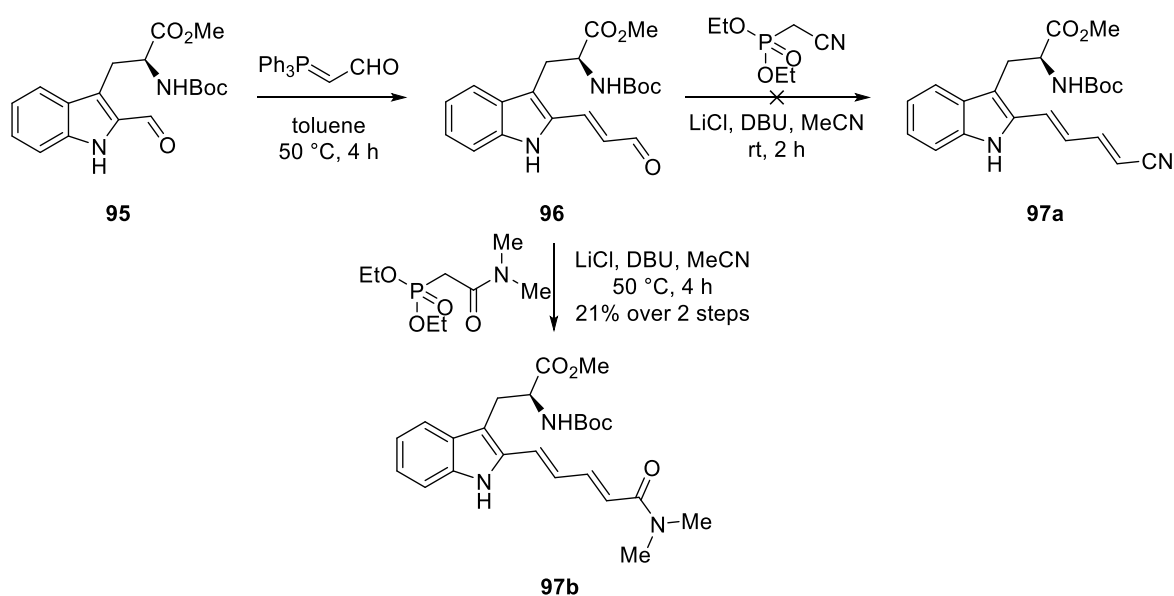


Figure 33. Absorbance (left) and emission (right) spectra of the synthesised tryptophan analogues **90**. Spectra were recorded in methanol at 5 μM concentration. Excitation was performed at the absorption maximum.

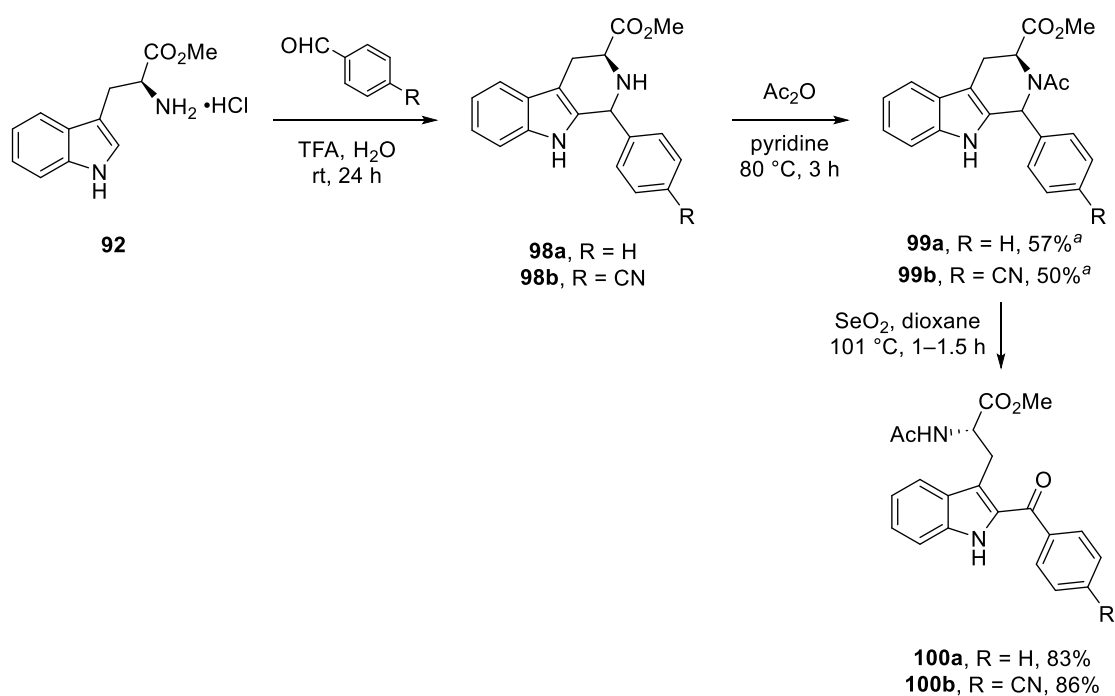
However, inspired by the results obtained, it was suggested that extending the conjugation further could enhance the quantum yield and consequently brightness of the tryptophan analogues. It was proposed to link the electron-withdrawing group to the indole ring via a diene chain. To achieve that 2-formyl tryptophan ester **95** was first subjected to a Wittig reaction with (triphenylphosphoranylidene)acetaldehyde at 50 °C (**Scheme 45**). This gave formyl derivative **96** as a single *E*-isomer, as confirmed by ¹H NMR spectroscopy. However, due to high reactivity of the formed species, it underwent further Wittig reaction with the phosphonium ylide. As the separation of the desired product **96** from the side products was quite challenging, it was used without further purification in the subsequent HWE reaction. Given that nitrile analogue **90e** demonstrated the best optical properties among the previously synthesised compounds, it was decided to synthesise nitrile-substituted diene derivative **97a** and evaluate whether the extended conjugation enhance photophysical properties. However, the attempted reaction of **96** with diethyl (cyanomethyl)phosphonate was unsuccessful, resulting in a complex mixture of unidentified products. So instead, the reaction of formyl derivative **96** with diethyl [(dimethylcarbamoyl)methyl]phosphonate was attempted, which gave desired tryptophan analogue **97b** in 21% over two steps.



Scheme 45. Synthesis of diene tryptophan analogues **97**.

Simultaneously, another library of the tryptophan analogues was proposed wherein electron-withdrawing substituents such as benzoyl would be directly attached to the indole core to investigate potential improvement in physicochemical properties. To

achieve that, synthesis of two benzoyl substituted compounds was investigated. In the Pictet-Spengler reaction of tryptophan methyl ester **92** with the corresponding benzaldehydes under acidic conditions, intermediates **98a** and **98b** were obtained (Scheme 46).¹⁸³ These β -carboline intermediates were subsequently subjected to the *N*-protection reaction, although this step proved to be quite challenging. For example, protection with Boc₂O and CbzCl was attempted under various reaction conditions, however, the starting materials remained unreacted. So instead, *N*-acetylation was performed using a literature procedure, which resulted in isolation of the desired products **99a** and **99b** in 50–57% yields.¹⁸³ This was then followed by oxidative cleavage using selenium dioxide under standard conditions, which provided the desired tryptophan analogues **100a** and **100b** in 83–86% yields. It is worth noting that the compound **100a** had been previously synthesised, however, the evaluation of physicochemical properties had not been performed.¹⁸³



Scheme 46. Synthesis of the 2-benzoyl tryptophan analogues **100**.

^aOver 2 steps.

With compounds **97b** and **100a/b** in hand, their photophysical properties were evaluated (Table 12, Figure 34). Although some of the data for diene **97b** appeared promising, showing red-shift emission maximum at 489 nm in methanol, the fluorescence intensity remained low. This tryptophan derivative exhibited a quantum yield below 0.01 and despite a high molar extinction coefficient ($>30000 \text{ cm}^{-1} \text{ M}^{-1}$),

the brightness was weak. For the benzoyl compounds **100a** and **100b**, the absorbance maxima were both found to be below 350 nm and neither compound exhibited fluorescence. Therefore, all compounds from this library were excluded from further evaluation.

Table 12. Photophysical study of the analogues **97b** and **100a/b**.

Compound	λ_{abs} (nm)	λ_{em} (nm)	Stokes Shift (nm)	ϵ (cm ⁻¹ M ⁻¹)	ϕ_F	Brightness (cm ⁻¹ M ⁻¹)
97b	374	489	115	33300	0.008	250
100a	326	--	--	--	--	--
100b	334	--	--	--	--	--

-- below the limit of detection

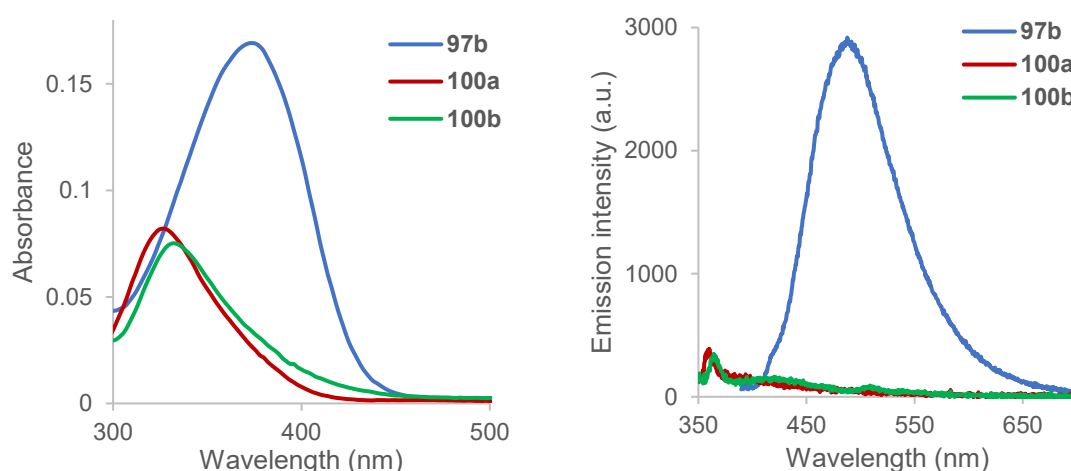
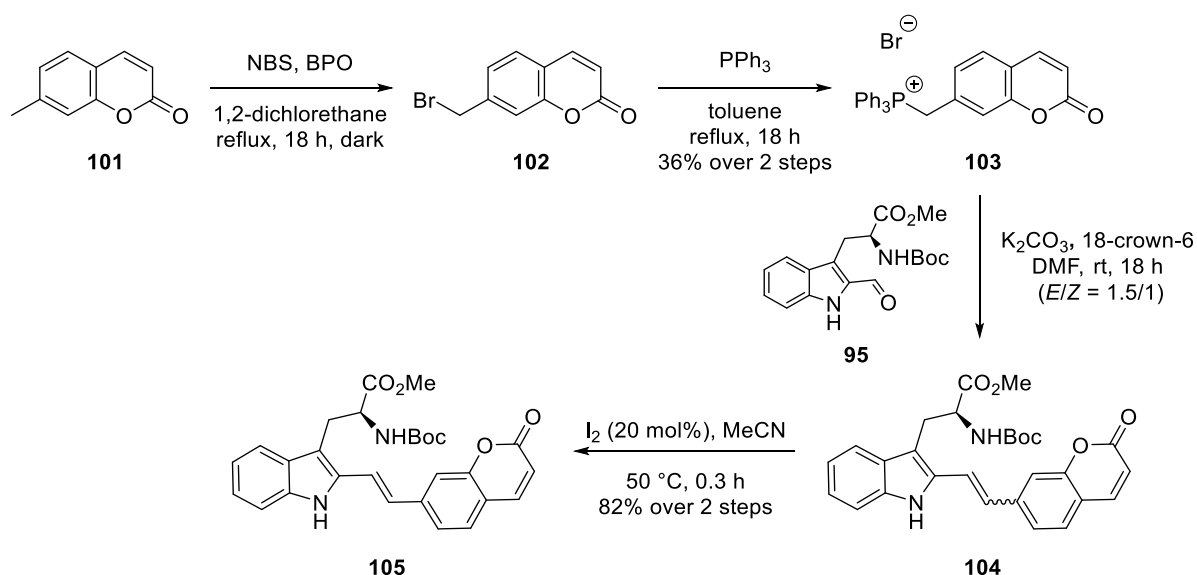


Figure 34. Absorbance (left) and emission (right) spectra of the synthesised tryptophan analogues **97b** and **100a/b**. Spectra were recorded in methanol at 5 μ M concentration. Excitation was performed at the absorption maximum.

Given that the photophysical properties of the initial tryptophan analogue library looked promising (**Table 11**), aside from the low quantum yields and brightness, it was decided to install a known fluorophore such as coumarin, through the same alkene conjugated system with the indole. It was previously reported that coumarin phosphonium salts could undergo Wittig reactions with various aldehydes, although for 2-formyl tryptophan **95** this reaction had not been reported before.¹⁸⁴ While this general class of compound had previously been synthesised via a manganese-

catalysed CH alkenylation using a pyridine directing group, the removal of the directing group in this approach proved to be unsuccessful, preventing full analysis of their photophysical properties.¹⁸⁵ Instead, our previously developed olefination of 2-formyl tryptophan **95** was employed. Coumarin phosphonium salt **103** was successfully synthesised by first brominating 7-methylcoumarin (**101**) using NBS in the presence of benzoyl peroxide, followed by reaction of the resulting bromocoumarin **102** with triphenylphosphine (**Scheme 47**).¹⁸⁶ The phosphonium salt was then subjected to the Wittig reaction with 2-formyl tryptophan **95** under basic conditions in the presence of 18-crown-6 ether, which facilitated the generation of a naked anion of carbonate and served as a phase-transfer catalyst for better dissolution of the inorganic base in the organic solvent. The Wittig reaction provided the coumarin tryptophan **104** as a mixture of *Z*- and *E*-isomers in a ratio of 1:1.5, respectively. These isomers could be separated; however, since the focus was primarily on a synthesis of a single isomer, the mixture was fully converted to the more stable *E*-isomer. The isomerisation reaction for alkenes can be performed using various approaches including thermal isomerisation, metal photocatalysis or acid/base-catalysed isomerisation.^{187,188} Another approach involves the use of iodine as a catalyst for radical isomerisation, which was employed in this work.¹⁸⁹ Treatment of isomeric mixture **104** with catalytic iodine (20 mol%), gave solely the *E*-isomer **105**, in 82% yield over the two steps.



Scheme 47. Synthesis of coumarin tryptophan analogue **105** via Wittig reaction.

After successful synthesis of compound **105** its photophysical properties were evaluated. This tryptophan analogue showed much improved, red-shifted absorbance maximum around 400 nm and emission maximum at 505 nm in dimethylsulfoxide (DMSO) (**Figure 35**). As the largest Stokes shift was observed in methanol (185 nm), the molar extinction coefficient and quantum yield of this compound were determined in this solvent. Although the molar extinction coefficient was exceptionally high ($43000\text{ cm}^{-1}\text{ M}^{-1}$), the fluorescence of this compound was found to be partly quenched in methanol (**Table 13**), as in the previous cases. Therefore, these parameters were determined in the solution of the other water miscible solvents such as tetrahydrofuran and DMSO. Changing the solvent improved quantum yield values reaching 0.48 and 0.52 in DMSO and THF, respectively, while maintaining the high molar extinction coefficient of $40000\text{ cm}^{-1}\text{ M}^{-1}$. Consequently, brightness of this compound was determined to be $19400\text{ cm}^{-1}\text{ M}^{-1}$ in both solvents, representing an excellent result and positioning it among the brightest fluorescent amino acids developed in the Sutherland group.

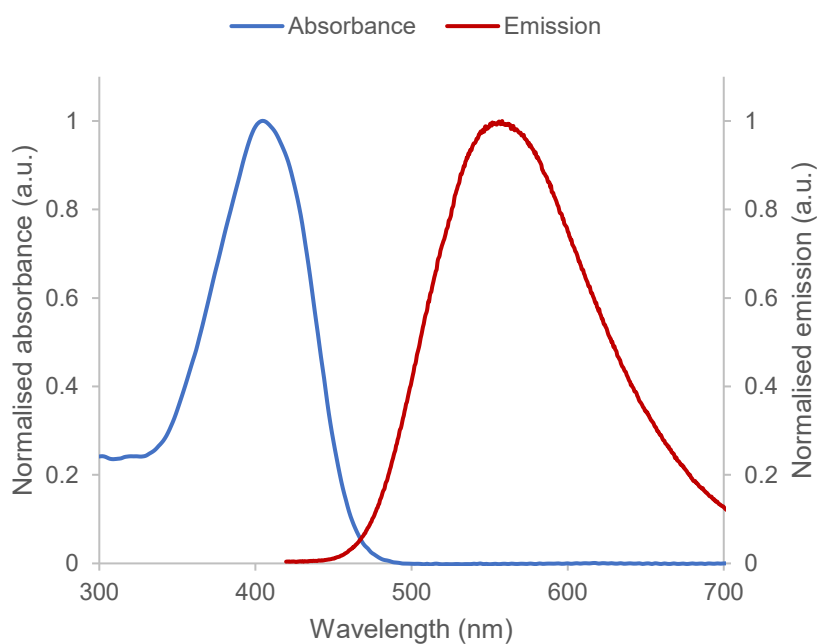


Figure 35. Normalised absorbance and emission spectra of **105**. Spectra were recorded in DMSO at 5 μM concentration. Excitation was performed at the absorption maximum.

Table 13. Photophysical properties of coumarin tryptophan **105** in various solvents.

Solvent	λ_{abs} (nm)	λ_{em} (nm)	Stokes Shift (nm)	ϵ (cm ⁻¹ M ⁻¹)	Φ_F	Brightness (cm ⁻¹ M ⁻¹)
MeOH	400	585	185	43500	--	--
THF	400	505	105	37100	0.52	19390
DMSO	406	560	154	40600	0.48	19410
EtOAc	395	500	105	N/D	N/D	N/D
CHCl ₃	400	520	120	N/D	N/D	N/D
CH ₂ Cl ₂	400	540	140	N/D	N/D	N/D
MeCN	390	540	150	N/D	N/D	N/D
IPA	405	550	145	N/D	N/D	N/D

N/D not determined; -- below the limit of detection.

Further solvatochromic study was performed to determine whether solvents influenced the photophysical properties of the compound **105**, which had been designed as a charge-transfer-based fluorophore (**Table 13**, **Figures 36** and **37**). Regarding absorbance, minimal changes in the absorbance maximum positions were observed across all the investigated solvents indicating negligible charge transfer between the indole and coumarin moieties in the ground state. On the contrary, the emission of **105** varied significantly across different solvents. For instance, fluorescence of **105** was partly quenched in methanol solution as noted previously. However, when another alcohol such as isopropanol was tested, the fluorescence intensity of **105** was only slightly reduced (by 17%) compared to that in THF. In addition, the emission maxima were highly dependent on the solvent polarity. For example, the emission maxima in ethyl acetate and THF were found at 505 and 508 nm respectively, while methanol exhibited the most red-shifted emission band at 585 nm, followed by DMSO at 560 nm and isopropanol at 550 nm. In acetonitrile and dichloromethane, compound **105** showed similar emission maxima around 540 nm. This environment sensitivity is characteristic of charge-transfer fluorophores, which are stabilised in more polar solvents.

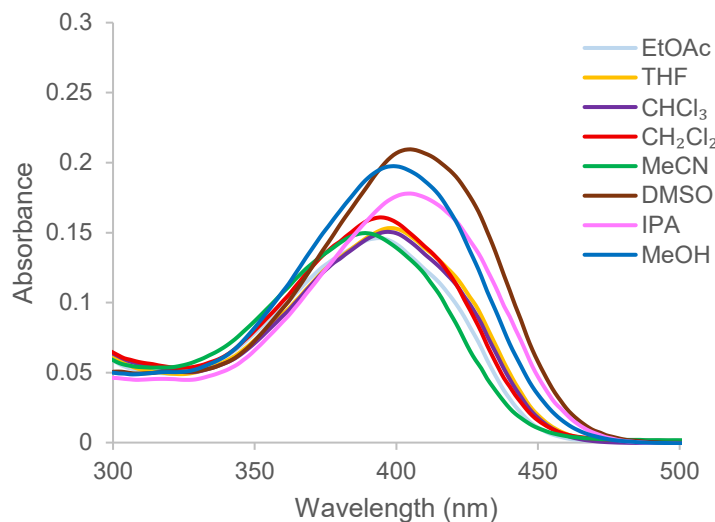


Figure 36. Absorbance spectrum of **105** in different solvents. Spectra were recorded at 5 μ M concentration.

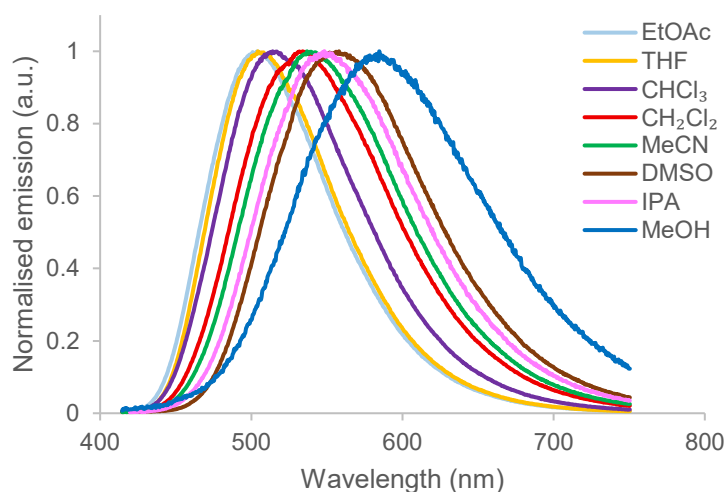


Figure 37. Normalised emission spectra of **105** in different solvents. Spectra were recorded at 5 μ M concentration. Excitation was performed at the absorption maximum.

To confirm the solvent sensitivity of compound **105** is due to polarity effects, a Lippert-Mataga plot was produced for the various solvent systems. The Lippert-Mataga plot, which represents the relationship between Stokes shifts and solvent polarizability, is illustrated by the Lippert-Mataga equation. This equation describes the influence of general solvent effects accounting for physical characteristics such as solvent dielectric constant, refractive index, variations in dipole moments on the emission maxima position.¹⁹⁰ However, the equation does not consider any specific solvent effects, such as hydrogen bonding or preferential solvation. As illustrated in **Figure 38**, a clear correlation is observed between the nature of the solvent and the

Stokes shifts of compound **105** in different solvents, suggesting that the general solvent effects primarily explained the variation. However, a slight deviation noted for water may be attributed to the aggregate-induced quenching as previously discussed. As part of the solvatochromic study, the sensitivity of coumarin tryptophan **105** to pH was also investigated. After recording the absorption and emission spectra of **105** at three different pH values (3, 6 and 8), it was concluded that only minimal differences in the absorption and emission intensities were observed (less than 20%, see **Figure S1, Appendix A**). Typically, major quenching is observed in the case of pH sensitive amino acid probes.¹⁹¹

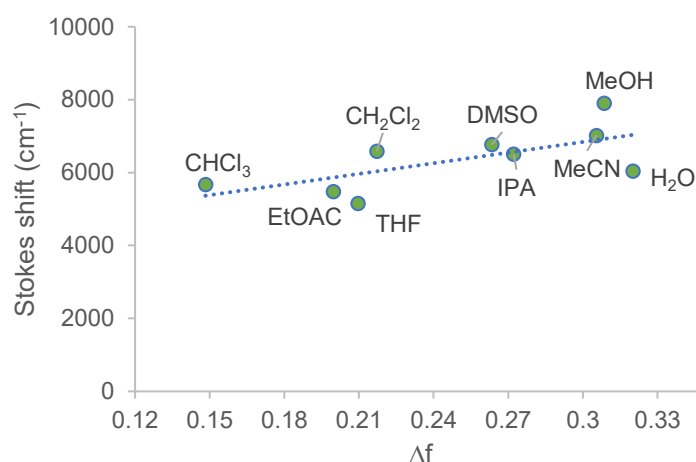


Figure 38. Lippert-Mataga plot for coumarin tryptophan analogue **105**.

It should be noted that coumarin compounds **105** was partly quenched in methanol but also in aqueous solvents such as water and phosphate-buffer saline (PBS) likely due to aggregate-induced quenching (**Figure 39**). However, as this compound showed such promising results in organic solvents, it was decided to also investigate its fluorescence in liposomes to evaluate its potential as a lipophilic probe for lipid-rich environments. Therefore, a solution of liposomes, commonly used to mimic biological environments, was prepared and coumarin tryptophan derivative **105** was dissolved in it, showing excellent fluorescence intensity once again. The emission intensity of **105** in the liposome solution was 48 times higher than in PBS and 35 times higher than in aqueous solution, highlighting the potential application of this compound as a lipid-sensitive probe.

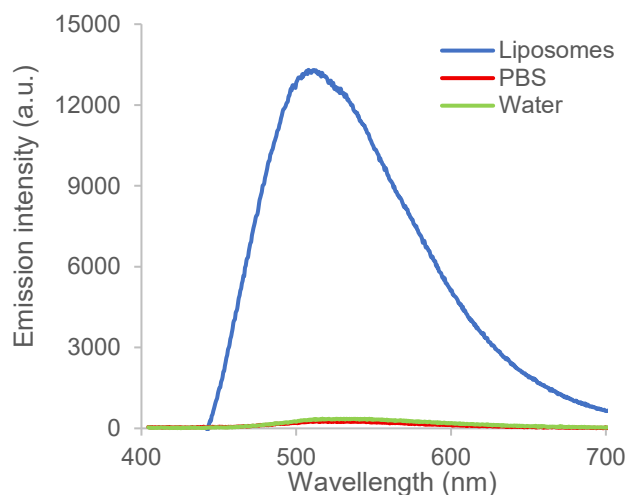
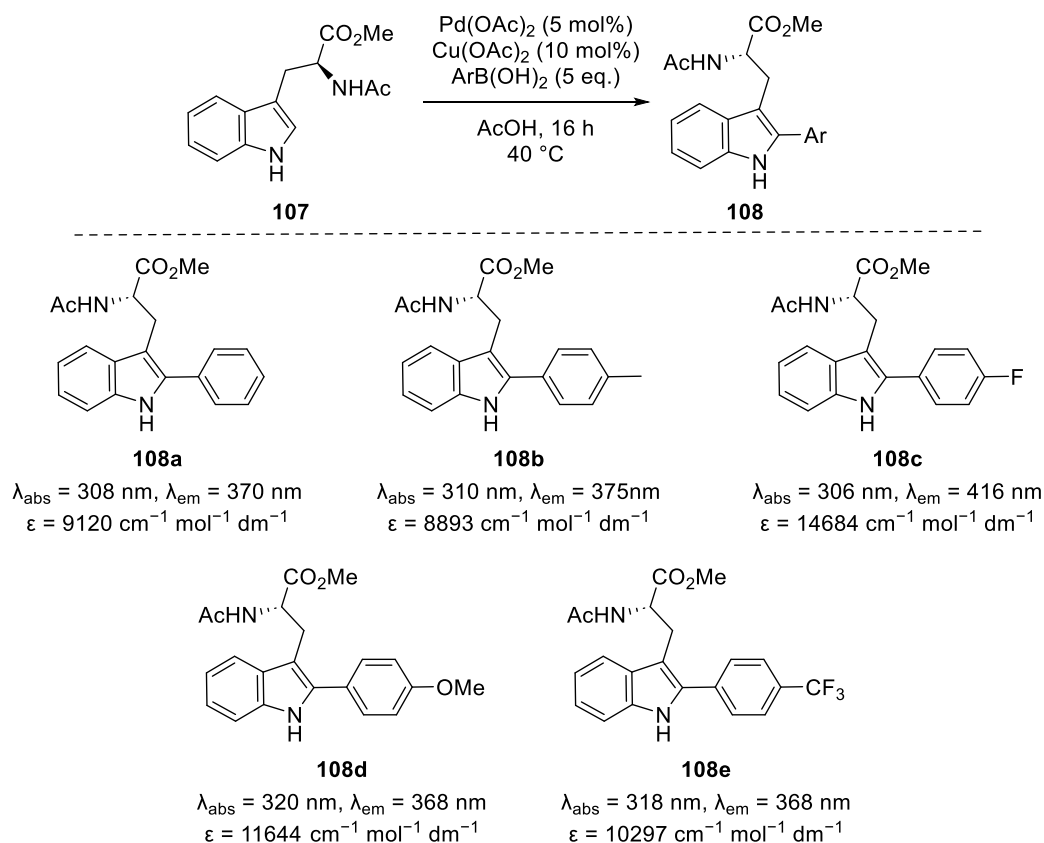


Figure 39. Emission spectra of **105** in water, PBS and liposome solutions. Spectra were recorded at 5 μM concentration. Excitation was performed at the absorption maximum.

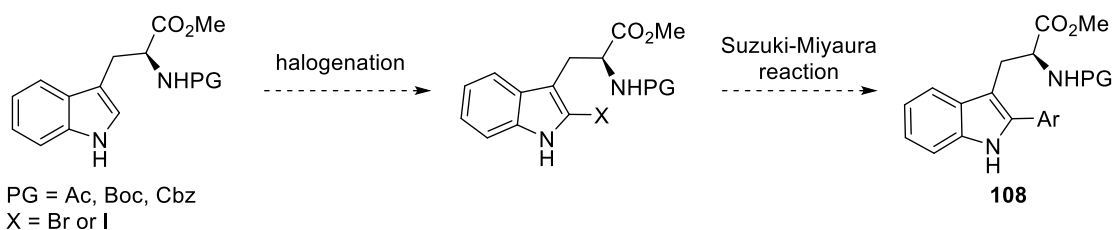
In addition to standard analysis, coumarin analogue **105** was also investigated by two-photon spectroscopy. In two-photon excitation, the fluorophore is excited using photon with a wavelength approximately twice as long as that used in standard one-photon excitation.¹⁷¹ This technique is particularly valuable in applications such as two-photon fluorescence microscopy. Using longer excitation wavelength in the far infrared region, where the biological tissues are transparent, results in deeper tissue imaging and higher spatial resolution.

The following study was performed by the Magennis group members, BSc student Niamh C. Radcliffe-Kennedy and PhD student Abigail Thom. Prior to conducting the two-photon excitation study, the fluorescence lifetime under one-photon excitation was measured and determined to be 4.02 nanoseconds. The two-photon excitation of coumarin tryptophan analogue **105** in DMSO was performed using a broadband Ti:sapphire laser with a central wavelength of 800 nm, resulting in an emission spectrum closely matching that obtained using one-photon excitation at 405 nm (**Figure S2, Appendix A**). The two-photon nature of the excitation was confirmed via a log-log plot of fluorescence intensity versus power, and the calculated slope of the plot was 1.99 (**Figure S3, Appendix A**). Subsequently, the two-photon cross section (σ_{2P}) of **105** was measured at 800 nm and found to be 81 GM. This was used to calculate the two-photon brightness ($\sigma_2\Phi_F$) for **105** yielding a value of 39 GM. This is a major improvement in two-photon brightness compared to the reported values for thiazoloindole amino acids **89** ($\sigma_2\Phi_F = 14\text{--}15$ GM), which had been



Scheme 49. Previously reported 2-aryl tryptophan derivatives by Fairlamb and co-workers.¹⁹²

To broaden the scope of the synthetic approach, it was decided to introduce a halogen leaving group rather than attempting a CH-activation of the C2-position of the indole ring (**Scheme 50**). The halogenated intermediate would be then subjected to an optimised Suzuki-Miyaura reaction with various boronic acids.



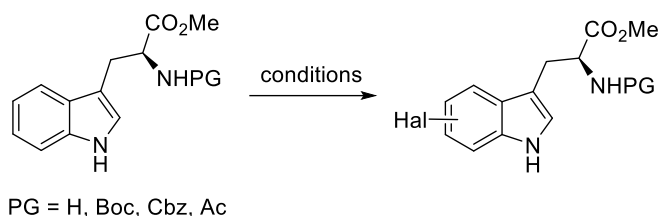
Scheme 50. A proposed synthetic route for 2-aryl tryptophans **108**.

To achieve this, a halogenation step was investigated. Several synthetic procedures were evaluated; however, the majority of the reactions did not afford the desired product. Bromination of unprotected tryptophan methyl ester using NBS in a mixture of acetic and formic acids was attempted (**Table 14**, entry 1). Despite full conversion of the starting material, no product could be isolated.¹⁹³ Assuming that the difficulties

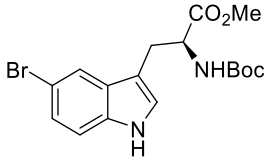
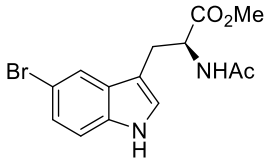
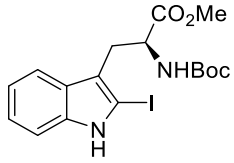
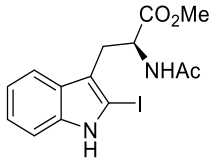
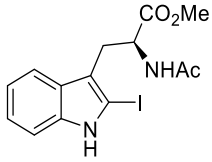
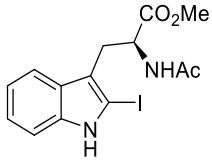
were related to the isolation of an unprotected amino acid **109**, bromination of *N*-Cbz-protected tryptophan ester was subsequently attempted, which resulted in the isolation of 5-bromotryptophan **110** as the major product, in 21% yield (entry 2). Switching to a radical bromination approach using NBS in the presence of benzoyl peroxide as a radical initiator led to the isolation of the same product as before in 21% yield (entry 3).¹⁹⁴ It was proposed that the Cbz-protecting group might be too bulky potentially hindering the 2-position of indole. Consequently, an alternative protecting group was evaluated. Bromination of *N*-Boc-protected tryptophan ester was subsequently performed under the same conditions, yet this reaction also led to bromination at C-5 to give **111** as the major product in 30% yield (entry 4). Increasing the reaction temperature did not result in any improvement (entry 5), so the approach was changed slightly, and bromination using only NBS was explored (entry 6).¹⁹⁵ Despite 90% of the starting material being consumed within 15 minutes of the reaction, a mixture of products was obtained, with no major products identified. When this reaction was attempted at a lower temperature, full conversion was achieved within 1 hour; however, only 5-bromotryptophan **111** was isolated in 11% yield (entry 7). Subsequent efforts to brominate *N*-acetyl tryptophan ester resulted in the isolation of brominated product **112** in 33% yield (entry 8). The reaction was found to be messy, and purification proved to be challenging. Since bromination reactions were unsuccessful, an iodination strategy was then investigated. Given that the Sutherland group has significant experience with iron-catalysed halogenation, and current focus is on iron-catalysed iodination, this approach was tested on the *N*-Boc protected tryptophan derivative. In the case of using a strong iodinating reagent such as *N*-iodosaccharin in the presence of iron(III) chloride as a Lewis base, the reaction did not proceed and only starting material was isolated (entry 9). When the super Lewis base, iron(III) triflimide, formed *in situ* from iron(III) chloride and 1-butyl-3-methylimidazolium triflimide ([BMIM]NTf₂) to activate *N*-iodosaccharin was used with in this case the *N*-acetyl tryptophan derivative, a mixture of unidentified products was isolated along with the unreacted starting material (entry 10). Consequently, iodination of *N*-acetyl tryptophan was then attempted using *N*-iodosuccinimide (NIS) in presence of a Brønsted acid, trifluoroacetic acid (TFA), which ultimately led to the successful isolation of desired product **114** in 25% yield (entry 11).¹⁹⁶ Further optimisation, including the addition of 1.8 equivalent of NIS in three portions over 1.5 hours, resulted in the isolation of the desired 2-iodotryptophan **114** in 55% yield (entry 12). Conducting the reaction in

the dark was essential as NIS decomposed rapidly under reaction conditions upon exposure to light.

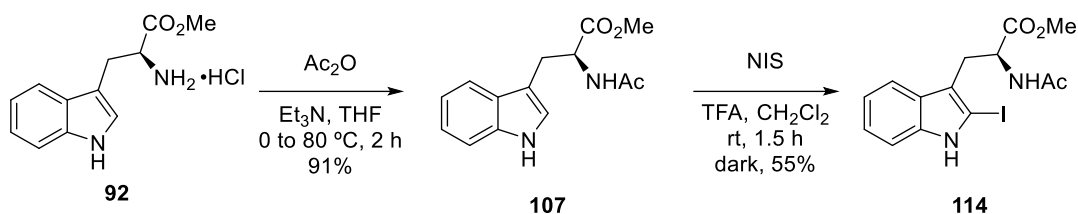
Table 14. Attempted halogenation of tryptophan methyl ester.



Entry	Conditions	Product	Yield
1	NBS (1.02 eq.), AcOH, HCO ₂ H rt, 0.3 h	 109	N/A
2	NBS (1.02 eq.), AcOH, HCO ₂ H rt, 1.5 h	 110	21%
3	NBS (1.3 eq.), benzoyl peroxide, 1,2-dichloroethane 40 °C, 3.5 h	 110	21%
4	NBS (1.6 eq.), benzoyl peroxide, 1,2-dichloroethane 40 °C, 2 h	 111	30%
5	NBS (1.6 eq.), benzoyl peroxide, 1,2-dichloroethane 76 °C, 0.5 h	 111	26%
6	NBS (1.1 eq.), CH ₂ Cl ₂ rt, 0.25 h	 111	N/A

7	NBS (1.8 eq.), CH ₂ Cl ₂ 0 °C, 1 h	 111	11%
8	NBS (1.3 eq.), benzoyl peroxide, 1,2-dichloroethane 40 °C, 1 h	 112	33%
9	<i>N</i> -iodosaccharin (1.2 eq.), FeCl ₃ (0.05 eq.), CHCl ₃ , rt, 4 h	 113	N/A
10	<i>N</i> -iodosaccharin (1.2 eq.), FeCl ₃ (0.05 eq.), [BMIM]NTf ₂ (0.15 eq.), CH ₂ Cl ₂ , 40 °C, 1.5 h	 114	N/A
11	NIS (1 eq.), TFA, CH ₂ Cl ₂ rt, 2 h, dark	 114	25%
12	NIS (1.8 eq.), TFA, CH ₂ Cl ₂ rt, 1.5 h, dark	 114	55%

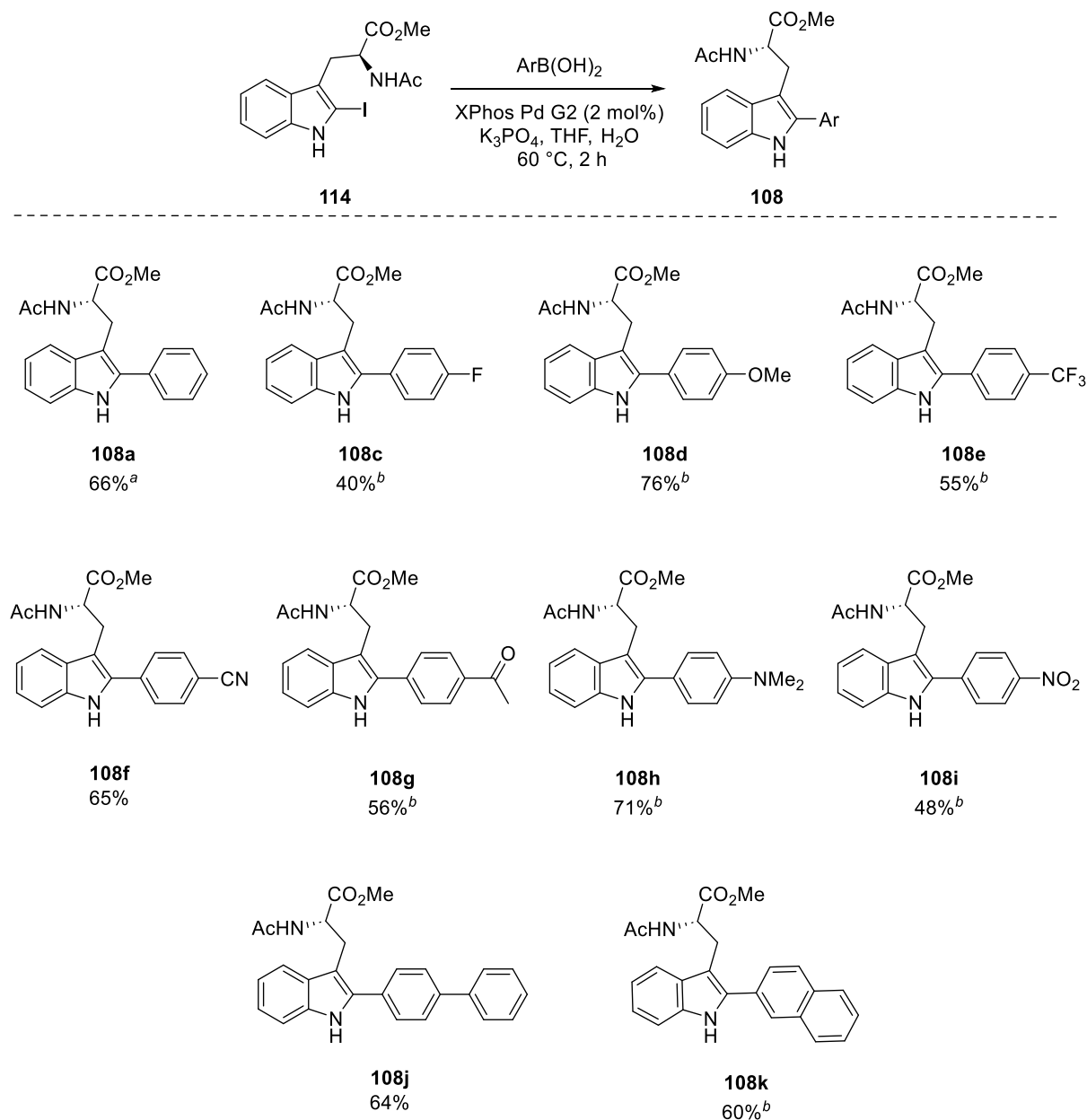
An optimised synthetic procedure for iodinated intermediate **114** is presented in **Scheme 51**. The acetyl protecting group was selected due to its greater stability under acidic conditions compared to Boc- and Cbz-protecting groups, which was critical for the iodination step. The protected intermediate **107** was synthesised from methyl tryptophan ester **92** under standard basic conditions using acetic anhydride and was generally employed in the subsequent step without further purification, as the crude material exhibited satisfactory purity by ¹H NMR spectroscopy.



Scheme 51. Optimised synthesis of iodinated intermediate **114**.

Having synthesised iodinated intermediate **114**, a Suzuki-Miyaura reaction was investigated with various aryl boronic acids using XPhos Pd G2 as the catalyst and potassium phosphate as the base at 60 °C (**Scheme 52**). The catalyst was selected based on previous successful cross-coupling reactions with other amino acids, where low catalyst loadings and short reactions times were consistently achieved.^{168,170} The use of this catalyst enabled the synthesis of previously reported phenyl tryptophan analogue **108a** in significantly shorter time compared to the Fairlamb procedure (3 h vs 16 h) and with a reduced catalyst loading (2 mol% instead of 5 mol%), although the reaction required slightly more forcing conditions (60 °C instead of 40 °C) and an inert atmosphere.¹⁹² Compound **108a** was isolated in a lower yield of 66% compared to the reported 93%. A similar result was achieved for 4-fluorophenyl analogue **108c**, which was obtained in 40% yield after 1.2 hours in contrast to 77% yield after a 16-hour reaction by the Fairlamb method. This and several other tryptophan analogues were synthesised by MSci student, Arthur Wong. In case of 4-trifluoromethylphenyl product **108e**, the isolated yield was comparable to that obtained using the previously reported procedure (55% vs 58%). However, for 4-methoxyphenyl analogue **108d** the developed method provided a significantly improved result, affording the product in 76% yield compared to the previously reported 28%. Overall, the current approach generally demonstrated broad tolerance to the various boronic acids bearing both electron-donating and electron-withdrawing substituents. To evaluate the effect of both types of substituents on the charge-transfer fluorescence properties of the tryptophan analogues, a series of derivatives were synthesised. Aryl tryptophan compounds bearing 4-cyanophenyl (**108f**) and 4-acetylphenyl groups (**108g**) were successfully obtained in good yields of 65% and 56%, respectively. A novel aryl tryptophan analogue **108i** bearing a 4-nitrophenyl side chain was isolated in a moderate 48% yield, which was considered satisfactory as the previous reported attempts to synthesise this compound had failed.¹⁹⁷ In addition, a new 4-dimethylaminophenyl substituted tryptophan derivative **108h** was also synthesised using this methodology and was isolated in a high 71%

yield. Other polyaromatic analogues, including biphenyl **108j** and naphthyl **108k** were also synthesised, with isolated yields of 64% and 60%, respectively.



Scheme 52. Tryptophan analogues **108** synthesised via Suzuki-Miyaura cross-coupling reaction. ^a 3-hour reaction time. ^b Synthesised by MSci student Arthur Wong.

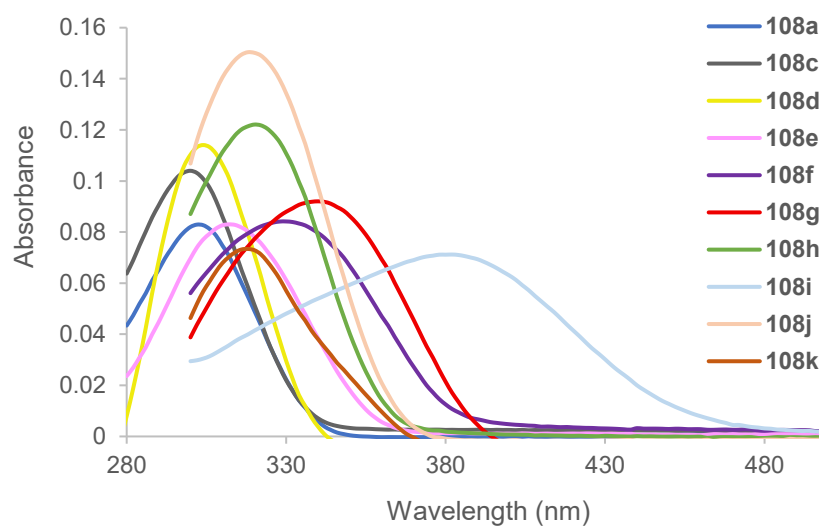
Following the successful synthesis of ten aryl tryptophan analogues **108**, each compound was subjected to comprehensive photophysical characterisation, including the determination of fluorescence quantum yield and brightness (**Table 15**). A pronounced bathochromic shift in the absorbance maxima was observed across the series compared to the parent tryptophan, with all compounds exhibiting

absorbance maxima above 300 nm in acetonitrile solution (**Figure 40**). The most red-shifted absorbance band was recorded for the 4-nitrophenyl tryptophan **108i** at 382 nm. Nevertheless, this tryptophan analogue was found to be non-fluorescent, a behaviour commonly observed for the nitro-aryl compounds, likely due to fluorescence quenching via photo-induced electron transfer (**Table 15**).¹⁹⁸ For the rest of the series, all compounds exhibited emission maxima above 360 nm, with the most red-shifted analogue **108g**, showing an emission band at 493 nm (**Figure 41**). However, the quantum yield of **108g** was among the lowest in the series (0.16), which resulted in rather low brightness value. Interestingly, the naphthol derivative **108k** also displayed a comparatively weak quantum yield of 0.4, which is still a reasonable value, though low relative to the rest of the series. Nevertheless, due to relatively high molar extinction coefficient, the brightness remained rather high albeit lower compared to most of the compounds in the library. The rest of the synthesised tryptophan analogues showed excellent fluorescent properties much improved compared to the parent tryptophan, with the quantum yield values of 0.73 and above. Remarkably, several compounds demonstrated near-unity quantum yield of 1, indicating that nearly all absorbed photons were re-emitted as fluorescence (*p*-methoxyphenyl tryptophan **108d** and biphenyl tryptophan **108j**). Among them, the compound **108j** displayed not only the highest molar extinction coefficient in the series, but also an exceptionally high brightness value of 35000 cm⁻¹ M⁻¹, nearly twice as high as the previously synthesised coumarin derivative **105**. This compound also featured a red-shifted emission maximum at 413 nm likely attributed to twisted intramolecular charge transfer. Another particularly notable compound was dimethyl aminophenyl analogue **108h**, which demonstrated strong brightness (>25000 cm⁻¹ M⁻¹) and an emission maximum near 400 nm in acetonitrile solution, further supporting its potential as a high-performance fluorophore.

Table 15. Photophysical properties evaluation of the compounds **108**.

Compound	λ_{abs} (nm)	λ_{em} (nm)	Stokes Shift (nm)	ϵ ($\text{cm}^{-1} \text{ M}^{-1}$)	Φ_{F}	Brightness ($\text{cm}^{-1} \text{ M}^{-1}$)
108a	302	369	67	17400	0.83	14360
108c	300	367	67	18700	0.76	14150
108d	304	361	57	10900	1.00	10900
108e	312	405	93	16000	0.76	12180
108f	330	445	115	18000	0.73	13180
108g	338	493	155	18100	0.16	2800
108h	320	385	65	32300	0.83	26640
108i	382	--	--	--	--	--
108j	318	413	95	35300	1.00	35300
108k	318	418	100	24600	0.40	9940

-- below the limit of detection

**Figure 40.** Absorbance spectrum of the compounds **108**. Spectra were recorded at 5 μM concentration in acetonitrile.

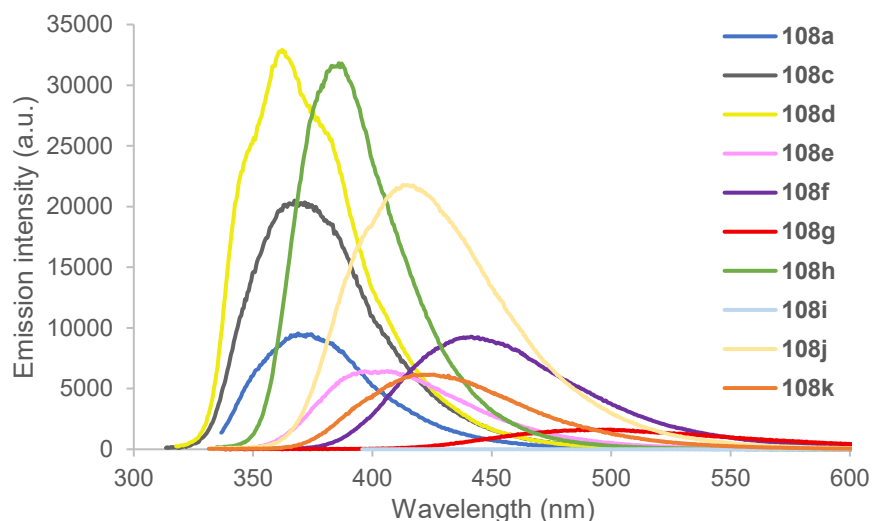
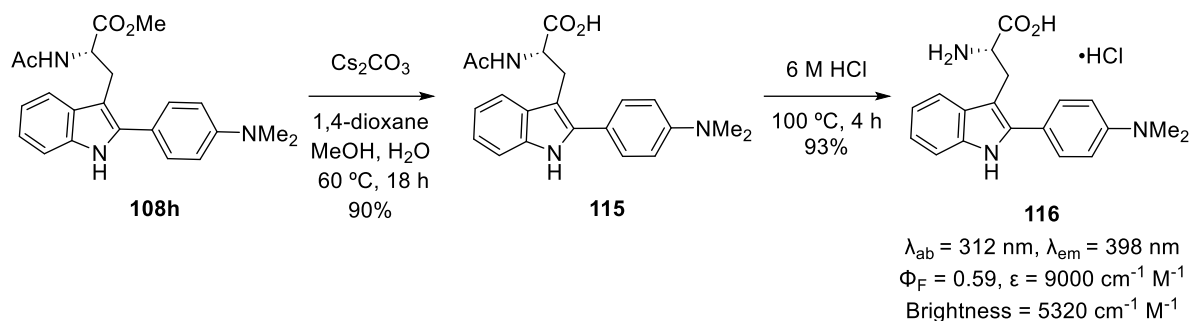


Figure 41. Emission spectra of the compounds **108**. Spectra were recorded at 5 μ M concentration in acetonitrile. Excitation was performed at the absorption maximum.

As dimethyl aminophenyl analogue **108h** compound demonstrated promising results as well as potential as an environmentally sensitive fluorophore due to the presence of the amino-substituent, further investigation was undertaken. This compound was subjected to deprotection reactions to evaluate photophysical properties of the unprotected amino acid and assess its suitability for solid phase peptide synthesis (**Scheme 53**). First, ester hydrolysis was performed under standard basic conditions at 60 °C overnight, which gave the intermediate carboxylic acid **115** in 90% yield. Subsequently, the acetyl protecting group was removed using 6 M HCl at 100 °C, which gave access to unprotected amino acid **116** in 93% yield. The photophysical characterisation of the synthesised amino acid **116** revealed that while absorbance and emission maxima did not change significantly, only shifting slightly to the blue-light region and red-light region correspondingly, the molar extinction coefficient and quantum yield values decreased notably. As a result, the brightness value dropped by 80% relative to the protected analogue. Nevertheless, the remaining brightness was still considered sufficient for potential future applications.



Scheme 53. Deprotection of **108h**. Conducted by Arthur Wong.

Further photophysical investigation were conducted, including solvatochromic and pH-dependent studies (**Figure 42**). Although compound **116** was designed as a charge-transfer probe, the solvatochromic study revealed no significant shift in emission maxima across different solvents as only the fluorescence intensity decreased in acetonitrile and water. In contrast, the compound exhibited high pH sensitivity, maintaining strong fluorescence at basic pH, but a significant decrease in intensity upon protonation of the dimethyl amino group. This protonation disrupted the charge-transfer process, leading to fluorescence quenching.

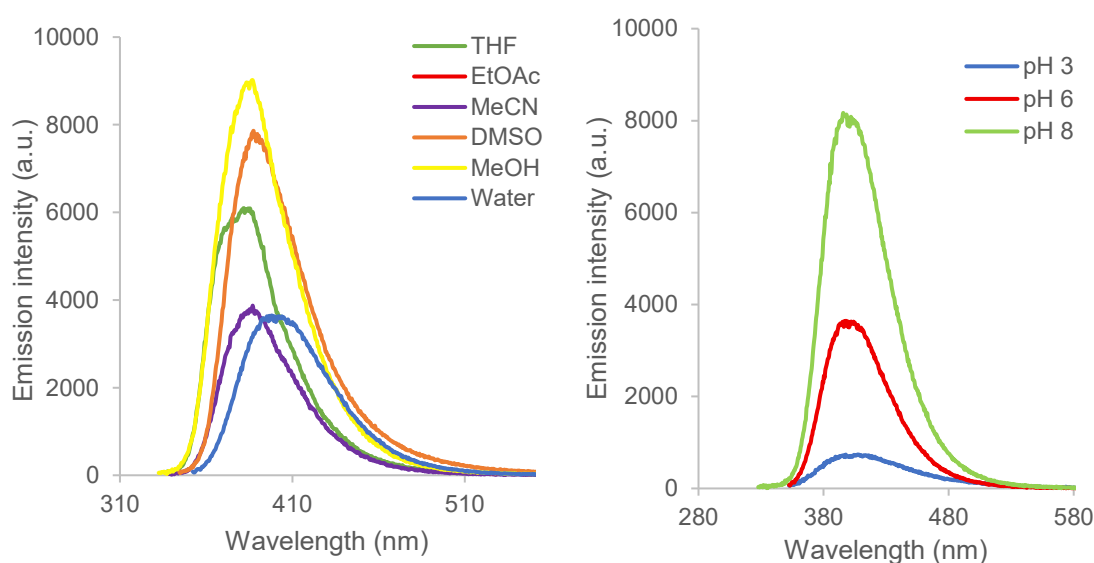
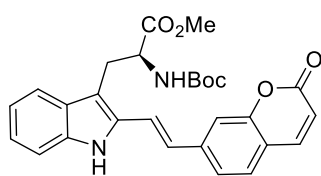


Figure 42. Fluorescence solvatochromic and pH studies of **116**. Conducted by Arthur Wong.

2.3.6 Conclusions and future work

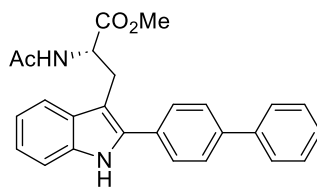
In summary, several novel fluorescent tryptophan analogues were synthesised via derivatisation of the tryptophan scaffold at C2-position of the indole ring. The first library comprised compounds bearing electron-withdrawing groups attached to the indole ring through an alkene bridge. These derivatives were accessed through a novel synthetic strategy involving alkenylation reactions of 2-formyl tryptophan. This approach enabled the synthesis of highly bright coumarin tryptophan derivative **105**, with a brightness value of $19400\text{ cm}^{-1}\text{ M}^{-1}$ (**Figure 43**). This compound exhibited excellent photophysical characteristics, including a significantly red-shifted emission beyond 500 nm, substantially different from the parent tryptophan amino acid. Its properties indicated strong potential as an environmentally sensitive probe as this tryptophan analogue exhibited bright fluorescence in lipid-rich environments but was quenched under aqueous conditions. Coumarin derivative **105** also proved to be applicable for two-photon excitation studies. This compound was successfully deprotected, generating a compound that could be used for future solid phase peptide synthesis applications. The next phase of this project will focus on incorporating this coumarin amino acid into a peptide to evaluate its fluorescent properties and explore its potential application in biological imaging.

The second library of tryptophan derivatives, featuring an aryl moiety at the C2-position also demonstrated exceptional photophysical properties with quantum yields reaching up to 1 and significantly outperforming parent tryptophan (e.g. **108j** and **108h**, **Figure 43**). The synthetic methodology developed for this library exhibited broad tolerance towards various aryl boronic acids with a range of substituents, enabling successful synthesis of derivatives, previously inaccessible by other methods. Dimethylaminophenyl analogue **116** showed promising results as a pH sensitive probe. Although when deprotected it exhibited decreased brightness, it still maintained strong potential as an effective fluorescent probe. Future work for this project will focus on incorporating the brightest amino acids into peptides and exploring further applications of these for fluorescent imaging.



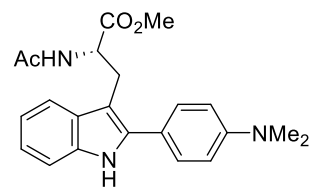
105

$\lambda_{ab} = 406 \text{ nm}$, $\lambda_{em} = 560 \text{ nm}$
 $\Phi_F = 0.48$, $\epsilon = 40600 \text{ cm}^{-1} \text{ M}^{-1}$
 Brightness = $19410 \text{ cm}^{-1} \text{ M}^{-1}$



108j

$\lambda_{ab} = 318 \text{ nm}$, $\lambda_{em} = 413 \text{ nm}$
 $\Phi_F = 1$, $\epsilon = 35300 \text{ cm}^{-1} \text{ M}^{-1}$
 Brightness = $35840 \text{ cm}^{-1} \text{ M}^{-1}$



108h

$\lambda_{ab} = 320 \text{ nm}$, $\lambda_{em} = 385 \text{ nm}$
 $\Phi_F = 0.83$, $\epsilon = 32300 \text{ cm}^{-1} \text{ M}^{-1}$
 Brightness = $26640 \text{ cm}^{-1} \text{ M}^{-1}$

Figure 43. Optimal fluorescent tryptophan analogues synthesised in this project.

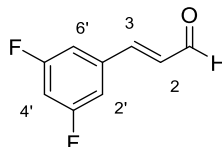
3. Experimental Section

3.1 General Experimental

All reactions were performed under an atmosphere of air unless otherwise stated. All reagents and starting materials were obtained from commercial sources unless otherwise stated. Brine refers to a saturated solution of sodium chloride. All dry solvents were purified using a PureSolv 500 MD solvent purification system. Flash column chromatography was carried out using Merck Geduran[®] Si 60 (40–63 μm). Merck Supelco aluminium-backed plates pre-coated with silica gel 60 were used for thin layer chromatography and were visualised under a UV lamp. ^1H NMR and ^{13}C NMR spectra were recorded on a Bruker DPX 400 spectrometer with chemical shift values in ppm relative to tetramethylsilane or residual chloroform or residual dimethyl sulfoxide or residual methanol as standard. J values are reported in Hz. The assignment of ^1H NMR spectra are based on COSY experiments and ^{13}C NMR spectra is based on DEPT, HSQC and HMBC experiments. The NMR data is provided only for major rotamer when the ratio of major-to-minor rotamer is equal to or over 2:1. Infrared spectra were recorded using a Jasco FTIR-4100 spectrometer directly as either a solid or liquid and mass spectra were obtained using a JEOL JMS-700 spectrometer or Agilent 6546 mass spectrometer. Melting points were determined on a Gallenkamp melting point apparatus or Stuart Scientific melting point apparatus. Optical rotations were determined as solutions irradiating with the sodium D line ($\lambda = 598 \text{ nm}$) using an Autopol V polarimeter. $[\alpha]_{\text{D}}$ values are reported in units $10^{-1} \text{ deg cm}^2 \text{ g}^{-1}$. Chiral HPLC spectra were obtained using Shimadzu LC-20AD prominence liquid chromatograph with a CBM-20A prominence communications bus module, DGU-20A5 prominence degasser, SPD-M20A prominence diode array detector (210 or 254 nm) and a Shimadzu CTO-20AC prominence column oven (25 $^{\circ}\text{C}$). Analysis was performed using 20 μL sample injections and methods were calibrated with the corresponding racemic mixtures. Data acquisition and processing was performed using LabSolutions 1.21 SP1 chromatography software.

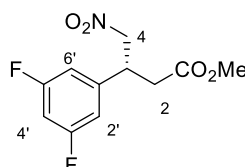
3.2 SV2A PET Imaging Agent Experimental

(*E*)-3-(3',5'-Difluorophenyl)prop-2-enal (**60**)⁵⁶



In the oven-dried flask, 3,5-difluorobenzaldehyde (**56**) (2.00 g, 14.1 mmol) and (triphenylphosphoranylidene)acetaldehyde (4.71 g, 15.5 mmol) were dissolved in anhydrous tetrahydrofuran (200 mL) under argon. The reaction mixture was heated to 50 °C and stirred for 18 h. The crude mixture was cooled to room temperature and concentrated *in vacuo*. The resulting residue was dissolved in ethyl acetate (100 mL) and washed with water (100 mL). The aqueous layer was extracted with ethyl acetate (2 × 100 mL). The combined organic layers were dried (MgSO₄), filtered and concentrated *in vacuo*. The crude material was purified by flash column chromatography eluting with 10% diethyl ether in petroleum ether (40–60) to give (*E*)-3-(3',5'-difluorophenyl)prop-2-enal (**60**) as a pale-yellow solid (1.84 g, 78%). Spectroscopic data were consistent with the literature.⁵⁶ δ_{H} (400 MHz, CDCl₃) 6.68 (1H, dd, *J* 16.0, 7.5 Hz, 2-H), 6.90 (1H, tt, *J* 8.6, 2.3 Hz, 4'-H), 7.07–7.10 (2H, m, 2'-H and 6'-H), 7.39 (1H, d, *J* 16.0 Hz, 3-H), 9.73 (1H, d, *J* 7.5 Hz, 1-H); δ_{C} (101 MHz, CDCl₃) 106.3 (t, ²*J*_{CF} 25.5 Hz, CH), 111.1 (dd, ²*J*_{CF} 19.2 Hz, ⁴*J*_{CF} 7.2 Hz, 2 × CH), 130.6 (CH), 137.2 (t, ³*J*_{CF} 9.5 Hz, C), 149.4 (t, ⁴*J*_{CF} 3.0 Hz, CH), 163.3 (dd, ¹*J*_{CF} 250.2 Hz, ³*J*_{CF} 12.7 Hz, 2 × C), 192.9 (CH); *m/z* (ESI) 191 (MNa⁺, 100%).

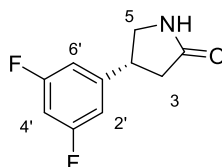
Methyl (3*R*)-3-(3',5'-difluorophenyl)-4-nitrobutanoate ((*R*)-**58**)⁵⁶



To a stirred solution of (*E*)-3-(3',5'-difluorophenyl)prop-2-enal (**60**) (0.068 g, 0.40 mmol) in methanol (1.2 mL) (*R*)- α,α -bisphenyl-2-pyrrolidinemethanol trimethylsilyl ether (**Cat-2**) (0.013 g, 0.040 mmol), benzoic acid (0.010 g, 0.080 mmol) and

nitromethane (0.065 mL, 1.2 mmol) were added. The reaction mixture was stirred for 18 h and then cooled to 0 °C. *N*-Bromosuccinimide (0.092 g, 0.52 mmol) was added, and the mixture was stirred for another 18 h slowly warming up to 15 °C. The mixture was then concentrated *in vacuo*. The crude material was purified by flash column chromatography eluting with 60% dichloromethane in hexane to give methyl (3*R*)-3-(3',5'-difluorophenyl)-4-nitrobutanoate ((**R**)-**58**) as a colourless oil, which solidified upon standing (0.053 g, 51% over two steps). $[\alpha]_{\text{D}}^{19} +9.6$ (c 0.1, CHCl₃). Spectroscopic data were consistent with the literature.⁵⁶ δ_{H} (400 MHz, CDCl₃) 2.75 (1H, d, *J* 16.6, 7.6 Hz, 2-*HH*), 2.75 (1H, d, *J* 16.6, 7.2 Hz, 2-*HH*), 3.67 (3H, s, OCH₃), 3.93–4.03 (1H, m, 3-H), 4.62 (1H, dd, *J* 13.0, 8.2 Hz, 4-*HH*), 4.73 (1H, dd, *J* 13.0, 6.6 Hz, 4-*HH*), 6.70–6.82 (3H, m, 4'-H, 2'-H and 6'-H); δ_{C} (101 MHz, CDCl₃) 37.1 (CH₂), 39.7 (t, ⁴*J*_{CF} 1.8 Hz, CH), 52.2 (CH₃), 78.7 (CH₂), 103.8 (t, ²*J*_{CF} 25.2 Hz, CH), 110.6 (dd, ²*J*_{CF} 18.8 Hz, ⁴*J*_{CF} 7.3 Hz, 2 × CH), 142.2 (t, ³*J*_{CF} 8.9 Hz, C), 163.4 (dd, ¹*J*_{CF} 250.2 Hz, ³*J*_{CF} 12.8 Hz, 2 × C), 170.5 (C); *m/z* (ESI) 282 (MNa⁺, 100%). The enantiomeric ratio was determined by HPLC analysis with a CHIRALCEL® AD-H column (95:5, hexane: *i*PrOH, flow rate of 1.0 mL/min): *t*_{major} = 14.28 min, *t*_{minor} = 11.84 min; 99:1 *er*.

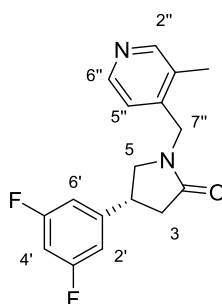
(4*R*)-4-(3',5'-Difluorophenyl)pyrrolidin-2-one ((R**)-**59**)**⁵⁶



To a stirred suspension of methyl (3*R*)-3-(3',5'-difluorophenyl)-4-nitrobutanoate ((**R**)-**58**) (0.124 g, 0.478 mmol) in a mixture of ethanol and water (4.5 mL, 2:1, v/v) was added ammonium chloride (0.768 g, 14.7 mmol) and iron powder (0.267 g, 4.78 mmol). After stirring for 1.5 h at room temperature, the reaction mixture was adjusted to pH 14 with 6 M aqueous sodium hydroxide solution (2 mL) and extracted with ethyl acetate (3 × 50 mL). The combined organic layers were dried (MgSO₄), filtered and concentrated *in vacuo*. The crude material was purified by flash column chromatography eluting with 5% methanol in diethyl ether to give (4*R*)-4-(3',5'-difluorophenyl)pyrrolidin-2-one ((**R**)-**59**) as a white solid (0.060 g, 63%). $[\alpha]_{\text{D}}^{19} -25.9$ (c 0.1, CHCl₃). Spectroscopic data were consistent with the literature.⁵⁶ δ_{H} (400

MHz, CDCl₃) 2.44 (1H, dd, *J* 16.9, 8.2 Hz, 3-*HH*), 2.75 (1H, dd, *J* 16.9, 9.0 Hz, 3-*HH*), 3.39 (1H, dd, *J* 9.6, 6.8 Hz, 5-*HH*), 3.61–3.72 (1H, m, 4-H), 3.75–3.83 (1H, m, 5-*HH*), 5.74 (1H, br s, NH), 6.72 (1H, tt, *J* 8.8, 2.4 Hz, 4'-H), 6.75–6.81 (2H, m, 2'-H and 6'-H); δ_C (101 MHz, CDCl₃) 37.7 (CH₂), 40.0 (t, ⁴*J*_{CF} 2.1 Hz, CH), 49.1 (CH₂), 102.8 (t, ²*J*_{CF} 25.2 Hz, CH), 109.9 (dd, ²*J*_{CF} 18.5 Hz, ⁴*J*_{CF} 7.0 Hz, 2 × CH), 146.2 (t, ³*J*_{CF} 8.8 Hz, C), 163.4 (dd, ¹*J*_{CF} 250.1 Hz, ³*J*_{CF} 12.9 Hz, 2 × C), 177.1 (C); *m/z* (ESI) 220 (MNa⁺, 100%).

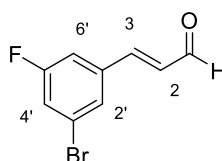
(4*R*)-4-(3',5'-Difluorophenyl)-1-[(3''-methylpyridin-4''-yl)methyl]pyrrolidin-2-one ((*R*)-7)⁵⁶



In an oven-dried flask under argon, sodium hydride (0.0810 g, 2.03 mmol, 60% dispersion in mineral oil) was added, washed with hexane (2 mL) and dried at the room temperature *in vacuo* for 0.5 h. Then it was suspended in anhydrous tetrahydrofuran (1 mL) and cooled to 0 °C. A solution of (4*R*)-4-(3',5'-difluoro-4'-iodophenyl)pyrrolidin-2-one ((*R*)-59) (0.182 g, 0.923 mmol) in anhydrous tetrahydrofuran (3 mL) was added to the mixture, followed by 4-(chloromethyl)-3-methylpyridine hydrochloride (0.181 g, 1.02 mmol) and tetrabutylammonium iodide (0.0170 g, 0.0462 mmol). The reaction mixture was warmed to room temperature and was stirred for 18 h. After cooling to 0 °C, the reaction was quenched with saturated aqueous sodium bicarbonate solution (5 mL) and extracted with chloroform (3 × 10 mL). The combined organic layers were dried (MgSO₄), filtered and concentrated *in vacuo*. The crude material was purified by flash column chromatography eluting with 10% methanol in diethyl ether to give (4*R*)-4-(3',5'-difluorophenyl)-1-[(3''-methylpyridin-4''-yl)methyl]pyrrolidin-2-one ((*R*)-7) as a white solid (0.237 g, 89%). [α]_D¹⁹ +21.9 (*c* 0.1, CHCl₃). Spectroscopic data were consistent with previously published data.⁵⁶ δ_H (400 MHz, CDCl₃) 2.31 (3H, s, 3''-CH₃), 2.60 (1H, dd, *J* 17.0, 8.2 Hz, 3-*HH*), 2.91 (1H, dd, *J* 17.0, 8.6 Hz, 3-*HH*), 3.24 (1H, dd, *J*

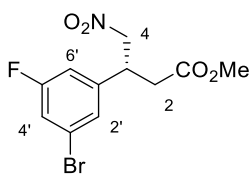
8.0, 5.6 Hz, 5-*HH*), 3.53–3.66 (2H, m, 4-H and 5-*HH*), 4.42 (1H, d, *J* 15.6 Hz, 7''-*HH*), 4.62 (1H, d, *J* 15.6 Hz, 7''-*HH*), 6.66–6.76 (3H, m, 2'-H, 4'-H and 6'-H), 7.04 (1H, d, *J* 5.2 Hz, 5''-H), 8.39–8.45 (2H, m, 2''-H and 6''-H); δ_{C} (101 MHz, CDCl_3) 16.1 (CH_3), 37.1 (t, $^4J_{\text{CF}}$ 2.1 Hz, CH), 38.2 (CH_2), 43.7 (CH_2), 53.5 (CH_2), 102.9 (t, $^2J_{\text{CF}}$ 25.4 Hz, CH), 109.8 (dd, $^2J_{\text{CF}}$ 18.6 Hz, $^4J_{\text{CF}}$ 7.0 Hz, 2 \times CH), 122.5 (CH), 131.7 (C), 142.8 (C), 145.8 (t, $^3J_{\text{CF}}$ 8.8 Hz, C), 148.1 (CH), 151.5 (CH), 163.4 (dd, $^1J_{\text{CF}}$ 250.4 Hz, $^3J_{\text{CF}}$ 12.8 Hz, 2 \times C), 173.2 (C); *m/z* (ESI) 303 (MH^+ , 100%). The enantiomeric ratio was determined by HPLC analysis with a CHIRALCEL[®] AD-H column (90:10, hexane:*i*PrOH, flow rate of 2.0 mL/min): t_{major} = 13.19 min, t_{minor} = 11.73 min; 98:2 *er*.

(*E*)-3-(3'-Bromo-5'-fluorophenyl)prop-2-enal (21**)**⁵⁶



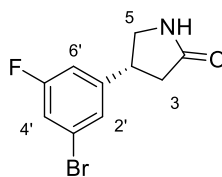
In the oven-dried flask, 3-bromo-5-fluorobenzaldehyde (**1**) (1.00 g, 4.92 mmol) and methyl (triphenylphosphoranylidene)acetaldehyde (1.65 g, 5.40 mmol) were dissolved in anhydrous tetrahydrofuran (70 mL), under argon. The reaction mixture was stirred at room temperature for 18 h and then concentrated *in vacuo*. The crude material was purified by flash column chromatography eluting with 10% diethyl ether in hexane to give (*E*)-3-(3'-bromo-5'-fluorophenyl)prop-2-enal (**21**) as a white solid (0.900 g, 80%). Spectroscopic data were consistent with previously published data.⁵⁶ δ_{H} (400 MHz, CDCl_3) 6.68 (1H, dd, *J* 16.0, 7.5 Hz, 2-H), 7.21 (1H, dt, *J* 8.9, 2.0 Hz, 6'-H), 7.32 (1H, dt, *J* 7.8, 2.0 Hz, 4'-H), 7.36 (1H, d, *J* 16.0 Hz, 3-H), 7.48–7.51 (1H, m, 2'-H), 9.72 (1H, d, *J* 7.5 Hz, 1-H); δ_{C} (101 MHz, CDCl_3) 113.6 (d, $^2J_{\text{CF}}$ 22.1 Hz, CH), 121.4 (d, $^2J_{\text{CF}}$ 24.6 Hz, CH), 123.4 (d, $^3J_{\text{CF}}$ 9.8 Hz, C), 127.4 (d, $^4J_{\text{CF}}$ 3.2 Hz, CH), 130.6 (CH), 137.5 (d, $^3J_{\text{CF}}$ 8.2 Hz, C), 149.0 (d, $^4J_{\text{CF}}$ 2.8 Hz, CH), 162.8 (d, $^1J_{\text{CF}}$ 252.3 Hz, C), 192.8 (CH); *m/z* (ESI) 250 (MNa^+ , 100%).

Methyl (3*R*)-3-(3'-bromo-5'-fluorophenyl)-4-nitrobutanoate ((*R*)-24**)**⁵⁶



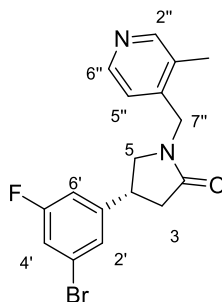
To a stirred solution of (*E*)-3-(3',5'-difluorophenyl)prop-2-enal (**21**) (0.900 g, 3.96 mmol) in methanol (12 mL) (*R*)- α,α -bisphenyl-2-pyrrolidinemethanol trimethylsilyl ether (**Cat-1**) (0.129 g, 0.396 mmol), benzoic acid (0.0960 mg, 0.793 mmol) and nitromethane (0.650 mL, 11.9 mmol) were added. The reaction mixture was stirred for 18 h and then cooled to 0 °C. *N*-Bromosuccinimide (0.917 g, 5.15 mmol) was added, and the mixture was stirred for another 18 h slowly warming up to 15 °C. The mixture was then concentrated *in vacuo*. The crude material was purified by flash column chromatography eluting with 60% dichloromethane in hexane to give methyl (3*R*)-3-(3'-bromo-5'-fluorophenyl)-4-nitrobutanoate ((*R*)-**24**) as a colourless oil, which solidified upon standing (0.495 g, 40% over two steps). $[\alpha]_D^{19} +7.6$ (c 0.1, CHCl₃). Spectroscopic data were consistent with the literature.⁵⁶ δ_H (400 MHz, CDCl₃) 2.74 (1H, d, *J* 16.6, 7.6 Hz, 2-*HH*), 2.74 (1H, d, *J* 16.6, 7.2 Hz, 2-*HH*), 3.67 (3H, s, OCH₃), 3.91–4.00 (1H, m, 3-*H*), 4.62 (1H, dd, *J* 13.2, 8.2 Hz, 4-*HH*), 4.73 (1H, dd, *J* 13.2, 6.4 Hz, 4-*HH*), 6.91 (1H, dt, *J* 8.9, 1.9 Hz, 4'-*H*), 7.15–7.21 (2H, m, 2'-*H* and 6'-*H*); δ_C (101 MHz, CDCl₃) 37.2 (CH₂), 39.6 (d, $^4J_{CF}$ 1.8 Hz, CH), 52.3 (CH₃), 78.7 (CH₂), 113.8 (d, $^2J_{CF}$ 22.1 Hz, CH), 119.1 (d, $^2J_{CF}$ 24.3 Hz, CH), 123.4 (d, $^3J_{CF}$ 9.9 Hz, C), 126.6 (d, $^4J_{CF}$ 3.2 Hz, CH), 142.5 (d, $^3J_{CF}$ 7.7 Hz, C), 162.8 (d, $^1J_{CF}$ 253.2 Hz, C), 170.6 (C); *m/z* (ESI) 341 (MNa⁺, 100%). The enantiomeric ratio was determined by HPLC analysis with a CHIRALCEL® AD-H column (98:2, hexane:*i*PrOH, flow rate of 1.0 mL/min): *t*_{major} = 12.72 min, *t*_{minor} = 11.48 min; 97:3 *er*.

(4*R*)-4-(3'-Bromo-5'-fluorophenyl)pyrrolidin-2-one ((*R*)-4)⁵⁶



To a stirred suspension of methyl (3*R*)-3-(3'-bromo-5'-fluorophenyl)-4-nitrobutanoate (**((*R*)-24)**) (0.495 g, 1.55 mmol) in a mixture of ethanol and water (16.5 mL, 2:1, v/v) was added ammonium chloride (2.48 g, 46.4 mmol) and iron powder (0.865 g, 15.5 mmol). After stirring for 18 h at room temperature, the reaction mixture was adjusted to pH 14 with 6 M aqueous sodium hydroxide solution (10 mL) and stirred for 2 h at room temperature. The mixture was filtered through Celite[®], washed with chloroform (200 mL) and water (100 mL), then concentrated *in vacuo*. The residue was diluted with chloroform (200 mL), which was washed with water (200 mL). The aqueous layer was then extracted with chloroform (200 mL). The combined organic layers were dried (MgSO₄), filtered and concentrated *in vacuo*. The crude material was purified by flash column chromatography eluting with 7% methanol in diethyl ether to give (4*R*)-4-(3'-bromo-5'-fluorophenyl)pyrrolidin-2-one (**((*R*)-4)**) as a white solid (0.290 g, 73%). [α]_D²⁰ -18.5 (*c* 0.1, CHCl₃). Spectroscopic data were consistent with the literature.⁵⁶ δ_{H} (400 MHz, CDCl₃) 2.44 (1H, dd, *J* 16.8, 8.4 Hz, 3-*HH*), 2.75 (1H, dd, *J* 16.8, 8.8 Hz, 3-*HH*), 3.39 (1H, dd, *J* 9.6, 6.8 Hz, 5-*HH*), 3.62–3.73 (1H, m, 4-H), 3.76–3.83 (1H, m, 5-*HH*), 5.73 (1H, br s, NH), 6.92 (1H, dt, *J* 9.2, 2.0 Hz, 6'-H), 7.12–7.21 (2H, m, 4'-H and 2'-H); δ_{C} (101 MHz, CDCl₃) 37.7 (CH₂), 39.8 (d, ⁴*J*_{CF} 1.8 Hz, CH), 49.1 (CH₂), 113.0 (d, ²*J*_{CF} 21.7 Hz, CH), 118.1 (d, ²*J*_{CF} 24.4 Hz, CH), 123.2 (d, ³*J*_{CF} 10.0 Hz, C), 126.0 (d, ⁴*J*_{CF} 3.1 Hz, CH), 146.4 (d, ³*J*_{CF} 7.7 Hz, C), 163.0 (d, ¹*J*_{CF} 252.5 Hz, C), 177.0 (C); *m/z* (ESI) 280 (MNa⁺, 100%).

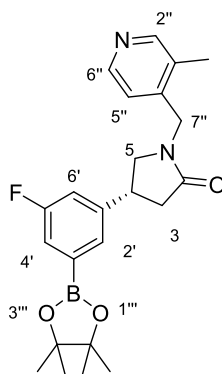
(4*R*)-4-(3'-Bromo-5'-fluorophenyl)-1-[(3''-methylpyridin-4''-yl)methyl]-pyrrolidin-2-one ((*R*)-5)⁵⁶



Sodium hydride (0.0980 g, 2.45 mmol, 60% dispersion in mineral oil) was added to an oven-dried flask under argon and cooled to 0 °C. This was washed with hexane (2 mL) and then dried *in vacuo* at room temperature for 15 min. The flask was cooled to 0 °C, and anhydrous tetrahydrofuran (2.5 mL) was added. To this solution was added (4*R*)-4-(3'-bromo-5'-fluorophenyl)pyrrolidin-2-one ((*R*)-4) (0.288 g, 1.11 mmol), 4-(chloromethyl)-3-methylpyridine hydrochloride (0.218 g, 1.22 mmol) and potassium iodide (0.0210 g, 0.0140 mmol). The reaction mixture was warmed to room temperature and then stirred for 19 h. After cooling to 0 °C, the reaction was quenched with saturated aqueous sodium bicarbonate solution (10 mL) and extracted with chloroform (3 × 20 mL). The combined organic layers were dried (MgSO₄), filtered and concentrated *in vacuo*. The crude material was purified by flash column chromatography eluting with 10% methanol in diethyl ether to give (4*R*)-4-(3'-bromo-5'-fluorophenyl)-1-[(3''-methylpyridin-4''-yl)methyl]pyrrolidin-2-one ((*R*)-5) as a pale yellow solid (0.309 g, 76%). [α]_D¹⁸ +28.9 (*c* 0.1, CHCl₃). Spectroscopic data were consistent with the literature.⁵⁶ δ_{H} (400 MHz, CDCl₃) 2.32 (3H, s, 3''-CH₃), 2.59 (1H, dd, *J* 17.0, 7.7 Hz, 3-*HH*), 2.92 (1H, dd, *J* 17.0, 8.6 Hz, 3-*HH*), 3.24 (1H, dd, *J* 9.2, 6.0 Hz, 5-*HH*), 3.53– 3.65 (2H, m, 4-H and 5-*HH*), 4.44 (1H, d, *J* 15.4 Hz, 7''-*HH*), 4.60 (1H, d, *J* 15.4 Hz, 7''-*HH*), 6.84 (1H, dt, *J* 9.2, 2.0 Hz, 6'-H), 7.04 (1H, d, *J* 4.8 Hz, 5''-H), 7.12 (1H, br t, *J* 2.0 Hz, 2'-H), 7.15 (1H, dt, *J* 8.0, 2.0 Hz, 4'-H), 8.41–8.46 (2H, m, 2''-H and 6''-H); δ_{C} (101 MHz, CDCl₃) 16.0 (CH₃), 36.7 (d, ⁴*J*_{CF} 1.9 Hz, CH), 38.1 (CH₂), 43.6 (CH₂), 53.4 (CH₂), 112.8 (d, ²*J*_{CF} 21.7 Hz, CH), 118.1 (d, ²*J*_{CF} 24.4 Hz, CH), 122.5 (CH), 123.2 (d, ³*J*_{CF} 9.1 Hz, C), 125.8 (d, ⁴*J*_{CF} 3.2 Hz, CH), 131.6 (C), 142.6 (C), 145.9 (d, ³*J*_{CF} 7.6 Hz, C), 148.2 (CH), 151.6 (CH), 162.9 (d, ¹*J*_{CF} 252.8 Hz, C), 173.0 (C); *m/z* (ESI) 363 (MH⁺, 100%). The enantiomeric ratio was determined by HPLC analysis with a CHIRALCEL[®] AD-H

column (92:8, hexane:*i*PrOH, flow rate of 1.5 mL/min): $t_{\text{major}} = 21.62$ min, $t_{\text{minor}} = 17.81$ min; 98:2 *er*.

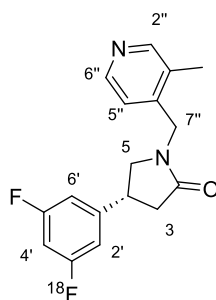
(4*R*)-4-(3'-(4''',4''',5''',5'''-tetramethyl-1''',3''',2'''-dioxaborolan-2'''-yl)-5'-fluorophenyl)-1-[(3''-methylpyridin-4''-yl)methyl]pyrrolidin-2-one ((*R*)-8)



(4*R*)-4-(3'-Bromo-5'-fluorophenyl)-1-[(3''-methylpyridin-4''-yl)methyl]pyrrolidin-2-one (**(*R*)-5**) (0.150 g, 0.413 mmol) was dissolved in anhydrous dioxane (2.8 mL) under argon. To the mixture was added bis(pinacolato)diboron (0.158 g, 0.620 mmol), [1,1'-bis(diphenylphosphino)ferrocene]palladium(II) dichloride (0.0160 g, 0.0206 mmol) and potassium acetate (0.203 g, 2.07 mmol). The reaction mixture was stirred for 1 h at 100 °C. The mixture was cooled to room temperature, filtered through Celite®, washed with chloroform (50 mL) and concentrated *in vacuo*. The resulting brown residue was then filtered through the silica plug, washed with the mixture of ethyl acetate and ethanol (4:1, 300 mL) and concentrated *in vacuo*. The resulting residue dissolved in minimal amounts of hot hexane and a few drops of chloroform and filtered while hot. The solution was cooled in a freezer for 24 h and the resulting solid was filtered off, washed with cold hexane and dried *in vacuo* to give (4*R*)-4-(3'-fluoro-5'-(4''',4''',5''',5'''-tetramethyl-1''',3''',2'''-dioxaborolan-2'''-yl)phenyl)-1-[(3''-methylpyridin-4''-yl)methyl]pyrrolidin-2-one (**(*R*)-8**) as beige solid (0.114 g, 67%). Mp 111–114 °C; $\nu_{\text{max}}/\text{cm}^{-1}$ (neat) 2977 (CH), 1687 (C=O), 1437, 1257, 1156, 1066; $[\alpha]_{\text{D}}^{18} +21.9$ (c 0.1, CHCl₃); δ_{H} (400 MHz, CDCl₃) 1.34 (12H, s, 4 × CH₃), 2.32 (3H, s, 3''-CH₃), 2.66 (1H, dd, J 16.8, 8.1 Hz, 3-*HH*), 2.91 (1H, dd, J 16.8, 8.1 Hz, 3-*HH*), 3.25–3.32 (1H, m, 4-*H*), 3.62 (2H, m, 5-CH₂), 4.42 (1H, d, J 15.5 Hz, 7''-*HH*), 4.62 (1H, d, J 15.5 Hz, 7''-*HH*), 6.98 (1H, dt, J 9.7, 2.4 Hz, 6'-*H*), 7.06 (1H, d, J 4.7 Hz, 5''-*H*), 7.37 (1H, dd, J 8.6, 2.4 Hz, 4'-*H*), 7.40 (1H, br s, 2'-*H*), 8.41–8.42 (2H, s, 2''-*H*), 8.42 (1H, d, J 4.7 Hz, 6''-*H*); δ_{C} (101 MHz, CDCl₃) 15.9 (CH₃), 24.9 (4 × CH₃),

37.0 (d, $^4J_{\text{CF}}$ 1.9 Hz, CH), 38.3 (CH₂), 43.6 (CH₂), 53.8 (CH₂), 84.3 (2 × C), 116.5 (d, $^2J_{\text{CF}}$ 21.8 Hz, CH), 119.9 (d, $^2J_{\text{CF}}$ 19.4 Hz, CH), 122.3 (CH), 128.6 (d, $^4J_{\text{CF}}$ 2.7 Hz, CH), 131.6 (C), 142.9 (C), 143.7 (d, $^3J_{\text{CF}}$ 6.4 Hz, C), 148.0 (CH), 151.3 (CH), 162.7 (d, $^1J_{\text{CF}}$ 247.9 Hz, C), 173.6 (C). The carbon directly attached to the boron atom was not detected, likely due to quadrupolar relaxation.¹⁹⁹ m/z (ESI) 411.2266 (MH⁺. C₂₃H₂₉BFN₂O₃ requires 411.2254).

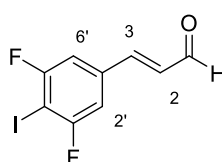
(4*R*)-4-(3'-[¹⁸F]fluoro-5'-fluorophenyl)-1-[(3"-methylpyridin-4"-yl)methyl]-pyrrolidin-2-one ((*R*)-[¹⁸F]7)⁵⁶



No-carrier added aqueous [¹⁸F]fluoride was produced *via* the ¹⁸O(p,n)¹⁸F nuclear reaction by irradiation of ¹⁸O-enriched water by a GE Healthcare PETtrace 860 cyclotron at the West of Scotland PET Centre. Fully automated radiosynthesis was performed on a customised RNPlus Synthra module. Immediately prior to delivering [¹⁸F]fluoride, (4*R*)-4-(3'-fluoro-5'-(4''',4''',5''',5'''-tetramethyl-1''',3''',2'''-dioxaborolan-2'''-yl)phenyl)-1-[(3"-methylpyridin-4"-yl)methyl]pyrrolidin-2-one (2.0 mg) ((*R*)-**8**), copper(II) trifluoromethanesulfonate (5.0 mg), and pyridine (10 μL) were dissolved in *N,N*-dimethylformamide (0.7 mL) and the solution was added to a reaction vessel. Cyclotron target water containing [¹⁸F]fluoride was transferred to and trapped on a QMA SepPakPlus Light cartridge. The trapped [¹⁸F]fluoride was eluted into a reaction vessel using a solution of tetrabutylammonium trifluoromethanesulfonate (9.3 mg) in 1:5 water/acetonitrile (0.6 mL). This solution was dried by stirring at 100 °C under vacuum and a stream of helium gas for 8 minutes. This process was repeated using acetonitrile (1 mL). The [¹⁸F]fluoride was then completely dried by applying full vacuum for 6 minutes. The mixture was cooled to 60 °C, then the solution of (4*R*)-4-(3'-fluoro-5'-(4''',4''',5''',5'''-tetramethyl-1''',3''',2'''-dioxaborolan-2'''-yl)phenyl)-1-[(3"-methylpyridin-4"-yl)methyl]pyrrolidin-2-one was added to the reaction vessel. The reaction mixture was heated to 115 °C for 20 minutes while being stirred. The reaction mixture was then cooled to 60 °C and diluted with

acetonitrile (2.0 mL). An aliquot was removed for analysis by analytical radioHPLC [C18 Phenomenex Synergi™ 4 µm Hydro-RP 80 Å (150 mm × 4.60 mm)], to allow radiochemical conversion and product identity. Analysis was performed using isocratic mobile phase acetonitrile:ammonium formate (0.1 M aq):acetic acid in a ratio of 400:600:0.5 at a flow rate of 1 mL min⁻¹. The eluent passing through the HPLC column was monitored continuously for radioactivity and absorbance at 230 nm. (4*R*)-4-(3'-[¹⁸F]Fluoro-5'-fluorophenyl)-1-[(3"-methylpyridin-4"-yl)methyl]-pyrrolidin-2-one ((*R*)-[¹⁸F]**7**) was afforded in 67% RCC (n = 4).

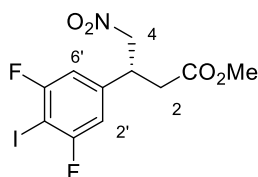
(*E*)-3-(3',5'-Difluoro-4'-iodophenyl)prop-2-enal (72**)**



In the oven-dried flask under argon, *N,N*-diisopropylethylamine (1.80 mL, 12.8 mmol) was dissolved in anhydrous tetrahydrofuran (18 mL). The resultant solution was cooled to -10 °C and a solution of *n*-butyllithium (4.90 mL, 2.5 M in hexane, 12.3 mmol) was added dropwise. The mixture was stirred for 0.5 h at -10 °C. The resulting solution was added dropwise to a solution of 3,5-difluorobenzonitrile (**69**) (1.03 g, 7.40 mmol) in anhydrous tetrahydrofuran (12 mL) at -78 °C under argon. After 10 minutes, a solution of iodine (2.25 g, 8.87 mmol) in anhydrous tetrahydrofuran (6 mL) was added dropwise. The reaction mixture was slowly warmed to room temperature and left stirring overnight under argon. After 18 h, the mixture was treated with a 10% aqueous solution of sodium thiosulfate (15 mL) and extracted with hexane/ethyl acetate mixture (v/v, 1:1, 3 × 24 mL). The combined organic layers were dried (MgSO₄), filtered and concentrated *in vacuo*. The resulting 3,5-difluoro-4-iodobenzonitrile (**70**) was obtained as a brown oil and was used without further purification. Diisobutylaluminium anhydride (9.10 mL, 1 M in dichloromethane, 9.10 mmol) was then added dropwise to a solution of 3,5-difluoro-4-iodobenzonitrile (**70**) (2.02 g, 7.62 mmol) in anhydrous dichloromethane (22 mL) under argon at 0 °C. The reaction was slowly warmed to room temperature, stirred for 2 h, and then quenched with an aqueous solution of 6 M hydrochloric acid (20 mL). The mixture was extracted with dichloromethane (3 × 50 mL). The combined organic layers were passed through Celite®, dried (MgSO₄), filtered and

concentrated *in vacuo* to afford 3,5-difluoro-4-iodobenzaldehyde (**71**) as a white solid, which was used without further purification. 3,5-Difluoro-4-iodobenzaldehyde (**71**) (1.50 g, 5.63 mmol) and (triphenylphosphoranylidene)acetaldehyde (1.88 g, 6.19 mmol) were dissolved in anhydrous tetrahydrofuran (60 mL) under argon. The reaction mixture was heated to 50 °C and stirred for 18 h. The crude mixture was cooled to room temperature and concentrated *in vacuo*. The resulting residue was dissolved in ethyl acetate (40 mL) and washed with water (20 mL). The aqueous layer was extracted with ethyl acetate (2 × 40 mL). The combined organic layers were dried (MgSO₄), filtered and concentrated *in vacuo*. The crude material was purified by flash column chromatography eluting with 10% diethyl ether in petroleum ether (40–60) to give (*E*)-3-(3',5'-difluoro-4'-iodophenyl)prop-2-enal (**72**) as a pale-yellow solid (1.16 g, 53% over 3 steps). Mp 152–154 °C; $\nu_{\text{max}}/\text{cm}^{-1}$ (neat) 2923 (CH), 2356, 1663 (C=O), 1559, 1422, 1128, 1020; δ_{H} (400 MHz, CDCl₃) 6.72 (1H, dd, *J* 16.0, 7.5 Hz, 2-H), 7.06–7.11 (2H, m, 2'-H and 6'-H), 7.36 (1H, d, *J* 16.0 Hz, 3-H), 9.74 (1H, d, *J* 7.5 Hz, 1-H); δ_{C} (101 MHz, CDCl₃) 74.3 (t, $^2J_{\text{CF}}$ 29.7 Hz, C), 110.7 (dd, $^2J_{\text{CF}}$ 25.9 Hz, $^4J_{\text{CF}}$ 2.6 Hz, 2 × CH), 130.7 (CH), 137.0 (t, $^3J_{\text{CF}}$ 9.2 Hz, C), 148.5 (t, $^4J_{\text{CF}}$ 3.0 Hz, CH), 163.4 (dd, $^1J_{\text{CF}}$ 248.3 Hz, $^3J_{\text{CF}}$ 6.3 Hz, 2 × C), 192.7 (CH); *m/z* (ESI) 292.9277 ([M–H][–]. C₉H₄F₂I₂O requires 292.9280).

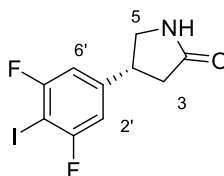
Methyl (3*R*)-3-(3',5'-difluoro-4'-iodophenyl)-4-nitrobutanoate ((*R*)-**75**)



To a stirred solution of (*E*)-3-(3',5'-difluoro-4'-iodophenyl)prop-2-enal (**72**) (0.18 g, 0.61 mmol) in methanol (1.3 mL) (*R*)- α,α -bisphenyl-2-pyrrolidinemethanol trimethylsilyl ether (**Cat-2**) (0.020 g, 0.061 mmol), benzoic acid (0.015 mg, 0.12 mmol) and nitromethane (0.21 mL, 1.8 mmol) were added. The reaction mixture was stirred for 21 h and then cooled to 0 °C. *N*-Bromosuccinimide (0.14 g, 0.80 mmol) was added, and the mixture was stirred for another 18 h slowly warming up to 15 °C. The mixture was then concentrated *in vacuo*. The crude material was purified by flash column chromatography eluting with 60% dichloromethane in hexane to give methyl (3*R*)-3-(3',5'-difluorophenyl)-4-nitrobutanoate ((*R*)-**75**) as a colourless

oil, which solidified upon standing (0.094 g, 40% over two steps) $\nu_{\max}/\text{cm}^{-1}$ (neat) 2958 (CH), 2360, 1732 (C=O), 1554 (C–NO₂), 1431, 1373 (C–NO₂), 1203, 1018, 856; $[\alpha]_{\text{D}}^{26} +1.3$ (c 0.1, CHCl₃); δ_{H} (400 MHz, CDCl₃) 2.72 (1H, dd, J 16.8, 7.6 Hz, 2-*HH*), 2.77 (1H, dd, J 16.8, 7.0 Hz, 2-*HH*), 3.67 (3H, s, OCH₃), 3.93–4.03 (1H, m, 3-H), 4.62 (1H, dd, J 13.0, 8.3 Hz, 4-*HH*), 4.73 (1H, dd, J 13.0, 6.5 Hz, 4-*HH*), 6.81 (1H, d, J 6.1 Hz, 2'-H and 6'-H); δ_{C} (101 MHz, CDCl₃) 36.9 (CH₂), 39.4 (d, $^4J_{\text{CF}}$ 2.0 Hz, CH), 52.3 (CH₃), 70.6 (t, $^2J_{\text{CF}}$ 29.4 Hz, C), 78.4 (CH₂), 110.7 (dd, $^2J_{\text{CF}}$ 25.6 Hz, $^4J_{\text{CF}}$ 2.7 Hz, 2 × CH), 142.2 (t, $^3J_{\text{CF}}$ 8.5 Hz, C), 163.0 (dd, $^1J_{\text{CF}}$ 248.5 Hz, $^3J_{\text{CF}}$ 6.3 Hz, 2 × C), 170.4 (C); m/z (ESI) 365.9438 (M–H–[H₂O])[–]. C₁₁H₇F₂INO₃ requires 365.9444). The enantiomeric ratio was determined by HPLC analysis with a CHIRALCEL[®] AD-H column (96:4, hexane:*i*PrOH, flow rate of 1.5 mL/min): t_{minor} = 9.68 min, t_{major} = 10.73 min; 97:3 *er*.

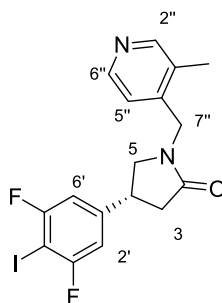
(4*R*)-4-(3',5'-Difluoro-4'-iodophenyl)pyrrolidin-2-one ((*R*)-77)



To a stirred suspension of methyl (3*R*)-3-(3',5'-difluoro-4'-iodophenyl)-4-nitrobutanoate ((*R*)-75) (0.127 g, 0.490 mmol) in a mixture of ethanol and water (4.5 mL, 2:1, v/v) was added ammonium chloride (0.785 g, 14.7 mmol) and iron powder (0.277 g, 4.90 mmol). After stirring for 2.5 h at room temperature, the reaction mixture was adjusted to pH 14 with a 6 M aqueous sodium hydroxide solution (2 mL) and extracted with ethyl acetate (3 × 50 mL). The combined organic layers were dried (MgSO₄), filtered and concentrated *in vacuo*. The crude material was purified by flash column chromatography eluting with 5% methanol in diethyl ether to give (4*R*)-4-(3',5'-difluoro-4'-iodophenyl)pyrrolidin-2-one ((*R*)-77) as a white solid (0.061 g, 63%). Mp 173–176 °C; $\nu_{\max}/\text{cm}^{-1}$ (neat) 2360, 1743 (C=O), 1689 (C=O), 1431, 1365, 1203, 1011, 852; $[\alpha]_{\text{D}}^{26} -10.9$ (c 0.1, CHCl₃); δ_{H} (400 MHz, CDCl₃) 2.43 (1H, dd, J 16.9, 8.2 Hz, 3-*HH*), 2.76 (1H, dd, J 16.9, 9.0 Hz, 3-*HH*), 3.39 (1H, dd, J 9.6, 6.7 Hz, 5-*HH*), 3.63–3.73 (1H, m, 4-H), 3.76–3.84 (1H, m, 5-*HH*), 6.47 (1H, br s, NH), 6.82 (2H, d, J 7.0 Hz, 2'-H and 6'-H); δ_{C} (101 MHz, CDCl₃) 37.4 (CH₂), 39.7 (t, $^4J_{\text{CF}}$ 2.2 Hz, CH), 48.8 (CH₂), 69.0 (t, $^2J_{\text{CF}}$ 29.6 Hz, C), 110.0 (dd, $^2J_{\text{CF}}$ 25.3 Hz, $^4J_{\text{CF}}$

2.7 Hz, 2 × CH), 146.2 (t, $^3J_{\text{CF}}$ 8.5 Hz, C), 163.0 (dd, $^1J_{\text{CF}}$ 247.8 Hz, $^3J_{\text{CF}}$ 6.5 Hz, 2 × C), 176.6 (C); m/z (ESI) 323.9694 (MH^+). $\text{C}_{10}\text{H}_9\text{F}_2\text{INO}$ requires 323.9691).

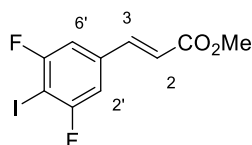
(4*R*)-4-(3',5'-Difluoro-4'-iodophenyl)-1-[(3''-methylpyridin-4''-yl)methyl]-pyrrolidin-2-one ((*R*)-78)



In an oven-dried flask under argon, sodium hydride (0.013 g, 0.37 mmol, 60% dispersion in mineral oil) was added, washed with hexane (1 mL) and dried at the room temperature *in vacuo* for 0.5 h. The sodium hydride was suspended in anhydrous tetrahydrofuran (0.1 mL) and cooled to 0 °C. A solution of (4*R*)-4-(3',5'-difluoro-4'-iodophenyl)pyrrolidin-2-one ((*R*)-77) (0.048 g, 0.15 mmol) in anhydrous tetrahydrofuran (1.3 mL) was added to the mixture, followed by 4-(chloromethyl)-3-methylpyridine hydrochloride (0.030 g, 0.16 mmol) and tetrabutylammonium iodide (0.0030 g, 0.0074 mmol). The reaction mixture was warmed to room temperature and stirred for 18 h. After cooling to 0 °C, the reaction was quenched with saturated aqueous sodium bicarbonate solution (1.5 mL) and extracted with chloroform (3 × 5 mL). The combined organic layers were dried (MgSO_4), filtered and concentrated *in vacuo*. The crude material was purified by flash column chromatography eluting with 7% methanol in diethyl ether to give (4*R*)-4-(3',5'-difluoro-4'-iodophenyl)-1-[(3''-methylpyridin-4''-yl)methyl]pyrrolidin-2-one ((*R*)-78) as a colourless oil, which solidified upon standing (0.015 g, 23%). Mp 152–154 °C; $\nu_{\text{max}}/\text{cm}^{-1}$ (neat) 2360, 1743 (C=O), 1689 (C=O), 1427, 1362, 1203, 1011, 852; $[\alpha]_{\text{D}}^{25} +37.2$ (c 0.1, CHCl_3); δ_{H} (400 MHz, CDCl_3) 2.30 (3H, s, 3''-CH₃), 2.58 (1H, dd, J 17.0, 8.0 Hz, 3-*HH*), 2.93 (1H, dd, J 17.0, 8.8 Hz, 3-*HH*), 3.21–3.25 (1H, m, 5-*HH*), 3.53–3.68 (2H, m, 4-*H* and 5-*HH*), 4.41 (1H, d, J 15.4 Hz, 7''-*HH*), 4.63 (1H, d, J 15.4 Hz, 7''-*HH*), 6.74 (2H, d, J 6.6 Hz, 2'-*H* and 6'-*H*), 7.04 (1H, d, J 5.0 Hz, 5''-*H*), 8.41–8.45 (2H, m, 2''-*H* and 6''-*H*); δ_{C} (101 MHz, CDCl_3) 16.0 (CH₃), 36.8 (t, $^4J_{\text{CF}}$ 2.0 Hz, CH), 38.0 (CH₂), 43.6 (CH₂), 53.2 (CH₂), 69.2 (t, $^2J_{\text{CF}}$ 29.5 Hz, C), 109.9 (dd, $^2J_{\text{CF}}$ 25.3 Hz, $^4J_{\text{CF}}$ 2.6 Hz, 2

× CH), 122.4 (CH), 131.6 (C), 142.6 (C), 145.8 (t, $^3J_{\text{CF}}$ 8.4 Hz, C), 148.1 (CH), 151.4 (CH), 163.0 (dd, $^1J_{\text{CF}}$ 248.2 Hz, $^3J_{\text{CF}}$ 6.5 Hz, 2 × C), 172.9 (C); m/z (ESI) 429.0269 (MH^+ . $\text{C}_{17}\text{H}_{16}\text{F}_2\text{IN}_2\text{O}$ requires 429.0270).

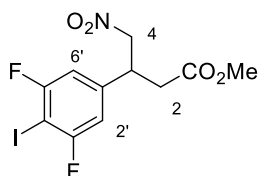
Methyl (*E*)-3-(3',5'-difluoro-4'-iodophenyl)propanoate (**76**)



In the oven-dried flask under argon, *N,N*-diisopropylethylamine (1.80 mL, 12.8 mmol) was dissolved in anhydrous tetrahydrofuran (18 mL). The resultant solution was cooled to $-10\text{ }^{\circ}\text{C}$ and a solution of *n*-butyllithium (4.90 mL, 2.5 M in hexane, 12.3 mmol) was added dropwise. The mixture was stirred for 0.5 h at $-10\text{ }^{\circ}\text{C}$. The resulting solution was added dropwise to a solution of 3,5-difluorobenzonitrile (**69**) (1.03 g, 7.40 mmol) in anhydrous tetrahydrofuran (12 mL) at $-78\text{ }^{\circ}\text{C}$ under argon. After 10 minutes, a solution of iodine (2.25 g, 8.87 mmol) in anhydrous tetrahydrofuran (6 mL) was added dropwise. The reaction mixture was slowly warmed to room temperature and left stirring overnight under argon. After 18 h, the mixture was treated with a 10% aqueous solution of sodium thiosulfate (15 mL) and extracted with hexane/ethyl acetate mixture (v/v, 1:1, 3 × 24 mL). The combined organic layers were dried (MgSO_4), filtered and concentrated *in vacuo*. The resulting 3,5-difluoro-4-iodobenzonitrile (**70**) was obtained as a brown oil and was used without further purification. Diisobutylaluminium anhydride (9.10 mL, 1 M in dichloromethane, 9.10 mmol) was then added dropwise to a solution of 3,5-difluoro-4-iodobenzonitrile (**70**) (2.02 g, 7.62 mmol) in anhydrous dichloromethane (22 mL) under argon at $0\text{ }^{\circ}\text{C}$. The reaction was slowly warmed to room temperature, stirred for 2 h, and then quenched with an aqueous solution of 6 M hydrochloric acid (20 mL). The mixture was extracted with dichloromethane (3 × 50 mL). The combined organic layers were passed through Celite®, dried (MgSO_4), filtered and concentrated *in vacuo* to afford 3,5-difluoro-4-iodobenzaldehyde (**71**) as a white solid, which was used without further purification. 3,5-Difluoro-4-iodobenzaldehyde (**71**) (0.200 g, 0.746 mmol) and methyl (triphenylphosphoranylidene)acetate (0.275 g, 0.821 mmol) were dissolved in anhydrous tetrahydrofuran (10 mL) under argon. The reaction mixture was stirred for 18 h at room temperature. The crude mixture

was concentrated *in vacuo*. The resultant residue was purified by flash column chromatography eluting with 10% diethyl ether in hexane to give methyl (*E*)-3-(3',5'-difluoro-4'-iodophenyl)propanoate (**76**) as a white solid (0.108 g, 55% over 3 steps). Mp 126–128 °C; $\nu_{\text{max}}/\text{cm}^{-1}$ (neat) 2846 (CH), 1733 (C=O), 1663 (C=O), 1628, 1422, 1125, 971; δ_{H} (400 MHz, CDCl_3) 3.82 (3H, s, OCH_3), 6.46 (1H, d, J 16.0 Hz, 2-H), 7.03 (2H, m, 2'-H and 6'-H), 7.55 (1H, d, J 16.0 Hz, 3-H); δ_{C} (101 MHz, CDCl_3) 52.0 (CH_3), 72.9 (t, $^2J_{\text{CF}}$ 29.6 Hz, C), 110.4 (dd, $^2J_{\text{CF}}$ 25.8 Hz, $^3J_{\text{CF}}$ 2.5 Hz, 2 \times CH), 121.0 (CH), 137.6 (t, $^3J_{\text{CF}}$ 9.2 Hz, C), 141.5 (t, $^4J_{\text{CF}}$ 2.9 Hz, CH), 163.0 (dd, $^1J_{\text{CF}}$ 247.6 Hz, $^3J_{\text{CF}}$ 6.4 Hz, 2 \times C), 166.54 (C); m/z (ESI) 324.9537 (MH^+). $\text{C}_{10}\text{H}_8\text{F}_2\text{IO}_2$ requires 324.9532).

Methyl 3-(3',5'-difluoro-4'-iodophenyl)-4-nitrobutanoate (*rac*-75)



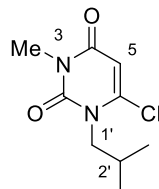
In the oven-dried flask under argon, methyl (*E*)-3-(3',5'-difluoro-4'-iodophenyl)propanoate (**76**) (0.100 g, 0.309 mmol) and nitromethane (0.083 mL, 1.55 mmol) were dissolved in anhydrous acetonitrile (1.5 mL). The solution was cooled down to 0 °C and 1,8-diazabicyclo[5.4.0]undec-7-ene (0.047 mg, 0.309 mmol) was added dropwise over 0.3 h. The reaction mixture was stirred for 18 h slowly warming up to 15 °C. The mixture was then concentrated *in vacuo*. The resultant residue was dissolved in ethyl acetate (5 mL) and washed with water (5 mL). The aqueous layer was extracted with ethyl acetate (2 \times 5 mL). The combined organic layers were dried (MgSO_4), filtered and concentrated *in vacuo*. The crude material was purified by flash column chromatography eluting with 60% dichloromethane in hexane to give methyl 3-(3',5'-difluorophenyl)-4-nitrobutanoate (*rac*-75) as a white solid (0.030 g, 25%). Mp 77–79 °C; $\nu_{\text{max}}/\text{cm}^{-1}$ (neat) 3091, 2966 (CH), 1734 (C=O), 1555 (C– NO_2), 1437, 1368 (C– NO_2), 1214, 1012; δ_{H} (400 MHz, CDCl_3) 2.75 (1H, d, J 16.7, 7.6 Hz, 2-*HH*), 2.75 (1H, d, J 16.7, 7.0 Hz, 2-*HH*), 3.67 (3H, s, OCH_3), 3.94–4.02 (1H, m, 3-H), 4.62 (1H, dd, J 13.0, 8.3 Hz, 4-*HH*), 4.73 (1H, dd, J 13.0, 6.5 Hz, 4-*HH*), 6.81 (1H, d, J 6.5 Hz, 2'-H and 6'-H); δ_{C} (101 MHz, CDCl_3) 36.9 (CH_2), 39.4 (t, $^4J_{\text{CF}}$ 2.0 Hz, CH), 52.3 (CH_3), 70.6 (t, $^2J_{\text{CF}}$ 29.2 Hz, C),

78.4 (CH₂), 110.6 (dd, ²J_{CF} 25.5 Hz, ³J_{CF} 2.7 Hz, 2 × CH), 142.2 (t, ³J_{CF} 8.4 Hz, C), 163.0 (dd, ¹J_{CF} 248.6 Hz, ³J_{CF} 6.3 Hz, C), 170.4 (C); *m/z* (APCI) 383.9552 ([M-H]⁻. C₁₁H₉F₂INO₄ requires 383.9550). The enantiomeric ratio was determined by HPLC analysis with a CHIRALCEL® AD-H column (96:4, hexane:*i*PrOH, flow rate of 1.5 mL/min): t₁ = 10.86 min, t₂ = 9.78 min.

3.3 New PET Imaging Agents Binding MCT1 and MCT2

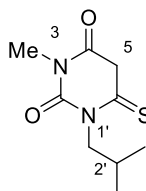
Experimental

6-Chloro-1-isobutyl-3-methyl-2,4-(1*H*,3*H*)-pyrimidinedione (**40**)⁸⁷



Isobutyl bromide (0.75 mL, 6.8 mmol) was added to a solution of 6-chloro-3-methyluracil (**39**) (1.0 g, 6.2 mmol) and potassium carbonate (1.0 g, 7.2 mmol) in dimethyl sulfoxide (10 mL). The mixture was heated to 60 °C and stirred for 72 h. The mixture was then cooled to room temperature and diluted with water (25 mL) and brine (25 mL). The product was then extracted with diethyl ether (3 × 40 mL). The organic layers were combined, dried (MgSO₄), filtered and concentrated *in vacuo*. Purification by flash column chromatography eluting with 20% ethyl acetate in petroleum ether gave 6-chloro-1-isobutyl-3-methyl-2,4-(1*H*,3*H*)-pyrimidinedione (**40**) as white crystals (0.54 g, 40%). Spectroscopic data were consistent with the literature.⁸⁷ δ_{H} (400 MHz, CDCl₃) 0.96 (6H, d, *J* 6.8 Hz, CH(CH₃)₂), 2.11–2.22 (1H, m, 2'-H), 3.34 (3H, s, 3-CH₃), 3.90 (2H, d, *J* 7.6 Hz, 1'-H₂), 5.92 (1H, s, 5-H); δ_{C} (101 MHz, CDCl₃) 19.7 (2 × CH₃), 28.1 (CH₃), 28.3 (CH), 53.5 (CH₂), 101.9 (CH), 146.0 (C), 151.2 (C), 160.9 (C); *m/z* (CI) 217 (MH⁺, 100%).

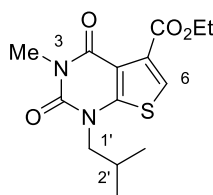
1-isobutyl-6-mercapto-3-methyl-2,4-(1*H*,3*H*)-pyrimidinedione (**41**)⁸⁷



Sodium hydrosulphide monohydrate (1.43 g, 19.4 mmol) was added to a stirred solution of 6-chloro-1-isobutyl-3-methyl-2,4-(1*H*,3*H*)-pyrimidinedione (**40**) (3.49 g, 16.1 mmol) in ethanol (45 mL) under argon. The mixture was stirred at room temperature for 16 h before further sodium hydrosulphide monohydrate (1.43 g, 19.4

mmol) was added and stirring continued at room temperature for a further 5 h under argon. The solution was concentrated *in vacuo* and the resulting oil diluted with water (40 mL) and washed with ethyl acetate (40 mL). The aqueous layer was acidified with an aqueous solution of 1 M hydrochloric acid and extracted with ethyl acetate (3 × 40 mL). The combined organic layers were dried (MgSO₄), filtered and concentrated *in vacuo* to give 1-isobutyl-6-mercapto-3-methyl-2,4-(1*H*,3*H*)-pyrimidinedione (**41**) as a pale beige solid (2.69 g, 78%). Spectroscopic data were consistent with the literature.⁸⁷ Mp 111–113 °C; δ_{H} (400 MHz, CDCl₃) 0.92 (6H, d, *J* 6.8 Hz, CH(CH₃)₂), 2.24–2.31 (1H, m, 2'-H), 3.29 (3H, s, 3-CH₃), 4.14 (2H, s, 5-H₂), 4.27 (2H, d, *J* 7.4 Hz, 1'-H₂); δ_{C} (101 MHz, CDCl₃) 20.1 (2 × CH₃), 26.6 (CH₃), 28.6 (CH), 49.2 (CH₂), 54.5 (CH₂), 150.3 (C), 164.8 (C), 197.2 (C); *m/z* (ESI) 237 (MNa⁺, 100%).

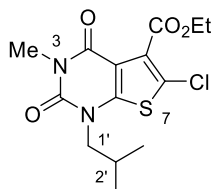
Ethyl 1-isobutyl-3-methyl-2,4-dioxo-1,2,3,4-tetrahydrothieno[2,3-*d*]pyrimidine-5-carboxylate (43**)⁸⁷**



Ethyl bromopyruvate (1.70 mL, 13.3 mmol) was added to a solution of 1-isobutyl-6-mercapto-3-methyl-2,4-(1*H*,3*H*)-pyrimidinedione (**41**) (1.90 g, 8.87 mmol) in ethanol (40 mL) and stirred at room temperature for 1 h. The reaction mixture was concentrated *in vacuo* to give a red oil. A mixture of the crude intermediate and polyphosphoric acid (10.0 g) was heated to 145 °C for 3 h and then cooled to room temperature. The mixture was diluted with water (15 mL), a saturated aqueous solution of sodium carbonate (15 mL) was added and the mixture extracted with ethyl acetate (3 × 25 mL). The combined organic layers were dried (MgSO₄), filtered and concentrated *in vacuo*. Purification by flash column chromatography eluting with 20% ethyl acetate in petroleum ether gave ethyl 1-isobutyl-3-methyl-2,4-dioxo-1,2,3,4-tetrahydrothieno[2,3-*d*]pyrimidine-5-carboxylate (**43**) as a dark pink solid (1.41 g, 54%). Mp 62–66 °C. Spectroscopic data were consistent with the literature.⁸⁷ δ_{H} (400 MHz, CDCl₃) 1.00 (6H, d, *J* 6.9 Hz, CH(CH₃)₂), 1.40 (3H, t, *J* 7.4 Hz, OCH₂CH₃), 2.26–2.38 (1H, m, 2'-H), 3.42 (3H, s, 3-CH₃), 3.81 (2H, d, *J* 7.6 Hz,

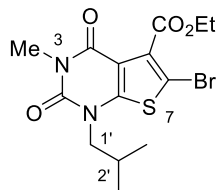
1'-H₂), 4.41 (2H, q, *J* 7.4 Hz, OCH₂CH₃), 7.29 (1H, s, 6-H); δ_C (101 MHz, CDCl₃) 14.2 (CH₃), 20.0 (2 × CH₃), 27.0 (CH), 28.5 (CH₃), 56.2 (CH₂), 61.9 (CH₂), 112.6 (C), 119.4 (CH), 132.3 (C), 150.8 (C), 154.2 (C), 157.0 (C), 162.9 (C); *m/z* (ESI) 333 (MNa⁺, 100%).

Ethyl 6-chloro-1-isobutyl-3-methyl-2,4-dioxo-1,2,3,4-tetrahydrothieno[2,3-*d*]pyrimidine-5-carboxylate (44**)⁸⁷**



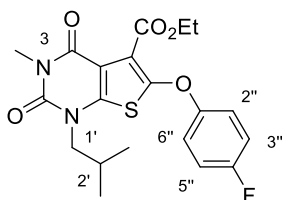
N-Chlorosuccinimide (0.031 g, 0.23 mmol) was added to a stirred solution of ethyl 1-isobutyl-3-methyl-2,4-dioxo-1,2,3,4-tetrahydrothieno[2,3-*d*]pyrimidine-5-carboxylate (**43**) (0.060 g, 0.19 mmol) in dichloromethane (0.5 mL) and acetic acid (0.5 mL). The mixture was stirred at room temperature for 5 h. The reaction mixture was azeotroped under vacuum in the presence of toluene (3 × 2 mL). Purification by flash column chromatography eluting with 20% ethyl acetate in petroleum ether gave ethyl 6-chloro-1-isobutyl-3-methyl-2,4-dioxo-1,2,3,4-tetrahydrothieno[2,3-*d*]pyrimidine-5-carboxylate (**44**) as a white solid (0.054 g, 82%). Mp 81–83 °C. Spectroscopic data were consistent with the literature.⁸⁷ δ_H (400 MHz, CDCl₃) 0.99 (6H, d, *J* 6.7 Hz, CH(CH₃)₂), 1.42 (3H, t, *J* 7.2 Hz, OCH₂CH₃), 2.24–2.32 (1H, m, 2'-H), 3.39 (3H, s, 3-CH₃), 3.72 (2H, d, *J* 7.6 Hz, 1'-H₂), 4.47 (2H, q, *J* 7.2 Hz, OCH₂CH₃); δ_C (101 MHz, CDCl₃) 14.1 (CH₃), 20.0 (2 × CH₃), 27.1 (CH₃), 28.4 (CH), 56.5 (CH₂), 62.5 (CH₂), 112.0 (C), 121.0 (C), 129.4 (C), 150.5 (C), 150.8 (C), 156.6 (C), 162.0 (C); *m/z* (ESI) 367 (MNa⁺, 100%).

Ethyl 6-bromo-1-isobutyl-3-methyl-2,4-dioxo-1,2,3,4-tetrahydrothieno[2,3-*d*]pyrimidine-5-carboxylate (45**)**⁸⁷



N-Bromosuccinimide (0.598 g, 3.36 mmol) was added to a stirred solution of ethyl 1-isobutyl-3-methyl-2,4-dioxo-1,2,3,4-tetrahydrothieno[2,3-*d*]pyrimidine-5-carboxylate (**43**) (0.870 g, 2.80 mmol) in dichloromethane (15 mL) and acetic acid (15 mL) and stirred at room temperature for 5 h. The reaction mixture was azeotroped under vacuum in the presence of toluene (3 × 30 mL). Purification by flash column chromatography eluting with 20% ethyl acetate in petroleum ether gave ethyl 6-bromo-1-isobutyl-3-methyl-2,4-dioxo-1,2,3,4-tetrahydrothieno[2,3-*d*]pyrimidine-5-carboxylate (**45**) as a white solid (0.911 g, 84%). Mp 110–114 °C; Spectroscopic data were consistent with the literature.⁸⁷ δ_{H} (400 MHz, CDCl₃) 0.99 (6H, d, *J* 6.7 Hz, CH(CH₃)₂), 1.42 (3H, t, *J* 7.1 Hz, OCH₂CH₃), 2.24–2.33 (1H, m, 2'-H), 3.40 (3H, s, 3-CH₃), 3.72 (2H, d, *J* 7.8 Hz, 1'-H₂), 4.48 (2H, q, *J* 7.1 Hz, OCH₂CH₃); δ_{C} (101 MHz, CDCl₃) 14.1 (CH₃), 20.0 (2 × CH₃), 27.0 (CH), 28.4 (CH₃), 56.5 (CH₂), 62.6 (CH₂), 103.5 (C), 113.1 (C), 132.5 (C), 150.5 (C), 153.2 (C), 156.4 (C), 162.7 (C); *m/z* (ESI) 410 (MNa⁺, 100%).

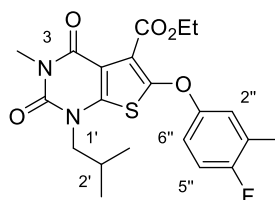
Ethyl 6-(4''-fluorophenoxy)-1-isobutyl-3-methyl-2,4-dioxo-1,2,3,4-tetrahydrothieno[2,3-*d*]pyrimidine-5-carboxylate (80a**)**



Ethyl 6-chloro-1-isobutyl-3-methyl-2,4-dioxo-1,2,3,4-tetrahydrothieno[2,3-*d*]pyrimidine-5-carboxylate (**44**) (0.400 g, 1.16 mmol) was dissolved in anhydrous *N,N'*-dimethylformamide (5 mL) under argon. Caesium carbonate (1.13 g, 3.48 mmol) and 4-fluorophenol (0.195 mg, 1.17 mmol) were added and the reaction

stirred at 100 °C for 16 h. The reaction mixture was then diluted with water (40 mL) and the product extracted with ethyl acetate (3 × 40 mL). The organic layers were washed with an aqueous solution of 5% lithium chloride (40 mL) and brine (40 mL). The combined organic layers were dried (MgSO₄), filtered and concentrated *in vacuo*. Purification by flash column chromatography eluting with 30% diethyl ether in petroleum ether gave ethyl 6-(4''-fluorophenoxy)-1-isobutyl-3-methyl-2,4-dioxo-1,2,3,4-tetrahydrothieno[2,3-*d*]pyrimidine-5-carboxylate (**80a**) as a colourless oil (0.0940 g, 81%). ν_{max} (neat)/cm⁻¹ 2963 (CH), 1705 (C=O), 1667 (C=O), 1551 (C=C), 1497, 1180, 841; δ_{H} (400 MHz, CDCl₃) 0.96 (6H, d, *J* 6.7 Hz, CH(CH₃)₂), 1.28 (3H, t, *J* 7.1 Hz, OCH₂CH₃), 2.20–2.30 (1H, m, 2'-H), 3.41 (3H, s, 3-CH₃), 3.70 (2H, d, *J* 7.7 Hz, 1'-H₂), 4.35 (2H, q, *J* 7.1 Hz, OCH₂CH₃), 7.02–7.07 (2H, m, 3''-H and 5''-H), 7.11 (2H, dd, *J* 9.3, 4.4 Hz, 2''-H and 6''-H); δ_{C} (101 MHz, CDCl₃) 14.0 (CH₃), 20.0 (2 × CH₃), 27.1 (CH₃), 28.3 (CH), 56.3 (CH₂), 62.2 (CH₂), 109.5 (C), 116.6 (d, ²*J*_{CF} 22.3 Hz, 2 × CH), 118.3 (C), 118.4 (d, ³*J*_{CF} 8.3 Hz, 2 × CH), 146.3 (C), 150.6 (C), 150.8 (C), 154.1 (d, ⁴*J*_{CF} 3.2 Hz, C), 157.2 (C), 160.5 (d, ¹*J*_{CF} 249.8 Hz, C), 162.0 (C); *m/z* (ESI) 443.1029 (MNa⁺. C₂₀H₂₁FN₂NaO₅S requires 443.1047).

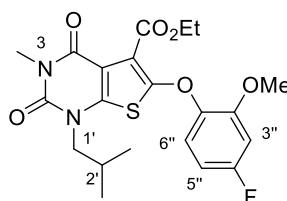
Ethyl 6-(4''-fluoro-3''-methylphenoxy)-1-isobutyl-3-methyl-2,4-dioxo-1,2,3,4-tetrahydrothieno[2,3-*d*]pyrimidine-5-carboxylate (80b)



The reaction was carried out according to the previously described procedure for 6-(4''-fluorophenoxy)-1-isobutyl-3-methyl-2,4-dioxo-1,2,3,4-tetrahydrothieno[2,3-*d*]pyrimidine-5-carboxylate (**80a**) using ethyl 6-chloro-1-isobutyl-3-methyl-2,4-dioxo-1,2,3,4-tetrahydrothieno[2,3-*d*]pyrimidine-5-carboxylate (**44**) (0.334 g, 0.970 mmol), 4-fluoro-3-methylphenol (0.184 g, 1.46 mmol) and caesium carbonate (0.948 g, 2.91 mmol). Purification by flash column chromatography eluting with 30% of diethyl ether in petroleum ether gave ethyl 6-(4''-fluoro-3''-methylphenoxy)-1-isobutyl-3-methyl-2,4-dioxo-1,2,3,4-tetrahydro-thieno[2,3-*d*]pyrimidine-5-carboxylate (**80b**) as a yellow oil (0.278 g, 66%). ν_{max} (neat)/cm⁻¹ 2963 (CH), 2291, 2110, 1898, 1735 (C=O), 1709 (C=O), 1667 (CO), 1550 (C=C), 1489, 1396, 1292, 1192, 667; δ_{H} (400

MHz, CDCl₃) 0.96 (6H, d, *J* 6.7 Hz, CH(CH₃)₂), 1.29 (3H, t, *J* 7.1 Hz, OCH₂CH₃), 2.20–2.30 (4H, m, 2'-H and 3''-CH₃), 3.41 (3H, s, 3-CH₃), 3.70 (2H, d, *J* 7.7 Hz, 1'-H₂), 4.35 (2H, q, *J* 7.1 Hz, OCH₂CH₃), 6.90–7.00 (3H, m, 2''-H, 5''-H and 6''-H); δ_C (101 MHz, CDCl₃) 14.0 (CH₃), 14.8 (d, ³*J*_{CF} 3.2 Hz, CH₃), 20.0 (2 × CH₃), 27.1 (CH₃), 28.3 (CH), 56.3 (CH₂), 62.1 (CH₂), 109.5 (C), 115.9 (d, ³*J*_{CF} 7.1 Hz, CH), 116.0 (d, ³*J*_{CF} 9.2 Hz, CH), 118.0 (C), 120.1 (d, ²*J*_{CF} 5.2 Hz, CH), 126.7 (d, ²*J*_{CF} 19.5 Hz, C), 146.2 (C), 150.8 (C), 150.9 (C), 153.7 (d, ⁴*J*_{CF} 2.7 Hz, C), 157.2 (C), 158.1 (d, ¹*J*_{CF} 242.4 Hz, C), 162.0 (C); *m/z* (ESI) 435.1394 (MH⁺. C₂₀H₂₁FN₂O₅S requires 435.1385).

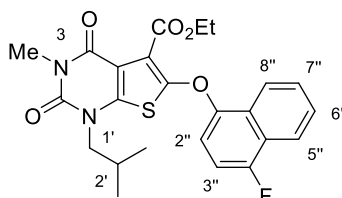
Ethyl 6-(4''-fluoro-2''-methoxyphenoxy)-1-isobutyl-3-methyl-2,4-dioxo-1,2,3,4-tetrahydrothieno[2,3-*d*]pyrimidine-5-carboxylate (80c)



The reaction was carried out according to the previously described procedure for ethyl 6-(4''-fluorophenoxy)-1-isobutyl-3-methyl-2,4-dioxo-1,2,3,4-tetrahydrothieno[2,3-*d*]pyrimidine-5-carboxylate (**80a**) using ethyl 6-chloro-1-isobutyl-3-methyl-2,4-dioxo-1,2,3,4-tetrahydrothieno[2,3-*d*]pyrimidine-5-carboxylate (**44**) (0.10 g, 0.29 mmol), 4-fluoro-2-methoxyphenol (0.050 mL, 0.44 mmol) and caesium carbonate (0.283 g, 0.870 mmol). Purification by flash column chromatography eluting with 20% ethyl acetate in petroleum ether gave ethyl 6-(4''-fluoro-2''-methoxyphenoxy)-1-isobutyl-3-methyl-2,4-dioxo-1,2,3,4-tetrahydro-thieno[2,3-*d*]pyrimidine-5-carboxylate (**80c**) as a yellow oil (0.058 g, 45%). *v*_{max} (neat)/cm⁻¹ 2963, 2917 (CH), 2361, 2176, 2014, 1732 (C=O), 1708 (C=O), 1662 (C=O), 1551 (C=C), 1501, 1397, 1292, 1180, 1026; δ_H (400 MHz, CDCl₃) 0.95 (6H, d, *J* 6.7 Hz, CH(CH₃)₂), 1.33 (3H, t, *J* 7.1 Hz, OCH₂CH₃), 2.23 (1H, m, 2'-H), 3.39 (3H, s, 3-CH₃), 3.67 (2H, d, *J* 7.7 Hz, 1'-H₂), 3.86 (3H, s, OCH₃), 4.37 (2H, q, *J* 7.1 Hz, OCH₂CH₃), 6.63 (1H, ddd, *J* 8.9, 7.7, 2.9 Hz, 5''-H), 6.73 (1H, dd, *J* 10.0, 2.9 Hz, 3''-H), 7.16 (1H, dd, *J* 8.9, 5.5 Hz, 6''-H); δ_C (101 MHz, CDCl₃) 14.0 (CH₃), 20.0 (2 × CH₃), 27.1 (CH₃), 28.3 (CH), 56.1 (CH₃), 56.3 (CH₂), 62.1 (CH₂), 101.3 (d, ²*J*_{CF} 27.4 Hz, CH), 106.9 (d, ²*J*_{CF} 23.4 Hz, CH), 109.6 (C), 115.6 (C), 120.8 (d, ³*J*_{CF} 10.3 Hz, CH), 142.8 (d, ⁴*J*_{CF} 3.3 Hz,

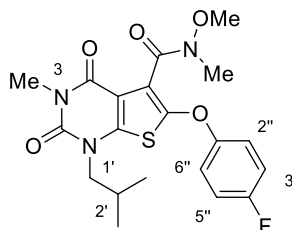
C), 145.3 (C), 150.9 (C), 151.6 (d, $^3J_{\text{CF}}$ 10.4 Hz, C), 153.0 (C), 157.3 (C), 160.6 (d, $^1J_{\text{CF}}$ 245.3 Hz, C), 162.2 (C); m/z (ESI) 473.1162 (MNa^+ . $\text{C}_{20}\text{H}_{20}\text{FN}_2\text{NaO}_5\text{S}$ requires 473.1154).

Ethyl 6-(4''-fluoro-1''-naphthyloxy)-1-isobutyl-3-methyl-2,4-dioxo-1,2,3,4-tetrahydrothieno[2,3-*d*]pyrimidine-5-carboxylate (80d)



The reaction was carried out according to the previously described procedure for ethyl 6-(4''-fluorophenoxy)-1-isobutyl-3-methyl-2,4-dioxo-1,2,3,4-tetrahydrothieno[2,3-*d*]pyrimidine-5-carboxylate (**80a**) using ethyl 6-chloro-1-isobutyl-3-methyl-2,4-dioxo-1,2,3,4-tetrahydrothieno[2,3-*d*]pyrimidine-5-carboxylate (**44**) (0.213 g, 0.618 mmol), 4-fluoro-1-naphthol (0.150 g, 0.927 mmol) and caesium carbonate (0.603 g, 1.85 mmol). Purification by flash column chromatography eluting with 20% ethyl acetate in petroleum ether gave ethyl 6-(4''-fluoro-1''-naphthyloxy)-1-isobutyl-3-methyl-2,4-dioxo-1,2,3,4-tetrahydrothieno[2,3-*d*]pyrimidine-5-carboxylate (**80d**) as yellow oil (0.161 g, 55%). ν_{max} (neat)/ cm^{-1} 2936 (CH), 2360, 1708 (C=O), 1662 (C=O), 1489, 1388, 1292, 768; δ_{H} (400 MHz, CDCl_3) 0.94 (6H, d, J 6.7 Hz, $\text{CH}(\text{CH}_3)_2$), 1.23 (3H, t, J 7.1 Hz, OCH_2CH_3), 2.17–2.27 (1H, m, 2'-H), 3.42 (3H, s, 3- CH_3), 3.66 (2H, d, J 7.7 Hz, 1'- H_2), 4.33 (2H, q, J 7.1 Hz, OCH_2CH_3), 7.08 (1H, dd, J 9.5, 8.5 Hz, 3''-H), 7.13 (1H, dd, J 8.5, 4.4 Hz, 2''-H), 7.64 (2H, dt, J 6.5, 3.5 Hz, 7''-H and ArH), 8.09–8.13 (1H, m, 5''-H), 8.23–8.28 (1H, m, ArH); δ_{C} (101 MHz, CDCl_3) 14.0 (CH_3), 20.0 (2 \times CH_3), 27.1 (CH_3), 28.3 (CH), 56.2 (CH_2), 62.1 (CH_2), 108.7 (d, $^2J_{\text{CF}}$ 22.5 Hz, CH), 109.6 (C), 112.0 (d, $^3J_{\text{CF}}$ 8.7 Hz, CH), 117.4 (C), 120.8 (d, $^3J_{\text{CF}}$ 4.6 Hz, CH), 121.4 (d, $^4J_{\text{CF}}$ 2.4 Hz, CH), 124.5 (d, $^2J_{\text{CF}}$ 18.3 Hz, C), 126.3 (d, $^3J_{\text{CF}}$ 5.2 Hz, C), 127.5 (d, $^4J_{\text{CF}}$ 1.9 Hz, CH), 127.7 (CH), 146.0 (C), 150.0 (d, $^4J_{\text{CF}}$ 3.5 Hz, C), 150.8 (C), 151.5 (C), 155.7 (d, $^1J_{\text{CF}}$ 250.2 Hz, C), 157.2 (C), 162.0 (C); m/z (ESI) 493.1206 (MNa^+ . $\text{C}_{24}\text{H}_{23}\text{FN}_2\text{NaO}_5\text{S}$ requires 493.1204).

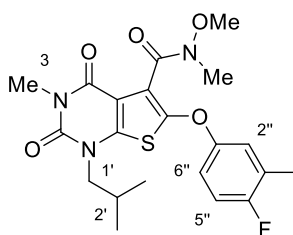
6-(4''-Fluorophenoxy)-1-isobutyl-3-methyl-2,4-dioxo-1,2,3,4-tetrahydrothieno[2,3-*d*]pyrimidine-5-(*N*-methoxy-*N*-methyl)carboxamide (37a)



Ethyl 6-(4''-fluorophenoxy)-1-isobutyl-3-methyl-2,4-dioxo-1,2,3,4-tetrahydrothieno[2,3-*d*]pyrimidine-5-carboxylate (**80a**) (0.10 g, 0.24 mmol) was dissolved in tetrahydrofuran (1.2 mL), methanol (0.7 mL) and water (0.2 mL). The mixture was stirred at 65 °C for 24 h. The reaction mixture was diluted with water (10 mL) and washed with diethyl ether (10 mL). The aqueous layer was acidified with an aqueous solution of 1 M hydrochloric acid (10 mL) and extracted with ethyl acetate (3 × 10 mL). The resulting white precipitate was filtered and dried in air. The combined organic layers were dried (MgSO₄), filtered and concentrated *in vacuo*. The combined solid was dissolved in acetonitrile (10 mL) and *O*-(benzotriazol-1-yl)-*N,N,N',N'*-tetramethyluronium hexafluorophosphate (0.084 g, 0.23 mmol), *N,N'*-diisopropylethylamine (0.052 mL, 0.30 mmol) and *N,O*-dimethylhydroxylamine (0.043 g, 0.45 mmol) were added. The mixture was then stirred at 40 °C for 16 h. The mixture was diluted with water (10 mL) and washed with saturated aqueous sodium bicarbonate solution (10 mL). The mixture was extracted with ethyl acetate (3 × 10 mL). The organic layers were combined and washed with an aqueous solution of 5% lithium chloride (30 mL) and brine (30 mL). The organic layer was dried (MgSO₄), filtered and concentrated *in vacuo* to give the crude product. Purification by flash column chromatography eluting with 40% ethyl acetate in petroleum ether gave 6-(4''-fluorophenoxy)-1-isobutyl-3-methyl-2,4-dioxo-1,2,3,4-tetrahydrothieno[2,3-*d*]pyrimidine-5-(*N*-methoxy-*N*-methyl)carboxamide (**37a**) as a yellow oil (0.042 g, 54% over two steps). ν_{\max} (neat)/cm⁻¹ 2929 (CH), 1706 (C=O), 1656 (C=O), 1549 (C=C), 1494, 1389, 1179, 1107, 729. NMR spectra showed a 5:1 mixture of rotational isomers. Only data for the major rotational isomer was recorded: δ_{H} (400 MHz, CDCl₃) 0.97 (6H, d, *J* 6.7 Hz, CH(CH₃)₂), 2.22–2.28 (1H, m, 2'-H), 3.38 (3H, s, NCH₃), 3.40 (3H, s, NCH₃), 3.60 (1H, dd, *J* 14.0, 7.9 Hz, 1'-HH), 3.64 (3H, s, OCH₃), 3.79 (1H, dd, *J* 14.0, 7.9 Hz, 1'-HH), 7.04 (2H, t, *J* 8.9 Hz, 2''-H and

6''-H), 7.16 (2H, dd, J 8.9, 4.3 Hz, 3''-H and 5''-H); δ_C (101 MHz, $CDCl_3$) 20.0 (CH_3), 20.1 (CH_3), 27.1 (CH_3), 28.3 (CH), 32.8 (CH_3), 56.3 (CH_2), 61.8 (CH_3), 109.8 (C), 116.5 (d, $^2J_{CF}$ 23.5 Hz, 2 \times CH), 119.1 (d, $^3J_{CF}$ 8.6 Hz, 2 \times CH), 119.6 (C), 146.3 (C), 147.3 (C), 151.0 (C), 154.2 (d, $^4J_{CF}$ 2.8 Hz, C), 157.6 (C), 160.5 (d, $^1J_{CF}$ 247.3 Hz, C), 163.3 (C); m/z (ESI) 458.1135 (MNa^+ . $C_{20}H_{22}FN_3NaO_5S$ requires 458.1156).

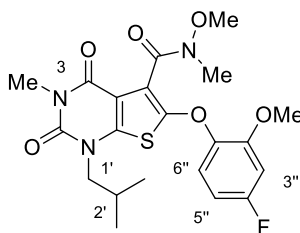
6-(4''-fluoro-3''-methylphenoxy)-1-isobutyl-3-methyl-2,4-dioxo-1,2,3,4-tetrahydrothieno[2,3-*d*]pyrimidine-5-(*N*-methoxy-*N*-methyl)carboxamide (37b)



Ethyl 6-(4''-fluoro-3''-methylphenoxy)-1-isobutyl-3-methyl-2,4-dioxo-1,2,3,4-tetrahydrothieno[2,3-*d*]pyrimidine-5-carboxylate (**80b**) (0.10 g, 0.15 mmol) was dissolved in ethanol (2.3 mL) and water (2.3 mL) and an aqueous solution of 4 M sodium hydroxide (0.9 mL) was added to the mixture. The mixture was stirred at 80 °C for 1.5 h. The reaction mixture was concentrated *in vacuo*, diluted with water (5 mL) and washed with diethyl ether (2 \times 5 mL). The aqueous layer was acidified with an aqueous solution of 1 M hydrochloric acid (5 mL) and extracted with ethyl acetate (3 \times 5 mL). The organic layers were combined, dried ($MgSO_4$), filtered and concentrated *in vacuo*. *N,N'*-Diisopropylethylamine (0.20 mL, 1.2 mmol) and *N,O*-dimethylhydroxylamine (0.056 g, 0.58 mmol) were dissolved in acetonitrile (5 mL) and stirred at room temperature for 10 min. The carboxylic acid was then dissolved in acetonitrile (5 mL) and added to the mixture, followed by *O*-(benzotriazol-1-yl)-*N,N,N',N'*-tetramethyluronium hexafluorophosphate (0.11 g, 0.29 mmol). The mixture was then stirred at 40 °C for 16 h. The mixture was diluted with water (10 mL) and washed with saturated aqueous sodium bicarbonate solution (10 mL). The mixture was extracted with ethyl acetate (3 \times 10 mL). The organic layers were combined and washed with an aqueous solution of 5% lithium chloride (25 mL) and brine (25 mL). The combined organic layers were dried ($MgSO_4$), filtered and concentrated *in vacuo* to give the crude product. Purification by flash column chromatography eluting with 2% methanol in chloroform gave 6-(4''-fluoro-3''-

methylphenoxy)-1-isobutyl-3-methyl-2,4-dioxo-1,2,3,4-tetrahydro-thieno[2,3-*d*]-pyrimidine-5-(*N*-methoxy-*N*-methyl) carboxamide (**37b**) as a yellow oil (0.039 g, 38% over two steps). ν_{max} (neat)/ cm^{-1} 2963 (CH), 1705 (C=O), 1663 (C=O), 1551 (C=C), 1492, 1424, 1389, 1192, 988, 748. NMR spectra showed a 5:1 mixture of rotational isomers. Only data for the major rotational isomer was recorded: δ_{H} (400 MHz, CDCl_3) 0.97 (6H, d, J 6.7 Hz, $\text{CH}(\text{CH}_3)_2$), 2.18–2.32 (4H, m, 2'-H and 3''-CH₃), 3.38 (3H, s, NCH₃), 3.40 (3H, s, NCH₃), 3.59–3.64 (4H, m, 1'-HH and OCH₃), 3.78 (1H, dd, J 14.2, 7.8 Hz, 1'-HH), 6.94–7.05 (3H, m, 3 × ArH); δ_{C} (101 MHz, CDCl_3) 14.8 (d, $^3J_{\text{CF}}$ 3.2 Hz, CH₃), 20.0 (CH₃), 20.1 (CH₃), 27.1 (CH₃), 28.3 (CH), 32.8 (CH₃), 56.3 (CH₂), 61.8 (CH₃), 109.8 (C), 115.9 (d, $^2J_{\text{CF}}$ 24.7 Hz, CH), 116.2 (d, $^3J_{\text{CF}}$ 8.4 Hz, CH), 119.3 (C), 120.5 (d, $^3J_{\text{CF}}$ 5.2 Hz, CH), 126.7 (d, $^2J_{\text{CF}}$ 19.5 Hz, C), 146.3 (C), 147.6 (C), 151.0 (C), 153.8 (C), 157.6 (C), 158.2 (d, $^1J_{\text{CF}}$ 242.4 Hz, C), 163.4 (C); m/z (ESI) 450.1495 (MH^+). $\text{C}_{21}\text{H}_{25}\text{FN}_3\text{O}_5\text{S}$ requires 450.1493).

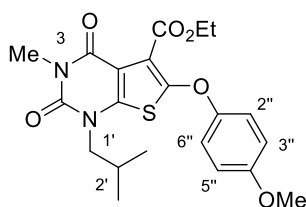
6-(4''-Fluoro-2''-methoxyphenoxy)-1-isobutyl-3-methyl-2,4-dioxo-1,2,3,4-tetrahydrothieno[2,3-*d*]pyrimidine-5-(*N*-methoxy-*N*-methyl)carboxamide (37c)



Ethyl 6-(4''-fluoro-2''-methoxyphenoxy)-1-isobutyl-3-methyl-2,4-dioxo-1,2,3,4-tetrahydrothieno[2,3-*d*]pyrimidine-5-carboxylate (**80c**) (0.058 g, 0.13 mmol) was dissolved in ethanol (1.3 mL) and water (3.3 mL) and an aqueous solution of 4 M sodium hydroxide (0.5 mL) was added to the mixture. The mixture was stirred at 80 °C for 0.7 h. The reaction mixture was concentrated *in vacuo*, diluted with water (3 mL) and washed with diethyl ether (2 × 3 mL). The aqueous layer was acidified with an aqueous solution of 1 M hydrochloric acid (3 mL) and extracted with ethyl acetate (3 × 3 mL). The organic layers were combined, dried (MgSO_4), filtered and concentrated *in vacuo*. *N,N'*-Diisopropylethylamine (0.14 mL, 0.80 mmol) and *N,O*-dimethylhydroxylamine (0.039 g, 0.40 mmol) were dissolved in acetonitrile (3.5 mL) and stirred at room temperature for 10 min. The carboxylic acid was then dissolved in acetonitrile (3.5 mL) and added to the mixture, followed by *O*-(benzotriazol-1-yl)-

N,N,N',N'-tetramethyluronium hexafluorophosphate (0.075 g, 0.20 mmol). The mixture was then stirred at 40 °C for 18 h. The mixture was diluted with water (8 mL) and washed with saturated aqueous sodium bicarbonate solution (8 mL). The mixture was extracted with ethyl acetate (3 × 8 mL). The organic layers were combined and washed with an aqueous solution of 5% lithium chloride (25 mL) and brine (25 mL). The combined organic layers were dried (MgSO₄), filtered and concentrated *in vacuo* to give the crude product. Purification by flash column chromatography eluting with 2% methanol in chloroform gave 6-(4''-fluoro-2''-methoxyphenoxy)-1-isobutyl-3-methyl-2,4-dioxo-1,2,3,4-tetrahydro-thieno[2,3-*d*]pyrimidine-5-(*N*-methoxy-*N*-methyl)carboxamide (**37c**) as yellow oil (0.019 g, 30% over two steps). ν_{max} (neat)/cm⁻¹ 2963, 2936 (CH), 2360, 1705 (C=O), 1651 (C=O), 1551 (C=C), 1392, 1180, 840, 729. NMR spectra showed a 5:1 mixture of rotational isomers. Only data for the major rotational isomer was recorded: δ_{H} (400 MHz, CDCl₃) 0.95 (6H, d, *J* 6.7 Hz, CH(CH₃)₂), 2.17–2.28 (1H, m, 2'-H), 3.38 (3H, s, NCH₃), 3.40 (3H, s, NCH₃), 3.56 (1H, dd, *J* 14.2, 7.4 Hz, 1'-HH), 3.66 (3H, s, 2''-OCH₃), 3.77 (1H, dd, *J* 14.2, 7.9 Hz, 1'-HH), 3.86 (3H, s, OCH₃), 6.63 (1H, ddd, *J* 8.9, 7.6, 2.9 Hz, 5''-H), 6.71 (1H, dd, *J* 10.0, 2.9 Hz, 3''-H), 7.25 (1H, dd, *J* 8.9, 5.6 Hz, 6''-H); δ_{C} (101 MHz, CDCl₃) 20.0 (2 × CH₃), 27.1 (CH₃), 28.2 (CH), 32.8 (CH₃), 56.1 (2 × CH₃), 61.8 (CH₂), 101.1 (d, ²*J*_{CF} 27.3 Hz, CH), 107.0 (d, ²*J*_{CF} 23.1 Hz, CH), 110.0 (C), 116.7 (C), 121.6 (d, ³*J*_{CF} 10.3 Hz, CH), 142.8 (C), 145.2 (C), 149.7 (C), 151.0 (C), 151.5 (d, ³*J*_{CF} 10.5 Hz, C), 157.6 (C), 160.6 (d, ¹*J*_{CF} 245.3 Hz, C), 163.6 (C); *m/z* (ESI) 488.1260 (MNa⁺. C₂₀H₂₂FN₃NaO₅S requires 488.1263).

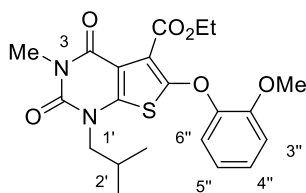
Ethyl 6-(4''-methoxyphenoxy)-1-isobutyl-3-methyl-2,4-dioxo-1,2,3,4-tetrahydrothieno[2,3-*d*]pyrimidine-5-carboxylate (80f)



Ethyl 6-chloro-1-isobutyl-3-methyl-2,4-dioxo-1,2,3,4-tetrahydrothieno[2,3-*d*]pyrimidine-5-carboxylate (**44**) (0.050 g, 0.15 mmol) was dissolved in dry *N,N'*-dimethylformamide (2.5 mL). Caesium carbonate (0.19 g, 0.58 mmol) and 4-methoxyphenol (0.036 g, 0.29 mmol) were added and the reaction mixture stirred at

100 °C for 18 h. The reaction mixture was concentrated *in vacuo*, then diluted with water (10 mL) and the product extracted with ethyl acetate (3 × 10 mL). The organic layers were washed with an aqueous solution of 5% lithium chloride (10 mL) and brine (10 mL). The combined organic layers were dried (MgSO₄), filtered and concentrated *in vacuo*. Purification by flash column chromatography eluting with 25% ethyl acetate in hexane gave ethyl 6-(4"-methoxyphenoxy)-1-isobutyl-3-methyl-2,4-dioxo-1,2,3,4-tetrahydrothieno[2,3-*d*]pyrimidine-5-carboxylate (**80f**) as pale-yellow oil (0.042 g, 62%). ν_{max} (neat)/cm⁻¹ 3019 (CH), 1703 (C=O), 1656 (C=O), 1501 (C=C), 1214, 667; δ_{H} (400 MHz, CDCl₃) 0.95 (6H, d, *J* 6.7 Hz, CH(CH₃)₂), 1.31 (3H, t, *J* 7.1 Hz, OCH₂CH₃), 2.16–2.30 (1H, m, 2'-H), 3.40 (3H, s, 3-CH₃), 3.68 (2H, d, *J* 7.7 Hz, 1'-H₂), 3.80 (3H, s, OCH₃), 4.37 (2H, q, *J* 7.1 Hz, OCH₂CH₃), 6.86–6.90 (2H, m, 2 × ArH), 7.07–7.12 (2H, m, 2 × ArH); δ_{C} (101 MHz, CDCl₃) 14.1 (CH₃), 20.0 (2 × CH₃), 27.1 (CH₃), 28.3 (CH), 55.7 (CH₃), 56.2 (CH₂), 62.1 (CH₂), 109.5 (C), 114.9 (2 × CH), 116.6 (C), 119.0 (2 × CH), 145.7 (C), 150.9 (C), 151.9 (C), 152.3 (C), 156.9 (C), 157.3 (C), 162.2 (C); *m/z* (ESI) 455.1259 (MNa⁺. C₂₁H₂₄N₂NaO₅S requires 455.1247).

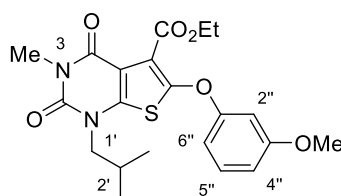
Ethyl 6-(2"-methoxyphenoxy)-1-isobutyl-3-methyl-2,4-dioxo-1,2,3,4-tetrahydrothieno[2,3-*d*]pyrimidine-5-carboxylate (80g)



Ethyl 6-chloro-1-isobutyl-3-methyl-2,4-dioxo-1,2,3,4-tetrahydrothieno[2,3-*d*]pyrimidine-5-carboxylate (**44**) (0.045 g, 0.13 mmol) was dissolved in anhydrous *N,N'*-dimethylformamide (2 mL) under argon. Caesium carbonate (0.17 g, 0.52 mmol) and 2-methoxyphenol (0.029 g, 0.26 mmol) were added and the reaction mixture stirred at 100 °C for 40 h. The reaction mixture was then diluted with water (10 mL) and the product extracted with ethyl acetate (3 × 10 mL). The organic layers were washed with an aqueous solution of 5% lithium chloride (10 mL) and brine (10 mL). The combined organic layers were dried (MgSO₄), filtered and concentrated *in vacuo*. Purification by flash column chromatography eluting with 25% ethyl acetate in hexane gave ethyl 6-(2"-methoxyphenoxy)-1-isobutyl-3-methyl-2,4-dioxo-1,2,3,4-

tetrahydrothieno[2,3-*d*]pyrimidine-5-carboxylate (**80g**) as yellow oil (0.026 g, 45%). ν_{\max} (neat)/cm⁻¹ 2962 (CH), 1705 (C=O), 1662 (C=O), 1497, 1297, 1178 1020, 762; δ_{H} (400 MHz, CDCl₃) 0.94 (6H, d, *J* 6.6 Hz, CH(CH₃)₂), 1.31 (3H, t, *J* 7.1 Hz, OCH₂CH₃), 2.18–2.28 (1H, m, 2'-H), 3.40 (3H, s, 3-CH₃), 3.67 (2H, d, *J* 7.7 Hz, 1'-H₂), 3.88 (3H, s, OCH₃), 4.35 (2H, q, *J* 7.1 Hz, OCH₂CH₃), 6.91–7.01 (2H, m, 3''-H and 6''-H), 7.16–7.20 (2H, m, 4''-H and 5''-H); δ_{C} (101 MHz, CDCl₃) 14.0 (CH₃), 20.0 (2 × CH₃), 27.1 (CH₃), 28.3 (CH), 55.1 (CH₃), 56.1 (CH₂), 61.9 (CH₂), 109.5 (C), 113.1 (CH), 115.9 (C), 119.7 (CH), 121.1 (CH), 126.4 (CH), 145.5 (C), 146.8 (C), 150.4 (C), 150.9 (C), 152.7 (C), 157.3 (C), 162.1 (C); *m/z* (ESI) 455.1262 (MNa⁺. C₂₁H₂₄N₂NaO₆S requires 455.1247).

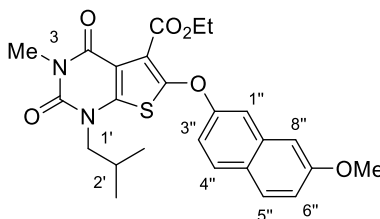
Ethyl 6-(3''-methoxyphenoxy)-1-isobutyl-3-methyl-2,4-dioxo-1,2,3,4-tetrahydrothieno[2,3-*d*]pyrimidine-5-carboxylate (80h)



Ethyl 6-chloro-1-isobutyl-3-methyl-2,4-dioxo-1,2,3,4-tetrahydrothieno[2,3-*d*]pyrimidine-5-carboxylate (**44**) (0.0500 g, 0.145 mmol) was dissolved in anhydrous *N,N'*-dimethylformamide (2.5 mL). Caesium carbonate (0.190 g, 0.580 mmol) and 3-methoxyphenol (0.0470 g, 0.290 mmol) were added and the reaction mixture stirred at 100 °C for 44 h. The reaction mixture was concentrated *in vacuo*, then diluted with water (10 mL) and the product extracted with ethyl acetate (3 × 10 mL). The organic layers were washed with an aqueous solution of 5% lithium chloride (10 mL) and brine (10 mL). The combined organic layers were dried (MgSO₄), filtered and concentrated *in vacuo*. Purification by flash column chromatography eluting with 40% diethyl ether in hexane gave ethyl 6-(3''-methoxyphenoxy)-1-isobutyl-3-methyl-2,4-dioxo-1,2,3,4-tetrahydrothieno[2,3-*d*]pyrimidine-5-carboxylate (**80h**) as colourless oil (0.0300 g, 44%). ν_{\max} (neat)/cm⁻¹ 2958 (CH), 1708 (C=O), 1662 (C=O), 1487, 1289, 1034, 772; δ_{H} (400 MHz, CDCl₃) 0.96 (6H, d, *J* 6.6 Hz, CH(CH₃)₂), 1.27 (3H, t, *J* 7.1 Hz, OCH₂CH₃), 2.20–2.31 (1H, m, 2'-H), 3.41 (3H, s, 3-CH₃), 3.70 (2H, d, *J* 7.7 Hz, 1'-H₂), 3.79 (3H, s, OCH₃), 4.34 (2H, q, *J* 7.1 Hz, OCH₂CH₃), 6.68–6.73 (3H, m, 3 × ArH), 7.23–7.28 (1H, t, *J* 8.1 Hz, 5''-H); δ_{C} (101 MHz, CDCl₃) 14.0 (CH₃),

20.0 (2 × CH₃), 27.1 (CH₃), 28.3 (CH), 55.5 (CH₃), 56.3 (CH₂), 62.1 (CH₂), 103.4 (CH), 109.2 (CH), 109.5 (C), 110.5 (CH), 118.5 (C), 130.4 (CH), 146.3 (C), 150.2 (C), 150.9 (C), 157.2 (C), 159.2 (C), 161 (C), 162.0 (C); *m/z* (ESI) 455.1249 (MNa⁺. C₂₁H₂₄N₂NaO₅S requires 455.1247).

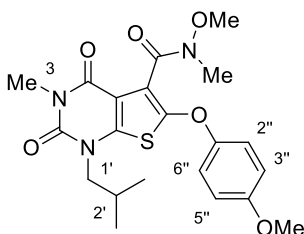
Ethyl 6-(7''-methoxy-2''-naphthyloxy)-1-isobutyl-3-methyl-2,4-dioxo-1,2,3,4-tetrahydrothieno[2,3-*d*]pyrimidine-5-carboxylate (80i**)**



Ethyl 6-chloro-1-isobutyl-3-methyl-2,4-dioxo-1,2,3,4-tetrahydrothieno[2,3-*d*]pyrimidine-5-carboxylate (**44**) (0.050 g, 0.15 mmol) was dissolved in dry *N,N'*-dimethylformamide (2.5 mL). Caesium carbonate (0.19 g, 0.58 mmol) and 7-methoxy-2-naphthol (0.051 g, 0.29 mmol) were added and the reaction mixture stirred at 100 °C for 24 h. The reaction mixture was then diluted with water (10 mL) and the product extracted with ethyl acetate (3 × 10 mL). The organic layers were washed with an aqueous solution of 5% lithium chloride (10 mL) and brine (10 mL). The combined organic layers were dried (MgSO₄), filtered and concentrated *in vacuo*. Purification by flash column chromatography eluting with 25% ethyl acetate in hexane gave ethyl 6-(7''-methoxy-2''-naphthyloxy)-1-isobutyl-3-methyl-2,4-dioxo-1,2,3,4-tetrahydro-thieno-[2,3-*d*]pyrimidine-5-carboxylate (**80i**) as orange oil (0.036 g, 53%). *v*_{max} (neat)/cm⁻¹ 2963 (CH), 2366, 1707 (C=O), 1662 (C=O), 1490, 1292, 1252, 771; δ_H (400 MHz, CDCl₃) 0.95 (6H, d, *J* 6.7 Hz, CH(CH₃)₂), 1.23 (3H, t, *J* 7.1 Hz, OCH₂CH₃), 2.20–2.30 (1H, m, 2'-H), 3.42 (3H, s, 3-CH₃), 3.70 (2H, d, *J* 7.6 Hz, 1'-H₂), 3.90 (3H, s, OCH₃), 4.32 (2H, q, *J* 7.1 Hz, OCH₂CH₃), 7.05 (1H, d, *J* 2.6 Hz, 8''-H), 7.10 (1H, dd, *J* 8.9, 2.6 Hz, 6''-H), 7.18 (1H, dd, *J* 8.9, 2.5 Hz, 3''-H), 7.37 (1H, d, *J* 2.5 Hz, 1''-H), 7.71 (1H, d, *J* 8.9 Hz, 5''-H), 7.76 (1H, d, *J* 8.9 Hz, 4''-H); δ_C (101 MHz, CDCl₃) 14.0 (CH₃), 20.0 (2 × CH₃), 27.1 (CH₃), 28.3 (CH), 55.3 (CH₃), 56.2 (CH₂), 62.1 (CH₂), 105.5 (CH), 109.5 (C), 112.0 (CH), 115.3 (CH), 118.4 (CH), 118.5 (C), 126.2 (C), 129.3 (CH), 130.0 (CH), 135.3 (C), 146.4 (C), 150.5 (C), 150.9 (C),

156.7 (C), 157.3 (C), 158.6 (C), 162.1 (C); m/z (ESI) 505.1415 (MNa^+ . $C_{25}H_{26}N_2NaO_6S$ requires 505.1404).

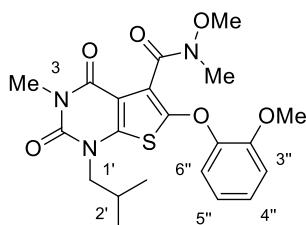
6-(4''-Methoxyphenoxy)-1-isobutyl-3-methyl-2,4-dioxo-1,2,3,4-tetrahydro-thieno[2,3-*d*]-pyrimidine-5-(*N*-methoxy-*N*-methyl)carboxamide (37f)



Ethyl 6-(4''-methoxyphenoxy)-1-isobutyl-3-methyl-2,4-dioxo-1,2,3,4-tetrahydro-thieno[2,3-*d*]pyrimidine-5-carboxylate (**80f**) (0.039 g, 0.090 mmol) was dissolved in ethanol (1 mL) and water (1 mL) and an aqueous solution of 4 M sodium hydroxide (0.4 mL) was added to the mixture. The mixture was stirred at 80 °C for 1 h. The reaction mixture was concentrated *in vacuo*, diluted with water (3 mL), and washed with diethyl ether (2 × 6 mL). The aqueous layer was acidified with an aqueous solution of 1 M hydrochloric acid (3 mL) and extracted with ethyl acetate (3 × 6 mL). The organic layers were combined, dried ($MgSO_4$), filtered and concentrated *in vacuo*. *N,N'*-Diisopropylethylamine (0.042 mL, 0.32 mmol) and *N,O*-dimethylhydroxylamine (0.016 g, 0.16 mmol) were dissolved in acetonitrile (1 mL) and stirred at room temperature for 10 min. The carboxylic acid was then dissolved in acetonitrile (1 mL) and added to the mixture, followed by *O*-(benzotriazol-1-yl)-*N,N,N',N'*-tetramethyluronium hexafluorophosphate (0.031 g, 0.081 mmol). The mixture was then stirred at 40 °C for 18 h. The mixture was diluted with water (4 mL) and washed with saturated aqueous sodium bicarbonate solution (4 mL). The mixture was extracted with ethyl acetate (3 × 10 mL). The organic layers were combined and washed with an aqueous solution of 5% lithium chloride (5 mL) and brine (5 mL). The combined organic layers were dried ($MgSO_4$), filtered and concentrated *in vacuo* to give the crude product. Purification by flash column chromatography eluting with 33% ethyl acetate and 33% of dichloromethane in hexane gave 6-(4''-methoxyphenoxy)-1-isobutyl-3-methyl-2,4-dioxo-1,2,3,4-tetrahydrothieno[2,3-*d*]pyrimidine-5-(*N*-methoxy-*N*-methyl)carboxamide (**37f**) as an orange oil (0.010 g, 23%). ν_{max} (neat)/ cm^{-1} 2957 (CH), 2365, 1704 (C=O), 1662

(C=O), 1501 (C=C), 1467, 1222, 1003, 771. NMR spectra showed a 5:1 mixture of rotational isomers. Only data for the major rotational isomer were recorded: δ_{H} (400 MHz, CDCl_3) 0.95 (6H, d, J 6.7 Hz, $\text{CH}(\text{CH}_3)_2$), 2.22–2.29 (1H, m, 2'-H), 3.39 (6H, s, $2 \times \text{NCH}_3$), 3.56–3.65 (4H, m, 1'-HH and NOCH_3), 3.75–3.82 (4H, m, 1'-HH and OCH_3), 6.84–6.89 (2H, m, $2 \times \text{ArH}$), 7.12–7.14 (2H, m, $2 \times \text{ArH}$); δ_{C} (101 MHz, CDCl_3) 20.0 (CH_3), 20.1 (CH_3), 27.1 (CH_3), 28.3 (CH), 32.8 (CH_3), 55.5 (CH_3), 56.2 (CH_2), 61.8 (CH_3), 114.9 ($2 \times \text{CH}$), 118.0 (C), 119.2 ($2 \times \text{CH}$), 145.8 (C), 148.9 (C), 151.0 (C), 152.0 (C), 156.9 (C), 157.6 (C), 163.6 (C); m/z (ESI) 470.1366 (MNa^+ . $\text{C}_{21}\text{H}_{25}\text{N}_3\text{NaO}_6\text{S}$ requires 470.1356).

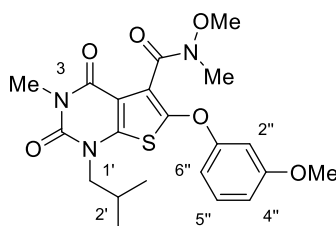
6-(2''-Methoxyphenoxy)-1-isobutyl-3-methyl-2,4-dioxo-1,2,3,4-tetrahydro-thieno[2,3-*d*]pyrimidine-5-(*N*-methoxy-*N*-methyl)carboxamide (37g)



Ethyl 6-(2''-methoxyphenoxy)-1-isobutyl-3-methyl-2,4-dioxo-1,2,3,4-tetrahydro-thieno[2,3-*d*]pyrimidine-5-carboxylate (**80g**) (0.026 g, 0.060 mmol) was dissolved in ethanol (0.65 mL) and water (0.65 mL) and an aqueous solution of 4 M sodium hydroxide (0.3 mL) was added to the mixture. The mixture was stirred at 80 °C for 1 h. The reaction mixture was concentrated *in vacuo*, diluted with water (2 mL) and washed with diethyl ether (2×5 mL). The aqueous layer was acidified with an aqueous solution of 1 M hydrochloric acid (2.5 mL) and extracted with ethyl acetate (3×5 mL). The organic layers were combined, dried (MgSO_4), filtered and concentrated *in vacuo*. *N,N'*-Diisopropylethylamine (0.058 mL, 0.34 mmol) and *N,O*-dimethylhydroxylamine (0.016 g, 0.16 mmol) were dissolved in acetonitrile (1 mL) and stirred at room temperature for 10 min. The carboxylic acid was then dissolved in acetonitrile (1 mL) and added to the mixture, followed by *O*-(benzotriazol-1-yl)-*N,N,N',N'*-tetramethyluronium hexafluorophosphate (0.032 g, 0.084 mmol). The mixture was then stirred at 40 °C for 18 h. The mixture was diluted with water (3 mL) and washed with saturated aqueous sodium bicarbonate solution (3 mL). The mixture was extracted with ethyl acetate (3×10 mL). The organic layers were

combined and washed with an aqueous solution of 5% lithium chloride (5 mL) and brine (5 mL). The combined organic layers were dried (MgSO₄), filtered and concentrated *in vacuo* to give the crude product. Purification by flash column chromatography eluting with 50% ethyl acetate in hexane gave 6-(3''-methoxyphenoxy)-1-isobutyl-3-methyl-2,4-dioxo-1,2,3,4-tetrahydrothieno[2,3-*d*]pyrimidine-5-(*N*-methoxy-*N*-methyl)carboxamide (**37g**) as yellow oil (0.011 g, 35%). ν_{max} (neat)/cm⁻¹ 2966 (CH), 1709 (C=O), 1662 (C=O), 1497 (C=C), 1257, 1114, 1020, 793. NMR spectra showed a 5:1 mixture of rotational isomers. Only data for the major rotational isomer were recorded: δ_{H} (400 MHz, CDCl₃) 0.94 (6H, d, *J* 6.7 Hz, CH(CH₃)₂), 2.18–2.28 (1H, m, 2'-H), 3.39 (3H, s, NCH₃), 3.39 (3H, s, NCH₃), 3.56 (1H, dd, *J* 14.1, 7.4 Hz, 1'-HH), 3.67 (3H, s, NOCH₃), 3.76 (1H, dd, *J* 14.1, 7.9 Hz, 1'-HH), 3.87 (3H, s, OCH₃), 6.94 (1H, dt, *J* 7.8, 1.5 Hz, ArH), 6.98 (1H, dd, *J* 8.0, 1.51 Hz, ArH), 7.17 (1H, dt, *J* 8.0, 1.6 Hz, ArH), 7.26 (1H, dd, *J* 7.8, 1.6 Hz, ArH); δ_{C} (101 MHz, CDCl₃) 20.0 (CH₃), 20.1 (CH₃), 27.1 (CH₃), 28.2 (CH), 32.8 (CH₃), 55.9 (CH₃), 56.1 (CH₂), 61.8 (CH₃), 110.0 (C), 112.9 (CH), 116.8 (C), 120.5 (CH), 121.2 (CH), 126.4 (CH), 145.3 (C), 146.8 (C), 149.5 (C), 150.5 (C), 151.0 (C), 157.7 (C), 163.7 (C); *m/z* (ESI) 448.1546 (MH⁺. C₂₁H₂₆N₃O₆S requires 448.1537).

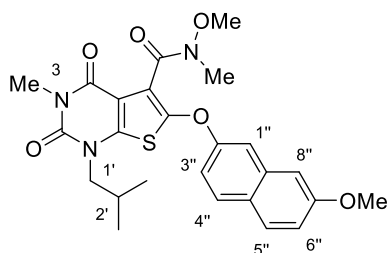
6-(3''-Methoxyphenoxy)-1-isobutyl-3-methyl-2,4-dioxo-1,2,3,4-tetrahydrothieno[2,3-*d*]pyrimidine-5-(*N*-methoxy-*N*-methyl)carboxamide (37h)



Ethyl 6-(3''-methoxyphenoxy)-1-isobutyl-3-methyl-2,4-dioxo-1,2,3,4-tetrahydrothieno[2,3-*d*]pyrimidine-5-carboxylate (**80h**) (0.025 g, 0.058 mmol) was dissolved in ethanol (0.6 mL) and water (0.6 mL) and an aqueous solution of 4 M sodium hydroxide (0.25 mL) was added to the mixture. The mixture was stirred at 80 °C for 1 h. The reaction mixture was concentrated *in vacuo*, diluted with water (2 mL) and washed with diethyl ether (2 × 3 mL). The aqueous layer was acidified with an aqueous solution of 1 M hydrochloric acid (2 mL) and extracted with ethyl acetate (3 × 3 mL). The organic layers were combined, dried (MgSO₄), filtered and

concentrated *in vacuo*. *N,N'*-Diisopropylethylamine (0.042 mL, 0.32 mmol) and *N,O*-dimethylhydroxylamine (0.016 g, 0.16 mmol) were dissolved in acetonitrile (1 mL) and stirred at room temperature for 10 min. The carboxylic acid was then dissolved in acetonitrile (1 mL) and added to the mixture, followed by *O*-(benzotriazol-1-yl)-*N,N,N',N'*-tetramethyluronium hexafluorophosphate (0.031 g, 0.081 mmol). The mixture was then stirred at 40 °C for 18 h. The mixture was diluted with water (3 mL) and washed with saturated aqueous sodium bicarbonate solution (3 mL). The mixture was extracted with ethyl acetate (3 × 5 mL). The organic layers were combined and washed with an aqueous solution of 5% lithium chloride (5 mL) and brine (5 mL). The combined organic layers were dried (MgSO₄), filtered and concentrated *in vacuo* to give the crude product. Purification by flash column chromatography eluting with 50% ethyl acetate in hexane gave 6-(3"-methoxyphenoxy)-1-isobutyl-3-methyl-2,4-dioxo-1,2,3,4-tetrahydrothieno[2,3-*d*]pyrimidine-5-(*N*-methoxy-*N*-methyl)carboxamide (**37h**) as an orange oil (0.012 g, 43%). ν_{max} (neat)/cm⁻¹ 2954 (CH), 2358, 2335, 1703 (C=O), 1662 (C=O), 1487 (C=C), 772. NMR spectra showed a 5:1 mixture of rotational isomers. Only data for the major rotational isomer were recorded: δ_{H} (400 MHz, CDCl₃) 0.97 (6H, d, *J* 6.9 Hz, CH(CH₃)₂), 2.21–2.33 (1H, m, 2'-H), 3.38 (3H, s, NCH₃), 3.40 (3H, s, NCH₃), 3.58–3.64 (4H, m, 1'-HH and NOCH₃), 3.77–3.86 (4H, m, 1'-HH and OCH₃), 6.70–6.77 (3H, m, 3 × ArH), 7.16 (2H, m, 5"-H); δ_{C} (101 MHz, CDCl₃) 20.0 (CH₃), 20.1 (CH₃), 27.1 (CH₃), 28.3 (CH), 32.8 (CH₃), 55.5 (CH₃), 56.3 (CH₂), 61.8 (CH₃), 103.7 (CH), 109.5 (CH), 109.9 (C), 110.7 (CH), 119.7 (C), 130.3 (CH), 146.4 (C), 146.9 (C), 151.0 (C), 157.6 (C), 159.2 (C), 161.0 (C), 163.4 (C); *m/z* (ESI) 470.1356 (MNa⁺. C₂₁H₂₅FN₃NaO₆S requires 470.1356).

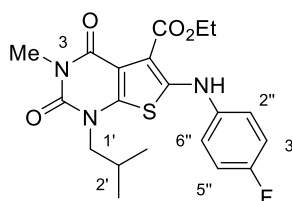
6-(7''-Methoxy-2''-phenoxy)-1-isobutyl-3-methyl-2,4-dioxo-1,2,3,4-tetrahydrothieno[2,3-*d*]pyrimidine-5-(*N*-methoxy-*N*-methyl)carboxamide (37i)



Ethyl 6-(7''-methoxy-2''-phenoxy)-1-isobutyl-3-methyl-2,4-dioxo-1,2,3,4-tetrahydrothieno[2,3-*d*]pyrimidine-5-carboxylate (**80i**) (0.034 g, 0.070 mmol) was dissolved in ethanol (0.8 mL) and water (0.8 mL) and an aqueous solution of 4 M sodium hydroxide (0.3 mL) was added to the mixture. The mixture was stirred at 80 °C for 1.5 h. The reaction mixture was concentrated *in vacuo*, diluted with water (2 mL), and washed with diethyl ether (2 × 5 mL). The aqueous layer was acidified with an aqueous solution of 1 M hydrochloric acid (2.5 mL) and extracted with ethyl acetate (3 × 5 mL). The organic layers were combined, dried (MgSO₄), filtered and concentrated *in vacuo*. *N,N*-Diisopropylethylamine (0.042 mL, 0.32 mmol) and *N,O*-dimethylhydroxylamine (0.016 g, 0.16 mmol) were dissolved in acetonitrile (1 mL) and stirred at room temperature for 10 min. The carboxylic acid was then dissolved in acetonitrile (1 mL) and added to the mixture, followed by *O*-(benzotriazol-1-yl)-*N,N,N',N'*-tetramethyluronium hexafluorophosphate (0.031 g, 0.081 mmol). The mixture was then stirred at 40 °C for 18 h. The mixture was diluted with water (2 mL) and washed with saturated aqueous sodium bicarbonate solution (3 mL). The mixture was extracted with ethyl acetate (3 × 10 mL). The organic layers were combined and washed with an aqueous solution of 5% lithium chloride (4 mL) and brine (4 mL). The combined organic layers were dried (MgSO₄), filtered and concentrated *in vacuo* to give the crude product. Purification by flash column chromatography eluting with 33% ethyl acetate and 33% of dichloromethane in hexane gave 6-(7''-methoxy-2''-phenoxy)-1-isobutyl-3-methyl-2,4-dioxo-1,2,3,4-tetrahydrothieno[2,3-*d*]pyrimidine-5-(*N*-methoxy-*N*-methyl)carboxamide (**37i**) as an orange oil (0.011 g, 31%). ν_{max} (neat)/cm⁻¹ 2958, 2360, 1706 (C=O), 1662 (C=O), 1635, 1491 (C=C), 1470, 1212, 765. NMR spectra showed a 5:1 mixture of rotational isomers. Only data for the major rotational isomer were recorded: δ_{H} (400 MHz, CDCl₃) 0.95 (6H, d, *J* 7.0 Hz, CH(CH₃)₂), 2.20–2.30 (1H, m, 2'-H), 3.38 (3H, s,

NCH₃), 3.41 (3H, s, NCH₃), 3.58–3.63 (1H, dd, *J* 14.2, 7.4 Hz, 1'-HH), 3.68 (3H, s, NOCH₃), 3.77–3.84 (1H, m, 1'-HH), 3.89 (3H, s, OCH₃), 7.05 (1H, d, *J* 2.5 Hz, 8"-H), 7.10 (1H, dd, *J* 8.8, 2.5 Hz, 6"-H), 7.20 (1H, dd, *J* 8.8, 2.5 Hz, 3"-H), 7.46 (1H, d, *J* 2.5 Hz, 1"-H), 7.71 (1H, d, *J* 8.8 Hz, 5"-H), 7.75 (1H, d, *J* 8.8 Hz, 4"-H); δ_c (101 MHz, CDCl₃) 20.0 (CH₃), 20.1 (CH₃), 27.1 (CH₃), 28.3 (CH), 32.8 (CH₃), 55.3 (CH₃), 56.2 (CH₂), 61.8 (CH₃), 105.6 (CH), 109.9 (C), 112.5 (CH), 115.5 (CH), 118.4 (CH), 119.7 (C), 126.3 (C), 129.3 (CH), 129.9 (CH), 135.4 (C), 146.5 (C), 151.0 (2 × C), 156.7 (C), 157.6 (C), 158.6 (C), 163.5 (C); *m/z* (ESI) 498.1703 (MH⁺. C₂₅H₂₈N₃O₆S requires 498.1693).

Ethyl 6-[(4"-fluorophenyl)amino]-1-isobutyl-3-methyl-2,4-dioxo-1,2,3,4-tetrahydrothieno[2,3-*d*]pyrimidine-5-carboxylate (83a)



A solution of bis(dibenzylideneacetone)palladium(0) (0.015 g, 0.026 mmol), *rac*-BINAP (0.016 g, 0.026 mmol), ethyl 6-bromo-1-isobutyl-3-methyl-2,4-dioxo-1,2,3,4-tetrahydrothieno[2,3-*d*]pyrimidine-5-carboxylate (**45**) (0.10 g, 0.26 mmol), and caesium carbonate (0.12 g, 0.36 mmol) in toluene (2.5 mL) was heated to 100 °C under an argon atmosphere. After 5 min, 4-fluoroaniline (0.026 mL, 0.27 mmol) was added and the reaction was left stirring at 100 °C for 24 h. After cooling to room temperature, the reaction mixture was diluted with tetrahydrofuran (5 mL) and filtered through Celite® pad. The resulting filtrate was concentrated *in vacuo*. Purification by flash column chromatography eluting with 30% ethyl acetate in petroleum ether gave ethyl 6-[(4"-fluorophenyl)amino]-1-isobutyl-3-methyl-2,4-dioxo-1,2,3,4-tetrahydrothieno[2,3-*d*]pyrimidine-5-carboxylate (**83a**) as a pale-yellow oil, solidifying on standing (0.062 g, 57%). Mp 135 °C ν_{\max} (neat)/cm⁻¹ 2963 (CH), 2824, 2673 (CH), 2110, 1748 (C=O), 1670 (C=O), 1604, 1304, 914, 667; δ_H (400 MHz, CDCl₃) 0.95 (6H, d, *J* 6.7 Hz, CH(CH₃)₂), 1.42 (3H, t, *J* 7.1 Hz, CH₂CH₃), 2.23 (1H, m, 2'-H), 3.42 (3H, s, 3-CH₃), 3.69 (2H, d, *J* 7.7 Hz, 1'-H₂), 4.41 (2H, q, *J* 7.1 Hz, CH₂CH₃), 7.05–7.12 (2H, m, 3"-H and 5"-H), 7.18–7.24 (2H, m, 2"-H and 6"-H); δ_c (101 MHz, CDCl₃) 14.3 (CH₃), 20.0 (CH₃), 27.3 (CH₃), 28.7 (CH), 55.9 (CH₂),

61.2 (CH₂), 104.9 (C), 110.7 (C), 116.7 (d, ²J_{CF} 22.9 Hz, 2 × CH), 122.8 (d, ³J_{CF} 8.2 Hz, 2 × CH), 136.9 (d, ⁴J_{CF} 2.8 Hz, C), 142.1 (C), 151.0 (C), 151.2 (C), 156.5 (C), 159.9 (d, ¹J_{CF} 245.1 Hz, C), 165.3 (C); *m/z* (ESI) 420.1386 (MH⁺. C₂₀H₂₃FN₃O₄S requires 458.1388).

HPLC Methods for Physicochemical Properties Analysis. Determination of Membrane Permeability (*P_m*) and Membrane Partition Coefficient (*K_m*)¹¹⁶

P_m and *K_m* values were determined using previously developed methodology on a Regis IAM.PC.DD2 (150 × 4.6 mm) column using a Dionex UltiMate 3000 series HPLC system, and data acquisition and processing carried out using Chromeleon 6.8 chromatography software. Both standard and test compounds solutions were prepared at a concentration of 0.5 mg/mL in the acetonitrile and 0.01 mM phosphate buffered saline (pH 7.4) mixture (1:1, v/v). Analysis was performed using 5 µL sample injections. The HPLC system oven was maintained to 25 °C, and UV detection was performed using a diode array detector (190–800 nm).

Acetonitrile and 0.01 mM phosphate buffered saline (pH 7.4) were used as the mobile phase at a flow rate of 1.0 mL min⁻¹. The retention time of each test compounds was measured under an isocratic mobile phase with acetonitrile concentrations ranging from 30 to 70%. For system corrections, the retention time of citric acid, an unretained compound, was determined using an isocratic mobile phase of 100% phosphate buffered saline. The following equations were used to calculate *P_m* and *K_m* of the test compounds:

$$k_{IAM} = \frac{(t_r - t_0)}{t_0}$$

where *k_{IAM}* – solute capacity factor on the IAM column, *t_r* – retention time of the test compound, *t₀* – retention time of citric acid (unretained compound).

$$k_{IAM} = \left(\frac{V_s}{V_m} \right) \times K_m$$

where V_s – volume of the IAM interphase created by the immobilised phospholipids, V_m – total volume of the solvent within the IAM column, K_m – membrane partition coefficient.

V_s is determined by the ligand density on the column, which is 70.0:6.7:1.2 (PhC:C₁₀:C₃) mg/g packing material.²⁰⁰ V_s is a sum of the different ligand volumes:

$$V_s = \frac{W_{\text{PhC}}}{\delta_{\text{PhC}}} + \frac{W_{\text{C10}}}{\delta_{\text{C10}}} + \frac{W_{\text{C3}}}{\delta_{\text{C3}}}$$

where the specific weight of PhC (δ_{PhC}) = 1.01779 g/mL, C₁₀/C₃ ($\delta_{\text{C10/C3}}$) = 0.86 g/mL; W_{PhC} = 133 mg, W_{C10} = 12.73 mg, W_{C3} = 2.28 mg.

$$V_m = f_r \times t_0$$

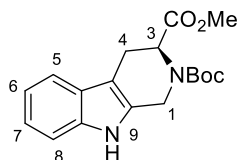
where f_r – flow rate.

$$P_m = \frac{K_m}{MW}$$

where P_m – permeability, MW – molecular weight of the test

3.4 Fluorescent Tryptophan Derivatives Experimental

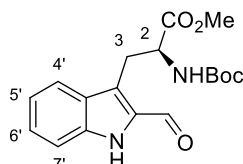
Methyl (3S)-2-(*tert*-butoxycarbonyl)-2,3,4,9-tetrahydro-1*H*-pyrido[3,4-*b*]indole-3-carboxylate (**94**)^{201,202}



Polyformaldehyde (0.0360 g, 1.20 mmol) was added to the solution of methyl L-tryptophanate hydrochloride (**92**) (0.255 g, 1.00 mmol) in acetic acid/methanol (10:1, 5 mL) under argon. The reaction mixture was stirred at 80 °C for 1.5 h and then cooled to room temperature. The mixture was basified to pH 9–10 using an aqueous solution of ammonium hydroxide and extracted with dichloromethane (3 × 7 mL). The combined organic layers were dried (MgSO₄), filtered and *in vacuo*. The resulting pale yellow solid (0.211 g) was then dissolved in dichloromethane (1.5 mL) and triethylamine (0.252 mL, 1.82 mmol) and di-*tert*-butyl dicarbonate (0.258 g, 1.18 mmol) were added to the solution. The reaction mixture was stirred at room temperature for 18 h and concentrated *in vacuo*. The crude material was purified by flash column chromatography eluting with 17% ethyl acetate in hexane to give methyl (3*S*)-2-(*tert*-butoxycarbonyl)-2,3,4,9-tetrahydro-1*H*-pyrido[3,4-*b*]indole-3-carboxylate (**94**) as a white solid (0.230 g, 69% over 2 steps). Spectroscopic data were consistent with the literature.²⁰² $[\alpha]_D^{18} +84.0$ (c 0.1, CHCl₃). NMR spectra showed a 1.2:1 mixture of rotational isomers. Only data for the major rotational isomer is presented: δ_H (400 MHz, CDCl₃) 1.54 (9H, C(CH₃)₃, minor), 1.54 (9H, C(CH₃)₃, major), 3.05–3.16 (1H, m, 4-*HH*), 3.42 (1H, d, *J* 16.3 Hz, 4-*HH*), 3.61 (3H, s, OCH₃, major), 3.63 (3H, s, OCH₃, minor), 4.52 (1H, d, *J* 16.2 Hz, 1-*HH*, minor), 4.58 (1H, d, *J* 16.2 Hz, 1-*HH*, major), 4.82 (1H, d, *J* 16.2 Hz, 1-*HH*, major), 4.91 (1H, d, *J* 16.2 Hz, 1-*HH*, minor), 5.21 (1H, d, *J* 5.2 Hz, 3-H, minor), 5.42 (1H, d, *J* 5.8 Hz, 3-H, major), 7.07–7.19 (2H, m, 2 × ArH), 7.30 (1H, dd, *J* 7.8, 3.4 Hz, ArH), 7.49 (1H, d, *J* 7.8 Hz, ArH), 7.81 (1H, br s, 9-H, major), 8.18 (1H, br s, 9-H, minor); δ_C (101 MHz, CDCl₃) 23.2 (CH₂, major), 23.5 (CH₂, minor), 28.4 (3 × CH₃), 40.2 (CH₂, minor), 40.6 (CH₂, major), 52.3 (CH₃, minor), 52.4 (CH₃, major), 52.4 (CH, major), 53.8 (CH, minor), 80.9 (C, major), 81.1 (C, minor), 105.6 (C, minor), 106.4 (C, major), 110.8

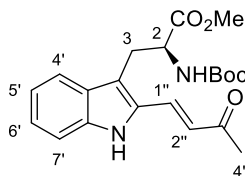
(CH, major), 110.8 (CH, minor), 118.1 (CH, minor), 118.2 (CH, major), 119.5 (CH, minor), 119.6 (CH, major), 121.8 (CH, minor), 122.0 (CH, major), 126.7 (C, minor), 126.8 (C, major), 129.7 (C, major), 129.8 (C, minor), 136.4 (C), 155.5 (C, minor), 155.8 (C, major), 172.1 (C); m/z (ESI) 231 ($[M-CO_2^tBu]+H^+$, 100%).

Methyl (2S)-2-[(*tert*-butoxycarbonyl)amino]-3-(2'-formyl-1'*H*-indol-3'-yl)propanoate (95)^{180,202}



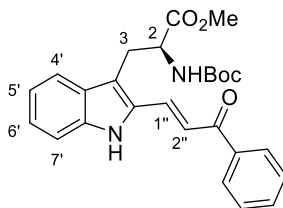
To a solution of methyl (3S)-2-(*tert*-butoxycarbonyl)-2,3,4,9-tetrahydro-1*H*-pyrido[3,4-*b*]indole-3-carboxylate (**94**) (0.856 g, 2.59 mmol) in anhydrous dioxane (21 mL) under argon was added selenium oxide (0.431 g, 3.89 mmol). The reaction mixture was stirred under reflux for 1.5 h, then cooled to room temperature, filtered through Celite® and concentrated *in vacuo*. The crude material was purified by flash column chromatography eluting with 30% ethyl acetate in hexane to give methyl (2S)-2-[(*tert*-butoxycarbonyl)amino]-3-(2'-formyl-1'*H*-indol-3'-yl)propanoate (**95**) as a yellow solid (0.608 g, 68%). Spectroscopic data were consistent with the literature.²⁰² $[\alpha]_D^{18} +88.3$ (c 0.1, $CHCl_3$); δ_H (400 MHz, $CDCl_3$) 1.45 (9H, s, $C(CH_3)_3$), 3.57–3.70 (5H, m, OCH_3 and 3- H_2), 4.69–4.78 (1H, m, 2-H), 5.23 (1H, d, J 7.6 Hz, 2-NH), 7.16 (1H, ddd, J 8.1, 5.6, 2.0 Hz, ArH), 7.34–7.42 (2H, m, 2 × ArH), 7.68 (1H, d, J 8.1 Hz, ArH), 9.15 (1H, s, 1'-H), 9.87 (1H, s, CHO); δ_C (101 MHz, $CDCl_3$) 26.8 (CH_2), 28.3 (3 × CH_3), 52.5 (CH_3), 54.3 (CH), 80.3 (C), 112.4 (CH), 120.9 (CH), 121.4 (CH), 121.9 (C), 127.6 (CH), 127.8 (C), 133.4 (C), 137.3 (C), 154.9 (C), 171.6 (C), 180.9 (C); m/z (ESI) 369 (MNa^+ , 100%).

Methyl (2S)-2-[(*tert*-butoxycarbonyl)amino]-3-(2'-[(1''*E*)-3''-oxo-1''-butenyl]-1'*H*-indol-3'-yl)propanoate (90a)



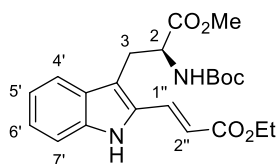
Lithium chloride (0.0090 g, 0.21 mmol) was added to a microwave vial and dried in an oven at 140 °C overnight. The oven-dried microwave vial was then cooled to room temperature *in vacuo* and then purged with argon. Methyl (2S)-2-[(*tert*-butoxycarbonyl)amino]-3-(2'-formyl-1'*H*-indol-3'-yl)propanoate (**95**) (0.060 g, 0.17 mmol) was dissolved in anhydrous acetonitrile (1.7 mL) under argon and added to the microwave vial. 1,8-Diazabicyclo(5.4.0)undec-7-ene (0.024 mL, 0.17 mmol) and diethyl (2-oxopropyl)phosphonate (0.034 mg, 0.21 mmol) were added, and the reaction mixture was stirred at 50 °C for 1.5 h. After cooling to room temperature, the reaction mixture was concentrated *in vacuo*. The crude material was purified by flash column chromatography eluting with ethyl acetate in hexane (gradient 2:1 to 1:1) to give methyl (2S)-2-[(*tert*-butoxycarbonyl)amino]-3-(2'-[(1''*E*)-3''-oxo-1''-butenyl]-1'*H*-indol-3'-yl)propanoate (**90a**) as a bright yellow solid (0.056 g, 84%). Mp 85–87 °C; $\nu_{\text{max}}/\text{cm}^{-1}$ (neat) 3347 (NH), 2979 (CH), 1691 (C=O), 1603 (C=O), 1357, 1263, 1164, 1064, 1003, 742; $[\alpha]_{\text{D}}^{21} +12.3$ (*c* 0.1, CHCl₃); δ_{H} (400 MHz, CDCl₃) 1.43 (9H, s, C(CH₃)₃), 2.40 (3H, s, 4''-H₃), 3.33–3.50 (2H, m, 3-H₂), 3.62 (3H, s, OCH₃), 4.64–4.76 (1H, m, 2-H), 5.18 (1H, d, *J* 7.8 Hz, 2-NH), 6.55 (1H, d, *J* 16.2 Hz, 2''-H), 7.09 (1H, dd, *J* 8.1, 7.1 Hz, 6'-H), 7.25 (1H, dd, *J* 8.2, 7.1 Hz, 5'-H), 7.34 (1H, d, *J* 8.2 Hz, 4'-H), 7.55 (1H, d, *J* 8.1 Hz, 7'-H), 7.61 (1H, d, *J* 16.2 Hz, 1''-H), 9.13 (1H, br s, 1'-H); δ_{C} (101 MHz, CDCl₃) 27.2 (CH₃), 27.7 (CH₂), 28.3 (3 × CH₃), 52.5 (CH₃), 54.6 (CH), 80.1 (C), 111.4 (CH), 117.6 (C), 119.9 (CH), 120.4 (CH), 124.0 (CH), 125.4 (CH), 128.8 (C), 131.1 (CH), 131.2 (C), 137.7 (C), 155.1 (C), 172.2 (C), 198.3 (C); *m/z* (ESI) 387.1919 (MH⁺. C₂₁H₂₇N₂O₅ requires 387.1914).

Methyl (2S)-2-[(*tert*-butoxycarbonyl)amino]-3-(2'-[(1''*E*)-3''-oxo-3''-phenyl-1''-propenyl]-1'*H*-indol-3'-yl)propanoate (90b**)**



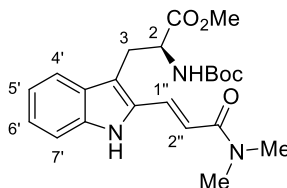
The reaction was carried out according to the previously described procedure for methyl (2S)-2-[(*tert*-butoxycarbonyl)amino]-3-(2'-[(1''*E*)-3''-oxo-1''-butenyl]-1'*H*-indol-3'-yl)propanoate (**90a**) using methyl (2S)-2-[(*tert*-butoxycarbonyl)amino]-3-(2'-formyl-1'*H*-indol-3'-yl)propanoate (**95**) (0.10 g, 0.29 mmol), anhydrous acetonitrile (2 mL), lithium chloride (0.017 g, 0.40 mmol), 1,8-diazabicyclo(5.4.0)undec-7-ene (0.062 mL, 0.40 mmol) and diethyl (2-oxo-2-phenylethyl)phosphonate (0.088 mL, 0.40 mmol). The reaction mixture was stirred at 50 °C for 19 h. Another portion of 1,8-diazabicyclo(5.4.0)undec-7-ene (0.018 mL, 0.13 mmol) and diethyl (2-oxo-2-phenylethyl)phosphonate (0.022 mL, 0.10 mmol) was added, and the reaction mixture was left stirring at 50 °C for 41 h. After cooling to room temperature, the reaction mixture was concentrated *in vacuo*. The crude material was purified by flash column chromatography eluting with ethyl acetate in hexane (gradient 4:1 to 3:1) to give methyl (2S)-2-[(*tert*-butoxycarbonyl)amino]-3-(2'-[(1''*E*)-3''-oxo-3''-phenyl-1''-propenyl]-1'*H*-indol-3'-yl)propanoate (**90b**) as a bright yellow solid (0.073 g, 57%). Mp 92–95 °C; $\nu_{\text{max}}/\text{cm}^{-1}$ (neat) 3332 (NH), 2976 (CH), 2359, 1681 (C=O), 1577, 1281, 1214, 1160, 1013, 746; $[\alpha]_{\text{D}}^{15} +180.8$ (c 0.1, CHCl₃); δ_{H} (400 MHz, CDCl₃) 1.41 (1H, s, C(CH₃)₃), 3.45 (1H, dd, *J* 14.6, 5.2 Hz, 3-*HH*), 3.50 (1H, dd, *J* 14.6, 5.2 Hz, 3-*HH*), 3.67 (3H, s, OCH₃), 4.69–4.77 (1H, m, 2-*H*), 5.10 (1H, d, *J* 8.3 Hz, 2-NH), 7.13 (1H, t, *J* 8.0 Hz, ArH), 7.26–7.37 (3H, m, 2''-H and 2 × ArH), 7.48–7.54 (2H, m, 2 × ArH), 7.57–7.63 (2H, m, 2 × ArH), 7.87 (1H, d, *J* 15.6 Hz, 1''-H), 8.01–8.06 (2H, m, 2 × ArH), 8.35 (1H, br s, 1'-H); δ_{C} (101 MHz, CDCl₃) 27.5 (CH₂), 28.3 (3 × CH₃), 52.5 (CH₃), 54.4 (CH), 80.0 (C), 111.2 (CH), 118.1 (C), 118.7 (CH), 120.2 (CH), 120.5 (CH), 125.5 (CH), 128.4 (2 × CH), 128.7 (2 × CH), 129.1 (C), 131.7 (CH), 131.9 (C), 132.8 (CH), 137.5 (C), 138.2 (C), 155.1 (C), 172.0 (C), 189.6 (C); *m/z* (ESI) 471.1893 (MNa⁺. C₂₆H₂₈N₂O₅Na requires 471.1890).

Methyl (2S)-2-[(*tert*-butoxycarbonyl)amino]-3-(2'-[(1''*E*)-3''-ethoxy-3''-oxo-1''-propenyl]-1'*H*-indol-3'-yl)propanoate (90c**)**²⁰³



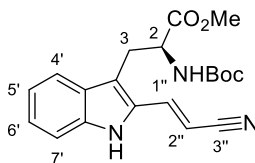
The reaction was carried out according to the previously described procedure for methyl (2S)-2-[(*tert*-butoxycarbonyl)amino]-3-(2'-[(1''*E*)-3''-oxo-1''-butenyl]-1'*H*-indol-3'-yl)propanoate (**90a**) using methyl (2S)-2-[(*tert*-butoxycarbonyl)amino]-3-(2'-formyl-1'*H*-indol-3'-yl)propanoate (**95**) (0.060 g, 0.17 mmol), anhydrous acetonitrile (1.7 mL), lithium chloride (0.015 g, 0.35 mmol), 1,8-diazabicyclo(5.4.0)undec-7-ene (0.040 mL, 0.26 mmol) and triethyl phosphonoacetate (0.070 mL, 0.35 mmol). The reaction mixture was stirred at 50 °C for 2 h. Another portion of 1,8-diazabicyclo(5.4.0)undec-7-ene (0.013 mL, 0.087 mmol) and triethyl carboxymethylphosphonate (0.018 mL, 0.091 mmol) was added and the reaction mixture was left stirring at 50 °C for 22 h. After cooling to room temperature, the reaction mixture was concentrated *in vacuo*. The crude material was purified by flash column chromatography eluting with ethyl acetate in hexane (4:1) to give methyl (2S)-2-[(*tert*-butoxycarbonyl)amino]-3-(2'-[(1''*E*)-3''-ethoxy-3''-oxo-1''-propenyl]-1'*H*-indol-3'-yl) propanoate (**90c**) as a beige solid (0.045 g, 67%). Mp 92–95 °C; $[\alpha]_{\text{D}}^{21} +14.4$ (*c* 0.1, CHCl₃); δ_{H} (400 MHz, CDCl₃) 1.33 (3H, t, *J* 7.1 Hz, OCH₂CH₃), 1.44 (9H, s, C(CH₃)₃), 3.39 (1H, dd, *J* 14.6, 4.6 Hz, 3-*HH*), 3.45 (1H, dd, *J* 14.6, 5.6 Hz, 3-*HH*), 3.71 (3H, s, OCH₃), 4.20–4.32 (2H, m, OCH₂CH₃), 4.72 (1H, ddd, *J* 8.3, 5.6, 4.6 Hz, 2-H), 5.14 (1H, d, *J* 8.3 Hz, 2-NH), 6.22 (H, d, 15.8 Hz, 2''-H), 7.07 (1H, t, *J* 7.9 Hz, ArH), 7.15–7.24 (2H, m, ArH), 7.55 (1H, d, *J* 7.9 Hz, ArH), 7.64 (1H, d, *J* 15.8 Hz, 1''-H), 8.70 (1H, br s, 1'-H); δ_{C} (101 MHz, CDCl₃) 14.4 (CH₃), 27.2 (CH₂), 28.3 (3 × CH₃), 52.6 (CH₃), 54.4 (CH), 60.6 (CH₂), 80.0 (C), 111.1 (CH), 115.2 (CH), 116.2 (C), 119.9 (CH), 120.3 (CH), 125.1 (CH), 128.8 (C), 131.2 (C), 131.5 (CH), 137.3 (C), 155.1 (C), 166.9 (C), 172.3 (C); *m/z* (ESI) 439.1850 (MNa⁺. C₂₂H₂₈N₂O₆Na requires 439.1840).

Methyl (2S)-2-[(*tert*-butoxycarbonyl)amino]-3-(2'-[(1''*E*)-3''-dimethylamino-3''-oxo-1''-propenyl]-1'*H*-indol-3'-yl)propanoate (90d)



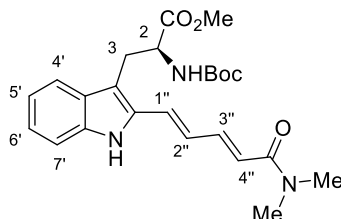
The reaction was carried out according to the previously described procedure for methyl (2S)-2-[(*tert*-butoxycarbonyl)amino]-3-(2'-[(1''*E*)-3''-oxo-1''-butenyl]-1'*H*-indol-3'-yl)propanoate (**90a**) using methyl (2S)-2-[(*tert*-butoxycarbonyl)amino]-3-(2'-formyl-1'*H*-indol-3'-yl)propanoate (**95**) (0.060 g, 0.17 mmol), anhydrous acetonitrile (1.7 mL), lithium chloride (0.010 g, 0.21 mmol), 1,8-diazabicyclo(5.4.0)undec-7-ene (0.026 mL, 0.17 mmol) and diethyl [(dimethylcarbamoyl)methyl]phosphonate (0.046 mg, 0.21 mmol). The reaction mixture was stirred at 50 °C for 3.5 h. After cooling to room temperature, the reaction mixture was concentrated *in vacuo*. The crude material was purified by flash column chromatography eluting with a 50–100% of ethyl acetate in hexane to give methyl (2S)-2-[(*tert*-butoxycarbonyl)amino]-3-(2'-[(1''*E*)-3''-dimethylamino-3''-oxo-1''-propenyl]-1'*H*-indol-3'-yl)propanoate (**90d**) as a yellow oil (0.050 g, 69%). $\nu_{\text{max}}/\text{cm}^{-1}$ (neat) 3258 (NH), 2976 (CH), 1688 (C=O), 1642 (C=O), 1584, 1499, 1364, 1245, 1153, 742; $[\alpha]_{\text{D}}^{21} +11.1$ (c 0.1, CHCl₃); δ_{H} (400 MHz, CDCl₃) 1.41 (9H, s, C(CH₃)₃), 3.06 (3H, s, N(CH₃)CH₃), 3.15 (3H, s, N(CH₃)CH₃), 3.34 (1H, dd, *J* 14.4, 5.2 Hz, 3-*HH*), 3.40 (1H, dd, *J* 14.4, 5.8 Hz, 3-*HH*), 3.67 (3H, s, OCH₃), 4.66 (1H, ddd, *J* 8.0, 5.8, 5.2 Hz, 2-H), 5.11 (1H, d, *J* 8.0 Hz, 2-NH), 6.72 (1H, d, *J* 15.4 Hz, 2''-H), 7.07 (1H, t, *J* 8.0 Hz, ArH), 7.20 (1H, t, *J* 8.0 Hz, ArH), 7.27 (1H, d, *J* 8.0 Hz, ArH), 7.55 (1H, *J* 8.0 Hz, ArH), 7.67 (1H, d, *J* 15.4 Hz, 1''-H), 8.83 (1H, br s, 1'-H); δ_{C} (101 MHz, CDCl₃) 27.4 (CH₂), 28.3 (3 × CH₃), 36.1 (CH₃), 37.4 (CH₃), 52.5 (CH₃), 54.4 (CH), 79.9 (C), 111.0 (CH), 114.8 (CH), 115.0 (C), 119.8 (CH), 120.2 (CH), 124.5 (CH), 129.1 (C), 130.0 (CH), 131.9 (C), 137.0 (C), 155.1 (C), 166.5 (C), 172.2 (C); *m/z* (ESI) 416.2193 (MH⁺. C₂₂H₃₀N₃O₅ requires 416.2180).

Methyl (2S)-2-[(*tert*-butoxycarbonyl)amino]-3-(2'-[(1''*E*)-2''-cyano-1''-ethenyl]-1'*H*-indol-3'-yl)propanoate (90e**)**



Lithium chloride (0.010 g, 0.021 mmol) was added to a microwave vial and dried in an oven at 140 °C overnight. The oven-dried microwave vial was cooled to room temperature *in vacuo* and then purged with argon. Methyl (2S)-2-[(*tert*-butoxycarbonyl)amino]-3-(2'-formyl-1'*H*-indol-3'-yl)propanoate (**95**) (0.060 g, 0.17 mmol) was dissolved in anhydrous acetonitrile (1.7 mL) under argon and added to the microwave vial. The mixture was cooled to 0 °C and 1,8-diazabicyclo(5.4.0)undec-7-ene (0.026 mL, 0.17 mmol) and diethyl (cyanomethyl)phosphonate (0.034 mL, 0.21 mmol) were added. The reaction mixture was then warmed to room temperature, stirred for 2 h and then concentrated *in vacuo*. The crude material was purified by flash column chromatography eluting with a 2–5% of ethyl acetate in dichloromethane to give methyl (2S)-2-[(*tert*-butoxycarbonyl)amino]-3-(2'-[(1''*E*)-2''-cyano-1''-ethenyl]-1'*H*-indol-3'-yl)propanoate (**90e**) as a pale yellow solid (0.030 g, 47%). Mp 166–169 °C; $\nu_{\text{max}}/\text{cm}^{-1}$ (neat) 3286 (NH), 2973 (CH), 2213 (C \equiv N), 1678 (C=O), 1606, 1527, 1435, 1278, 1158 1061, 746; $[\alpha]_{\text{D}}^{22} +11.6$ (*c* 0.1, CHCl₃); δ_{H} (400 MHz, CDCl₃) 1.46 (9H, s, C(CH₃)₃), 3.33–3.42 (2H, m, 3-H₂), 3.68 (3H, s, OCH₃), 4.64–4.71 (1H, m, 2-H), 5.13 (1H, d, *J* 8.0, 2-NH), 5.51 (1H, d, *J* 16.5 Hz, 2''-H), 7.09–7.16 (1H, m, ArH), 7.27–7.31 (2H, m, ArH), 7.35 (1H, d, *J* 16.5 Hz, 1''-H), 7.55 (1H, d, *J* 8.1 Hz, ArH), 8.36 (1H, br s, 1'-H); δ_{C} (101 MHz, CDCl₃) 27.4 (CH₂), 28.3 (3 × CH₃), 52.6 (CH₃), 54.3 (CH), 80.4 (C), 92.1 (CH), 111.4 (CH), 117.3 (C), 118.6 (C), 120.2 (CH), 120.8 (CH), 125.9 (CH), 128.4 (C), 130.6 (C), 137.3 (CH), 137.6 (C), 155.0 (C), 171.8 (C); *m/z* (ESI) 392.1587 (MNa⁺. C₂₀H₂₃N₃O₄Na requires 392.1581).

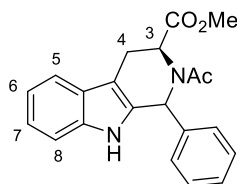
Methyl (2S)-2-[(*tert*-butoxycarbonyl)amino]-3-(2'-[(1''*E*,3''*E*)-5''-dimethylamino-5''-oxo-1'',3''-pentadienyl]-1'*H*-indol-3'-yl)propanoate (97b)



In the oven-dried flask under argon, methyl (2S)-2-[(*tert*-butoxycarbonyl)amino]-3-(2'-formyl-1'*H*-indol-3'-yl)propanoate (**95**) (0.200 g, 0.577 mmol) was dissolved in anhydrous toluene (3 mL). (Triphenylphosphoranylidene)acetaldehyde (0.194 g, 0.636 mmol) was added and the reaction mixture was heated at 50 °C for 4 h. After cooling to room temperature, the reaction mixture was concentrated *in vacuo*. The crude material was purified by flash column chromatography eluting with 30% ethyl acetate in hexane to give methyl (2S)-2-[(*tert*-butoxycarbonyl)amino]-3-(2'-[(1''*E*)-3''-oxo-1''-propenyl]-1'*H*-indol-3'-yl)propanoate (**96**) as a bright yellow solid. Lithium chloride (0.0250 g, 0.590 mmol) was added to a microwave vial and dried in an oven at 140 °C overnight. The oven-dried microwave vial was then cooled to room temperature *in vacuo* and then purged with argon. The resulting methyl (2S)-2-[(*tert*-butoxycarbonyl)amino]-3-(2'-[(1''*E*)-3''-oxo-1''-propenyl]-1'*H*-indol-3'-yl)propanoate (**96**) was dissolved in anhydrous acetonitrile (4.5 mL) under argon and added to the microwave vial. 1,8-Diazabicyclo(5.4.0)undec-7-ene (0.0740 mL, 0.494 mmol) and diethyl [(dimethylcarbamoyl)methyl]phosphonate (0.0960 g, 0.429 mmol) were added, and the reaction mixture was heated at 50 °C for 4 h. Another portion of 1,8-diazabicyclo(5.4.0)undec-7-ene (0.00900 mL, 0.0593 mmol) and diethyl [(dimethylcarbamoyl)methyl]phosphonate (0.0120 g, 0.0515 mmol) was added, and the reaction mixture was left stirring at 50 °C for 22 h. After cooling to room temperature, the reaction was concentrated *in vacuo*. The crude material was purified by flash column chromatography eluting with a 50–67% ethyl acetate in hexane to give methyl (2S)-2-[(*tert*-butoxycarbonyl)amino]-3-(2'-[(1''*E*,3''*E*)-5''-dimethylamino-5''-oxo-1'',3''-pentadienyl]-1'*H*-indol-3'-yl)propanoate (**97b**) as a bright yellow oil (0.0540 g, 21% after two steps). $\nu_{\text{max}}/\text{cm}^{-1}$ (neat) 3254 (NH), 2952 (CH), 1707 (C=O), 1634 (C=O), 1590, 1498, 1165, 1120; $[\alpha]_{\text{D}}^{16} +97.0$ (c 0.1, CHCl₃). NMR spectra showed a 9:1 mixture of rotational isomers. Only data for the major rotational isomer is presented: δ_{H} (400 MHz, CDCl₃) 1.42 (9H, s, C(CH₃)₃), 3.05 (3H, s, NMe₂), 3.75 (3H, s, CO₂Me), 4.15 (1H, d, H-1''), 4.25 (1H, d, H-1''), 4.35 (1H, d, H-1''), 4.45 (1H, d, H-1''), 4.55 (1H, d, H-1''), 4.65 (1H, d, H-1''), 4.75 (1H, d, H-1''), 4.85 (1H, d, H-1''), 4.95 (1H, d, H-1''), 5.05 (1H, d, H-1''), 5.15 (1H, d, H-1''), 5.25 (1H, d, H-1''), 5.35 (1H, d, H-1''), 5.45 (1H, d, H-1''), 5.55 (1H, d, H-1''), 5.65 (1H, d, H-1''), 5.75 (1H, d, H-1''), 5.85 (1H, d, H-1''), 5.95 (1H, d, H-1''), 6.05 (1H, d, H-1''), 6.15 (1H, d, H-1''), 6.25 (1H, d, H-1''), 6.35 (1H, d, H-1''), 6.45 (1H, d, H-1''), 6.55 (1H, d, H-1''), 6.65 (1H, d, H-1''), 6.75 (1H, d, H-1''), 6.85 (1H, d, H-1''), 6.95 (1H, d, H-1''), 7.05 (1H, d, H-1''), 7.15 (1H, d, H-1''), 7.25 (1H, d, H-1''), 7.35 (1H, d, H-1''), 7.45 (1H, d, H-1''), 7.55 (1H, d, H-1''), 7.65 (1H, d, H-1''), 7.75 (1H, d, H-1''), 7.85 (1H, d, H-1''), 7.95 (1H, d, H-1''), 8.05 (1H, d, H-1''), 8.15 (1H, d, H-1''), 8.25 (1H, d, H-1''), 8.35 (1H, d, H-1''), 8.45 (1H, d, H-1''), 8.55 (1H, d, H-1''), 8.65 (1H, d, H-1''), 8.75 (1H, d, H-1''), 8.85 (1H, d, H-1''), 8.95 (1H, d, H-1''), 9.05 (1H, d, H-1''), 9.15 (1H, d, H-1''), 9.25 (1H, d, H-1''), 9.35 (1H, d, H-1''), 9.45 (1H, d, H-1''), 9.55 (1H, d, H-1''), 9.65 (1H, d, H-1''), 9.75 (1H, d, H-1''), 9.85 (1H, d, H-1''), 9.95 (1H, d, H-1'').

s, N(CH₃)CH₃), 3.10 (3H, s, N(CH₃)CH₃), 3.34 (2H, d, *J* 5.1 Hz, 3-H₂), 3.60 (3H, s, OCH₃), 4.64 (1H, dt, *J* 8.2, 5.1 Hz, 2-H), 5.11 (1H, d, *J* 8.2 Hz, 2-NH), 6.43 (1H, d, *J* 14.6 Hz, 4''-H), 6.70 (1H, dd, *J* 15.5, 11.0 Hz, 2''-H), 6.85 (1H, d, *J* 15.5 Hz, 1''-H), 7.07 (1H, t, *J* 8.0 Hz, 6'-H), 7.19 (1H, t, *J* 8.0 Hz, 5'-H), 7.27 (1H, d, *J* 8.0 Hz, 4'-H), 7.44 (1H, dd, *J* 14.6, 11.0 Hz, 3''-H), 7.51 (1H, d, *J* 8.0 Hz, 7'-H), 8.61 (1H, br s, 1'-H); δ_c (101 MHz, CDCl₃) 27.4 (CH₂), 28.4 (3 \times CH₃), 35.9 (CH₃), 37.4 (CH₃), 52.4 (CH₃), 54.4 (CH), 79.9 (C), 110.7 (CH), 113.0 (C), 119.5 (CH), 120.1 (CH), 120.3 (CH), 124.0 (CH), 125.0 (CH), 126.3 (CH), 129.1 (C), 133.1 (C), 137.0 (C), 142.1 (CH), 155.0 (C), 166.7 (C), 172.2 (C); *m/z* (ESI) 464.2159 (MNa⁺. C₂₄H₃₁N₃O₅Na requires 464.2156).

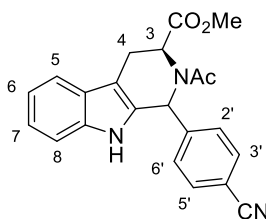
Methyl (2*S*)-1-phenyl-2-acetylamino-2,3,4,9-tetrahydro-1*H*-pyrido[3,4-*b*]indole-3-carboxylate (99a**)**¹⁸³



Benzaldehyde (0.072 mL, 0.55 mmol) was added to the solution of methyl L-tryptophanate hydrochloride (**92**) (0.13 g, 0.50 mmol) in trifluoroacetic acid/water (10:1, v/v, 1.9 mL) under argon. The reaction mixture was stirred at room temperature for 18 h. The mixture was quenched with saturated aqueous sodium bicarbonate solution (5 mL) and extracted with ethyl acetate (3 \times 7 mL). The combined organic layers were dried (MgSO₄), filtered and concentrated *in vacuo*. The resulting oil was dissolved in anhydrous pyridine (0.12 mL, 1.5 mmol), then acetic anhydride (0.094 mL, 1.0 mmol) was then added to the solution. The reaction mixture was stirred at 80 °C for 3 h and concentrated *in vacuo*. The mixture was then diluted with water (2 mL), basified to pH 9–10 using an aqueous solution of ammonium hydroxide and extracted with ethyl acetate (3 \times 5 mL). The combined organic layers were dried (MgSO₄), filtered and concentrated *in vacuo*. The crude material was purified by flash column chromatography eluting with ethyl acetate in hexane (gradient 2:1 to 1:1) to give methyl (2*S*)-1-phenyl-2-acetylamino-2,3,4,9-tetrahydro-1*H*-pyrido[3,4-*b*]indole-3-carboxylate (**99a**) as a yellow oil (0.099 g, 57% over 2 steps). The resulting material was isolated as a mixture of diastereomers

(2:1). Signals for major diastereomer are recorded. $\nu_{\max}/\text{cm}^{-1}$ (neat) 3276 (NH), 1735 (C=O), 1639 (C=O), 1392, 1220, 743; $[\alpha]_{\text{D}}^{19} +169.1$ (c 0.1, CHCl_3); δ_{H} (400 MHz, CDCl_3) 2.30 (3H, s, 2-NAc), 2.95 (3H, s, OCH_3), 3.07 (1H, dd, J 15.8, 6.9 Hz, 4-*HH*), 3.67 (1H, br d, J 15.8 Hz, 4-*HH*), 4.84 (1H, d, J 6.9 Hz, 3-H), 7.06 (1H, s, 1-H), 7.10 (8H, m, 8 \times ArH), 7.59 (1H, d, J 7.8 Hz, 8-H), 7.95 (1H, br s, 9-H); δ_{C} (101 MHz, CDCl_3) 21.8 (CH_2), 22.5 (CH_3), 51.0 (CH), 51.9 (CH_3), 53.7 (CH), 107.6 (C), 111.0 (CH), 118.5 (CH), 119.7 (CH), 122.4 (CH), 126.5 (C), 127.9 (CH), 128.2 (2 \times CH), 129.4 (2 \times CH), 130.1 (C), 136.4 (C), 139.5 (C), 170.6 (C), 170.8 (C); m/z (ESI) 371.1365 (MNa^+ . $\text{C}_{21}\text{H}_{20}\text{N}_2\text{O}_3\text{Na}$ requires 371.1366).

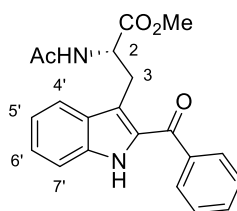
Methyl (2S)-1-(4'-cyanophenyl)-2-acetylamino-2,3,4,9-tetrahydro-1H-pyrido-[3,4-*b*]indole-3-carboxylate (99b)



4-Cyanobenzaldehyde (0.131 mL, 1.00 mmol) was added to the solution of methyl L-tryptophanate (**92**) (0.255 g, 1.00 mmol) in trifluoroacetic acid/water (10:1, v/v, 3.8 mL) under argon. The reaction mixture was stirred at room temperature for 18 h. The mixture was quenched with saturated aqueous sodium bicarbonate solution (5 mL) and extracted with ethyl acetate (3 \times 7 mL). The combined organic layers were dried (MgSO_4), filtered and concentrated *in vacuo*. The resulting oil was then dissolved in anhydrous pyridine (0.242 mL, 3 mmol) and acetic anhydride (0.190 mL, 2.00 mmol) was added to the solution. The reaction mixture was stirred at 80 °C for 4 h and concentrated *in vacuo*. The mixture was then diluted with water (6 mL), basified to pH 9–10 using an aqueous solution of ammonium hydroxide and extracted with chloroform₃ (3 \times 10 mL). The combined organic layers were dried (MgSO_4), filtered and concentrated *in vacuo*. The crude material was purified by flash column chromatography eluting with ethyl acetate in hexane (gradient 2:1 to 1:1) to give methyl (2S)-1-(4'-cyanophenyl)-2-acetylamino-2,3,4,9-tetrahydro-1H-pyrido[3,4-*b*]indole-3-carboxylate (**99b**) as a yellow oil (0.0810 g, 50% over 2 steps). The resulting material was isolated as a mixture of diastereomers (1.2:1). Signals

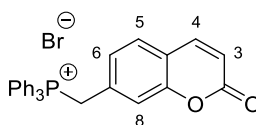
for major diastereomer are presented. $\nu_{\max}/\text{cm}^{-1}$ (neat) 3271 (NH), 2952 (CH), 2364 ($\text{C}\equiv\text{N}$), 1736 ($\text{C}=\text{O}$), 1645 ($\text{C}=\text{O}$), 1390, 1307, 1223, 1197, 741; $[\alpha]_{\text{D}}^{19} +28.8$ (c 0.1, CHCl_3); NMR spectra showed a 9:1 mixture of rotational isomers. Only data for the major rotational isomer is presented: δ_{H} (400 MHz, $\text{DMSO}-d_6$) 2.27 (3H, s, 2-NAc), 2.91 (3H, s, OCH_3), 3.07 (1H, dd, J 15.9, 6.7 Hz, 4-*HH*), 3.45 (1H, br d, J 15.9 Hz, 4-*HH*), 5.26 (1H, d, J 6.7 Hz, 3-H), 6.96 (1H, s, 1-H), 7.04 (1H, t, J 7.8 Hz, ArH), 7.12 (1H, t, J 7.8 Hz, ArH), 7.25 (2H, d, J 8.2 Hz, 2 \times ArH), 7.30 (1H, d, J 7.8 Hz, 5-H), 7.56 (1H, d, J 7.8 Hz, 8-H), 7.78 (2H, d, J 8.2 Hz, 2 \times ArH), 10.89 (1H, s, 9-H); δ_{C} (101 MHz, $\text{DMSO}-d_6$) 21.7 (CH_3), 22.7 (CH_2), 50.4 (CH), 51.9 (CH_3), 53.6 (CH), 107.4 (C), 110.7 (C), 111.8 (CH), 118.7 (CH), 119.2 (C), 119.2 (CH), 122.2 (CH), 126.4 (C), 129.6 (C), 130.1 (2 \times CH), 132.4 (2 \times CH), 136.9 (C), 146.0 (C), 171.2 (C), 171.4 (C); m/z (ESI) 372.1355 ($[\text{M}-\text{H}]^-$. $\text{C}_{22}\text{H}_{18}\text{N}_3\text{O}_3$ requires 372.1354).

Methyl (2*S*)-2-acetylamino-3-(2'-benzoyl-1'*H*-indol-3'-yl)propanoate (**100a**)¹⁸³



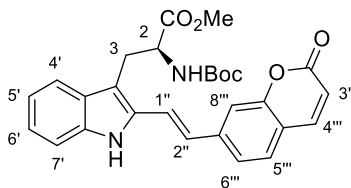
To a solution of methyl (2*S*)-1-phenyl-2-acetylamino-2,3,4,9-tetrahydro-1*H*-pyrido[3,4-*b*]indole-3-carboxylate (**99a**) (0.074 g, 0.21 mmol) in anhydrous dioxane (5 mL) under argon was added selenium oxide (0.071 g, 0.64 mmol). The reaction mixture was stirred under reflux for 1 h, then cooled to room temperature, filtered through Celite® and concentrated *in vacuo*. The crude material was purified by flash column chromatography eluting with 30% ethyl acetate in hexane to give methyl (2*S*)-2-acetylamino-3-(2'-benzoyl-1'*H*-indol-3'-yl)propanoate (**100a**) as a pale yellow solid (0.064 g, 83%). Spectroscopic data were consistent with the literature.¹⁸³ Mp 91–94 °C; $[\alpha]_{\text{D}}^{16} +27.6$ (c 0.1, CHCl_3). δ_{H} (400 MHz, CDCl_3) 1.86 (3H, s, NHAc), 3.49 (2H, dd, J 6.2, 4.9 Hz, 3- CH_2), 3.64 (3H, s, OCH_3), 4.67 (1H, ddd, J 8.2, 6.2, 4.9 Hz, 2-H), 7.19 (1H, ddd, J 8.0, 4.5, 3.5 Hz, ArH), 7.35 (2H, m, 2 \times ArH), 7.51 (2H, t, J 7.6 Hz, 2 \times ArH), 7.60 (1H, t, J 7.6 Hz, ArH), 7.69 (1H, d, J 6.2 Hz, 2-NH), 7.74 (1H, d, J 8.0 Hz, ArH), 7.78–7.84 (2H, m, 2 \times ArH), 9.01 (1H, s, 1'-H); δ_{C} (101 MHz, CDCl_3) 22.9 (CH_3), 26.8 (CH_2), 52.4 (CH_3), 54.3 (CH), 112.5 (CH), 119.8 (C), 120.7 (CH), 121.1 (CH), 126.6 (CH), 127.7 (C), 128.8 (2 \times CH), 129.6 (2 \times CH), 132.0 (C),

(2-Oxo-2H-chromen-7-yl)methyltriphenylphosphonium bromide (103)¹⁸⁶



7-Methylcoumarin (**101**) (0.33 g, 2.1 mmol), benzoyl peroxide (0.030 g, 0.18 mmol) and *N*-bromosuccinimide (0.45 g, 2.5 mmol) were dissolved in anhydrous 1,2-dichloroethane (7.5 mL) under argon. The reaction mixture was degassed for 0.15 h and then heated under reflux for 18 h in the dark. After cooling to room temperature and stirring the mixture for 0.5 h, the white precipitate formed was filtered off. The resulted solution was concentrated *in vacuo* and recrystallised from ethanol. The resulting 7-(bromomethyl)coumarin (**102**) was obtained as a pale yellow oil and was used without further purification. In an oven-dried microwave vial under argon, 7-(bromomethyl)coumarin (**102**) (0.23 g, 0.96 mmol) and triphenylphosphine (0.38 g, 1.4 mmol) were suspended in anhydrous toluene (7 mL). The reaction mixture was heated under reflux for 18 h. After cooling to the room temperature, the reaction mixture was diluted with dichloromethane, and the white precipitate was filtered off. The resulted solution was poured into hot ether, and the white precipitate was filtered off again and combined with the previous material. The combined solids were washed with cold dichloromethane and dried *in vacuo*. This gave (2-oxo-2H-chromen-7-yl)methyltriphenylphosphonium bromide (**103**) as a white solid (0.37 g, 36% over 2 steps). Spectroscopic data were consistent with the literature.¹⁸⁶ δ_{H} (400 MHz, CDCl_3) 5.76 (2H, d, $^2J_{\text{PH}}$ 15.3 Hz, CH_2P), 6.31 (1H, d, J 9.6 Hz, 3-H), 6.80 (1H, t, $^4J_{\text{PH}}$ 1.8 Hz, 8-H), 7.29 (1H, d, J 8.0 Hz, 5-H), 7.45 (1H, dt, J 8.0, 1.8 Hz, 6-H), 7.59–7.69 (7H, m, 4-H and 6 \times ArH), 7.72–7.88 (9H, m, 9 \times ArH); δ_{C} (101 MHz, CDCl_3) 30.3 (d, $^1J_{\text{CP}}$ 46.9 Hz, CH_2), 116.9 (d, $^6J_{\text{CP}}$ 1.8 Hz, CH), 117.4 (d, $^1J_{\text{CP}}$ 86.0 Hz, 3 \times C), 118.4 (d, $^4J_{\text{CP}}$ 3.6 Hz, C), 118.8 (d, $^3J_{\text{CP}}$ 5.7 Hz, CH), 128.3 (d, $^4J_{\text{CP}}$ 3.2 Hz, CH), 128.7 (d, $^3J_{\text{CP}}$ 5.5 Hz, CH), 130.2 (d, $^2J_{\text{CP}}$ 12.7 Hz, 6 \times CH), 132.3 (d, $^2J_{\text{CP}}$ 8.9 Hz, C), 134.5 (d, $^3J_{\text{CP}}$ 10.0 Hz, 6 \times CH), 135.2 (d, $^4J_{\text{CP}}$ 3.1 Hz, 3 \times CH), 143.2 (CH), 153.2 (d, $^5J_{\text{CP}}$ 3.6 Hz, C), 160.3 (C); m/z (ESI) 421 (M^+ , 100%).

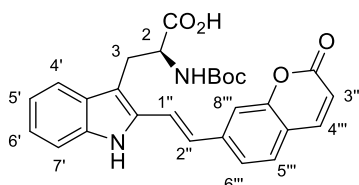
Methyl (2S)-2-[(*tert*-butoxycarbonyl)amino]-3-(2'-[(1''*E*)-2''-(2'''-oxo-2'''*H*-chromen-7'''-yl)ethenyl]-1'*H*-indol-3'-yl)propanoate (105)



Methyl (2S)-2-[(*tert*-butoxycarbonyl)amino]-3-(2'-formyl-1'*H*-indol-3'-yl)propanoate (**95**) (0.064 g, 0.19 mmol), (2-oxo-2*H*-chromen-7-yl)methyltriphenylphosphonium bromide (**103**) (0.12 g, 0.24 mmol), potassium carbonate (0.052 mg, 0.38 mmol) and 18-crown-6 (0.010 g, 0.038 mmol) were dissolved in anhydrous DMF (2 mL). After stirring for 18 h, the reaction mixture was diluted with water (5 mL) and extracted with ethyl acetate (3 × 10 mL). The combined organic layers were washed with a 5% aqueous solution of lithium chloride (7 mL), dried (MgSO₄), filtered and concentrated *in vacuo*. The resulting methyl (2S)-2-[(*tert*-butoxycarbonyl)amino]-3-(2'-[2''-(2'''-oxo-2'''*H*-chromen-7'''-yl)ethenyl]-1'*H*-indol-3'-yl)propanoate (**104**) was obtained a mixture of *Z/E*-isomers (1:1.5) and was used without further purification. Methyl (2S)-2-[(*tert*-butoxycarbonyl)amino]-3-(2'-[2''-(2'''-oxo-2'''*H*-chromen-7'''-yl)ethenyl]-1'*H*-indol-3'-yl)propanoate (**104**) (0.092 g, 0.19 mmol) was dissolved in acetonitrile and iodine (0.010 g) was then added. After stirring for 0.3 h at room temperature, the reaction mixture was concentrated *in vacuo*. The crude material was purified by flash column chromatography eluting with a 50% of ethyl acetate in hexane to give methyl (2S)-2-[(*tert*-butoxycarbonyl)amino]-3-(2'-[(1''*E*)-2''-(2'''-oxo-2'''*H*-chromen-7'''-yl)ethenyl]-1'*H*-indol-3'-yl)propanoate (**105**) as a bright yellow solid (0.074 g, 82%). Mp 199–200 °C; $\nu_{\text{max}}/\text{cm}^{-1}$ (neat) 3343 (NH), 2945 (CH), 1718 (C=O), 1688 (C=O), 1603, 1519, 1248, 1160, 1126, 830; $[\alpha]_{\text{D}}^{19} +72.6$ (c 0.1, CHCl₃); δ_{H} (400 MHz, CDCl₃) 1.40 (9H, s, C(CH₃)₃), 3.40 (1H, dd, *J* 14.4, 6.4 Hz, 3-*HH*), 3.46 (1H, dd, *J* 14.4, 4.4 Hz, 3-*HH*), 3.57 (3H, s, OCH₃), 4.65–4.74 (1H, m, 2-H), 5.16 (1H, d, *J* 7.8 Hz, 2-NH), 6.40 (1H, d, *J* 9.3 Hz, 3'''-H), 6.92 (1H, d, *J* 16.3 Hz, 2''-H), 7.10 (1H, t, *J* 7.6 Hz, ArH), 7.23 (1H, t, *J* 7.6 Hz, ArH), 7.34 (1H, d, *J* 8.0 Hz, ArH), 7.34 (1H, d, *J* 16.3 Hz, 1''-H), 7.43 (1H, s, 8'''-H), 7.46 (1H, d, *J* 8.0 Hz, ArH), 7.50–7.56 (2H, m, 2 × ArH), 7.70 (1H, d, *J* 9.3 Hz, 4'''-H), 8.52 (1H, s, 1'-H); δ_{C} (101 MHz, CDCl₃) 27.6 (CH₂), 28.3 (3 × CH₃), 52.4 (CH₃), 54.6 (CH), 80.0 (C), 110.9 (CH), 112.7 (C), 114.7 (CH), 115.8 (CH), 118.0 (C), 119.3 (CH), 119.8 (CH), 120.1 (CH),

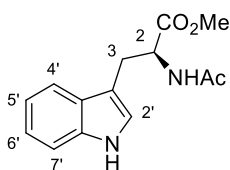
121.6 (CH), 124.0 (CH), 124.7 (CH), 128.1 (CH), 129.0 (C), 133.2 (C), 136.9 (C), 141.3 (C), 143.2 (CH), 154.6 (C), 155.1 (C), 161.1 (C), 172.4 (C); m/z (ESI) 487.1873 ($[M-H]^-$). $C_{28}H_{27}N_2O_6$ requires 487.1875).

(2S)-2-[(*tert*-Butoxycarbonyl)amino]-3-(2'-[(1''*E*)-2''-(2'''-oxo-2'''*H*-chromen-7'''-yl)ethenyl]-1'*H*-indol-3'-yl)propionic acid (106**)**



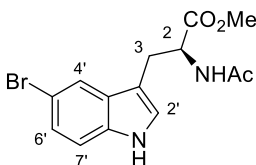
Methyl (2S)-2-[(*tert*-butoxycarbonyl)amino]-3-(2'-[(1''*E*)-2''-(2'''-oxo-2'''*H*-chromen-7'''-yl)ethenyl]-1'*H*-indol-3'-yl)propanoate (**105**) (0.040 g, 0.082 mmol) and caesium carbonate (0.035 g, 0.11 mmol) were dissolved in a mixture of dioxane (2 mL), water (1 mL) and methanol (0.8 mL). After stirring for 24 h at 60 °C, an additional portion of caesium carbonate (0.0080 g, 0.025 mmol) in water (0.4 mL) was added and the mixture was stirred for another 18 h. The reaction mixture was concentrated *in vacuo*, diluted with water (10 mL) and adjusted to pH 1 with an aqueous solution of 1 M hydrochloric acid, then extracted with ethyl acetate (3 × 10 mL). The combined organic layers were dried (MgSO₄), filtered and concentrated *in vacuo*. The resulting (2S)-2-[(*tert*-butoxycarbonyl)amino]-3-(2'-[(1''*E*)-2''-(2'''-oxo-2'''*H*-chromen-7'''-yl)ethenyl]-1'*H*-indol-3'-yl)propionic acid (**106**) was obtained as a yellow solid (0.036 g, 92%). Mp 263–265 °C; $\nu_{\max}/\text{cm}^{-1}$ (neat) 3362 (NH), 2923 (CH), 1701 (C=O), 1697 (C=O), 1601, 1156, 1126, 832; $[\alpha]_D^{19}$ +90.1 (*c* 0.1, MeOH); δ_H (400 MHz, CD₃OD) 1.21 (9H, s, C(CH₃)₃), 3.15 (1H, dd, *J* 14.4, 9.2 Hz, 3-*HH*), 3.26–3.37 (1H, m, 3-*HH*), 4.13 (1H, td, *J* 9.2, 4.0 Hz, 2-*H*), 6.44 (1H, d, *J* 9.5 Hz, 3'''-*H*), 7.01 (1H, t, *J* 8.0 Hz, ArH), 7.12–7.18 (2H, m, 2 × ArH), 7.18 (1H, d, *J* 16.4 Hz, 2''-*H*), 7.33 (1H, d, *J* 8.0 Hz, ArH), 7.52–7.58 (2H, m, 2 × ArH), 7.63 (1H, d, *J* 16.4 Hz, 1''-*H*), 7.69–7.74 (2H, m, 2 × ArH), 8.05 (1H, d, *J* 9.5 Hz, 4'''-*H*), 11.28 (1H, s, 1'-*H*); δ_C (101 MHz, CD₃OD) 26.2 (CH₂), 28.0 (3 × CH₃), 54.9 (CH), 77.9 (C), 111.0 (CH), 112.7 (CH), 113.7 (C), 115.1 (CH), 117.8 (C), 118.5 (CH), 119.0 (CH), 121.0 (CH), 123.0 (CH), 123.0 (CH), 124.7 (CH), 128.1 (C), 128.7 (CH), 133.7 (C), 137.1 (C), 141.5 (C), 144.0 (CH), 154.2 (C), 155.4 (C), 160.2 (C), 173.8 (C); m/z (ESI) 473.1709 ($[M-H]^-$). $C_{27}H_{26}N_2O_6$ requires 473.1718).

(2S)-N-Acetyltryptophan methyl ester (107)¹⁹²



Methyl L-tryptophanate hydrochloride (**92**) (0.255 mg, 1.00 mmol) was suspended in anhydrous tetrahydrofuran (10 mL) under argon and cooled to 0 °C. Triethylamine (0.104 mL, 1.10 mmol) was added dropwise followed by acetic anhydride (0.146 mL, 1.05 mmol). The mixture was heated to 80 °C and stirred for 2 h. The reaction mixture was quenched with water (30 mL) and extracted with ethyl acetate (3 × 30 mL). The combined organic layers were washed with 1 M hydrochloric acid solution (6 mL), saturated aqueous sodium bicarbonate solution (6 mL) and brine (6 mL). The organic layer was dried (MgSO₄), filtered and concentrated *in vacuo* to give (2S)-N-acetyltryptophan methyl ester (**107**) as a white solid (0.237 g, 91%). Spectroscopic data were consistent with the literature.¹⁹² [α]_D¹⁷ +83.4 (c 0.1, CHCl₃); δ_H (400 MHz, CDCl₃) 1.96 (3H, s, NHAc), 3.30 (1H, dd, *J* 14.7, 5.3 Hz, 3-*HH*), 3.36 (1H, dd, *J* 14.7, 5.5 Hz, 3-*HH*), 3.70 (3H, s, OCH₃), 4.96 (1H, ddd, *J* 7.5, 5.5, 5.3 Hz, 2-H), 6.01 (1H, d, *J* 7.5 Hz, 2-NH), 6.97 (1H, d, *J* 2.5 Hz, 2'-H), 7.12 (1H, t, *J* 7.8 Hz, ArH), 7.20 (1H, t, *J* 7.8 Hz, ArH), 7.36 (1H, d, *J* 7.8 Hz, ArH), 7.53 (1H, d, *J* 7.8 Hz, ArH), 8.22 (1H, br s, 1'-H); δ_C (101 MHz, CDCl₃) 23.3 (CH₃), 27.6 (CH₂), 52.4 (CH₃), 53.1 (CH), 110.1 (C), 111.3 (CH), 118.5 (CH), 119.7 (CH), 122.3 (CH), 122.7 (CH), 127.8 (C), 136.1 (C), 169.7 (C), 172.4 (C); *m/z* (ESI) 261 (MH⁺, 100%).

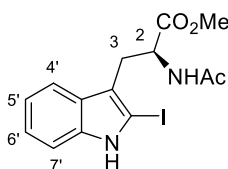
(2S)-N-Acetyl-5'-bromotryptophan methyl ester (112)²⁰⁴



(2S)-N-Acetyltryptophan methyl ester (**92**) (0.100 mg, 0.314 mmol) was dissolved in anhydrous 1,2-dichloroethane (3 mL) under argon. N-Bromosuccinimide (0.0890 g, 0.408 mmol) and benzoyl peroxide (0.00400 g, 0.0160 mmol) were then added to the solution. The mixture was stirred at 40 °C for 2 h. The reaction mixture was

concentrated *in vacuo*. The crude material was purified by flash chromatography eluting with 33% ethyl acetate in hexane to give (2*S*)-*N*-acetyl-2'-bromotryptophan methyl ester (**112**) as a yellow oil (0.0370 g, 30%). Spectroscopic data were consistent with the literature.²⁰⁴ $[\alpha]_D^{17} +76.5$ (*c* 0.1, CHCl₃); δ_H (400 MHz, CDCl₃) 2.00 (3H, s, NHAc), 3.25 (1H, dd, *J* 14.8, 5.0 Hz, 3-*HH*), 3.31 (1H, dd, *J* 14.8, 5.3 Hz, 3-*HH*), 3.72 (3H, s, OCH₃), 4.94 (1H, ddd, *J* 7.7, 5.3, 5.0 Hz, 2-H), 6.04 (1H, d, *J* 7.7 Hz, 2-NH), 6.98 (1H, d, *J* 2.0 Hz, 2'-H), 7.22 (1H, d, *J* 8.5 Hz, 7'-H), 7.26 (1H, dd, *J* 8.5, 1.5 Hz, 6'-H), 7.63 (1H, m, 4'-H), 8.29 (1H, br s, 1'-H); δ_C (101 MHz, CDCl₃) 23.3 (CH₃), 27.6 (CH₂), 52.5 (CH₃), 53.0 (CH), 109.9 (C), 112.8 (CH), 113.0 (C), 121.4 (CH), 124.0 (CH), 125.1 (CH), 129.5 (C), 134.7 (C), 169.8 (C), 172.3 (C); *m/z* (ESI) 339 (MH⁺, 100%).

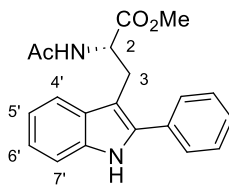
(2*S*)-*N*-Acetyl-2'-iodotryptophan methyl ester (**114**)



(2*S*)-*N*-Acetyltryptophan methyl ester (**107**) (0.125 g, 0.480 mmol) was dissolved in a mixture of dichloromethane (15 mL) and trifluoroacetic acid (1.5 mL). *N*-Iodosuccinimide (0.225 g, 1.00 mmol) was then added to the solution in the dark. The mixture was stirred at room temperature for 0.5 h, and then another portion of *N*-iodosuccinimide was added (0.0900 g, 0.400 mmol) and the reaction was stirred for another 0.5 h. The reaction mixture was concentrated *in vacuo* at room temperature. The crude material was purified by flash chromatography eluting with 25% of ethyl acetate in dichloroethane to give (2*S*)-*N*-acetyl-2'-iodotryptophan methyl ester (**114**) as a white solid (0.102 g, 55%). Mp 52–55 °C. $\nu_{\max}/\text{cm}^{-1}$ (neat) 3259 (NH), 2949 (CH), 1731 (C=O), 1649 (C=O), 1520, 1433, 1338, 1211, 741; $[\alpha]_D^{18} +28.6$ (*c* 0.1, CHCl₃); δ_H (400 MHz, CDCl₃) 1.97 (3H, s, NHAc), 3.22 (1H, dd, *J* 14.7, 5.6 Hz, 3-*HH*), 3.26 (1H, dd, *J* 14.7, 6.0 Hz, 3-*HH*), 3.70 (3H, s, OCH₃), 4.94 (1H, ddd, *J* 8.1, 6.0, 5.6 Hz, 2-H), 6.06 (1H, d, *J* 8.1 Hz, 2-NH), 7.05–7.15 (2H, m, 2 × ArH), 7.28 (1H, d, *J* 7.8 Hz, 4'-H), 7.49 (1H, d, *J* 7.8 Hz, 7'-H), 8.44 (1H, br s, 1'-H); δ_C (101 MHz, CDCl₃) 23.4 (CH₃), 29.5 (CH₂), 52.5 (CH₃), 52.7 (CH), 79.4 (C),

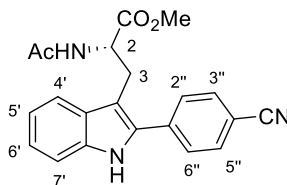
110.6 (CH), 116.5 (C), 117.8 (CH), 120.1 (CH), 122.6 (CH), 127.7 (C), 138.9 (C), 169.8 (C), 172.3 (C); *m/z* (ESI) 409.0026 (MNa⁺. C₁₄H₁₅N₂O₃Na requires 409.0020).

Methyl (2S)-2-acetylamino-3-(2'-phenyl-1'H-indol-3'-yl)propanoate (108a)¹⁹²



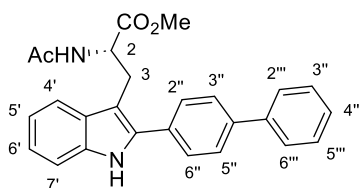
A solution of (2S)-*N*-acetyl-2'-iodotryptophan methyl ester (**114**) (0.050 g, 0.13 mmol), phenyl boronic acid (0.024 g, 0.19 mmol) and potassium phosphate (0.055 g, 0.26 mmol) in tetrahydrofuran/water (1:1, 4 mL) in a microwave vial was degassed under argon for 0.1 h. To this was added XPhos Pd G2 (0.0020 g, 0.0026 mmol), the vial was sealed, and the reaction mixture was stirred at 60 °C for 3 h. After cooling to room temperature, the reaction mixture was concentrated *in vacuo* and diluted with water (5 mL). The mixture was extracted with ethyl acetate (3 × 10 mL). The combined organic layers were dried (MgSO₄), filtered and concentrated *in vacuo*. The crude material was purified by flash column chromatography eluting with 50% ethyl acetate in hexane to give methyl (2S)-2-acetylamino-3-(2'-phenyl-1'*H*-indol-3'-yl)propanoate (**108a**) as a white solid (0.029 g, 66%). Spectroscopic data were consistent with the literature.¹⁹² [α]_D¹⁹ +65.7 (c 0.11, CHCl₃); δ_{H} (400 MHz, CDCl₃) 1.66 (3H, s, NHAc), 3.30 (3H, s, OCH₃), 3.53 (1H, dd, *J* 14.8, 5.2 Hz, 3-*HH*), 3.57 (1H, dd, *J* 14.8, 5.5 Hz, 3-*HH*), 4.84 (1H, ddd, *J* 8.1, 5.5, 5.2 Hz, 2-H), 5.78 (1H, d, *J* 8.1 Hz, 2-NH), 7.14 (1H, t, *J* 7.8 Hz, 6'-H), 7.20 (1H, t, *J* 7.8 Hz, 5'-H), 7.31–7.41 (2H, m, 2 × ArH), 7.47 (2H, t, *J* 7.6 Hz, 2 × ArH), 7.54–7.60 (3H, m, 3 × ArH), 8.25 (1H, br s, 1'-H); δ_{C} (101 MHz, CDCl₃) 22.9 (CH₃), 26.6 (CH₂), 52.0 (CH₃), 52.8 (CH), 106.8 (C), 110.9 (CH), 118.9 (CH), 120.0 (CH), 122.6 (CH), 128.1 (CH), 128.3 (2 × CH), 129.2 (2 × CH), 129.5 (C), 133.2 (C), 135.7 (C), 136.0 (C), 169.6 (C), 172.2 (C); *m/z* (ESI) 359 (MNa⁺. 100%).

Methyl (2S)-2-acetylamino-3-(2'-[4''-cyanophenyl]-1'H-indol-3'-yl)propanoate (108f)



The reaction was carried out according to the previously described procedure for methyl (2S)-2-acetylamino-3-(2'-phenyl-1'H-indol-3'-yl)propanoate (**108a**) using methyl (2S)-*N*-acetyl-2'-iodotryptophan methyl ester (**114**) (0.12 g, 0.30 mmol), 4-cyanophenyl boronic acid (0.066 g, 0.45 mmol), potassium phosphate (0.13 g, 0.60 mmol) and XPhos Pd G2 (0.0050 g, 0.0064 mmol). The reaction mixture was heated at 60 °C for 1.25 h. Another portion of XPhos Pd G2 (0.0020 g, 0.0025 mmol) was added, and the reaction mixture was left stirring at 60 °C for 2 h. After cooling to room temperature, the reaction mixture was concentrated *in vacuo* and diluted with water (10 mL). The mixture was extracted with ethyl acetate (3 × 10 mL). The combined organic layers were dried (MgSO₄), filtered and concentrated *in vacuo*. The crude material was purified by flash column chromatography eluting with 50% ethyl acetate in hexane followed by 33% hexane and 17% of dichloromethane in ethyl acetate to give methyl (2S)-2-acetylamino-3-(2'-[4''-cyanophenyl]-1'H-indol-3'-yl)propanoate (**108f**) as a white solid (0.071 g, 65%). Mp 196–201 °C; $\nu_{\text{max}}/\text{cm}^{-1}$ (neat) 3285 (NH), 2951 (CH), 2224 (C≡N), 1735 (C=O), 1650 (C=O), 1604, 1526, 1215, 840, 744; $[\alpha]_{\text{D}}^{19}$ +49.5 (c 0.1, CHCl₃). NMR spectra showed a 9:1 mixture of rotational isomers. Only data for the major rotational isomer is presented: δ_{H} (400 MHz, CDCl₃) 1.73 (3H, s, NHAc), 3.36 (3H, s, OCH₃), 3.51 (1H, dd, *J* 14.7, 5.3 Hz, 3-*HH*), 3.55 (1H, dd, *J* 14.7, 6.1 Hz, 3-*HH*), 4.86 (1H, ddd, *J* 7.9, 6.1, 5.3 Hz, 2-H), 5.88 (1H, d, *J* 7.9 Hz, 2-NH), 7.17 (1H, t, *J* 7.8 Hz, 6'-H), 7.25 (1H, t, *J* 7.8 Hz, 5'-H), 7.38 (1H, d, *J* 7.8 Hz, 4'-H), 7.60 (1H, d, *J* 7.8 Hz, 7'-H), 7.71 (2H, d, *J* 8.6 Hz, 2 × ArH), 7.76 (2H, d, *J* 8.6 Hz, 2 × ArH), 8.25 (1H, br s, 1'-H); δ_{C} (101 MHz, CDCl₃) 23.0 (CH₃), 27.2 (CH₂), 52.2 (CH₃), 52.9 (CH), 109.2 (C), 111.3 (CH and C), 118.5 (C), 119.3 (CH), 120.5 (CH), 123.7 (CH), 128.5 (2 × CH), 129.4 (C), 132.8 (2 × CH), 133.5 (C), 136.2 (C), 137.6 (C), 169.5 (C), 172.1 (C); *m/z* (ESI) 362.1500 (MH⁺. C₂₁H₂₀N₃O₃ requires 362.1499).

Methyl (2S)-2-acetylamino-3-(2'-[biphen-4''-yl]-1'H-indol-3'-yl)propanoate (108j)



The reaction was carried out according to the previously described procedure for methyl (2S)-2-acetylamino-3-(2'-phenyl-1'H-indol-3'-yl)propanoate (**108a**) using methyl (2S)-*N*-acetyl-2'-iodotryptophan methyl ester (**114**) (0.050 g, 0.13 mmol), 4-biphenyl boronic acid (0.066 g, 0.45 mmol), potassium phosphate (0.038 g, 0.19 mmol), tetrahydrofuran/water (1:1, 4 mL) and XPhos Pd G2 (0.0020 g, 0.0026 mmol). The reaction mixture was heated at 60 °C for 2 h. After cooling to room temperature, the reaction mixture was concentrated *in vacuo* and diluted with water (5 mL). The mixture was extracted with ethyl acetate (3 × 10 mL). The combined organic layers were dried (MgSO₄), filtered and concentrated *in vacuo*. The crude material was purified by flash column chromatography eluting with 50% ethyl acetate in hexane to give methyl (2S)-2-acetylamino-3-(2'-[biphen-4''-yl]-1'H-indol-3'-yl)propanoate (**108j**) as a white solid (0.038 g, 64%). Mp 200–202 °C; $\nu_{\text{max}}/\text{cm}^{-1}$ (neat) 3248 (NH), 2952 (CH), 1734 (C=O), 1654 (C=O), 1435, 1213, 843, 743; $[\alpha]_{\text{D}}^{17} +43.3$ (c 0.1, CHCl₃); δ_{H} (400 MHz, CDCl₃) 1.67 (3H, s, NHAc), 3.32 (3H, s, OCH₃), 3.58 (1H, dd, *J* 14.9, 5.2 Hz, 3-*HH*), 3.62 (1H, dd, *J* 14.9, 5.6 Hz, 3-*HH*), 4.88 (1H, ddd, *J* 8.0, 5.6, 5.3 Hz, 2-H), 5.81 (1H, d, *J* 8.0 Hz, 2-NH), 7.16 (1H, t, *J* 7.8 Hz, 6'-H), 7.22 (1H, t, *J* 7.8 Hz, 5'-H), 7.36–7.42 (2H, m, 2 × ArH), 7.45–7.51 (2H, m, 2 × ArH), 7.60 (2H, d, *J* 7.8 Hz, 7'-H), 7.61–7.68 (4H, m, 4 × ArH), 7.73 (2H, d, *J* 8.2 Hz, 2 × ArH), 8.19 (1H, br s, 1'-H); δ_{C} (101 MHz, CDCl₃) 23.4 (CH₃), 27.2 (CH₂), 52.5 (CH₃), 53.3 (CH), 107.6 (C), 111.4 (CH), 119.4 (CH), 120.6 (CH), 123.1 (CH), 127.4 (2 × CH), 128.2 (3 × CH), 129.0 (2 × CH), 129.4 (2 × CH), 130.0 (C), 132.5 (C), 136.0 (C), 136.2 (C), 140.6 (C), 141.3 (C), 170.0 (C), 172.6 (C); *m/z* (ESI) 435.1678 (MNa⁺. C₂₆H₂₄N₂O₃Na requires 435.1679).

Absorption and fluorescence data acquisition and fluorescence quantum yield calculations

Standard 10 mm path length fluorescence cuvettes were used for the measurements. Both UV-Vis absorbance and fluorescence spectra were recorded on a Horiba Duetta Fluorescence and Absorbance spectrometer. The following parameters were used: an integration time of 0.05 s and a band pass of 5 nm for absorbance spectra; band pass of 5 nm, an integration time of 0.25 s, and with detector accumulations set to 3 for fluorescence spectra. Measurements were performed at a minimum of five different concentrations, and the concentrations were chosen to ensure the absorption value was below 0.1 to avoid re-absorption effects. The corresponding standard samples were recorded using the same parameters. The integrated fluorescence intensity of each compound was determined from the fluorescence emission spectra obtained. The integrated fluorescence intensity was plotted against the measured absorbance and a gradient of the graph was calculated. Quantum yields were determined using a comparative method against standard samples with known quantum yield values: anthracene ($\Phi_F = 0.27$ in ethanol), L-tryptophan ($\Phi_F = 0.14$ in water) and 9,10-diphenylanthracene ($\Phi_F = 0.90$ in cyclohexane) according to the following equation:

$$\Phi_X = \Phi_{ST} \left(\frac{\text{Grad}_X}{\text{Grad}_{ST}} \right) \left(\frac{\eta_X^2}{\eta_{ST}^2} \right)$$

where subscripts ST and X stand for standard and sample respectively, Φ is the quantum yield; Grad is the gradient of the graph of integrated fluorescence intensity vs absorbance; η is the refractive index of the solvent ($\eta = 1.330$ for water, 1.361 for ethanol, 1.328 for methanol, 1.4793 for dimethyl sulfoxide, 1.407 for tetrahydrofuran).

Liposome and liposome sample preparation

Liposomes were prepared following a previously reported method.²⁰⁵ L- α -Phosphatidylcholine (egg yolk) (75 mg) and cholesterol (11 mg) (7:1 PC:cholesterol) were dissolved in chloroform (15 mL). The solution was concentrated *in vacuo* to form a thin film on the inner wall of the flask. Next, 10 mL of 10 mM sodium phosphate buffer (PBS pH 7.4) was added, and the flask was swirled in a water bath

at 37 °C for 10 minutes to form a suspension. The suspension was kept at 25 °C for 2 hours, sonicated for 3 minutes, and then kept at 25 °C for additional 2 hours. It was then centrifuged at 4000 rcf for 0.5 h and the resulting pellet was resuspended in 10 mM PBS (10 mL) to give a 7.5 mg/mL PC liposome concentration. The liposomes were stored in the fridge and brought to room temperature before use.

For photophysical studies, the liposome solution was diluted to the desired concentration in potassium phosphate buffer (pH 7.4). Sample solutions (5 μ M) were prepared by addition of the compound of interest in methanol (0.2 mg/mL) to the liposome solution. The resulting sample solutions were inverted several times, prior to absorption and emission spectra recording.

4. References

- 1 W. C. Röntgen, *J. Franklin Inst.*, 1896, **141**, 183–191.
- 2 D. L. Bailey, D. W. Townsend, Maisey, P. E. Valk and M. N, *Positron Emission Tomography: Basic Sciences*, Springer, 2005.
- 3 T. Jones and P. Price, *Lancet Oncol.*, 2012, **13**, 116–125.
- 4 V. Burianova, S. Kalinin, C. T. Supuran and M. Krasavin, *Eur. J. Med. Chem.*, 2021, **213**, 113046.
- 5 I. Mohammadi, F. Castro, A. Rahmim and J. Veloso, *Phys. Med. Biol.*, 2022, **67**, 02TR02.
- 6 M. Cerqueira and A. Jacobson, *Am. J. Roentgenol.*, 1989, **153**, 477–483.
- 7 J. S. Duncan and K. Trimmel, *Curr. Opin. Neurol.*, 2022, **35**, 189–195.
- 8 R. Ganai, S. Mehta, M. Shiroya, M. Mondal, Z. Ahammed and S. Chattopadhyay, in *XXII DAE High Energy Physics Symposium*, 2018, pp. 125–128.
- 9 J. Lau, E. Rousseau, D. Kwon, K.-S. Lin, F. Bénard and X. Chen, *Cancers (Basel)*, 2020, **12**, 1312.
- 10 J. Wenz, F. Arndt and S. Samnick, *EJNMMI Radiopharm. Chem.*, 2022, **7**, 1–14.
- 11 W. Wadsak and M. Mitterhauser, *Eur. J. Radiol.*, 2010, **73**, 461–469.
- 12 Division of Imaging and Radiation Medicine (DIRM), 2023. *FDA Briefing Document—PET Diagnostic Radiopharmaceutical Drugs*. Available at: <https://www.fda.gov/media/170658/download> (Accessed: 20/03/2025)
- 13 M. J. Niaz, M. Sun, M. Skafida, M. O. Niaz, J. Ivanidze, J. R. Osborne and E. O'Dwyer, *Clin. Imaging*, 2021, **79**, 278–288.
- 14 G. Treglia, B. Muoio, G. Trevisi, M. V. Mattoli, D. Albano, F. Bertagna and L. Giovanella, *Int. J. Mol. Sci.*, 2019, **20**, 4669.
- 15 C. Beadsmoore, D. Newman, D. MacIver and D. Pawaroo, *Can. Assoc. Radiol. J.*, 2015, **66**, 332–347.
- 16 J. Sorensen, in *Nuclear Medicine and Molecular Imaging*, Elsevier, 2022, pp. 200–209.
- 17 R. Wilcken, M. O. Zimmermann, A. Lange, A. C. Joerger and F. M. Boeckler, *J. Med. Chem.*, 2013, **56**, 1363–1388.
- 18 C. M. Le, *Nat. Chem.*, 2022, **14**, 476.
- 19 K. Kaseda, *Diagnostics*, 2020, **10**, 561.

- 20 R. H. J. A. Slart, R. H. J. A. Slart, A. W. J. M. Glaudemans, P. Chareonthaitawee, G. Treglia, F. L. Besson, T. A. Bley, D. Blockmans, R. Boellaard, J. Bucerius, J. M. Carril, W. Chen, M. C. Cid, B. Dagupta, S. Dorbala, O. Gheysens, F. Hyafil, S. Jain, T. Klink, C. J. van der Laken, F. Lomeña, M. Massollo, S. Prieto-González, R. Luqmani, A. Roivainen, C. Salvarani, A. Saraste, M. Schirmer, H. J. Verberne, A. Versari, A. E. Voskuyl, M. A. Walter, D. Camellino, E. Brouwer, M. A. Cimmino, A. Abidov, D. Agostini, R. S. Beanlands, R. C. Delgado-Bolton, A. J. Einstein, A. Gimelli, E. J. Miller, R. Sciagrà, A. Signore, R. H. J. A. Slart and G. Treglia, *Eur. J. Nucl. Med. Mol. Imaging*, 2018, **45**, 1250–1269.
- 21 E. Lotan, K. P. Friedman, T. Davidson and T. M. Shepherd, *Isr. Med. Assoc. J.*, 2020, **22**, 178–184.
- 22 S. Annunziata, R. C. Delgado Bolton, C. H. Kamani, J. O. Prior, D. Albano, F. Bertagna and G. Treglia, *Pharmaceuticals*, 2020, **13**, 1–11.
- 23 B. T. Kung, S. M. Seraj, M. Z. Zadeh, C. Rojulpote, E. Kothekar, C. Ayubcha, K. S. Ng, K. K. Ng, T. K. Au-Yong, T. J. Werner, H. Zhuang, S. J. Hunt, S. Hess and A. Alavi, *Am. J. Nucl. Med. Mol. Imaging*, 2019, **9**, 255–273.
- 24 J. P. Pijl, P. H. Nienhuis, T. C. Kwee, A. W. J. M. Glaudemans, R. H. J. A. Slart and L. C. Gormsen, *Semin. Nucl. Med.*, 2021, **51**, 633–645.
- 25 P. Brust, H. Rodig, J. Römer, H. Kasch, R. Bergmann, F. Füchtner, D. Zips, M. Baumann, J. Steinbach and B. Johannsen, *Appl. Radiat. Isot.*, 2002, **57**, 687–695.
- 26 J. Kwiecinski, *J. Nucl. Cardiol.*, 2024, **35**, 101845.
- 27 V. R. Bollineni, G. M. Kramer, E. P. Jansma, Y. Liu and W. J. G. Oyen, *Eur. J. Cancer*, 2016, **55**, 81–97.
- 28 L. R. Drake, A. T. Hillmer and Z. Cai, *Molecules*, 2020, **25**, 568.
- 29 A. F. Voter, R. A. Werner, K. J. Pienta, M. A. Gorin, M. G. Pomper, L. B. Solnes and S. P. Rowe, *Expert Rev. Anticancer Ther.*, 2022, **22**, 681–694.
- 30 R. Halder and T. Ritter, *J. Org. Chem.*, 2021, **86**, 13873–13884.
- 31 M. Failla, G. Floresta and V. Abbate, *RSC Med. Chem.*, 2023, **14**, 592–623.
- 32 E. A. Pérès, J. Toutain, L.-P. Paty, D. Divoux, M. Ibazizène, S. Guillouet, L. Barré, A. Vidal, M. Cherel, M. Bourgeois, M. Bernaudin and S. Valable, *EJNMMI Res.*, 2019, **9**, 114.
- 33 P. Mohr, J. van Sluis, M. N. Lub-de Hooge, A. A. Lammertsma, A. H. Brouwers and C. Tsoumpas, *Front. Nucl. Med.*, 2024, **4**, 1360710.

- 34 J.-K. Yoon, B.-N. Park, E.-K. Ryu, Y.-S. An and S.-J. Lee, *Int. J. Mol. Sci.*, 2020, **21**, 4309.
- 35 R. Rossi, S. Arjmand, S. L. Bærentzen, A. Gjedde and A. M. Landau, *Front. Neurosci.*, 2022, **16**, 864514.
- 36 S. J. Finnema, S. Li, Z. Cai, M. Naganawa, M.-K. Chen, D. Matuskey, N. Nabulsi, I. Esterlis, S. E. Holmes, R. Radhakrishnan, T. Toyonaga, Y. Huang and R. E. Carson, in *PET and SPECT of Neurobiological Systems*, Springer International Publishing, Cham, 2021, pp. 993–1019.
- 37 K. Heurling, N. J. Ashton, A. Leuzy, E. R. Zimmer, K. Blennow, H. Zetterberg, J. Eriksson, M. Lubberink and M. Schöll, *Mol. Cell. Neurosci.*, 2019, **97**, 34–42.
- 38 S. L. Martin, C. Uribe and A. P. Strafella, *J. Neurosci. Res.*, 2024, **102**, e25253.
- 39 M. E. Serrano, E. Kim, M. M. Petrinovic, F. Turkheimer and D. Cash, *Front. Neurosci.*, 2022, **16**, 796129.
- 40 H. Cai, T. J. Mangner, O. Muzik, M. W. Wang, D. C. Chugani and H. T. Chugani, *ACS Med. Chem. Lett.*, 2014, **5**, 1152–1155.
- 41 A. Johansen, V. Beliveau, E. Colliander, N. R. Raval, V. H. Dam, N. Gillings, S. Aznar, C. Svarer, P. Plavén-Sigraý and G. M. Knudsen, *J. Neurosci.*, 2024, **44**, e1750232024.
- 42 S. Li, Z. Cai, W. Zhang, D. Holden, S. fei Lin, S. J. Finnema, A. Shirali, J. Ropchan, S. Carre, J. Mercier, R. E. Carson, N. Nabulsi and Y. Huang, *Eur. J. Nucl. Med. Mol. Imaging*, 2019, **46**, 1952–1965.
- 43 C. C. Constantinescu, C. Tresse, M. Q. Zheng, A. Gouasmat, V. M. Carroll, L. Mistico, D. Alagille, C. M. Sandiego, C. Papin, K. Marek, J. P. Seibyl, G. D. Tamagnan and O. Barret, *Mol. Imaging Biol.*, 2019, **21**, 509–518.
- 44 M. Xiong, S. Roshanbin, D. Sehlin, H. D. Hansen, G. M. Knudsen, J. Rokka, J. Eriksson and S. Syvänen, *Neuroimage*, 2023, **277**, 120230.
- 45 K. B. Andersen, A. K. Hansen, K. Knudsen, A. C. Schacht, M. F. Damholdt, D. J. Brooks and P. Borghammer, *Nucl. Med. Biol.*, 2022, **112–113**, 52–58.
- 46 L. Michiels, A. Delva, J. van Aalst, J. Ceccarini, W. Vandenberghe, M. Vandenbulcke, M. Koole, R. Lemmens and K. Van Laere, *Neuroimage*, 2021, **232**, 117877.
- 47 Z. Cai, S. Li, W. Zhang, R. Pracitto, X. Wu, E. Baum, S. J. Finnema, D. Holden, T. Toyonaga, S. Lin, M. Lindemann, A. Shirali, D. C. Labaree, J. Ropchan, N. Nabulsi, R. E. Carson and Y. Huang, *ACS Chem. Neurosci.*, 2020, **11**, 592–603.

- 48 Z. Jiang, X. Cheng, H. Chen, W. Zheng, Y. Sun, Z. Yu, T. Yang, L. Zhang, D. Fan, Z. Yang, Y. Liu, L. Ai and Z. Wu, *ACS Med. Chem. Lett.*, 2022, **13**, 720–726.
- 49 S. Li, Z. Cai, X. Wu, D. Holden, R. Pracitto, M. Kapinos, H. Gao, D. Labaree, N. Nabulsi, R. E. Carson and Y. Huang, *ACS Chem. Neurosci.*, 2019, **10**, 1544–1554.
- 50 K. J. Makaravage, A. F. Brooks, A. V. Mossine, M. S. Sanford and P. J. H. Scott, *Org. Lett.*, 2016, **18**, 5440–5443.
- 51 M. Tredwell, S. M. Preshlock, N. J. Taylor, S. Gruber, M. Huiban, J. Passchier, J. Mercier, C. Génicot and V. Gouverneur, *Angew. Chem. Int. Ed.*, 2014, **53**, 7751–7755.
- 52 L. Chen, X. Li, Y. Ge, H. Li, R. Li, X. Song, J. Liang, W. Zhang, X. Li, X. Wang, Y. Wang, Y. Wu, Y. Bai and M. Wang, *EJNMMI Radiopharm. Chem.*, 2024, **9**, 66.
- 53 N. B. Nabulsi, J. Mercier, D. Holden, S. Carré, S. Najafzadeh, M.-C. Vandergeten, S. Lin, A. Deo, N. Price, M. Wood, T. Lara-Jaime, F. Montel, M. Laruelle, R. E. Carson, J. Hannestad and Y. Huang, *J. Nucl. Med.*, 2016, **57**, 777–784.
- 54 P. Chauhan and S. S. Chimni, *RSC Adv.*, 2012, **2**, 737–758.
- 55 Holly McErlain (2022) *The Development of Novel PET Imaging Agents for the Poly(ADP-Ribose) Polymerase 1 and Synaptic Vesicle 2A Proteins*. PhD thesis. University of Glasgow.
- 56 H. McErlain, E. B. McLean, T. E. F. Morgan, V. K. Burianova, A. A. S. Tavares and A. Sutherland, *J. Org. Chem.*, 2022, **87**, 14443–14451.
- 57 M. E. Morris and N. V. Kwatra, in *Drug Transporters*, Wiley, 2022, pp. 143–164.
- 58 M. A. Felmlee, R. S. Jones, V. Rodriguez-Cruz, K. E. Follman and M. E. Morris, *Pharm. Rev.*, 2020, **72**, 466–485.
- 59 T. D. Bannister, in *Encyclopedia of Cancer*, Elsevier, Third edit., 2018, vol. 2, pp. 266–278.
- 60 A. Silva, B. Antunes, A. Batista, F. Pinto-Ribeiro, F. Baltazar and J. Afonso, *Molecules*, 2021, **27**, 181.
- 61 S. J. Park, C. P. Smith, R. R. Wilbur, C. P. Cain, S. R. Kallu, S. Valasapalli, A. Sahoo, M. R. Guda, A. J. Tsung and K. K. Velpula, *Am. J. Cancer Res.*, 2018, **8**, 1967–1976.
- 62 M. Singh, J. Afonso, D. Sharma, R. Gupta, V. Kumar, R. Rani, F. Baltazar and V. Kumar, *Semin. Cancer Biol.*, 2023, **90**, 1–14.

- 63 F. Lauritzen, T. Eid and L. H. Bergersen, *Brain Struct. Funct.*, 2015, **220**, 1–12.
- 64 Y. Wang, L. Qin, W. Chen, Q. Chen, J. Sun and G. Wang, *Eur. J. Med. Chem.*, 2021, **226**, 113806.
- 65 M. C. Wilson, D. Meredith, C. Bunnun, R. B. Sessions and A. P. Halestrap, *J. Biol. Chem.*, 2009, **284**, 20011–20021.
- 66 M. C. Wilson, D. Meredith, J. E. M. Fox, C. Manoharan, A. J. Davies and A. P. Halestrap, *J. Biol. Chem.*, 2005, **280**, 27213–27221.
- 67 N. Wang, X. Jiang, S. Zhang, A. Zhu, Y. Yuan, H. Xu, J. Lei and C. Yan, *Cell*, 2021, **184**, 370–383.e13.
- 68 S. Gurrapu, S. K. Jonnalagadda, M. A. Alam, C. T. Ronayne, G. L. Nelson, L. N. Solano, E. A. Lueth, L. R. Drewes and V. R. Mereddy, *Bioorg. Med. Chem. Lett.*, 2016, **26**, 3282–3286.
- 69 S. Sharma, S. Wijerathna, K. Wu, A. Tyagi, S.-Y. Wu, K. Watabe, N. Kuklin, J. Escobedo and V. Sandanayaka, *Cancer Res.*, 2023, **83**, P3-07–21.
- 70 R. C. Lynch, P. N. Munster, R. H. Advani, M. Hamadani, D. R. Spigel, G. S. Falchook, M. R. Patel, D. S. D. Siegel, N. Beri, G. S. Nowakowski, N. Palmisiano, M. L. Burness, K. N. Moore, G. Shapiro, D. Juric, W. D. Bradley, T. J. O'Shea, M. F. Renschler, J. M. Englert and T. A. Yap, *J. Clin. Oncol.*, 2022, **40**, 3084–3084.
- 71 R. C. Lynch, P. N. Munster, G. S. Falchook, M. L. Burness, T. A. Yap, G. Shapiro, D. R. Spigel, M. R. Patel, K. N. Moore, D. Juric, S. Doleman, W. D. Bradley, T. J. O'Shea, J. M. Englert, M. F. Renschler and N. Beri, *J. Clin. Oncol.*, 2023, **41**, 3099–3099.
- 72 E. S. Tsang and P. N. Munster, *Onco Targets Ther.*, 2022, **15**, 1509–1518.
- 73 B. Bradley, M. A. Belmonte, S. Kansara, J. L. Blank, L. Cryan, N. M. Reilly, V. Murali, D. H. Miller and J. P. Secrist, *Eur. J. Cancer*, 2022, **174**, S24–S25.
- 74 S. Puri, K. Stefan, S. L. Khan, J. Pahnke, S. M. Stefan and K. Juvale, *J. Med. Chem.*, 2023, **66**, 657–676.
- 75 M. Quanz, E. Bender, C. Kopitz, S. Grünewald, A. Schlicker, W. Schwede, A. Eheim, L. Toschi, R. Neuhaus, C. Richter, J. Toedling, C. Merz, R. Lesche, A. Kamburov, H. Siebeneicher, M. Bauser and A. Hägebarth, *Mol. Cancer Ther.*, 2018, **17**, 2285–2296.
- 76 S. E. R. Halford, H. Walter, P. McKay, W. Townsend, K. Linton, K. Heinzmann, I. Dragoni, L. Brotherton, G. Veal, A. Siskos, H. C. Keun, C. Bacon, S. Wedge, M. J. S. Dyer and E. R. Plummer, *J. Clin. Oncol.*, 2021, **39**, 3115–3115.

- 77 S. E. R. Halford, P. Jones, S. Wedge, S. Hirschberg, S. Katugampola, G. Veal, G. Payne, C. Bacon, S. Potter, M. Griffin, M. Chenard-Poirier, G. Petrides, G. Holder, H. C. Keun, U. Banerji and E. R. Plummer, *J. Clin. Oncol.*, 2017, **35**, 2516–2516.
- 78 A. Silva, B. Antunes, A. Batista, F. Pinto-Ribeiro, F. Baltazar and J. Afonso, *Molecules*, 2021, **27**, 181.
- 79 N. J. Curtis, L. Mooney, L. Hopcroft, F. Michopoulos, N. Whalley, H. Zhong, C. Murray, A. Logie, M. Revill, K. F. Byth, A. D. Benjamin, M. A. Firth, S. Green, P. D. Smith and S. E. Critchlow, *Oncotarget*, 2017, **8**, 69219–69236.
- 80 T. Koltai and L. Fliegel, *Explor Target Antitumor Ther*, 2024, **5**, 135–169.
- 81 K. Graham, A. Müller, L. Lehmann, N. Koglin, L. Dinkelborg and H. Siebeneicher, *J. Labelled Comp. Radiopharm.*, 2014, **57**, 164–171.
- 82 V. F. Van Hée, D. Labar, G. Dehon, D. Grasso, V. Grégoire, G. G. Muccioli, R. Frédérick and P. Sonveaux, *Oncotarget*, 2017, **8**, 24415–24428.
- 83 H. Tateishi, A. B. Tsuji, K. Kato, H. Sudo, A. Sugyo, T. Hanakawa, M.-R. Zhang, T. Saga, Y. Arano and T. Higashi, *Bioorg. Med. Chem. Lett.*, 2017, **27**, 4893–4897.
- 84 M. Sadeghzadeh, R.-P. Moldovan, S. Fischer, B. Wenzel, F.-A. Ludwig, R. Teodoro, W. Deuther-Conrad, S. Jonnalagadda, S. K. Jonnalagadda, E. Gudelis, A. Šačkus, K. Higuchi, V. Ganapathy, V. R. Mereddy, L. R. Drewes and P. Brust, *J. Labelled Comp. Radiopharm.*, 2019, **62**, 411–424.
- 85 D. Gündel, M. Sadeghzadeh, W. Deuther-Conrad, B. Wenzel, P. Cumming, M. Toussaint, F.-A. Ludwig, R.-P. Moldovan, M. Kranz, R. Teodoro, B. Sattler, O. Sabri and P. Brust, *Int. J. Mol. Sci.*, 2021, **22**, 1645.
- 86 K. M. O'Rourke (2018) *The Synthesis of Novel PET and SPECT Imaging Agents and the Development of New Radioiododeboronation Procedures*. PhD thesis. University of Glasgow.
- 87 K. M. O'Rourke, E. S. Johnstone, H. M. Becker, S. L. Pimlott and A. Sutherland, *Tetrahedron*, 2018, **74**, 4086–4094.
- 88 H. M. Becker, D. Hirnet, C. Fecher-Trost, D. Sültemeyer and J. W. Deitmer, *J. Biol. Chem.*, 2005, **280**, 39882–39889.
- 89 J. E. M. Fox, D. Meredith and A. P. Halestrap, *J. Physiol.*, 2000, **529**, 285–293.

- 90 C. Zheng, D. Holden, M.-Q. Zheng, R. Pracitto, K. C. Wilcox, M. Lindemann, Z. Felchner, L. Zhang, J. Tong, K. Fowles, S. J. Finnema, N. Nabulsi, R. E. Carson, Y. Huang and Z. Cai, *Eur. J. Nucl. Med. Mol. Imaging*, 2022, **49**, 1482–1496.
- 91 M. Naganawa, S. Li, N. Nabulsi, S. Henry, M.-Q. Zheng, R. Pracitto, Z. Cai, H. Gao, M. Kapinos, D. Labaree, D. Matuskey, Y. Huang and R. E. Carson, *J. Nucl. Med.*, 2021, **62**, 561–567.
- 92 Y. Hayashi, in *Catalytic Asymmetric Synthesis*, Wiley, 2022, pp. 1–28.
- 93 J. von Liebig, *Justus Liebigs Ann. Chem.*, 1860, **113**, 246–247.
- 94 Z. G. Hajos and D. R. Parrish, *J. Org. Chem.*, 1974, **39**, 1615–1621.
- 95 U. Eder, G. Sauer and R. Wiechert, *Angew. Chem. Int. Ed. Engl.*, 1971, **10**, 496–497.
- 96 K. A. Ahrendt, C. J. Borths and D. W. C. MacMillan, *J. Am. Chem. Soc.*, 2000, **122**, 4243–4244.
- 97 B. List, R. A. Lerner and C. F. Barbas, *J. Am. Chem. Soc.*, 2000, **122**, 2395–2396.
- 98 M. Marigo, T. C. Wabnitz, D. Fielenbach and K. A. Jørgensen, *Angew. Chem. Int. Ed.*, 2005, **44**, 794–797.
- 99 Y. Hayashi, H. Gotoh, T. Hayashi and M. Shoji *Angew. Chem. Int. Ed.*, 2005, **44**, 4212–4215.
- 100 J. L. Vicario, E. Reyes, D. Badía and L. Carrillo, in *Catalytic Asymmetric Conjugate Reactions*, Wiley, 2010, pp. 219–293.
- 101 K. L. Jensen, P. H. Poulsen, B. S. Donslund, F. Morana and K. A. Jørgensen, *Org. Lett.*, 2012, **14**, 1516–1519.
- 102 R. Lindroth, H. P. Bryce-Rogers, T. P. M. Merke and C. J. Wallentin, *Photochem. Photobiol. Sci.*, 2022, **21**, 819–824.
- 103 A. V. Mossine, A. F. Brooks, V. Bernard-Gauthier, J. J. Bailey, N. Ichiishi, R. Schirmacher, M. S. Sanford and P. J. H. Scott, *J. Labelled Comp. Radiopharm.*, 2018, **61**, 228–236.
- 104 N. Griem-Krey, A. B. Klein, M. Herth and P. Wellendorph, *J. Vis. Exp.*, 2019, **Mar. 12**, 145.
- 105 A. Metaxas, C. Thygesen, S. R. R. Briting, A. M. Landau, S. Darvesh and B. Finsen, *Front. Cell. Neurosci.*, 2019, **13**, 538.
- 106 M. B. Thomsen, J. Jacobsen, T. P. Lillethorup, A. C. Schacht, M. Simonsen, M. Romero-Ramos, D. J. Brooks and A. M. Landau, *J. Cereb. Blood Flow Metab.*, 2021, **41**, 819–830.

- 107 P. Sadasivam, X. T. Fang, T. Toyonaga, S. Lee, Y. Xu, M.-Q. Zheng, J. Spurrier, Y. Huang, S. M. Strittmatter, R. E. Carson and Z. Cai, *Mol. Imaging Biol.*, 2021, **23**, 372–381.
- 108 M. H. Haindl, M. B. Schmid, K. Zeitler and R. M. Gschwind, *RSC Adv.*, 2012, **2**, 5941–5943.
- 109 J. Franzén, M. Marigo, D. Fielenbach, T. C. Wabnitz, A. Kjærsgaard and K. A. Jørgensen, *J. Am. Chem. Soc.*, 2005, **127**, 18296–18304.
- 110 A. Kamlah and F. Bracher, *Lett. Org. Chem.*, 2018, **16**, 931–934.
- 111 K. Jones and M. L. Escudero-Hernandez, *Tetrahedron*, 1998, **54**, 2275–2280.
- 112 S. Li, Z. Cai, W. Zhang, D. Holden, S. fei Lin, S. J. Finnema, A. Shirali, J. Ropchan, S. Carre, J. Mercier, R. E. Carson, N. Nabulsi and Y. Huang, *Eur. J. Nucl. Med. Mol. Imaging*, 2019, **46**, 1952–1965.
- 113 Ø. Torkildsen, L. A. Brunborg, K.-M. Myhr and L. Bø, *Acta Neurol. Scand.*, 2008, **117**, 72–76.
- 114 V. Ramaglia, M. Dubey, M. A. Malpede, N. Petersen, S. I. de Vries, S. M. Ahmed, D. S. W. Lee, G. J. Schenk, S. M. Gold, I. Huitinga, J. L. Gommerman, J. J. G. Geurts and M. H. P. Kole, *Acta Neuropathol.*, 2021, **142**, 643–667.
- 115 S. Gingele, T. M. Möllenkamp, F. Henkel, L. Schröder, M. W. Hümmert, T. Skripuletz, M. Stangel and V. Gudi, *Brain Pathol.*, 2024, **34**, e13218.
- 116 A. A. S. Tavares, J. Lewsey, D. Dewar and S. L. Pimlott, *Nucl. Med. Biol.*, 2012, **39**, 127–135.
- 117 S. D. Guile, J. R. Bantick, M. E. Cooper, D. K. Donald, C. Eyssade, A. H. Ingall, R. J. Lewis, B. P. Martin, R. T. Mohammed, T. J. Potter, R. H. Reynolds, S. A. St-Gallay and A. D. Wright, *J. Med. Chem.*, 2007, **50**, 254–263.
- 118 J. Hou, M. S. Kovacs, S. Dhanvantari and L. G. Luyt, *J. Med. Chem.*, 2018, **61**, 1261–1275.
- 119 A. Begouin, S. Hesse, M.-J. R. Queiroz and G. Kirsch, *Synthesis*, 2005, 2373–2378.
- 120 A. A. S. Tavares, J. Lewsey, D. Dewar and S. L. Pimlott, *Nucl. Med. Biol.*, 2012, **39**, 127–135.
- 121 Y. Sun, T. Hou, X. He, V. H. Man and J. Wang, *J. Comput. Chem.*, 2023, **44**, 1300–1311.
- 122 MolInspiration, *Calculation of Molecular Properties*. Available at: <https://www.molinspiration.com/cgi/properties> (Accessed 15/09/2023).

- 123 Biosig Lab, *Computational Biology and Clinical Informatics*. Available at: <https://biosig.lab.uq.edu.au/deeppk/prediction> (Accessed 15/09/2023).
- 124 S. Ong, H. Liu, X. Qiu, G. Bhat and C. Pidgeon, *Anal. Chem.*, 1995, **67**, 755–762.
- 125 T. Bohnert and L.-S. Gan, *J. Pharm. Sci.*, 2013, **102**, 2953–2994.
- 126 L. D. Adair and E. J. New, *Curr. Opin. Biotechnol.*, 2023, **83**, 102973.
- 127 S. M. Hickey, B. Ung, C. Bader, R. Brooks, J. Lazniewska, I. R. D. Johnson, A. Sorvina, J. Logan, C. Martini, C. R. Moore, L. Karageorgos, M. J. Sweetman and D. A. Brooks, *Cells*, 2021, **11**, 35.
- 128 R. Nordstrom, S. Cherry, A. Azhdarinia, E. Sevic-Muraca and H. VanBrocklin, *Biomed. Opt. Express*, 2013, **4**, 2751.
- 129 H. M. Schouw, L. A. Huisman, Y. F. Janssen, R. H. J. A. Slart, R. J. H. Borra, A. T. M. Willemsen, A. H. Brouwers, J. M. van Dijk, R. A. Dierckx, G. M. van Dam, W. Szymanski, H. H. Boersma and S. Kruijff, *Eur. J. Nucl. Med. Mol. Imaging*, 2021, **48**, 4272–4292.
- 130 P. A. Sutton, M. A. van Dam, R. A. Cahill, S. Mieog, K. Polom, A. L. Vahrmeijer and J. van der Vorst, *BJS Open*, 2023, **7**, zrad049.
- 131 C. A. Combs, *Curr. Protoc. Neurosci.*, 2010, **50**, 2.1.1–2.1.14.
- 132 F. Rost, in *Encyclopedia of Spectroscopy and Spectrometry*, Elsevier, 2010, pp. 619–624.
- 133 K. Jeong, S.-H. Kong, S.-W. Bae, C. R. Park, F. Berth, J. H. Shin, Y.-S. Lee, H. Youn, E. Koo, Y.-S. Suh, D. J. Park, H.-J. Lee and H.-K. Yang, *J. Gastric Cancer*, 2021, **21**, 191–202.
- 134 N. Kosaka, M. Ogawa, P. L. Choyke and H. Kobayashi, *Future Oncol.*, 2009, **5**, 1501–11.
- 135 H. Khraishah and F. A. Jaffer, *Front. Cardiovasc. Med.*, 2020, **7**, 587100.
- 136 H. Chen, M. Zhang, B. Li, D. Chen, X. Dong, Y. Wang and Y. Gu, *Biomaterials*, 2015, **53**, 532–544.
- 137 X. Shi, P. Xu, C. Cao, Z. Cheng, J. Tian and Z. Hu, *Eur. J. Nucl. Med. Mol. Imaging*, 2022, **49**, 4325–4337.
- 138 S. Hu and L. V. Wang, *J. Biomed. Opt.*, 2010, **15**, 011101.
- 139 P. K. Upputuri and M. Pramanik, *WIREs Nanomed. and Nanobiotechnol.*, 2020, **12**, e1618.
- 140 M. Zimmer, *Chem. Rev.*, 2002, **102**, 759–782.

- 141 G. R. V. Hammond, C. E. J. Cheetham and T. Balla, in *Encyclopedia of Cell Biology*, Elsevier, 2016, pp. 51–61.
- 142 E. L. Snapp, *Trends Cell. Biol.*, 2009, **19**, 649–655.
- 143 P. J. Cranfill, B. R. Sell, M. A. Baird, J. R. Allen, Z. Lavagnino, H. M. de Gruiter, G.-J. Kremers, M. W. Davidson, A. Ustione and D. W. Piston, *Nat. Methods*, 2016, **13**, 557–562.
- 144 A. Hoffman, R. Atreya, T. Rath and M. F. Neurath, *Visc. Med*, 2020, **36**, 95–103.
- 145 U.S. Food and Drug Administration (FDA), *Drugs@FDA: FDA-Approved Drugs*. Available at: <https://www.accessdata.fda.gov/scripts/cder/daf/index.cfm> (accessed: 29/05/2025).
- 146 Q.-Y. Chen, J.-W. Xie, Q. Zhong, J.-B. Wang, J.-X. Lin, J. Lu, L.-L. Cao, M. Lin, R.-H. Tu, Z.-N. Huang, J.-L. Lin, H.-L. Zheng, P. Li, C.-H. Zheng and C.-M. Huang, *JAMA Surg.*, 2020, **155**, 300.
- 147 C. Egloff-Juras, L. Bezdetnaya, G. Dolivet and H.-P. Lassalle, *Int. J. Nanomedicine*, 2019, **14**, 7823–7838.
- 148 J. T. Alander, I. Kaartinen, A. Laakso, T. Pätälä, T. Spillmann, V. V. Tuchin, M. Venermo and P. Välisuo, *Int. J. Biomed. Imaging*, 2012, **2012**, 1–26.
- 149 H. A. Galema, T. M. van Ginhoven, G. J. H. Franssen, J. Hofland, C. G. O. T. Bouman, C. Verhoef, A. L. Vahrmeijer, M. Hutteman, D. E. Hilling and S. Keereweer, *Br. J. Surg.*, 2023, **110**, 541–544.
- 150 D. Seah, Z. Cheng and M. Vendrell, *ACS Nano*, 2023, **17**, 19478–19490.
- 151 L. E. Lamberts, M. Koch, J. S. de Jong, A. L. L. Adams, J. Glatz, M. E. G. Kranendonk, A. G. T. Terwisscha van Scheltinga, L. Jansen, J. de Vries, M. N. Lub-de Hooge, C. P. Schröder, A. Jorritsma-Smit, M. D. Linssen, E. de Boer, B. van der Vegt, W. B. Nagengast, S. G. Elias, S. Oliveira, A. J. Witkamp, W. P. Th. M. Mali, E. Van der Wall, P. J. van Diest, E. G. E. de Vries, V. Ntziachristos and G. M. van Dam, *Clin. Cancer Res.*, 2017, **23**, 2730–2741.
- 152 R. Atreya, H. Neumann, C. Neufert, M. J. Waldner, U. Billmeier, Y. Zopf, M. Willma, C. App, T. Münster, H. Kessler, S. Maas, B. Gebhardt, R. Heimke-Brinck, E. Reuter, F. Dörje, T. T. Rau, W. Uter, T. D. Wang, R. Kiesslich, M. Vieth, E. Hannappel and M. F. Neurath, *Nat. Med.*, 2014, **20**, 313–318.
- 153 G. Lu, N. S. van den Berg, B. A. Martin, N. Nishio, Z. P. Hart, S. van Keulen, S. Fakurnejad, S. U. Chirita, R. C. Raymundo, G. Yi, Q. Zhou, G. A. Fisher, E. L. Rosenthal and G. A. Poultides, *Lancet Gastroenterol. Hepatol.*, 2020, **5**, 753–764.

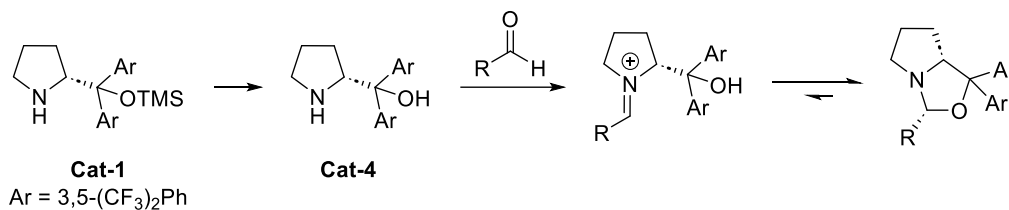
- 154 F. J. Voskuil, P. J. Steinkamp, T. Zhao, B. van der Vegt, M. Koller, J. J. Doff, Y. Jayalakshmi, J. P. Hartung, J. Gao, B. D. Sumer, M. J. H. Witjes, G. M. van Dam, Y. Albaroodi, L. B. Been, F. Dijkstra, B. van Etten, Q. Feng, R. J. van Ginkel, K. Hall, K. Havenga, J. W. Haveman, P. H. J. Hemmer, L. Jansen, S. J. de Jongh, G. Kats-Ugurlu, W. Kelder, S. Kruijff, I. Kruithof, E. van Loo, J. L. N. Roodenburg, N. Shenoy, K. P. Schepman and S. A. H. J. de Visscher, *Nat. Commun.*, 2020, **11**, 3257.
- 155 E. K. Nyren-Erickson, M. K. Haldar, Y. Gu, S. Y. Qian, D. L. Friesner and S. Mallik, *Anal. Chem.*, 2011, **83**, 5989–5995.
- 156 R. Philip, A. Penzkofer, W. Bäuml, R. M. Szeimies and C. Abels, *J. Photochem. Photobiol. A Chem.*, 1996, **96**, 137–148.
- 157 S. Selvam and I. Sarkar, *J. Pharm. Anal.*, 2017, **7**, 71–75.
- 158 R. F. Kubin and A. N. Fletcher, *J. Lumin.*, 1982, **27**, 455–462.
- 159 S. L. Jacques and S. A. Prahl, *OMLC: PhotoChemCAD Chemicals*. Available at: <https://omlc.org/spectra/PhotochemCAD/> (Accessed: 02/06/2025).
- 160 Z. Cheng, E. Kuru, A. Sachdeva and M. Vendrell, *Nat. Rev. Chem.*, 2020, **4**, 275–290.
- 161 A. Acharyya, I. A. Ahmed and F. Gai, *Methods Enzymol.*, 2020, **639**, 191–215.
- 162 A. H. Harkiss and A. Sutherland, *Org. Biomol. Chem.*, 2016, **14**, 8911–8921.
- 163 E. Kuru, S. Tekkam, E. Hall, Y. V Brun and M. S. Van Nieuwenhze, *Nat. Protoc.*, 2015, **10**, 33–52.
- 164 R. Subiros-Funosas, V. C. L. Ho, N. D. Barth, L. Mendive-Tapia, M. Pappalardo, X. Barril, R. Ma, C.-B. Zhang, B.-Z. Qian, M. Sintès, O. Ghashghaei, R. Lavilla and M. Vendrell, *Chem. Sci.*, 2020, **11**, 1368–1374.
- 165 J. G. Marmorstein, V. V. Pagar, E. Hummingbird, I. G. Saleh, H. A. T. Phan, Y. Chang, K. D. Shaffer, Y. Venkatesh, I. J. Dmochowski, K. J. Stebe and E. J. Petersson, *Bioconjug. Chem.*, 2024, **35**, 1913–1922.
- 166 L. S. Fowler, D. Ellis and A. Sutherland, *Org. Biomol. Chem.*, 2009, **7**, 4309.
- 167 L. Zeng, O. Marshall, R. McGrory, R. Clarke, R. J. Brown, M. Kadodwala, A. R. Thomson and A. Sutherland, *Org. Lett.*, 2025, **27**, 2475–2479.
- 168 O. Marshall, R. McGrory, S. Songsri, A. R. Thomson and A. Sutherland, *Chem. Sci.*, 2025, **16**, 3490–3497.
- 169 R. Clarke, L. Zeng, B. C. Atkinson, M. Kadodwala, A. R. Thomson and A. Sutherland, *Chem. Sci.*, 2024, **15**, 5944–5949.

- 170 A. C. Dodds, H. G. Sansom, S. W. Magennis and A. Sutherland, *Org. Lett.*, 2023, **25**, 8942–8946.
- 171 J. D. Bell, T. E. F. Morgan, N. Buijs, A. H. Harkiss, C. R. Wellaway and A. Sutherland, *J. Org. Chem.*, 2019, **84**, 10436–10448.
- 172 N. Elia, *FEBS J.*, 2021, **288**, 1107–1117.
- 173 R. Verma, S. Pyreddy, C. E. Redmond, F. Qazi, A. Khalid, N. M. O'Brien-Simpson, R. Shukla and S. Tomljenovic-Hanic, *Anal. Chim. Acta*, 2023, **1282**, 341925.
- 174 E. F. Joest, C. Winter, J. S. Wesalo, A. Deiters and R. Tampé, *ACS Synth. Biol.*, 2022, **11**, 1466–1476.
- 175 R. Chaniyara, S. Tala, C.-W. Chen, X. Zang, R. Kakadiya, L.-F. Lin, C.-H. Chen, S.-I. Chien, T.-C. Chou, T.-H. Tsai, T.-C. Lee, A. Shah and T.-L. Su, *J. Med. Chem.*, 2013, **56**, 1544–1563.
- 176 K. Iterbeke, G. Laus, P. Verheyden and D. Tourwé, *Lett. Pept. Sci.*, 1998, **5**, 121–123.
- 177 J. Ye, J. Wu, T. Lv, G. Wu, Y. Gao and H. Chen, *Angew. Chem. Int. Ed.*, 2017, **56**, 14968–14972.
- 178 H. Chen, F. Ye, J. Luo and Y. Gao, *Org. Lett.*, 2019, **21**, 7475–7477.
- 179 J. Chauhan, T. Luthra and S. Sen, *Eur. J. Org. Chem.*, 2018, 4776–4786.
- 180 A. Chiotellis, A. Müller Herde, S. L. Rössler, A. Brekalo, E. Gedeonova, L. Mu, C. Keller, R. Schibli, S. D. Krämer and S. M. Ametamey, *J. Med. Chem.*, 2016, **59**, 5324–5340.
- 181 D. Gao and L. Jiao, *J. Org. Chem.*, 2021, **86**, 5727–5743.
- 182 M. A. Blanchette, W. Choy, J. T. Davis, A. P. Essinfeld, S. Masamune, W. R. Roush and T. Sakai, *Tetrahedron Lett.*, 1984, **25**, 2183–2186.
- 183 F. Gatta and D. Misiti, *J. Heterocycl. Chem.*, 1987, **24**, 1183–1187.
- 184 L. Wang, H. Zou, D. Ye and D. Cao, *J. Heterocycl. Chem.*, 2013, **50**, 551–556.
- 185 A. Kopp, T. Oyama and L. Ackermann, *Chem. Commun.*, 2024, **60**, 5423–5426.
- 186 D. Ivanova, V. Kolev, T. Lazarova and E. Padros, *Tetrahedron Lett.*, 1999, **40**, 2645–2648.
- 187 J. Wang, J. Gu, J.-Y. Zou, M.-J. Zhang, R. Shen, Z. Ye, P.-X. Xu and Y. He, *Nat. Commun.*, 2024, **15**, 3254.

- 188 H. Liu, M. Xu, C. Cai, J. Chen, Y. Gu and Y. Xia, *Org. Lett.*, 2020, **22**, 1193–1198.
- 189 S. S. Hepperle, Q. Li and A. L. L. East, *J. Phys. Chem. A*, 2005, **109**, 10975–10981.
- 190 Y. Ni, W. Fang and M. A. Olson, *Molecules*, 2023, **28**, 3217.
- 191 S. Songsri, A. H. Harkiss and A. Sutherland, *J. Org. Chem.*, 2023, **88**, 13214–13224.
- 192 T. J. Williams, A. J. Reay, A. C. Whitwood and I. J. S. Fairlamb, *Chem. Commun.*, 2014, **50**, 3052–3054.
- 193 F. Y. Miyake, K. Yakushijin and D. A. Horne, *Org. Lett.*, 2004, **6**, 711–713.
- 194 S. Kato, Y. Hamada and T. Shioiri, *Tetrahedron Lett.*, 1988, **29**, 6465–6466.
- 195 P. Ashworth, B. Broadbelt, P. Jankowski, P. Kocienski, A. Pimm and R. Bell, *Synthesis*, 1995, **2**, 199–206.
- 196 M. Horikawa, S. T. Joy, L. S. Sharninghausen, X. Shao, A. K. Mapp, P. J. H. Scott and M. S. Sanford, *Chem. Sci.*, 2023, **14**, 12068–12072.
- 197 A. J. Reay, L. A. Hammarback, J. T. W. Bray, T. Sheridan, D. Turnbull, A. C. Whitwood and I. J. S. Fairlamb, *ACS Catal.*, 2017, **7**, 5174–5179.
- 198 C.-X. Zhao, T. Liu, M. Xu, H. Lin and C.-J. Zhang, *Chin. Chem. Lett.*, 2021, **32**, 1925–1928.
- 199 B. Wrackmeyer, *Prog. Nucl. Magn. Reson. Spectrosc.*, 1979, **12**, 227–259.
- 200 A. Taillardat-Bertschinger, A. Galland, P.-A. Carrupt and B. Testa, *J. Chromatogr. A*, 2002, **953**, 39–53.
- 201 R. Chaniyara, S. Tala, C.-W. Chen, X. Zang, R. Kakadiya, L.-F. Lin, C.-H. Chen, S.-I. Chien, T.-C. Chou, T.-H. Tsai, T.-C. Lee, A. Shah and T.-L. Su, *J. Med. Chem.*, 2013, **56**, 1544–1563.
- 202 H. Chen, F. Ye, J. Luo and Y. Gao, *Org. Lett.*, 2019, **21**, 7475–7477.
- 203 J. Liu, P. Wang, W. Zeng, Q. Lu and Q. Zhu, *Chem. Commun.*, 2021, **57**, 11661–11664.
- 204 C.-M. Chio, Y.-C. Huang, Y.-C. Chou, F.-C. Hsu, Y.-B. Lai and C.-S. Yu, *ACS Med. Chem. Lett.*, 2020, **11**, 589–596.
- 205 N. van Rooijen and R. van Nieuwmegen, *Cell Tissue Res.*, 1984, **238**, 355–358.

5. Appendices

Appendix A. Figures and Schemes



Scheme S1. Possible catalytic cycle in the presence of catalyst **Cat-4**. (M. B. Schmid, K. Zeitler and R. M. Gschwind. *J. Am. Chem. Soc.* 2011, **133**, 18, 7065–7074.)

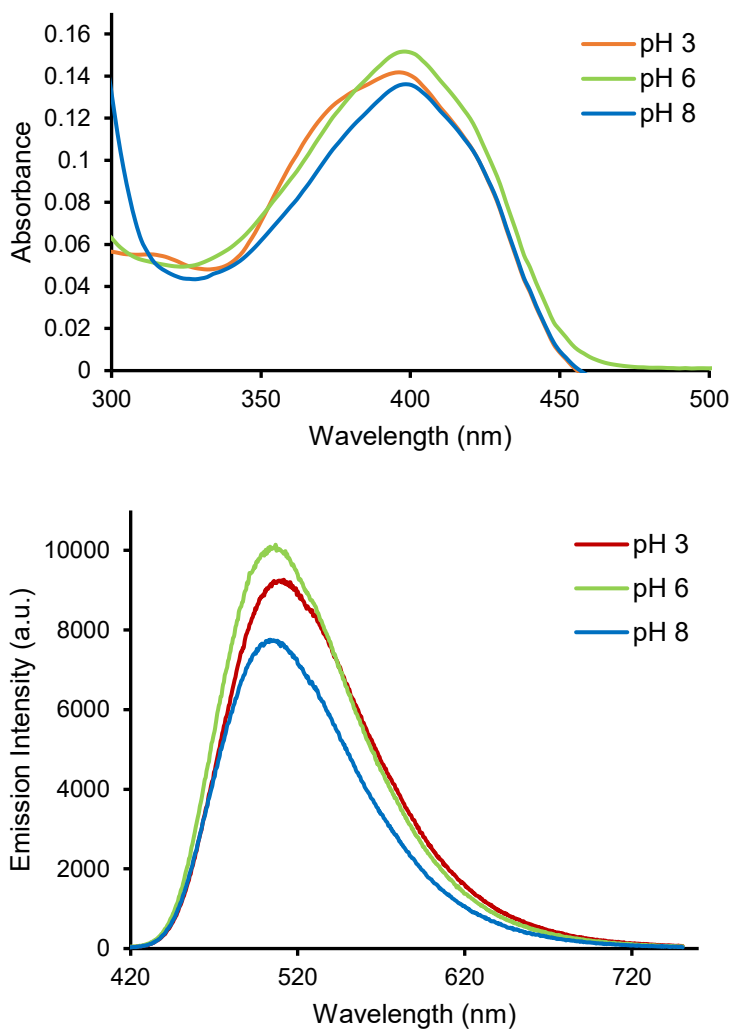


Figure S1. Absorbance and emission spectra for pH study of **105** (5 μ M solutions in THF. pH adjusted using Et₃N (pH 8) or 1 M HCl (pH 3)).

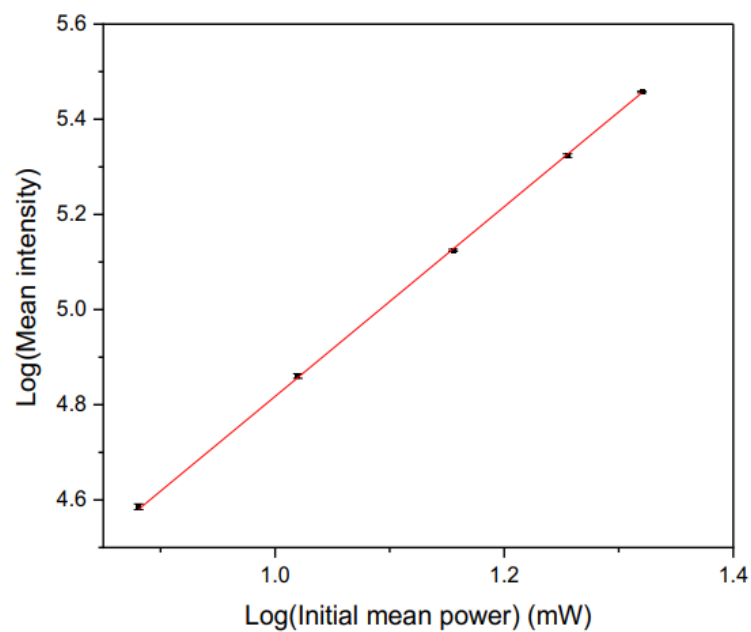


Figure S2. Log-Log plot, confirming two-photon excitation of **105**. Slope value is 1.993 ± 0.012 . Spectra were recorded in DMSO at $14.22 \mu\text{M}$ concentration.

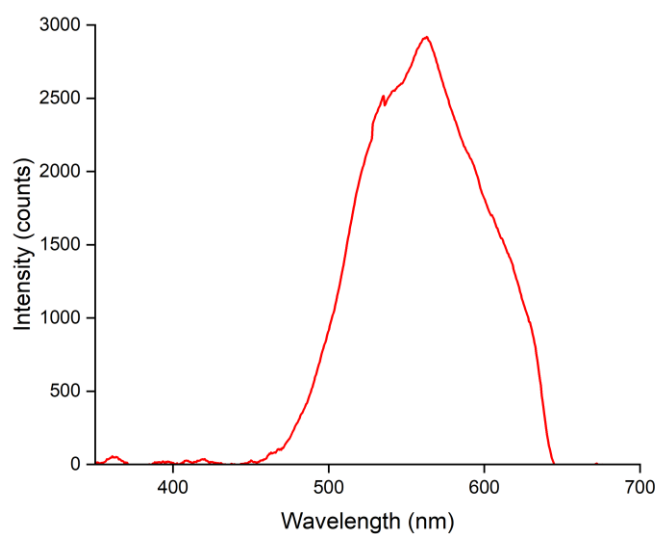
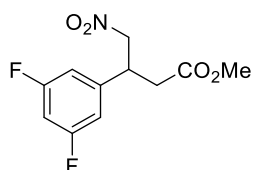


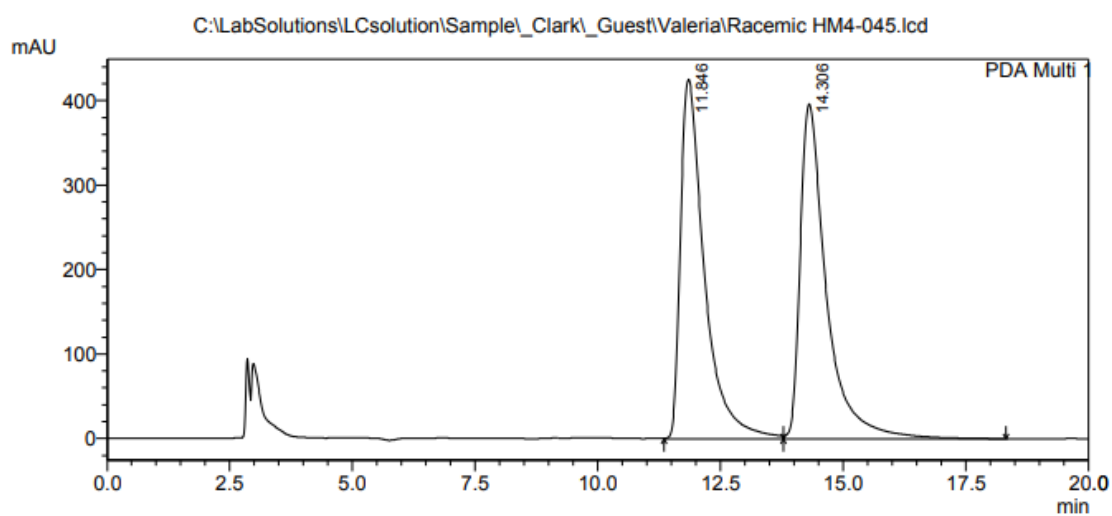
Figure S3. Emission spectra of **105** after two-photon excitation at 800 nm. Spectra were recorded in DMSO at $14.22 \mu\text{M}$ concentration.

Appendix B. Chiral HPLC Traces

Methyl 3-(3',5'-difluorophenyl)-4-nitrobutanoate (*rac*-58)



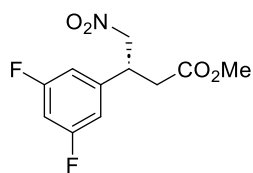
Acquired by : Admin
Sample Name : Racemic HM4-045
Sample ID : Racemic HM4-045
Injection Volume : 20 μ L
Data File Name : Racemic HM4-045.lcd
Method File Name : AD-H_5%IPA-Hexane_1mL-min_20min.lcm
Data Acquired : 05/12/2022 12:38:50
Data Processed : 08/12/2022 13:16:22
Racemic HM4-045
AD-H_5% IPA in hexane @ 1.0 mL/min for 20 min



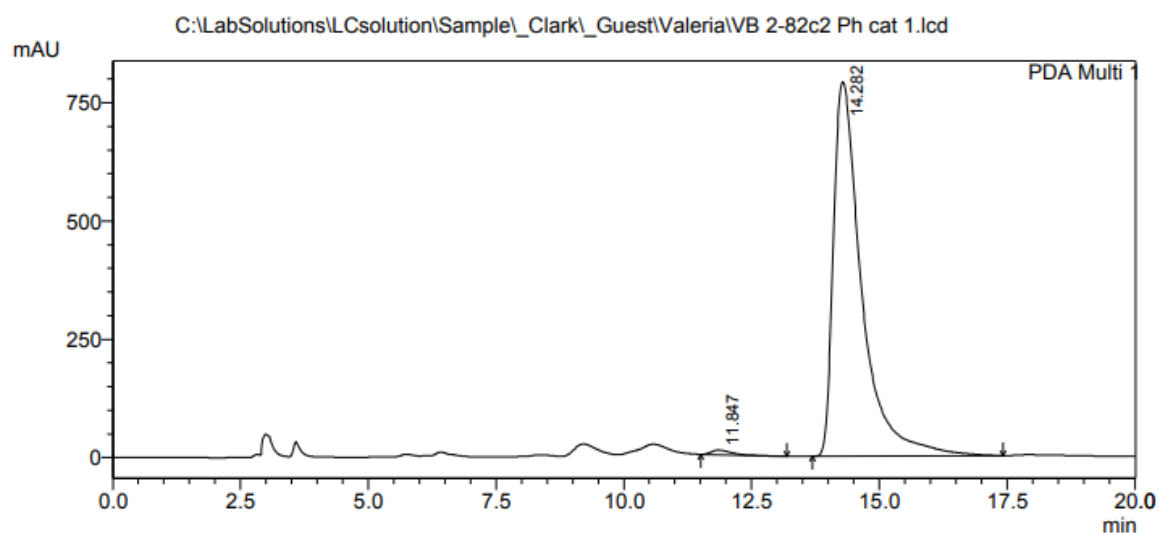
PDA Ch1 210nm 4nm

Peak#	Ret. Time	Area	Height	Area %	Height %
1	11.846	14458995	425387	49.526	51.752
2	14.306	14736011	396591	50.474	48.248
Total		29195006	821978	100.000	100.000

Methyl (3R)-3-(3',5'-difluorophenyl)-4-nitrobutanoate ((R)-58)



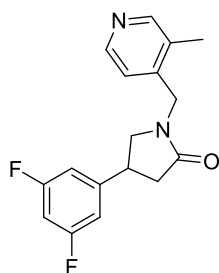
C:\LabSolutions\LCsolution\Sample_Clark_Guest\Valeria\VB 2-82c2 Ph cat 1.lcd
 Acquired by : Admin
 Sample Name : VB 2-82c2 Ph cat 1
 Sample ID : VB 2-82c2 Ph cat 1
 Injection Volume : 20 uL
 Data File Name : VB 2-82c2 Ph cat 1.lcd
 Method File Name : AD-H_5% iPrOH-Hexane_1mL-min_20min.lcm
 Data Acquired : 08/12/2022 12:10:15
 Data Processed : 08/12/2022 13:05:45
 VB 2-82c2 Ph cat 10% 1
 AD-H_5% IPA in hexane @ 1.0 mL/min for 20 min



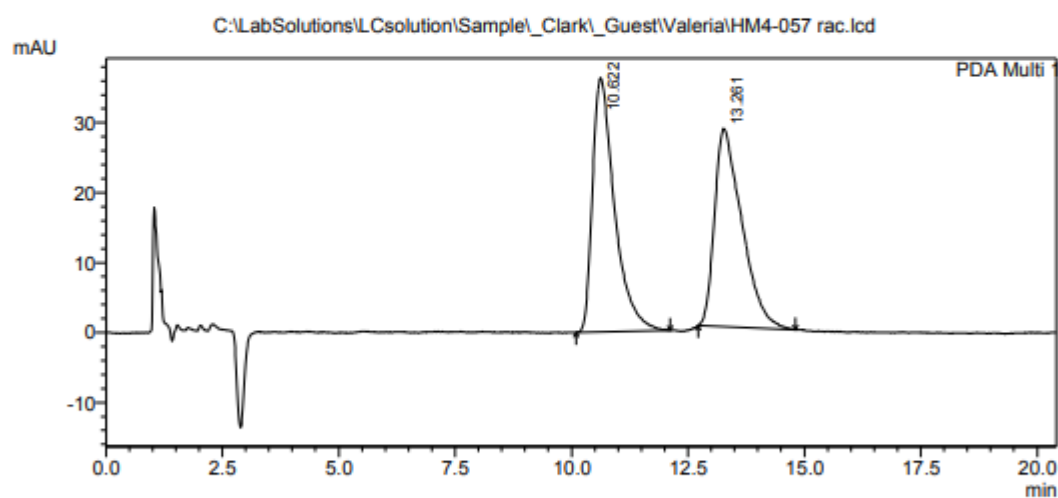
PDA Ch1 210nm 4nm

Peak#	Ret. Time	Area	Height	Area %	Height %
1	11.847	276990	9849	0.902	1.231
2	14.282	30418800	790506	99.098	98.769
Total		30695791	800355	100.000	100.000

**4-(3',5'-Difluorophenyl)-1-[(3''-methylpyridin-4''-yl)methyl]pyrrolidin-2-one
(rac-7)**



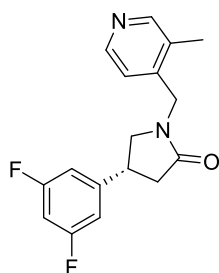
Acquired by : Admin
Sample Name : HM4-057 rac
Sample ID : HM4-057 rac
Injection Volume : 20 uL
Data File Name : HM4-057 rac.lcd
Method File Name : AD-H_10%iPrOH-Hexane_2mL-min_40min.lcm
Data Acquired : 31/07/2023 15:12:22
Data Processed : 31/07/2023 16:10:10
HM4-057 rac
AD-H column
10% iPrOH in hexane @ 2 mL/min
20 uL
25C



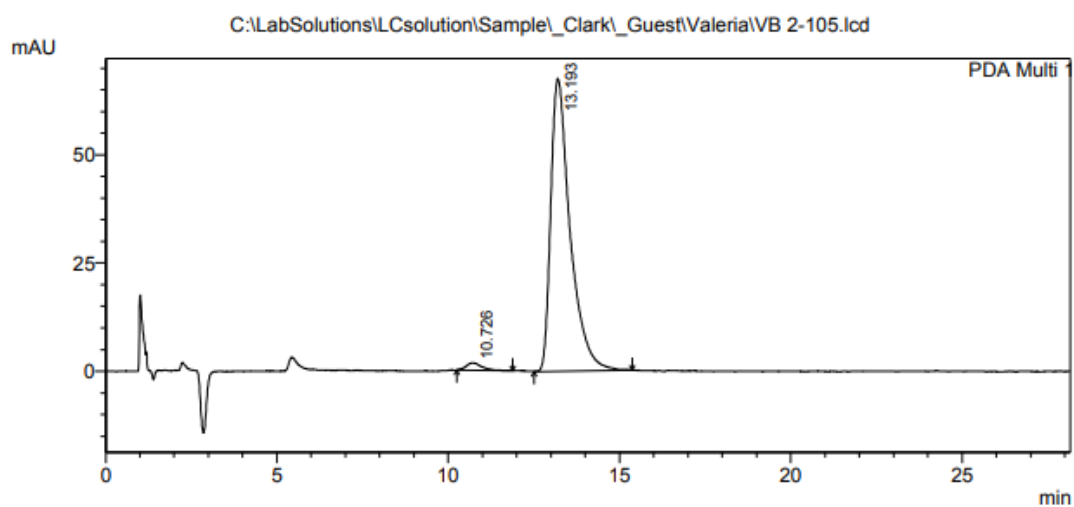
PDA Ch1 254nm 4nm

Peak#	Ret. Time	Area	Height	Area %	Height %
1	10.622	1197852	36329	50.893	56.191
2	13.261	1155803	28324	49.107	43.809
Total		2353655	64653	100.000	100.000

(4*R*)-4-(3',5'-Difluorophenyl)-1-[(3''-methylpyridin-4''-yl)methyl]pyrrolidin-2-one ((*R*)-7)



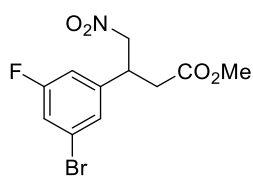
C:\LabSolutions\LCsolution\Sample_Clark_Guest\Valeria\VB 2-105.lcd
 Acquired by : Admin
 Sample Name : VB 2-105
 Sample ID : VB 2-105
 Injection Volume : 20 uL
 Data File Name : VB 2-105.lcd
 Method File Name : AD-H_10%iPrOH-Hexane_2mL-min_40min.lcm
 Data Acquired : 31/07/2023 15:37:17
 Data Processed : 31/07/2023 16:09:11
 VB 2-105
 AD-H column
 10% iPrOH in hexane @ 2 mL/min
 20 uL
 25C



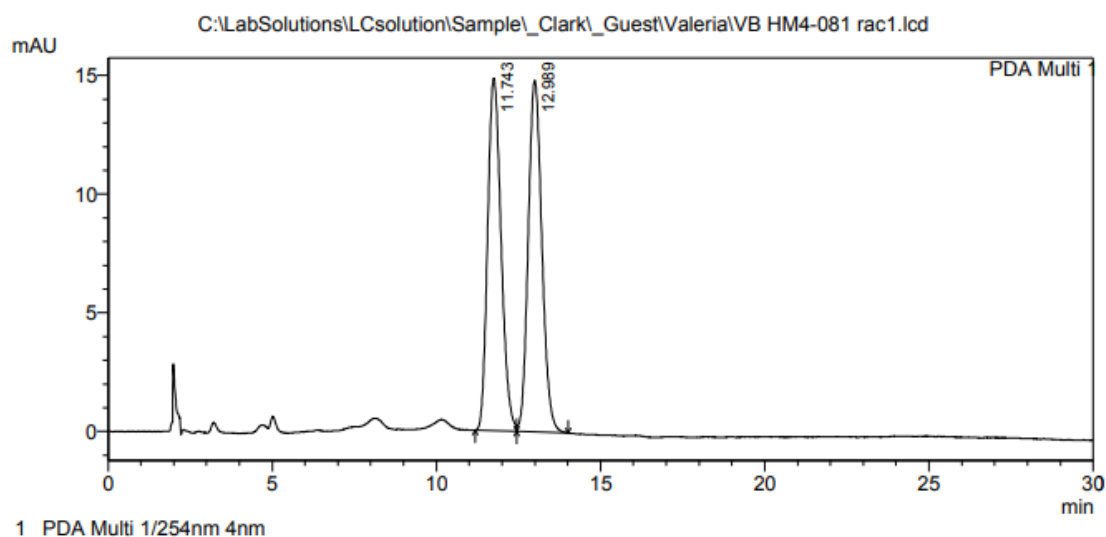
PDA Ch1 254nm 4nm

Peak#	Ret. Time	Area	Height	Area %	Height %
1	10.726	51971	1702	1.919	2.456
2	13.193	2656186	67596	98.081	97.544
Total		2708157	69298	100.000	100.000

Methyl 3-(3'-bromo-5'-fluorophenyl)-4-nitrobutanoate (*rac*-24)



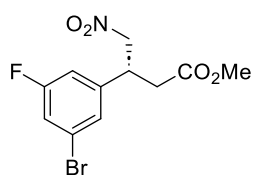
C:\LabSolutions\LCsolution\Sample_Clark_Guest\Valeria\VB HM4-081 rac1.lcd
 Acquired by : Admin
 Sample Name : VB HM4-081 rac
 Sample ID : VB HM4-081 rac
 Injection Volume : 20 uL
 Data File Name : VB HM4-081 rac1.lcd
 Method File Name : AD-H_2%IPA/Hexane_1mL-min_30min.lcm
 Data Acquired : 18/11/2012 11:05:39
 Data Processed : 18/11/2012 11:35:42
 VB HM4-081 rac
 AD-H_2%IPA/Hexane_1mL_30min



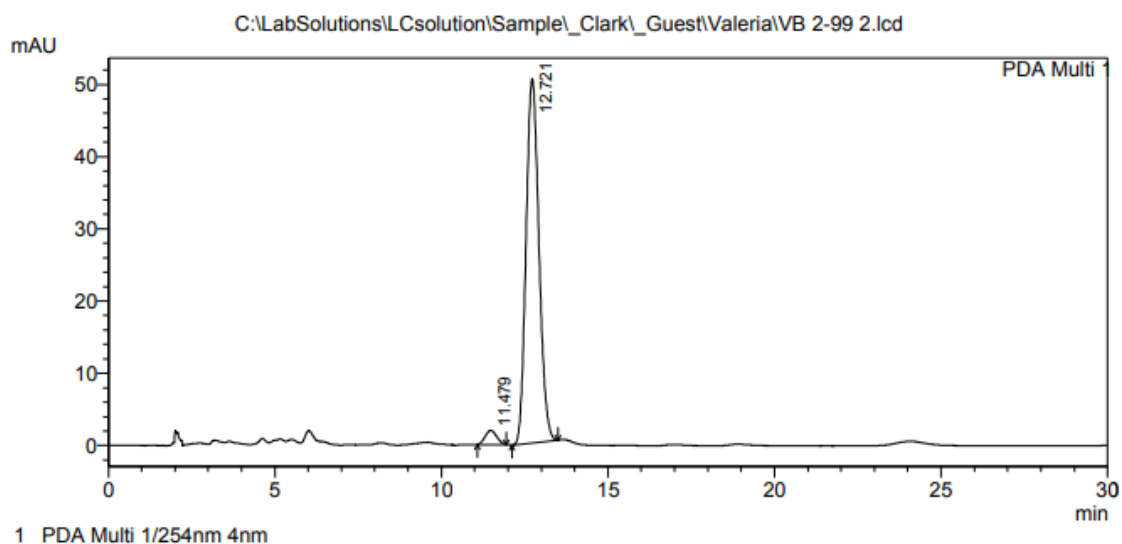
PDA Ch1 254nm 4nm

Peak#	Ret. Time	Area	Height	Area %	Height %
1	11.743	422146	14852	49.737	50.045
2	12.989	426618	14825	50.263	49.955
Tota		848764	29677	100.000	100.000

Methyl (3R)-3-(3'-bromo-5'-fluorophenyl)-4-nitrobutanoate ((R)-24)



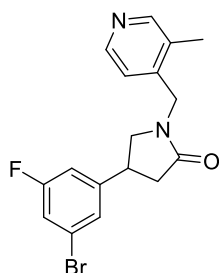
C:\LabSolutions\LCsolution\Sample_Clark_Guest\Valeria\VB 2-99 2.lcd
 Acquired by : Admin
 Sample Name : VB 2-99 1
 Sample ID : VB 2-99 1
 Injection Volume : 20 uL
 Data File Name : VB 2-99 2.lcd
 Method File Name : AD-H_2%IPA-Hexane_1mL-min_30min.lcm
 Data Acquired : 18/11/2012 11:44:49
 Data Processed : 18/11/2012 12:14:50
 VB 2-99 1
 AD-H_2%IPA/Hexane_1mL_30min



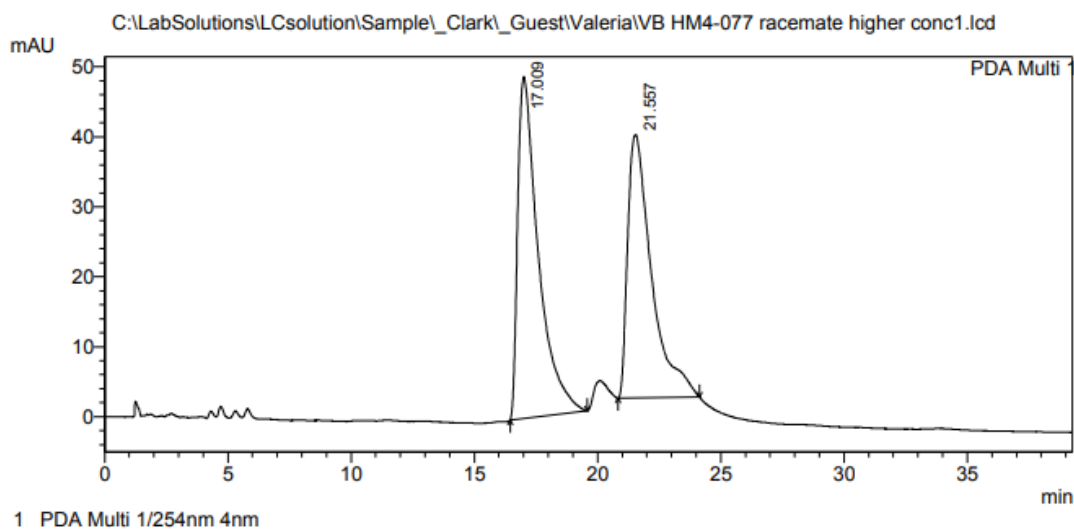
PDA Ch1 254nm 4nm

Peak#	Ret. Time	Area	Height	Area %	Height %
1	11.479	47149	1951	3.383	3.725
2	12.721	1346454	50429	96.617	96.275
Total		1393603	52380	100.000	100.000

4-(3'-Bromo-5'-fluorophenyl)-1-[(3"-methylpyridin-4"-yl)methyl]-pyrrolidin-2-one (rac-5)



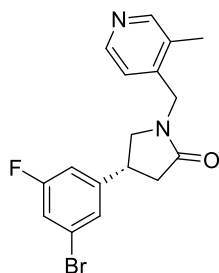
C:\LabSolutions\LCsolution\Sample_Clark_Guest\Valeria\VB HM4-077 racemate higher conc1.lcd
 Acquired by : Admin
 Sample Name : VB HM4-077 racemate higher conc
 Sample ID : VB HM4-077 racemate higher conc
 Injection Volume : 20 uL
 Data File Name : VB HM4-077 racemate higher conc1.lcd
 Method File Name : AD-H_8%IPrOH-Hexane_1.5mL-min_45min.lcm
 Data Acquired : 29/03/2023 16:30:19
 Data Processed : 29/03/2023 17:09:35
 VB HM4-077 racemate higher conc
 45 minutes 1.5 ml/min @ 25 C
 8% IPA in Hex
 ADH
 Load in IPA/Hexane 1:1, 20 uL



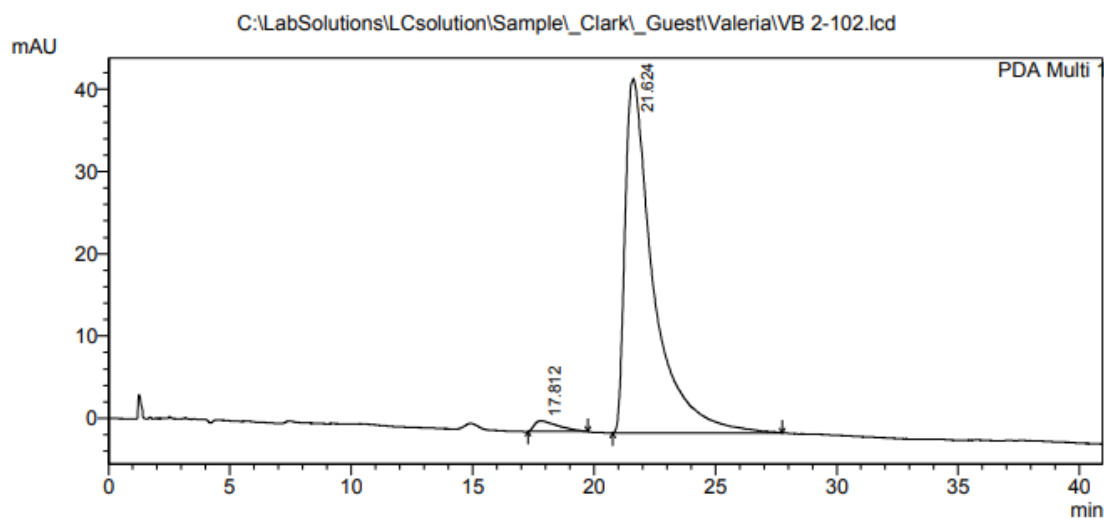
PDA Ch1 254nm 4nm

Peak#	Ret. Time	Area	Height	Area %	Height %
1	17.009	2846266	48830	52.906	56.521
2	21.557	2533638	37563	47.094	43.479
Total		5379904	86393	100.000	100.000

(4*R*)-4-(3'-Bromo-5'-fluorophenyl)-1-[(3"-methylpyridin-4"-yl)methyl]-pyrrolidin-2-one ((*R*)-5)



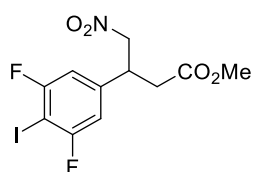
C:\LabSolutions\LCsolution\Sample_Clark_Guest\Valeria\VB 2-102.lcd
 Acquired by : Admin
 Sample Name : VB 2-101
 Sample ID : VB 2-101
 Injection Volume : 20 uL
 Data File Name : VB 2-102.lcd
 Method File Name : AD-H_8%IPA-Hexane_1.5mL-min_45min.lcm
 Data Acquired : 29/03/2023 15:48:07
 Data Processed : 29/03/2023 16:29:06
 VB 2-101
 45 minutes 1.5 ml/min @ 25 C
 8% IPA in Hex
 ADH
 Load in IPA/Hexane 1:1, 20 uL



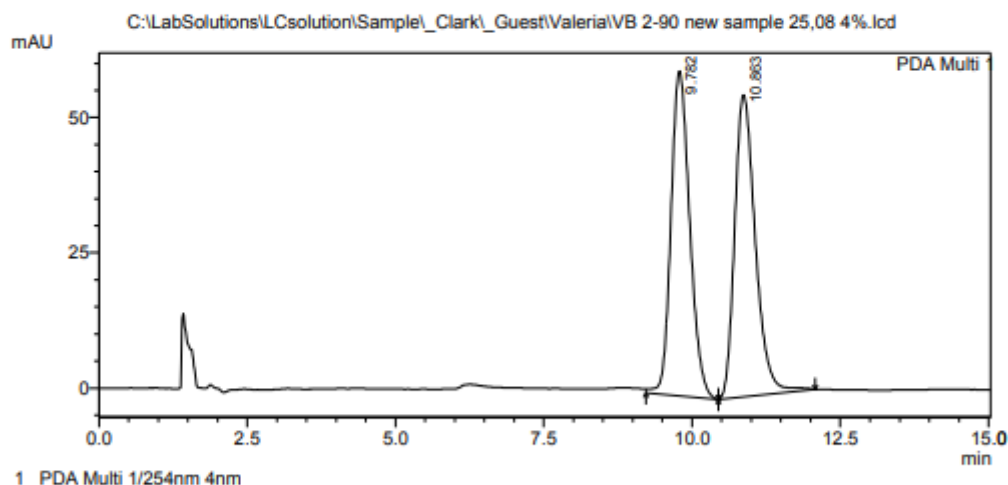
PDA Ch1 254nm 4nm

Peak#	Ret. Time	Area	Height	Area %	Height %
1	17.812	86218	1282	2.412	2.891
2	21.624	3488361	43073	97.588	97.109
Total		3574579	44355	100.000	100.000

Methyl 3-(3',5'-difluoro-4'-iodophenyl)-4-nitrobutanoate (*rac*-75)



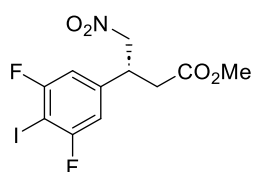
C:\LabSolutions\LCsolution\Sample\Clark\Guest\Valeria\VB 2-90 new sample 25,08 4%.lcd
 Acquired by : Admin
 Sample Name : VB 2-90 new sample 25,08 4%
 Sample ID : VB 2-90 new sample 25,08 4%
 Injection Volume : 20 uL
 Data File Name : VB 2-90 new sample 25,08 4%.lcd
 Method File Name : AD-H_4%iPrOH-Hexane_1.5mL-min_40min.lcm
 Data Acquired : 25/08/2023 15:08:53
 Data Processed : 25/08/2023 15:23:56
 VB 2-90
 4% iPrOH in hexane @ 1.5 mL/min
 AD-H column
 20 uL
 25 degrees



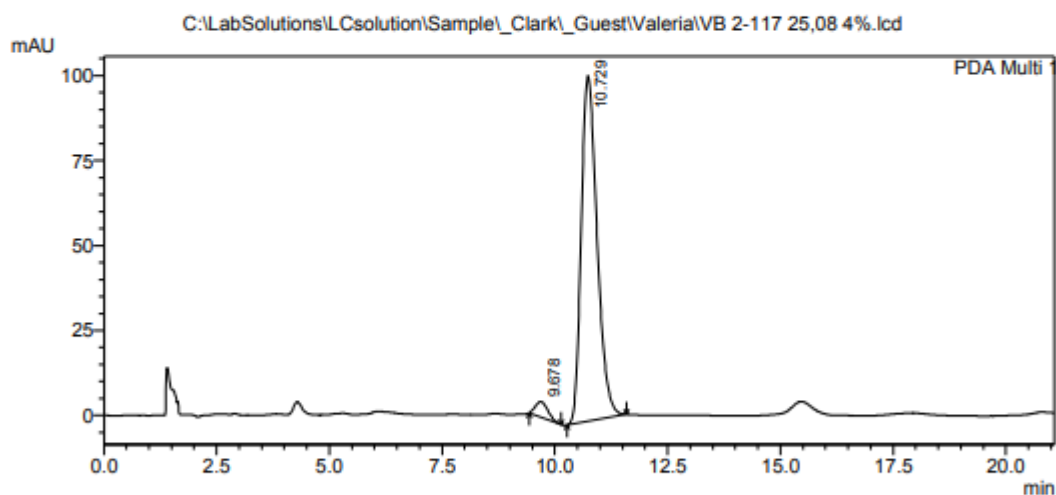
PDA Ch1 254nm 4nm

Peak#	Ret. Time	Area	Height	Area %	Height %
1	9.782	1319956	59920	49.459	51.785
2	10.863	1348824	55790	50.541	48.215
Total		2668780	115710	100.000	100.000

Methyl (3R)-3-(3',5'-difluoro-4'-iodophenyl)-4-nitrobutanoate ((R)-75)



C:\LabSolutions\LCsolution\Sample_Clark_Guest\Valeria\VB 2-117 25,08 4%.lcd
 Acquired by : Admin
 Sample Name : VB 2-117 25,08 4%
 Sample ID : VB 2-117 25,08 4%
 Injection Volume : 20 uL
 Data File Name : VB 2-117 25,08 4%.lcd
 Method File Name : AD-H_4%iPrOH-Hexane_1.5mL-min_40min.lcm
 Data Acquired : 25/08/2023 15:30:34
 Data Processed : 25/08/2023 15:51:40
 VB 2-117
 4% iPrOH in hexane @ 1.5 mL/min
 AD-H column
 20 uL
 25 degrees



PDA Ch1 254nm 4nm

Peak#	Ret. Time	Area	Height	Area %	Height %
1	9.678	87250	4506	3.402	4.248
2	10.729	2477329	101563	96.598	95.752
Total		2564579	106069	100.000	100.000

Appendix C. Determination of Physicochemical Properties

Membrane Permeability (P_m) and Membrane Partition Coefficient (K_m) via Immobilised Artificial Membrane (IAM) Chromatography

Compound	%	30	40	50	60
37a	1	7.000	3.267	2.37	2.077
	2	6.933	3.267	2.373	2.077
	3	6.947	3.267	2.373	2.077
	Average	6.960	3.267	2.372	2.077
Compound	%	30	40	50	60
37b	1	9.923	3.807	2.520	2.130
	2	9.920	3.807	2.520	2.130
	3	9.937	3.803	2.520	2.130
	Average	9.927	3.806	2.520	2.130
Compound	%	30	40	50	60
37c	1	6.723	3.173	2.337	2.067
	2	6.727	3.173	2.340	2.063
	3	6.713	3.170	2.340	2.063
	Average	6.721	3.172	2.339	2.064
Compound	%	30	40	50	60
37f	1	6.663	3.203	2.367	2.083
	2	6.693	3.200	2.367	2.083
	3	6.703	3.197	2.363	2.087
	Average	6.686	3.200	2.366	2.084
Compound	%	30	40	50	60
37h	1	7.197	3.320	2.400	2.097
	2	7.223	3.320	2.400	2.097
	3	7.237	3.323	2.397	2.097
	Average	7.219	3.321	2.399	2.097
Compound	%	30	40	50	60
37g	1	5.873	3.033	2.323	2.073
	2	5.867	3.040	2.323	2.073
	3	5.870	3.040	2.323	2.073
	Average	5.870	3.038	2.323	2.073
Compound	%	30	40	50	60
37i	1	18.31	5.060	2.840	2.247
	2	18.333	5.060	2.840	2.247
	3	18.343	5.070	2.840	2.247
	Average	18.329	5.063	2.840	2.247
Citric Acid	1	1.877			
	2	1.880			
	3	1.880			
	Average	1.879			

Comp.	30	40	50	60	t_r (min)	k'	V_s	V_s/V_m	K_m	MW	P_m
37a	6.960	3.267	2.372	2.077	12.475	5.6391	0.1481	0.0788	71.53	435.5	0.1643
37b	9.927	3.806	2.520	2.130	18.978	9.0998	0.1481	0.0788	115.43	449.5	0.2568
37c	6.721	3.172	2.339	2.064	12.007	5.3898	0.1481	0.0788	68.37	465.5	0.1469
37f	6.686	3.200	2.366	2.084	11.886	5.3258	0.1481	0.0788	67.56	447.5	0.1510
37g	5.870	3.037	2.323	2.073	10.114	4.3828	0.1481	0.0788	55.60	447.5	0.1242
37h	7.219	3.321	2.399	2.097	13.028	5.9336	0.1481	0.0788	75.27	447.5	0.1682
37i	18.329	5.063	2.840	2.247	37.780	19.1062	0.1481	0.0788	242.36	497.6	0.4871